Response of high-temperature superconductors to electromagnetic radiation: (A Review)

A. V. Velichko and N. T. Cherpak

*A. Usikov Institute of Radiophysics and Electronics, National Academy of Sciences of the Ukraine, 310085, Kharkov, Ukraine**

(Submitted May 15, 1997; revised January 5, 1998)
Fiz. Nizk. Temp. **24**, 395–428 (May 1998)

Nonequilibrium processes resulting from the interaction of high-temperature superconductors with electromagnetic radiation are considered from microwave to optical range. Emphasis is laid on the dependence of surface or dc resistance on external parameters (temperature, bias current, modulation frequency, magnetic field, radiation power, and frequency), which is characteristic of every nonbolometric response mechanism considered by us. The most frequently used methods for monitoring the response of HTSC to electromagnetic radiation are described. © *1998 American Institute of Physics.* [S1063-777X(98)00105-4]

INTRODUCTION

A high superconducting transition temperature T_c (>77.3 K) together with a small coherence length ξ and a strong anisotropy are responsible for diverse and unusual electromagnetic properties of HTSC as compared to conventional superconductors. Among other things, the concept of vortex lattice and of the shape and dynamics of the vortices themselves have been revised significantly (see, for example, the review by Blatter *et al.*[1]) The transformation of magnetic vortices and the peculiarities of their mutual interaction associated with a strong anisotropy and fluctuational effects have led to various phase transitions and new states of the vortex lattice, e.g., lattice fusion, thermally induced depinning, collective flux creep, and $2D-3D$ transition. All these peculiarities call for a detailed and thorough analysis of the electromagnetic properties of HTSC which is interesting not only from a scientific, but also from a technical point of view.[2] For example, one of the most important and relatively simple applications of HTSC is the development of electromagnetic radiation (EMR) detectors. A negligibly small dispersion (for frequencies $\nu \ll 2\Delta/\hbar$, 2Δ being the band gap in the quasiparticle spectrum), steepness of the HTSC transition, and the use of a cheap coolant (liquid nitrogen) urged scientists to explore the possibility of creating HTSC bolometers working at liquid nitrogen temperature.[3,4] The main drawback of such devices is that a compromise has to be sought between sensitivity and high-speed response. Hence it is preferable to use nonbolometric detectors. In this connection, the study of nonequilibrium mechanisms for monitoring the response of HTSC to EMR assumes a special significance. By response we mean the variation of a certain characteristic of the material under the effect of an external agency (in the present work, we shall take for such a characteristic the resistance R of the sample exposed to EMR).

In the general form, the response mechanisms can be divided into two large groups covering bolometric (equilibrium) and nonbolometric (nonequilibrium) response. The bolometric mechanism is one of the most thoroughly investigated mechanisms[4] and hence we shall not consider it in the present work.

In recent publications devoted to the study of optical response[5–8] of microbridges made of epitaxial YBaCuO films, it is assumed that nonbolometric mechanisms are realized not only in granular samples, but also in high-quality HTSC. However, the controversy in the observed values of sensitivity and response time for the same nonthermal mechanisms has not been resolved so far. Most probably, it is linked not with the intrinsic properties of HTSC, but with various external conditions (temperature, bias current, magnetic field, radiation power, wavelength, pulse duration, etc.) under which these characteristics are obtained.[9] In this connection, it is necessary to study nonbolometric mechanisms in samples of the same quality under identical external conditions, and to investigate the conditions for optimizing the characteristics of detectors.

In this communication, we present a review of the most typical results on the investigation of nonequilibrium mechanisms of the response of HTSC to EMR, and systematize the existing mechanisms from the point of view of the most general physical effects characterizing superconductors. We shall not consider in this review the results of investigations in the fields of Raman scattering, generation of harmonics of the fundamental signal, photoluminescence, etc.

The review consists of the following parts. Typical methods for monitoring the response to EMR from the microwave (MW) to optical range are described in Sec. 1. Section 2 is devoted to a review of experimental works on the nonbolometric response mechanisms in HTSC, and to their classification into subgroups. The main results obtained in this field are summarized at the end of the review.

1. METHODS OF RESPONSE MONITORING

In response monitoring, it is important to take into consideration the frequency of the incident radiation and the technique used for monitoring. The former determines the processes induced by the incident radiation, and the latter

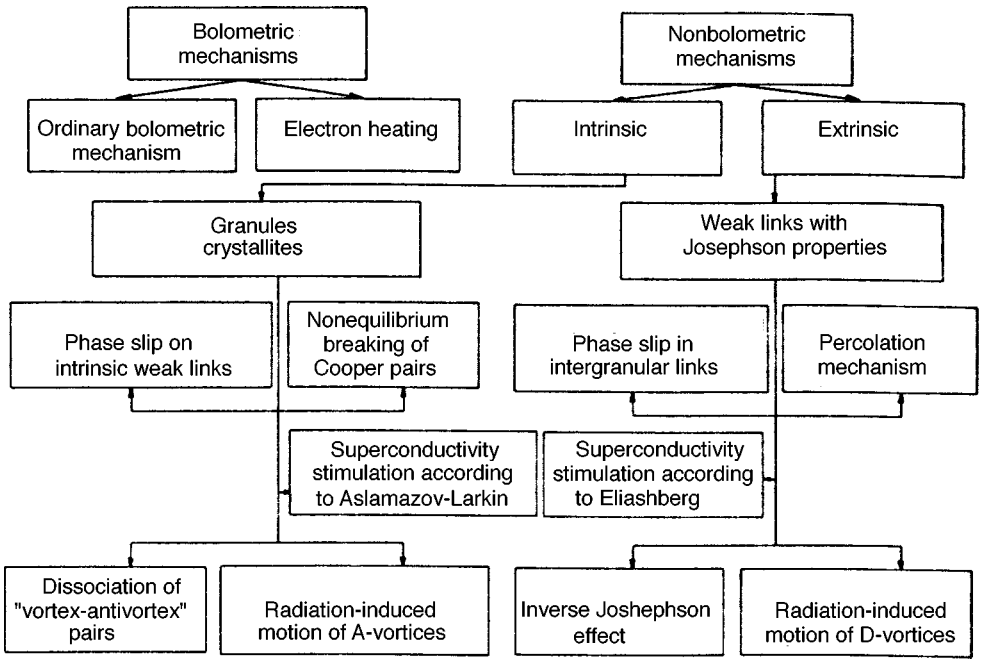

FIG. 1. Mechanisms of electromagnetic radiation monitoring by superconductors.

indicates the processes that may be discovered. The response is conventionally measured in direct current. In spite of the high sensitivity associated with the steepness of the superconducting transition in dc measurements, this method has a number of significant drawbacks. In the first place, special restrictions are imposed on the sample geometry: the thickness of the HTSC film must be smaller than or of the order of the radiation penetration depth δ. Otherwise, a part of the sample in which the radiation does not penetrate will shunt the layer whose properties have changed under exposure, and no response will be detected. Moreover, since the dc resistance of the sample in the superconducting state is equal to zero, the HTSC sample has to be processed with a view toward creating an element with nonzero resistance. In turn, this restricts the range of mechanisms available for monitoring the response. Besides, significant constraints on the noise characteristics of HTSC detectors are imposed by contact resistances of the order of 1 Ω, which are inescapable in such a detection technique.[10] These drawbacks are eliminated in the rf-technique for monitoring the response, although the sensitivity may decrease in this case due to a less steep superconducting transition and a smaller drop in the rf resistance as compared with the dc resistance. The rf-technique used by us for the first time[11] to monitor the response is based on the inductive technique[12] at radiofrequencies (rf) as well as the resonant technique[13] for measuring the MW response. Obviously, the problems associated with fluctuational noise and the degradation of the HTSC element due to contact phenomena are eliminated during rf monitoring of the response. Moreover, the constraints on sample thickness are less stringent in this case, since the only requirement is the overlapping of the incident radiation and the probing radiation penetration regions. Finally, the rf-technique for monitoring the response allows the detection of nonequilibrium processes even in the superconducting transition region, while a large value of the contact resistance and strong nonlinear effects associated with a constant measuring current lead to thermal instability and an ''avalanche''-type crossover to the bolometric regime.

Another effective method of studying the optical response of HTSC is the pump-probe technique[14,15] based on the use of the same agency (usually, a laser) as the source of radiation incident on the sample, and for monitoring the response by measuring the reflectivity of the probing signal. In this case, the nonequilibrium processes can be monitored over a wide range of wavelengths (from 10 μm to ultraviolet). The measuring signal is usually much weaker and is delayed relative to the pumping signal. The resolving power of such a technique is determined by the minimum possible duration of the laser pulse. For an optimal construction of the sensitive element, the amplitude of the nonthermal component is higher than the amplitude of the bolometric component at $T>80$ K by an order of magnitude.[6]

2. CLASSIFICATION OF RESPONSE MECHANISMS

We are not aware of any classification for the mechanisms of HTSC response to EMR showing their mutual relation with the most typical physical phenomena in superconductors. Such a classification is essential for a proper understanding of the processes stimulated in HTSC by the incident radiation. We believe that, while speaking of nonequilibrium response mechanisms, we must indicate clearly whether a particular mechanism is a property of the given sample or a common feature of the entire class of HTSC. In this respect, all nonbolometric response mechanisms can be divided into two groups, viz., intrinsic and extrinsic (see block diagram in Fig. 1). The intrinsic properties of HTSC are determined by the quality of single crystals and granules (for granular samples). At present, it is assumed that weak links between granules act as a chain of series- and parallel-connected Josephson junctions (JJ) responding synchro-

nously to the incident radiation. Hence the extrinsic properties of HTSC are mainly determined by the properties of a solitary JJ. Apparently, the intrinsic properties of HTSC are mainly similar to the properties of low-temperature type II superconductors with some differences associated with the peculiarities of the HTSC structure. Each of the above-mentioned large categories contains several mechanisms that are common to both groups.

2.1. Radiation-induced creep and flow of magnetic flux

The idea of thermally induced creep was put forth by Anderson,[16] while Zel'dov *et al.*[17] and Frenkel *et al.*[18] were among the first to detect the motion of magnetic flux induced in HTSC by radiation. Zel'dov *et al.*[17] studied the response of microbridges made of epitaxial YBaCuO films on $LaGaO_3$ and $SrTiO_3$ substrates to optical radiation (He–Ne laser, wavelength $\Lambda = 633$ nm), and found that the peak on the temperature dependence of the response is displaced by several degrees towards lower temperatures relative to the dR/dT peak characterizing the bolometric response. They also noticed a significant suppression of the response ΔR with increasing bias current, which was not observed in the temperature dependence of dR/dT. Moreover, the quantity $\Delta R/(dR/dT)$ characterizing the heating of the film in a purely bolometric effect increases sharply and has a peak at a temperature slightly lower than the superconducting transition temperature T_c. Since the thermal properties of the substrate, film, or the interface between them should not vary significantly in this temperature range, the authors concluded that the response is of nonbolometric type. Considering a strong correlation between the behavior of transport properties upon irradiation and without radiation, Zel'dov *et al.*[17] interpreted their results as magnetic flux creep induced by optical radiation. A similar interpretation of the results on the measurement of optical response was given by Frenkel *et al.*[18] who reported the observation of photo-induced depinning of magnetic flux. According to Frenkel,[19] the necessary condition for the emergence of flux flow is that the radiation quantum energy $h\nu$ must exceed the activation energy U_0 of the vortex lattice. The author believes that the photon energy is transferred thermally to flux lines, although other mechanisms of energy transfer (for example, the Lorentz force exerted on a vortex by the induced current) cannot be ruled out.

Eideloth[20] observed the response of BiSrCaCuO ceramic bridges and a meander made of epitaxial YBaCuO film on MgO substrate to optical radiation of wavelength $\Lambda = 633$ nm and concluded that his results can also be explained by the model of the photo-induced flux flow (PIFF). Moreover, the results of measurement on the BiSrCaCuO samples are described correctly by the PIFF model as well as the model of JJ network in which phase slip centers (PSC) are formed under the action of light as a vortex moves through the junction. It was also observed[20] that since the value of U_0 in the PIFF model and the energy barrier $2E_c$ in the JJ network model are close, these two mechanisms can be distinguished only by measuring the temperature dependence of the activation energy.

The contribution to the dc resistivity made by thermally activated flux creep in the case of a linear current–voltage characteristic (IVC) of the sample is described by the expression (see, for example, Ref. 21)

$$\rho = \frac{2\nu_0 \Phi_0^2 L_c}{k_B T} \exp(-U_0/k_B T), \tag{1}$$

where ν_0 is the attempt frequency, i.e., characteristic frequency of attempts by vortices to break away from the pinning center ($\sim 10^{12}$ Hz for YBaCuO single crystals), Φ_0 is the magnetic flux quantum, L_c is the coherence length along a flux line or a vortex bundle (which may vary from fractions of d for very thin samples to d for thick samples, d being the film thickness), and the energy $U_0 \sim 2 \cdot 10^5$ K for YBaCuO single crystals at $T \ll T_c$.[21] As a result, we obtain for the pre-exponential factor in formula (1) $\rho_0 = 10^5\ \mu\Omega \cdot$cm. Note that formula (1) is in good agreement with the experiment for $\rho < 10^{-2}\rho_n$, where ρ_n is the resistivity in the normal state. For $\rho > 10^{-2}\rho_n$, an excellent agreement is obtained with Tinkham's theory[22] in which it is assumed that resistance, which is associated with flux creep, depends on U_0 in the same way as in the case of dissipation due to thermally induced phase slip in a JJ suppressed strongly by the transport current. According to the Ambegaokar-Halperin theory,[23] the JJ resistance in a strongly suppressed state has the form

$$\rho/\rho_n = [I_0(\gamma_0/2)]^{-2}, \tag{2}$$

where I_0 is the modified Bessel function, and $\gamma_0 = U_0/k_B T$. The following dependence on temperature and magnetic field H is proposed for U_0:

$$U_0 \propto \frac{(1 - T/T_c)^{3/2}}{H}. \tag{3}$$

Palstra *et al.*[21] reported that the dependence (3) is valid only over a limited temperature range, and a different temperature- and magnetic field dependence for U_0 obtained, for example, in the vortex glass model[24,25] or the thermally activated flow model,[26] cannot be ruled out.

If the Lorentz force F_L exerted on vortices by the transport current flowing through the sample is such that they acquire an energy $U_L = U_0$, depinning of vortices and a transition to the flux flow regime take place.[27] According to the Bardeen–Stefan theory,[27] the flux flow resistance is described by the expression

$$\rho_{ff} = \rho_n H/H_{c2}, \tag{4}$$

where H_{c2} is the upper critical field.

As regards the rf response associated with the flux flow, it was shown by Ji *et al.*[28] that at temperatures not very close to T_c and for $h\nu \ll 2\Delta$, the specific impedance taking into account the contribution from flux flow can be presented in the form

$$\rho = \frac{\Phi_0 B_{\text{eff}}}{\eta c^2} + \frac{4\pi\omega\lambda_L^2}{c^2}, \tag{5}$$

where η is the viscosity, $\omega = 2\pi\nu$ the angular frequency, λ_L the field penetration depth, and B_{eff} the effective magnetic

flux density responding to the rf field. According to Portis *et al.*,[29] the surface resistance taking vortex dissipation into account can be represented in the form

$$R_s = X_0 \left[\frac{-1+(1+4B_{\rm eff}^2/B_0^2)^{1/2}}{2} \right]^{1/2}, \qquad (6)$$

where $X_0 = 4\pi\omega\lambda_L^2/c^2$ is the surface reactance for $B_{\rm eff}=0$, and $B_0 = 8\pi\omega\eta\lambda_L^2/\Phi_0$ is the characteristic value of $B_{\rm eff}$ for which the surface impedance Z_s is defined by the vortex movement. It was assumed by Portis *et al.*[29] that $B_{\rm eff}=fH$, where f is the density of free or weakly pinned fluxons ($f \sim 0.1$). However, Ji *et al.*[28] interpreted f as a part of the length of all vortices intersecting the intergranular region in the sample. They assume that there exist intergranular vortices having a number density n_J which do not pass through granules, and intragranular vortices having a number density n_g which are pinned inside granules. Besides, the main contribution to dissipation comes only from vortices intersecting weak links since the viscosity η_J of intergranular region is much higher than that of intragranular regions η_g due to a higher resistance of the intergranular regions. According to Ji *et al.*,[28] $B_{\rm eff}=(n_J+xn_g)\Phi_0$, where x is the ratio of the intergranular volume to the total volume of the sample.

The method of contactless monitoring of the HTSC response to millimeter (mm) waves was developed by our group in the beginning of 1990's (see Refs. 11 and 30). The technique is based on monitoring using rf bias whose advantages over conventional four-probe technique were known long before the discovery of HTSC.[31] Medvedev *et al.*[31] showed that the use of rf bias increases the sensitivity of detectors and improves their noise characteristics. This method makes it possible to monitor the response simultaneously in two frequency ranges, viz., rf ($\sim$10 MHz) by including a superimposed inductance coil in the resonance circuit of the quality-factor meter, and the mm range ($\sim$36 GHz) by using a quasioptical dielectric resonator which is also used for supplying a powerful mm-range signal. Details of the experimental technique are described in Refs. 30 and 32.

Investigations of the rf response of ceramic and thin-film samples of YBaCuO to mm radiation show[30,32,33] that, in the superconducting transition region, the response is complex and contains bolometric and nonbolometric components. It was found that the peak of the overall response is displaced relative to the peak of the temperature derivative dR_s/dT of the surface resistance, which describes the purely bolometric effect, by 0.4–0.7 K, depending on the quality of the sample. The displacement of peaks on the temperature scale was reduced by improving the electromagnetic characteristics of the samples (by decreasing R_s and reducing the transition width ΔT). Measurements of the relaxation response after switching off the mm wave pumping radiation[32,33] show a good agreement with various theoretical models describing the relaxation of magnetization of superconductors in the magnetic flux creep regime. The activation energy $U_0 = 0.05-0.5$ eV obtained from our measurements in the temperature range 77–86 K are in reasonable agreement with the experimental results presented in Refs. 28 and 34. Finally the

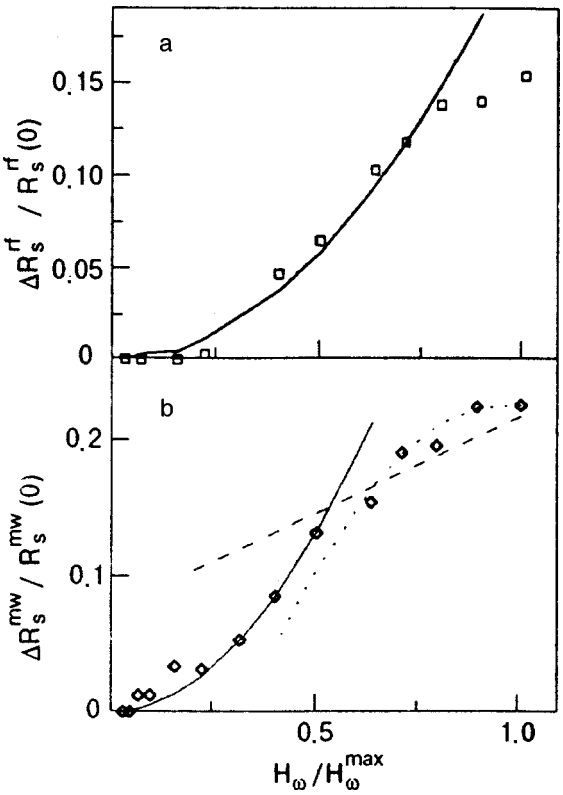

FIG. 2. Magnetic-field dependences of normalized responses of a YBaCuO thin film TF1 at $T=86.7$ K: radiofrequency response $\Delta R_s^{\rm rf}/R_s^{\rm rf}(0)$ (a) and microwave response $\Delta R_s^{\rm mw}/R_s^{\rm mw}(0)$ (b). Solid curves describe the approximation according to the Halbritter theory[35] (from Velichko *et al.*[32]).

amplitude dependences of the response of YBaCuO samples of various qualities are also described quite well by theoretical models taking into account the formation and movement of magnetic vortices under the action of a strong rf radiation.[35–37] Figures 2 and 3 show the amplitude dependences of rf and MW response of two thin films of YBaCuO deposited on a $LaAlO_3$ substrate and a YBaCuO ceramic plate, as well as the theoretical dependences obtained by using the models proposed by Halbritter,[35] Sridhar[36] and Gurevich,[37] which are in good agreement with the experimental results. Thus, it can be assumed on the basis of the results of measurements that the rf response of YBaCuO superconductors contains a nonbolometric component in the superconducting transition region. In all probability, the nonequilibrium response mechanism is associated with the creation and movement of Josephson vortices or similar magnetic vortices in inter- and intragranular weak couplings under the effect of millimeter radiation.

Salient features and conditions for realization of the mechanism

(1) The contribution to the dc resistance from the vortex movement is described by formulas (1) (in the case of creep), (4) (for flux flow), and (5) for rf R_s.
(2) The flux creep regime is characterized by an exponential temperature dependence of the resistance (see formula (1)).
(3) The flux creep regime is characterized by a linear IVC for bias currents I satisfying the condition $IHV_c r_p$

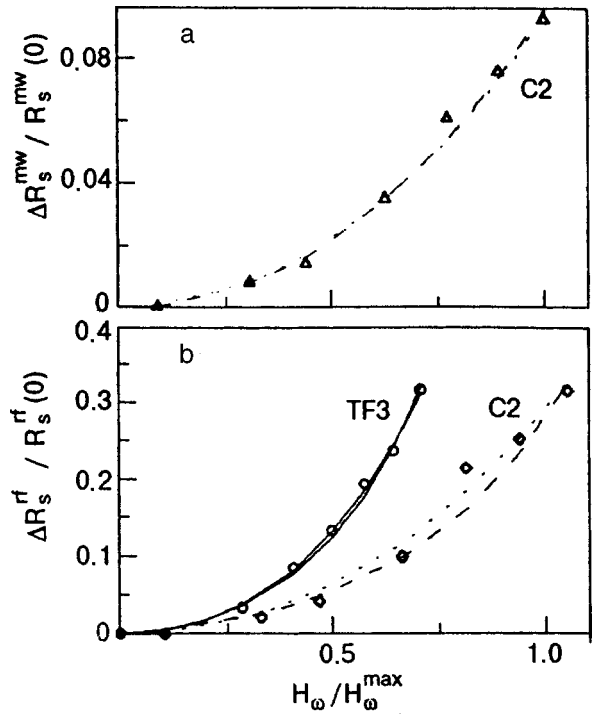

FIG. 3. Magnetic field dependence of the normalized microwave response $\Delta R_s^{mw}/R_s^{mw}(0)$ for a YBaCuO ceramic plate C2 (*a*) and radiofrequency response $\Delta R_s^{rf}/R_s^{rf}(0)$ for C2 ceramics and thin film TF3 (*b*) for 86.1 K $<T<$90.5 K. Solid and dotted curves correspond to the approximation according to Gurevich[34] and Sridhar[36] (from Velichko *et al.*[30]).

$\leqslant k_BT$ (V_c is the correlation volume and r_p is the pinning potential range), and by an exponential $V(I)$ dependence for large currents.

(4) The magnetic field dependence of resistance is described by formula (2) and is determined by the magnetic field dependence (3) of the activation energy.
(5) The response amplitude ΔR is proportional to $f_{\rm mod}^{1/2}$, where $f_{\rm mod}$ is the modulation frequency of the radiation.
(6) The flux flow regime is characterized by a linear magnetic field dependence (see formula (4)) and a linear IVC ($V \approx I$).

2.2. Phase slip

A special resistive state is formed in long and narrow superconducting channels [transverse size of the channel $d_c < \xi(T)$], as well as in narrow and even wide thin films for $I > I_c$ both for $I_c = I_c^{\rm GL}$ ($I_c^{\rm GL}$ is the Ginzburg–Landau depairing current) and in an external magnetic field higher than a certain value H_e' ($H_e' = \pi\Phi_0/4w^2$ is the field corresponding to penetration of metastable vortices into a film, and w is the film width). This state cannot be explained just in terms of a dynamic mixed state (DMS)[38] since for high voltages emerging under these conditions, the vortex velocity $v = V/LB$, where L is the sample length and B the magnetic induction, must be of the order of the Fermi velocity, which is evidently not feasible from a physical point of view. High condensate velocities v_s lead to depairing and the number density n_s of pairs begins to depend on v_s. The dependence of the superconducting current density $J_s(v_s)$ passes through a peak corresponding to $J_c^{\rm GL}$. For $J > J_c^{\rm GL}$, the number of superconducting electrons is not sufficient for the passage of transport current, and in contrast to the static case, the total current now contains the normal component J_n as well. The superconducting state continues to be thermodynamically more advantageous since $n_s(v_m) = (2/3)n_s(0)$ at the peak.

Webb and Warburton (see Ref. 19 in the paper by Dmitrenko[38]) detected in 1968 a regular structure of voltage steps on the IVC of tin whiskers and came to the conclusion that individual resistive centers are formed upon an increase in current. The sample resistance (slope of the IVC) increases after the emergence of each step. Later, Tinkham proposed a model of the resistive center called the phase slip center (PSC). He observed the main features of PSC, viz., the magnitude and constancy of differential resistance, as well as oscillations of J_s with Josephson frequency. The formation of the first PSC takes place in a narrow superconducting channel when the current becomes equal to the depairing current at the weakest spot in the sample. A further increase in current results in the motion of normal electrons, which leads to the emergence of an electric field accelerating the superconducting electrons to critical velocity. In this region, the order parameter ψ vanishes and the entire current is transported only by the normal component. However, the formation of Cooper pairs is advantageous as before, hence ψ emerges once again and a part of the current is transported by the condensate. For each such cycle, the phase difference for wave functions of Cooper pairs from opposite sides of the ''weak'' region will vary by 2π. Hence this site is called a phase slip center. Its characteristic size is determined by the distance over which ψ pulsates, and amounts to $\sim 2\lambda_E(T)$, where λ_E is the length of the voltage drop region.

For $|\psi| = 0$, this region lies in the normal state, and the electric field penetrates the adjacent superconducting regions to a depth $\sim\lambda_E$. Hence the formation of one PSC leads to the emergence of a resistance $2\rho\lambda_E/S$, where ρ is the resistivity of the material of the filament and S its cross-sectional area. The voltage drop across this resistance is associated only with the normal component $I_n = I - I_s$. Averaging of voltage across one PSC over time (taking into consideration the fact that the total current is constant and independent of time, while the supercurrent I_s pulsates between I_c and 0) gives

$$\overline{V} = 2\lambda_E\rho(I - \beta I_c)/S, \tag{7}$$

where $\beta \sim 0.5$. This simple formula correctly describes the experimental IVC. A further increase in current leads to the formation of new PSC's since new resistive regions come into play each time.[39]

Dmitrenko *et al.* (see Refs. 18 and 55 in their paper[38]) were the first to observe oscillations of the first derivatives of IVC of wide films in the vicinity of T_c, which were interpreted as analogs of PSC. For an applied magnetic field $H_\perp = 0$, the critical current I_c is close to the depairing current and decreases linearly with H as it increases to a certain value H' after which it oscillates with a period ΔH, while the oscillation amplitude increases with decreasing temperature. The period of these oscillations is associated with the

periodic modulation of the screening current of the potential edge barrier which hinders the vortex movement. Such a step structure of IVC of wide films was interpreted as the emergence of phase slip lines (PSL) (see Refs. 57 and 58 in the paper[38]). It was found that the IVC of a vortex-free state of a film of width $w \geqslant \lambda_\perp$ ($\lambda_\perp = 2\lambda^2/d$ is the effective field penetration depth in a film of thickness d) for $H < H'$ is similar to the IVC of a narrow superconducting channel with PSC, as in the case $H_\perp = 0$. However, the emergence and movement of vortices in a film for $H > H'$ does not change qualitatively the character of steps on the IVC. The voltage jump is preceded by a nonlinear region corresponding to DMS. Vortex movement is also a phase slip, since the passage of a single vortex through the film corresponds to a variation of the phase difference at the film edges by 2π. However, the mechanisms of PSC and PSL in wide films are quite different from the vortex mechanism.[38] It turns out that the stringent condition of a ''narrow'' ($d, w \ll \lambda_\perp$) superconducting channel is not necessary for the formation of a PSC. Moreover, the step structure of IVC of wide films is observed in zero magnetic fields also.

One of the first observations of radiation-induced phase slip in HTSC was reported by Leung *et al.*[10] who studied the optical response of granular YBaCuO films on sapphire substrates. Between T_c (temperature corresponding to zero resistance) and T_{c0} (temperature corresponding to the onset of superconducting transition), most intergranular links become nonsuperconducting, and the dc conductivity is associated with individual isolated channels in which the Josephson coupling is still strong. The size and number of such channels decreases with increasing temperature, and the response amplitude becomes smaller.[10] Obviously, the peak of the response emerges at a temperature at which most of the JJ with almost identical critical parameters (critical current, etc.) change upon exposure to radiation. The dependence of the phase slip resistance on activation energy for strongly suppressed JJ was obtained theoretically by Ambegaokar and Halperin [formula (2) in Ref. 23], and can be presented in the following form if we take into account the temperature and magnetic field dependence of U_0 from the theory developed by Yeshurun and Malozemoff (formula (3) in Ref. 24):

$$\rho_{ps}(H,T) = \rho_n \left[I_0 \left(\frac{A_T (1 - T/T_c)^{3/2}}{2H} \right) \right]^2 \tag{8}$$

where A_T is a coefficient. According to Blackstead *et al.*,[40] the passage of transport current with energy exceeding U_0 for $H > H_{c1}$ (H_{c1} is the lower critical field) causes a flux flow whose resistance is defined by formula (4). However, $\rho_{ff} = \rho_n$ in the vicinity of T_c, and hence the resistance in this region will be double the normal state resistance, which is apparently not possible physically. This can be avoided by making the substitution $\rho_n \to \rho_n - \rho(H,T)$. This gives

$$\rho_{ff} = [\rho_n - \rho(H,T)] \frac{H}{H_{c2}}. \tag{9}$$

Here, $\rho(H,T) \equiv \rho_{ps}(H,T)$ from formula (8). Taking into consideration the angle φ between the current and the magnetic field in the (**ab**) plane, we obtain[40]

$$\rho_{ff} = [\rho_n - \rho(H,T)] \frac{H}{H_{c2}} \sin^2(\varphi). \tag{10}$$

Thus, two competing mechanisms exist for $H > H_{c1}$, viz., the flux flow and the phase slip. The phase slip process is independent of the relative orientation of the current and magnetic field, and accounts for the non-Lorentzian dissipation observed in a number of works (see, for example, Ref. 41). It should be remarked that a dependence of the type (8) is manifested clearly only in the case when $H \| I$. In all other cases, the dependence $\rho(H,T)$ is determined by the flux creep regime (see Eq. (1)).

Formula (8) was obtained by Tinkham[22] for describing the dependence of the superconducting transition width on the magnetic field. However, as $H \to 0$, formula (8) gives a nonphysical value of the resistance and zero transition width. This contradiction is removed by assuming the existence of an effective intrinsic field $H_0 \neq 0$ which ensures a finite height of the energy barrier U_0 even in a zero external field. The existence of such a field is explained physically by the Kosterlitz–Thouless theory[42] which assumes the existence of thermally induced ''vortex–antivortex'' pairs below T_c. It is found that the current-induced depairing of vortex pairs leads to nonohmic losses for $H = 0$.[43] Taking such a dependence into account, we can present formula (8) in the form[43]

$$\rho_{ps}(H,T) = \rho_n \left\{ I_0 \left(\frac{A_T (1 - T/T_c)^{3/2}}{2(H + H_0)} \right) \left(1 - \frac{I}{I_{c0}} \right)^{3/2} \right\}^{-2}. \tag{11}$$

Typical values of H_0 for high-quality YBaCuO samples are $\sim 0.1 - 0.25$ T, while $H_0 \sim 0.05$ T for BiSrCaCuO.[43] For high-quality YBaCuO single crystals (see Ref. 41), the experimental data for $H = 0$ are approximated quite well for $A_T = 10.044 k_B T$. It is found that the narrower the superconducting transition, the higher the value of A_T. Moreover, the resistance calculated by using formula (11) is quite sensitive to the choice of T_{c0}, and hence a variation of T_{c0} even by 0.05 K strongly affects the value of ρ:

$$\rho = \rho_{ff} + \rho_{ps}. \tag{12}$$

It is also assumed that T_{c0} does not change in an applied magnetic field.

According to Blackstead,[43] the disordered distribution of oxygen in Cu–O planes leads to discontinuities, and a network of JJ parallel to the **c**-axis is formed between overlapping regions of adjacent planes and creates conducting channels between planes. The critical current of the entire channel is determined by the weakest junction. Thermal fluctuations lead to a relative displacement of fragments of the Cu–O planes, and perturbation of vortices pinned at these fragments leads to a time-dependent local phase difference. This results in a field dependence of resistance that is not associated with the Lorentz force.

Thus, in view of the leading role of thermal fluctuations near T_c, the dominating loss mechanism is the phase slip associated with the nanogranular nature of HTSC, i.e., with the thermal-phonon-modulated bonds between planes. According to Blackstead,[43] the resistance to flux flow dominates

at lower temperatures and hence determines the losses in granules (for YBaCuO, this temperature range corresponds to $T \leqslant 85$ K).[40]

Formula (12), in which ρ_{ff} and ρ_{ps} are defined by formulas (10) and (11) respectively, corresponds to the dc resistance. In order to determine the MW response, it is essential to know the behavior of R_s. According to Blackstead,[40] we obtain by taking residual resistance $\rho_{00} \sim 2.5 \cdot 10^{-4} \rho_n$ into consideration:

$$R_s = [(\rho_{ff} + \rho_{ps} + \rho_{00})(\omega\mu/2)]^{1/2}, \tag{13}$$

where μ is the permeability.

Dmitriev *et al.*[44] studied the effect of MW field on the behavior of PSC and observed a suppression (even disappearance) of the critical current of samples by MW radiation. They also found that in the bridges made of YBaCuO ceramics (MW radiation leads to the emergence of discrete formations that are multiples of current PSC and are called ''rf PSC'').[44] Among other things, this is confirmed by the root dependence of the response on radiation power which is characteristic of the PSC formation mechanism. It is interesting to study the dynamics of rf and current PSC observed by Dmitriev *et al.*[44] The rf PSC vanishes in a direct current, and is replaced by a current PSC. This is accompanied by a transition of the sample to the ''unperturbed'' resistive state (with zero radiation power $P_\omega = 0$).

Salient features and conditions for realization of the mechanism

(1) The IVC of superconducting channels in which PSC are formed is described by Eq. (7).
(2) The dependence of phase slip resistance on temperature, magnetic field and bias current is described by formula (11). This mechanism is especially clearly manifested for parallel orientation of current and magnetic field along the **c**-axis since there is no contribution from the flux flow in this case. In view of the thermal activation nature of the process, it is manifested quite strongly in the vicinity of T_c.
(3) The phase slip resistance is independent of the angle between the current and the magnetic field.
(4) The response amplitude increases in proportion to the square root of the radiation power.

2.3. Breaking of ''vortex–antivotex'' pairs

A large number of publications (see, for example, Ref. 45) report on the nonbolometric detection of infrared (IR) radiation in thin HTSC films. This regime is characterized by an anomalously large responsivity R_v approaching the quantum limit $R_v = 1/(2e\nu)$. In order to explain this effect, Kadin *et al.*[46] proposed a model for photon-induced dissociation of vortex pairs existing in two-dimensional superconductors. The theory of vortices in two-dimensional superconductors[42] assumes the presence of ''vortex–antivortex'' (V-AV) pairs below T_c which effectively screen vortex interaction at high temperatures and lead to the formation of free vortices. Under the action of transport current, these vortices move and lead to energy dissipation. As the temperature is lowered, most of the vortex pairs ''freeze out'' and a second phase

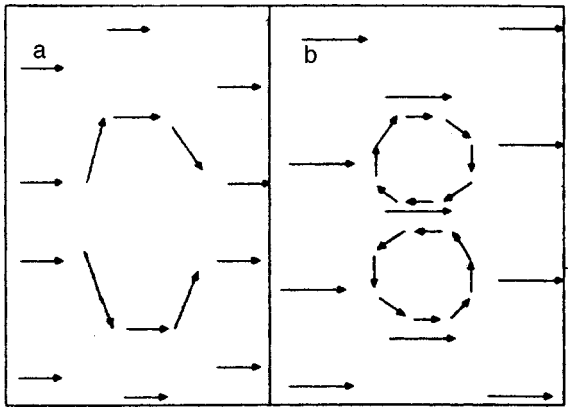

FIG. 4. The pattern of current flow near a ''vortex–antivortex'' pair generated for a large transport current: total current (*a*) and the same configuration with separated vortex currents (*b*) (from Kadin *et al.*[46]).

transition, called Kosterlitz–Thouless transition, occurs at a temperature T_{KT} and is accompanied by a pairing of all free vortices. Below T_{KT}, all vortices are paired, and there is no dissipation associated with their movement.[46] The formation of vortex pairs takes place through the emergence of a vortex ''core'' on the scale of the coherence length ξ with a local suppression of the order parameter ($\Delta = 0$). This may be caused by thermal fluctuations or by the photons of the incident radiation.[47] If vortices are separated in space, i.e., do not overlap, the currents circulating around the core become significant and the vortices are stable. The energy of such a pair, separated by a distance $r \gg \xi$, can be represented in the form[47]

$$E_v = E_{v0} \ln(r/\xi) = \Phi_0^2 d/2\pi\lambda_L^2 \ln(r/\xi). \tag{14}$$

For two closely-spaced vortices, the minimum energy E_{v0} of the vortex pair is of the order of energy of condensation in two vortex cores. As a rule, this energy is much higher than Δ. The above equation also gives the energy of attraction between vortices which is overcome by the Lorentz force emerging as a result of the passage of a current with density $J = E_{v0}/\Phi_0 r d$. For $r = \xi$, the current density J approaches the critical value J_c, thus indicating that a vortex pair may be formed by current alone. Such a model is a two-dimensional generalization of the model of PSC formation in a superconducting microstrip.[48] Figure 4 shows the current configuration in the vicinity of a vortex-pair being formed. For $T < T_{\mathrm{KT}} = E_{v0}/4k_B$, the breaking of the vortex pair may be caused by the current, resulting in a nonlinear IVC of the type $V \approx I^n$. Depending on temperature, three regimes with different IVC can be singled out:

$$V(I) = \begin{cases} \sim (I - I_c)^n, \quad n > 3 & \text{for } T \ll T_{KT}, \quad I > I_c, \\ \sim I^3 & \text{for } T = T_{KT}, \\ \sim I \text{ for } T > T_{KT} & \text{for small } I. \end{cases} \tag{15}$$

Such a form of IVC is caused by thermal activation processes leading to a nonlinear resistance of the form

$$R(J) \sim \exp\left(-\frac{E_v(J)}{2k_B T}\right) \simeq (J/J_c)^{E_{v0}/2k_B T}. \tag{16}$$

This equation is valid for $J \leqslant J_c$. For very small bias currents, the resistance is defined by the expression

$$R/R_{\max} = a \exp[-2(b/\tau)^{1/2}], \quad (17)$$

where $\tau = (T - T_{\mathrm{KT}})/(T_{c0} - T)$, a and b are constants, and $R_{\max}$ is the resistance at temperatures above T_{c0}.

Kadin *et al.*[46] propose the following microscopic mechanism of formation of V-AV pairs as a result of photon absorption. A photon with energy $h\nu \gg 2\Delta$ is absorbed in a certain region (spot) at the surface of a $2D$ film, giving rise to a pair of highly excited quasiparticles which break additional Cooper pairs over a time period of the order of a few microseconds and distribute the excess energy among a large number of quasiparticles. These quasiparticles diffuse into the film over a depth $\sim\xi$ over a time $\sim h/k_B T_{KT}$ and suppress the order parameter Δ in this layer, as well as the critical current I_c. If the value of I_c in the region of the spot is smaller than the transport current I, this will lead to instability and a local collapse of Δ, causing the screening current to bend around this ''hot spot.'' This process is analogous to phase slip induced by the phonon absorption, which provides the additional energy required by the current for the formation of a vortex pair (see Fig. 4). As a result of further diffusion of nonequilibrium quasiparticles into the film, the hot spot vanishes. However, the vortices continue to move at right angles to the current until they reach the edge of the film, leading to the emergence of a magnetic flux Φ_0 through the film which is equivalent to an integral voltage pulse. The time-averaged responsivity is given by $R_v = 1/(2e\nu)$.

The model described above, which was proposed for a homogeneous (on the scale $\sim\xi$) two-dimensional superconductor, can also be used for describing a $2D$ chain of weakly coupled JJ. It should be recalled that the effective field penetration depth λ_{eff} corresponding to weak intergranular currents may be quite large. Intergranular vortices with a reduced nucleation energy, and hence with a reduced pair dissociation energy, may emerge in such films. This explains the observed transition to vortex depairing in ordered chains of junctions as well as in granular superconductors. As soon as a vortex pair is formed, it behaves essentially in the same way as in a homogeneous film. For a granular superconductor with granule size $\leqslant\xi$, a photon absorbed in one of the granules suppresses Δ over the entire film, and reduces the critical currents linking it with the adjoining granules. This causes a local deviation of the current (Fig. 4a) followed by the formation of a vortex pair (Fig. 4b). In superconductors with a large size of the granules, however, a photon absorbed at the center of a granule hardly affects the intergranular currents. If the coupling between granules is not quite uniform, the vortex pairs formed in such granules cannot be dissociated by the current passing through them. In both these cases, the quantum efficiency of the process will be considerably reduced, which explains the large spread in the experimentally observed values of responsivity for granular thin-film HTSC detectors.

In spite of the fact that the formation of vortex pairs in this model occurs due to local heating, it was observed[49] that this is a nonequilibrium process and hence does not suffer from the drawbacks of bolometric detection. In this case, the total heating of the film is quite insignificant while the local heating may be quite strong. Kadin *et al.*[49] proposed two possible regimes of formation of vortex pairs. For $h\nu < \Delta$, the absorption of a quantum is linked directly with the formation of a vortex pair. Such a pair is formed in two cases: (1) if the energy of the quantum at a given temperature is higher than the nucleation energy E_{v0}, and (2) if the total current $I_\Sigma = I + I_\omega$ (I is the bias current and I_ω the ac amplitude) exceeds the critical current I_c over a time long enough for the formation of a vortex. For $h\nu > \Delta$, Cooper pairs are dissociated at first. This is followed by the formation of a vortex pair as a result of local heating.

The response time in this model is determined by the fluxon velocity $v = J\Phi_0/\eta = J\rho_n 2\pi\xi^2/\Phi_0$ in a direction perpendicular to the applied current, where η is the viscosity of vortices in the Bardeen–Stefan theory, and ρ_n is the resistivity in the normal state. For $J \sim J_c$, since $J_c\rho_n \simeq \Delta/e\xi$, we obtain the velocity $v \simeq \Delta\xi/h$ which approaches the Fermi velocity $v_F = 10^7 - 10^8$ cm/s for a pure superconductor. For a film of width $w = 10\ \mu$m and $v_F = 10^7$ cm/s, we obtain the response time $t_R = 100$ ps. For sensitivity optimization, the working temperature must be lower than T_{KT} since the sensitivity at higher temperatures will be limited by the background voltage associated with thermally activated unpaired vortices and the magnetic field induced by the current.[49] The most suitable material for a detector is a film with uniformly linked small granules, for which the injection of vortices from the film edges is restricted. The absorption of a photon in HTSC leads to the formation of a vortex ring (three-dimensional analog of a $2D$ vortex pair) which is enlarged by the transport current and splits into a V–AV pair upon reaching the (lower and upper) film surface, leading to the same responsivity $R_v = \Phi_0/h\nu$. In the one-dimensional case of a long wire with cross-sectional size $\sim\xi$, the absorption of a photon leads to the formation of a PSC which produces voltage steps.[46] For the one-dimensional case, the photon absorption may be accompanied by the formation of more than one PSC, which leads to an enhanced sensitivity below the quantum limit. In all other cases, the sensitivity of a film displaced in the vicinity of J_c is confined by the quantum limit since the violation of superconductivity due to the absorption of a photon is always connected with some kind of phase slip or a vortex process for which the magnetic flux quantum is a characteristic quantity.

Johnson *et al.*[50] studied the response of 10 nm-thick granular NbN films (with a grain size of the order of the film thickness) on Si substrates to optical radiation of wavelength $\Lambda = 632$ and 670 nm with a modulation frequency < 3.7 kHz and > 100 kHz, respectively. Meander-shaped structures with a constant surface area of 10^{-4} cm^2 ($5 \times 200\mu$m, $10 \times 100\mu$m, etc.) were prepared from these films. Below T_c, the authors[50] observed a slow bolometric response associated with film heating together with the substrate. It was found that radiation with wavelength $\leqslant 1\ \mu$m is absorbed strongly by Si and produces charge carriers in it. If the NbN film is displaced towards higher differential resistance, the conducting Si substrate partially shunts the response of the superconductor. In this case, the response becomes negative, i.e., the response amplitude decreases with increasing radiation

power. While the total response to continuous irradiation is positive, an increase in the modulation frequency transforms a slow positive signal into a fast negative signal. For high modulation frequencies, the slow bolometric response cannot ''catch up'' with the negative shunting component, and the net response is negative. In the absence of a bias current, when the laser beam is centered in the meander region, a rapid response which does not depend on the modulation frequency f_{mod} was observed up to 100 kHz. The authors associate this response with the photoelectric effect at the interface between NbN and Si. The photoelectric effect was not observed during optimization of the rapid positive component through an appropriate choice of the position of the laser beam.

The authors studied the transient and steady-state response as a function of the bias current I_b and temperature for $I_b<I_c$ and $T<T_c$. It was found that the dependences of the response δV_{ac} on $(\delta V/\delta T)_I$ are considerably nonlinear, especially in a constant weak magnetic field (up to 100 Oe). The nonlinear part of the dependence was observed for I_b corresponding to the highest differential resistance, and hence the shunting effect of the substrate was very strong. Measurement of $(\delta V/\delta T)_{I_b}$ for small I_b were used by the authors to estimate the effective sample heating δT_{eff} $\sim$150 mK. The highest responsivity R_v was observed in currents close to I_b and was 125 V/W. Under the assumption that the positive response is associated only with the bolometric effect, the effective heating is theoretically estimated at 1–11 mK, which is much smaller than the experimental value. It is assumed that the observed response may be caused by two nonequilibrium mechanisms, i.e., either by electron heating effect, or by the kinetic inductivity mechanism. The former gives an extremely low value of δT_{eff} $\sim$1 mK, as well as an underestimated value of responsivity. The authors believe that the photofluxon model of vortex-pair formation may explain the observed response, although the value of responsivity $R_v \sim 10^4$ V/W predicted by this model is much higher than the experimental value of 125 V/W. To prevent the excitation of photocarriers in Si and to avoid shunting of the response by the substrate, the same authors used a longer wavelength radiation source, viz., a diode laser with $\Lambda = 1300$ nm, in their later work[9] for a clearer differentiation of the response mechanisms. In the absence of a bias current, the responsivity of the response at radiation wavelengths 670 and 1300 nm was $\sim$20 V/W. When the laser beam was centered on the meander, a positive response was observed. This response persisted as the frequency f_{mod} was increased to 1 MHz, and was attributed by the authors to the heating of the NbN film relative to the substrate. The response amplitude varied linearly with the radiation intensity, and the modulated response signal remained purely sinusoidal without any harmonics. The responsivity for rapid response was estimated at $\sim$1500 V/W. The maximum possible heating of the sample did not exceed 2 mK.

Measurements of the dependence of the response on bias current and IVC at various temperatures led to the resistance $R_{\mathrm{eff}}^{(T)}$ of the thermal boundary between the film and the substrate. It was found that $R_{\mathrm{eff}}^{(T)}$ depends strongly on I_b, while for a purely thermal effect it should not depend on current, but must have a significant temperature dependence. A comparison of the experimental results with the hot spot model[51] reveals a good agreement for the temperature dependence of $R_{\mathrm{eff}}^{(T)}$ near the transition, while the value of $R_{\mathrm{eff}}^{(T)}$ obtained from the model for a deep superconducting state is found to be too low. It is borne out by computations[9] that the thermal resistance $R_{e\mathrm{ph}}^{(T)}$ associated with a finite time $\tau_{e\mathrm{ph}}$ of energy transfer from electrons to phonons in the film makes a decisive contribution to the time characteristics of the response as compared with the Kapitza thermal resistance R_{K} due to a finite time of energy transfer from the phonons in the film to the phonons in the substrate.

Since the thermal conductivity estimates used in the model include the electron heating effect, and the quantity $(\partial V/\partial T)_{I_b}$ (which is also used in the model) takes into account the thermal effects associated with the weak links between granules, the authors do not believe that these effects can explain the observed response. The response amplitude estimated from the kinetic inductivity variation mechanism is also too low (0.04 μW obtained from theory against an experimental value 100 μW). However, the experimentally observed response time of about 1 ns is of the same order as the value estimated by using the photofluxon model. For an unambiguous conclusion concerning the applicability of the photofluxon model, we must carry out experiments with a subnanosecond resolution and measure the dependence of the response time on the film thickness, which must be linear.[9]

Salient features and conditions for realization of the mechanism

(1) The dependence of the resistance associated with the dissociation of the V–AV pairs on temperature and bias current I is obtained by using formulas (16) and (17).
(2) Formula (15) describes the IVC at different temperatures and for different bias currents.
(3) The limiting sensitivity of this mechanism is equal to $\Phi_0/h\nu$.
(4) The response time for $v_F = 10^7$ cm/s and a film width $w = 10$ μm is $\sim$100 ps.
(5) The sensitivity can be increased right up to the quantum limit by decreasing the working temperature to below T_{KT} and selecting a film made of uniformly linked small size granules.

2.4. Inverse AC Josephson effect

The emergence of a dc voltage across JJ formed by a low-temperature superconductor under the action of microwave radiation was observed for the first time by Langerberg *et al.*[52] This phenomenon known as the inverse ac Josephson effect served as an impetus in the study of possible applications of JJ as EMR detectors. The discovery of HTSC stimulated a number of publications[53–56] in which the observed nonbolometric response of HTSC was interpreted as a modulation of weak-link parameters (critical current, order parameter phase, etc.) by an induced rf current.

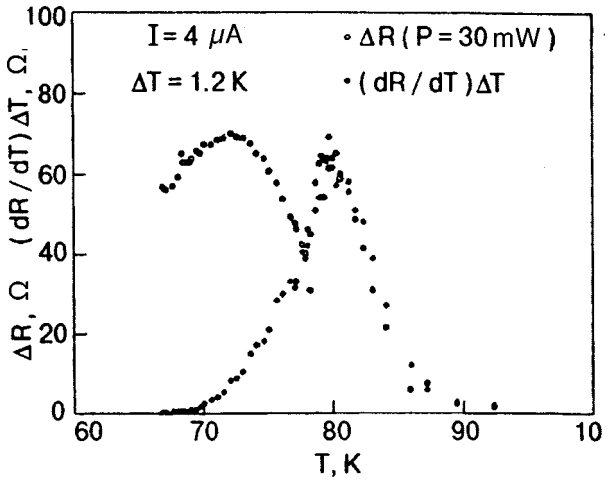

FIG. 5. Temperature dependences of the response ΔR and derivative dR/dT multiplied by the constant $\Delta T = 1.2$ K for a YBaCuO film (from Chang *et al.*[54]).

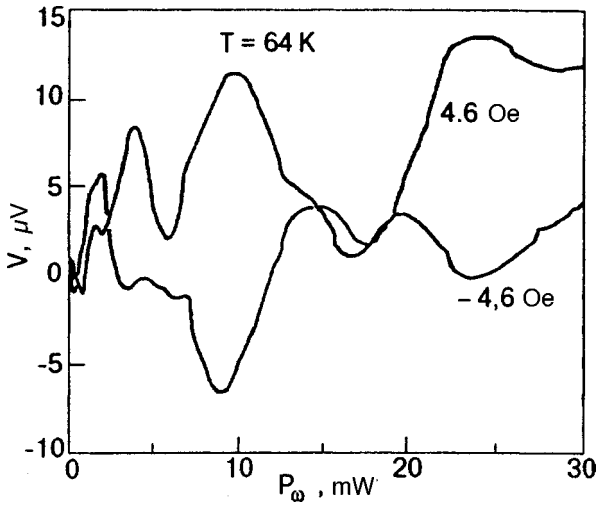

FIG. 6. Dependence of the voltage V induced by microwave radiation on the microwave power of a YBaCuO film in the absence of a constant bias for two different directions of the constant magnetic field at $T = 64$ K (from Chang *et al.*[54]).

Durny *et al.*[53] studied YBaCuO ceramic samples in the form of rectangular bars placed in the cavity of EPR spectrometer. The voltage induced in the sample by MW radiation (9.42 GHz) was measured as a function of temperature T, constant field H, and radiation power P_ω. It was found that the magnetic field suppresses the response for any field polarity. The amplitude ΔV of the response increased with decreasing T and increasing P_ω. The $\Delta V(P_\omega)$ dependence was linear in the P_ω range from 1 to 100 mW at low ($\sim$31 K) and high ($\sim$81 K) temperatures. In the intermediate temperature range (50–70 K), weak saturation of the $\Delta V(P_\omega)$ dependence was observed for $P_\omega \sim 20-30$ mW. Durny at al.[53] associate the response mechanism with the motion of Josephson vortices formed in weak links under the action of the Lorentz force exerted by the transport current.

Chang *et al.*[54] studied granular YBaCuO films in the form of an ''H''-structure. An ''H''-shaped film was placed in a rectangular waveguide so that the electric field $\mathbf{E}_\omega$ was parallel to the ''bridge,'' while the magnetic field $\mathbf{H}_\omega$ was perpendicular to the plane of the H-structure. Such an experimental geometry makes it possible to create an optimal coupling with $\mathbf{H}_\omega$ and prevents the interaction with the electric component, which permits to avoid ordinary rectification effects which are not associated with the physics of HTSC. A quasi-homogeneous chain of JJ is formed in the bridge of the H-structure, for which the dependence of ΔV on H (or H_ω) is strictly periodic in contrast to a randomly oriented $3D$ chain, since weak links respond to radiation synchronously. Chang *et al.*[54] discovered that the temperature dependence of the response $\Delta R = R(P_\omega) - R(0)$ exhibits two peaks (Fig. 5). The high-temperature peak is correctly described by the dependence

$$\Delta R = (dR/dT)\Delta T, \tag{18}$$

typical of the bolometric mechanism. The low-temperature peak of the response is in the tail of the resistive transition, where $dR/dT \to 0$ and is obviously not of thermal origin. The dependence on microwave power ($P_\omega^{\max} \sim 30$ mW) is linear in the region of the high-temperature peak, which confirms the bolometric nature of the response, while $\Delta R \propto \log(P_\omega)$ in the temperature range in which a nonbolometric response is observed. According to Chang *et al.*,[54] the time variation of the order parameter phase φ induced in a long JJ by MW radiation (even in zero magnetic field) leads to the formation of vortices which can move under the action of a direct transport current. The response amplitude ΔV in this case is proportional to the number of JJ that respond synchronously to radiation for a given I_b. It was found that the nonbolometric peak of the response increases and is displaced towards low temperatures upon an increase in the bias current as well as in the MW power. The response appears under the condition $I_b > I_c$. Chang *et al.*[54] state that the mechanism of induced motion of vortices proposed by them causes a response similar to that observed during dissociation of V–AV pairs in the course of a Kosterlitz–Thouless transition.[45] However, the IVC is linear ($V \approx I$) for this mechanism in the vicinity of T_c, while $V \approx I^3$ in the case of dissociation of vortex pairs. In addition, the oscillating dependence of ΔV on P_ω for $H = \text{const}$ (Fig. 6) and on H for $P_\omega = \text{const}$ unambiguously suggest the Josephson mechanism of the response, in which the vortices generated by a weak magnetic field move under the action of the current induced by MW radiation, leading to voltage oscillations.

Gallop *et al.*[55] observed the dependence of the differential resistance dV/dI of YBaCuO and BiSrCaCuO films on a MgO substrate on the bias voltage V_b under the effect of MW radiation ($\sim$10 mW) of frequency 8–20 GHz. The difference in the differential resistance in the presence of radiation and without it is of a periodic oscillating form with peaks at $V_b = n\Phi_0\nu$, where n is an integer and ν the radiation frequency. We assume that the fluxon lattice observed in YBaCuO at low temperatures moves under the action of the rf current, which induces the voltage $V = d\Phi/dT = mv(I_b\Phi_0)$ according to Faraday's law (m is the number of fluxons per unit area and $v(I_b)$ the velocity of fluxons, which strongly depends on the bias current I_b). The motion of flow

in this case is synchronized with the applied MW voltage within a limited range of V_b so that the velocity of fluxon motion through a superconducting microstrip is $dN/dt = n\nu$. In this case, the voltage drop across the film in this synchronized state is $V=\Phi_0(dN/dt)=n\Phi_0\nu$. This condition is similar to the condition for the formation of a Shapiro step in a solitary JJ.

Boone *et al.*[56] also studied the response of YBaCuO films in the form of 2000×600 μm strips of thickness 1.3–2 μm to pulsed MW radiation of frequency 9 GHz. The response observed in the region of resistive ''tail'' increases with I_b and with MW power ($P_\omega^{\max}\sim 100$ mW). It was found that the response amplitude is independent of the modulation frequency, which is typical of a nonbolometric response. The noise voltage measured with the help of a synchronous detector (in the absence of radiation), as well as the response itself, had a peak in the region of the resistive tail. The noise measurements permitted the estimation of the noise equivalent power (NEP) $P_{\text{eq}}\sim 6\cdot 10^{-10}$ W/$\sqrt{\text{Hz}}$, the responsivity being 136 V/W. Among possible mechanisms of response, the radiation-induced flux flow within intergranular weak links is considered. The mechanisms of dissociation of V–AV pairs,[45] photoinduced flux creep,[17] and synchronization of the fluxon lattice with the MW field[55] are not ruled out either.

Huggard *et al.*[57] studied the response of BiSrCaCuO thin-film bridges to the pulsed ($\tau=65$ ns) IR radiation ($\Lambda = 447$ μm) with the pulse repetition frequency of 165 Hz. The observed broadening of the decreasing component to the output pulse as compared to the input pulse can be explained by the nonlinearity of the response. As the current I_b increases, the peak of the response corresponding to the end of the resistive tail was shifted towards low temperatures right up to complete vanishing of the response for $I_b>100$ μA. The amplitude of the response was proportional to $\sqrt{P_\omega}$ in the case of high radiation powers and was linear in P_ω for low powers. The two methods of estimating NEP and responsivity mentioned above lead to the following results: $P_{\text{eq}}=5\cdot 10^{-9}$ W/Hz$^{1/2}$, $R_v=0.6$ V/W($1\text{ mW}<P_\omega<50$ mW) and $P_{\text{eq}}=3\cdot 10^{-12}$ W/Hz$^{1/2}$, $R_v=1.2\cdot 10^{-2}$ V/W($0<P_\omega<1$ mW). All the estimates were obtained in a detection band of 50 MHz. Huggard *et al.*[57] ruled out the bolometric origin of the response since, according to Barone and Patterno,[59] the critical current is independent of temperature at $T<T_c/3$, while the response in Ref. 57 was observed at $T=17\text{ K}\ll T_c/3$ ($T_c\sim 85$ K).

Computer simulation proved[58] that for frequencies $h\nu \ll 2\Delta$ and $I_\omega/I_0<1$, the maximum nondissipative current $I_c=I_0(1-\gamma I_\omega)$, where γ is a constant, I_ω the amplitude of the current induced by radiation, and I_0 the characteristic spread in the critical currents of JJ forming a bridge. At a working point with the differential resistance $\delta V/\delta I=R$, the voltage across the junction satisfies the equation

$$V=\gamma I_0 R I_\omega, \tag{19}$$

or $V\sim\sqrt{P_\omega}$. For $I_\omega\ll I_0$, a linear dependence on P_ω is expected.[59] Thus, Huggard *et al.*[57] proved that the response of a bridge to IR radiation is correctly described by the model of a solitary JJ in which I_c is replaced by a certain effective value I_0. This confirms the hypothesis on synchronous response of weak links to EMR.[60]

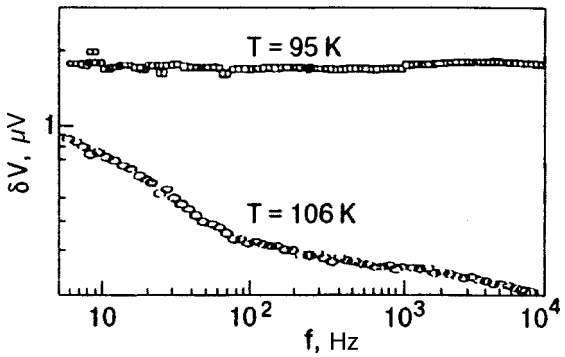

FIG. 7. Photoresponse of a BiSrCaCuO thin film as a function of the modulation frequency for the bolometric ($T=106$ K) and nonbolometric ($T=95$ K) components, $I=1$ mA and $P=2.5$ mW/cm^2 (from Ngo Phong and T. Shih[62]).

Schneider *et al.*[61] studied the frequency dependence of the response of BiSrCaCuO microbridges in the frequency range (10–1000) cm^{-1}. For frequencies varying from 10 to 100 cm^{-1}, only a nonbolometric response with a time constant $\tau\sim 4$ ns was detected with the dependence $\Delta V\sim P_\omega^{1/2}$ in the range from 3 to 30 mW. At a frequency 939 cm^{-1}, a bolometric response is also observed in addition to the nonthermal component near T_c. For $P_\omega<1$ mW, both components are linear functions of power. In this case, the response amplitude $\Delta V\sim\sqrt{P_\omega}$ for $\omega<100$ cm^{-1}, while this quantity is proportional to P_ω for $\omega=939$ cm^{-1}. The frequency dependence of the response in the frequency range from 10 to 1000 cm^{-1} is correctly described by a power law with the exponent 2.3. The obtained results confirm the Josephson nature of the nonbolometric response and rule out nonequilibrium mechanisms associated with electron heating and hot spots exhibiting a linear power dependence and *a weak frequency dependence*.

Ngo Phong and T. Shih[62] measured the response of strip structures of BiSrCaCuO granular films to 5-mm radiation. The response had high-temperature bolometric and low-temperature nonthermal components. The heating near T_c was estimated at ~ 0.3 mK. With increasing bias current, the dynamics typical of both components was observed: the high-temperature component of the response increased linearly and remained at the same temperature, while the low-temperature component increased nonlinearly, attaining saturation for large values of I_b, and was shifted towards lower temperatures. The high-temperature component as a function of modulation frequency decreased abruptly in the range $0<f_{\text{mod}}<100$ Hz and then diminished more smoothly up to 10 kHz. At the same time, the low-temperature component was virtually independent of f_{mod} (Fig. 7). The transformation of the MW pulse ($\tau\sim 50$ ms) after the interaction with the sample was also studied at three temperatures (Fig. 8). In the region of low-temperature component, the shape of the output pulse was exactly the same as that of the input pulse, demonstrating a short response time (the leading front <250 ns). The high-temperature component was character-

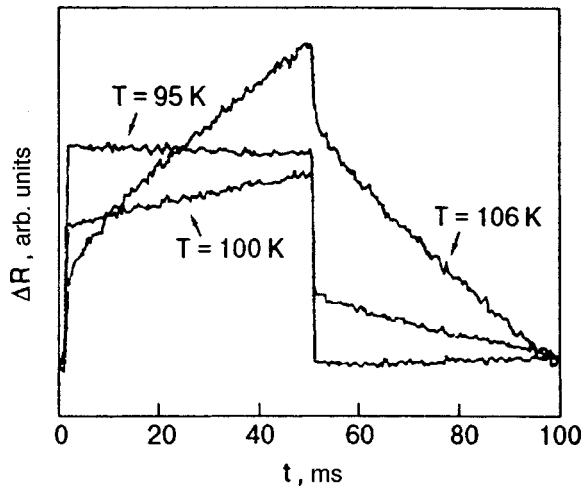

FIG. 8. Transient response ΔR of a thin YBaCuO film induced by MW ($\Lambda = 5$ mm) pulsed radiation at various temperatures near T_c, $I = 1$ mA, $f_{\text{mod}} = 10$ Hz, and $P = 2.5$ mW/cm^2 (from Ngo Phong and T. Shih[62]).

ized by a ''smeared'' asymmetric output pulse (the rise and fall times ~ 1 ms and ~ 20 ms respectively). For the intermediate temperature, the steepness of the leading front of the output pulse varied with time, indicating the presence of a thermal as well as a nonthermal component in the response. The amplitude of the nonthermal component decreased with the extent of granular structure in the sample, and the nonbolometric response was not observed at all for samples with $J_c \sim 10^5$ A/cm^2 at 77 K. The estimates of responsivity and detectability D^* under nonbolometric conditions give the values of $R_v = 10$ V/W and $D^* = 1.1 \cdot 10^8$ cm$\cdot$Hz$^{1/2}$/W. For both components, the power dependence was linear. A dependence of the form $\Delta V \sim P_\omega^{1/2}$ typical of JJ for large values of power[59] was not observed since large power levels were inaccessible. Finally, an analysis of the temperature dependence of the optical ($\Lambda \sim 1.06\ \mu$m and $\Lambda \sim 1.56\ \mu$m) and MW ($\Lambda \sim 5$ mm) responses in the same sample showed that only the bolometric component is left for $h\nu > 2\Delta$. It was emphasized that the Josephson detection mode is typical only for $h\nu < 2\Delta$.

Schneider *et al.*[3] studied recently the response of microstrips made of BiSrCaCuO films on MgO substrates to pulsed ($\sim 80\ \mu$s) IR radiation ($\Lambda \simeq 0.5$ mm) in a constant magnetic field up to 8 T. The magnetic field dependence of the response is determined by the dependence of critical current on B for a solitary rectangular JJ of thickness $d \ll \lambda_L$ and length l in a transverse magnetic field:

$$I_c(B) = I_c(0)\left|\frac{\sin[\pi(\Phi/\Phi_0)]}{\pi(\Phi/\Phi_0)}\right|. \tag{20}$$

The interference pattern is blurred in view of the spread in the parameters of weak links. Schneider *et al.*[3] proved that, according to (20), the magnetic field can either suppress ($I_b > I_c$) or enhance ($I_b < I_c$) the response depending on the relation between I_b and I_c for I_b varying from 2 to 100 μA in the magnetic field range 1 mT$< B <$ 50 mT. Since $I_c(B)$ depends on the length of the junction, Schneider *et al.* could estimate the characteristic size of junctions ($l_J \simeq 0.5\ \mu$m). For $B < 50$ mT, the $\Delta V(B)$ dependence has a plateau which is attributed by the authors to the presence of weak links of the nanometric scale with considerably higher values of I_c, which are ''immersed'' in grain boundaries. The characteristic size of such ''strong'' weak links, which was estimated from the period of the diffraction pattern, is $l_a \leqslant 1$ nm. The dependence of the response on H also exhibits a hysteresis (memory effects), and the response remains suppressed for $I_c > 20\ \mu A$ even after the removal of the field. This can be due to flux trapping in the network of granules and to the presence of weak links with high values of I_c, which form a barrier preventing the escape of vortices. However, Schneider *et al.*[3] rule out the trapping in granules themselves since it would decrease the intergranular field and lead to stimulation rather than suppression of the response.

Irie and Oya[63] studied in 1995 the response of BSCCO single crystals having a size of 1×1 to 3×5 mm and thickness 0.1–0.2 mm to MW radiation (of frequency 8–10 GHz). The measurements of the response by the four-probe technique along the **c**-axis revealed that the IVC of an exposed sample contains multiple resistive branches which are attributed by the authors to interplanar chains of series-connected JJ of the SIS type in the single crystal. For $I_b > I_c^{\min}$, a voltage is induced across the weakest junction, and a further increase in I_b leads to the formation of N jumps on IVC, corresponding to transition to the resistive state in N Josephson junctions. For low radiation power levels, the steps on IVC satisfy the relation $V_n = mn\nu/2e$, where m is the number of synchronized junctions, n is an integer (number of steps), and the shape of the IVC is similar to that for a solitary JJ. In the case of high-intensity radiation, when the signal frequency coincides with one of bulk modes of the resonator, the IVC changes significantly. It acquires steps corresponding to synchronization of fluxons with MW radiation. Finally, for large values of power, when the MW frequency does not coincide with resonator modes, vortices are not synchronized with external radiation. In this case, the flux flow mode can dominate over Josephson properties of the junction, which is also confirmed by the power dependence of the height of voltage steps, having the form $V_n \sim P_\omega^{1/2}$. In this case, neither the voltage V_p corresponding to the formation of steps, nor the amplitude I_p of a step depend on frequency in the range 8–10 GHz. In this case, the steps are considerably blurred (broadened) since the motion of fluxons is not associated with resonant modes, and irradiation plays the role of a trigger that controls the arrival of vortices in the junction.

Ling *et al.*[64] used the four-probe technique to study the response of YBaCuO single crystals to MW radiation (8–12 GHz) with or without direct measuring current along the **c**-axis. The sample was mounted at the end of the waveguide so that the MW fields H_ω and E_ω were parallel to the (ab) plane and the **c**-axis, respectively. The sliding short located at the end of the waveguide made it possible to control the position of the peaks of the electric and magnetic fields relative to the sample.

The dependence of response on the bias current in the normal state ($T = 94$ K) for various radiation powers (from 1 to 7 mW) was linear with a negative slope due to the fact that

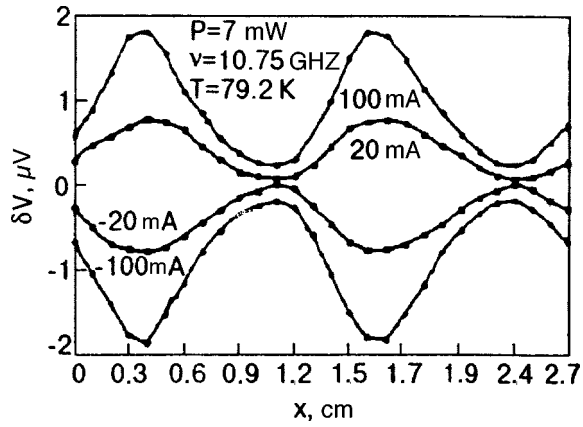

FIG. 9. Constant voltage δV induced by microwave radiation as a function of the sample coordinate for a strong current (from Ling *et al.*[64]).

the resistance along the **c**-axis in the normal state varies in proportion to $1/T$. In the superconducting state, the dependence of response on I_b has the shape of a curve with a peak displaced towards smaller currents upon an increase in the power P_ω. The response has positive polarity and an amplitude two orders of magnitude larger than in the normal state. At the same time, the current corresponding to the maximum response is equal to the critical current. The dependence of the response along the **c**-axis on the position x of the sample exhibits bipolar oscillating behavior with a period equal to 1/2 wavelength in the waveguide. The frequency dependence of the response in the range 8–12 GHz is also oscillating. This rules out rectification and differential heating associated with sample inhomogeneity as possible reasons of the response. On the other hand, such a behavior is in accord with ordinary time-dependent Josephson effect in which induced voltage varies as a Bessel's function. For $I_b=0$, no correlation between the ΔV peaks and the components E_ω and H_ω of the MW field was observed, while an increase in I_b led to clearly manifested displacement of oscillatory peaks towards maxima of the magnetic field H_ω. The height of the peaks increased with the bias current, and for large values of I_b (>20 mA) the polarity of the peaks was strictly determined by the polarity of bias current (Fig. 9). Ling *et al.*[64] attribute the observed response to the presence of intrinsic Josephson junctions in YBaCuO in the direction of the **c**-axis, in which the NW radiation induces pairs of Josephson vortices and antivortices. If $I_b\neq 0$, the formed pair of vortices is carried by current in various directions, leading to the emergence in the sample of a voltage with polarity coinciding with the polarity of I_b. For $I_b\neq 0$, the peaks of the response must coincide with the peaks of H_ω, and the polarity must be the same as that of I_b.

For $I_b=0$, vortices move under the action of MW electric field E_ω with a phase shift θ relative to H_ω in view of different phase relations for H_ω and E_ω in the Josephson junction. The resultant pattern of $\Delta V(x)$ depends on θ and has peaks separated by $\Lambda/2$. The polarity changes with the position x of the sample and can be purely positive or negative for $\theta=\pm\pi/2$.

Main features and conditions for realization of the mechanism

(1) The presence of a peak on the temperature dependence of response at temperatures much lower than the peak of the bolometric response.
(2) Displacement of the peak of the nonbolometric response towards low temperatures and a nonlinear increase (with saturation) of its amplitude with the bias current.
(3) Linear IVC of an HTSC bridge in the region of temperature corresponding to the maximum response.
(4) Independence of response of modulation frequency.
(5) Increase in the response amplitude with the extent of granular structure in the sample.
(6) Decrease in the response amplitude with the radiation frequency approximately in proportion to $\omega^{2.3}$.
(7) Linear and root dependence on radiation power for large and small power levels respectively.
(8) Stimulation of the response by a weak magnetic field for $I_b<I_c$ and its suppression for $I_b>I_c$.

2.5. Nonequilibrium breaking of cooper pairs

The properties of a superconductor below T_c are very sensitive to external excitations such as electrons, phonons, and photons.[65] In the case of MW frequencies for which $h\nu<2\Delta$. Cooper pairs cannot be broken, and the absorption of a photon is reduced to the energy redistribution of quasiparticles, which can stimulate superconductivity under certain conditions due to an increase in the gap width.[66,67] Cooper pairs can break under the interaction of the superconductor with EMR whose energy quantum $h\nu>2\Delta$ (light and IR radiation). Optical photons have energy of the order of several eV, while the energy corresponding to the gap in typical HTSC is of the order of tens of meV (e.g., the gap $2\Delta\simeq 30$ meV for YBaCuO).

The interaction between optical radiation and a superconductor is presented in Fig. 10.[65] Photons incident on a superconductor break Cooper pairs and generate quasiparticles with energies $E\gg 2\Delta$ (see Fig. 10a). Electrons possessing such high energies relax very rapidly (through electron–electron and electron–phonon collisions) to states with energies in the range of the gap energy (see Figs. 10b and c). An absorption of a photon generated a large number of quasiparticles and phonons in the range of energy gap during a very short period of time (see Fig. 10d). The recombination of excited quasiparticles is accompanied by the creation of Cooper pairs and emission of phonons (see Fig. 10e). Pair breaking by phonons with energies $>2\Delta$ occurs during the characteristic time τ_B (see Fig. 10f). Over the time τ_{es}, phonons escape from the film to the substrate (see Fig. 10g). Other processes with their own characteristic times also exist, including the scattering of excited quasiparticles accompanied with absorption (see Fig. 10h) or emission (see Fig. 10i) of a phonon. The time of energy relaxation of electrons through the electron–phonon interaction is an important parameter characterizing the intensity of this interaction.

Nonequilibrium effects in HTSC materials are mainly observed in structures with Josephson properties (bridges and junctions in edge steps as well as bicrystalline sub-

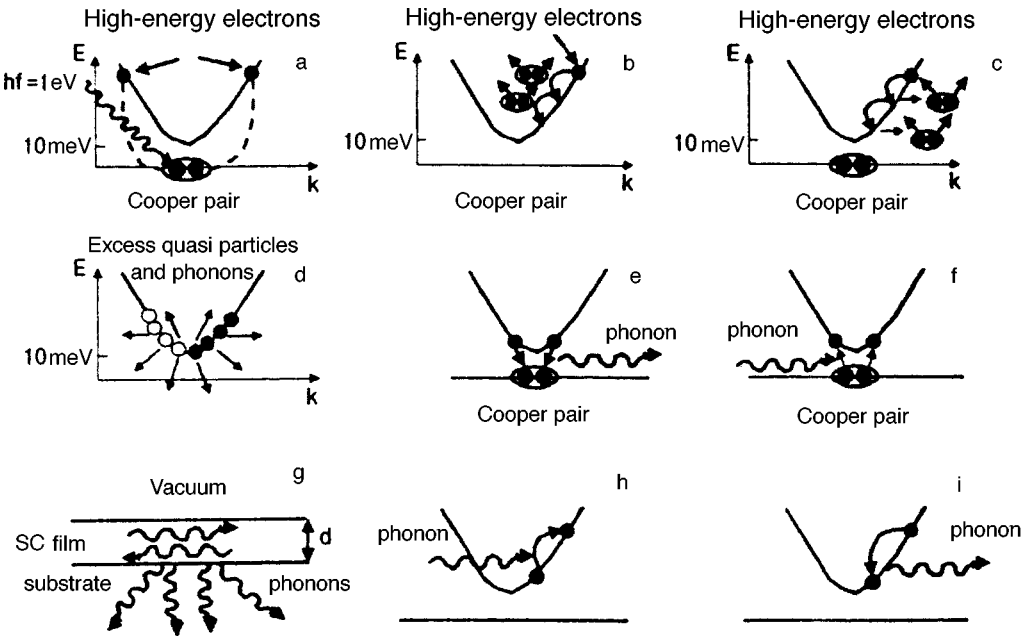

FIG. 10. Interaction between photons, quasiparticles, and phonons in superconductors (see the text) (from Gilabert[65]).

strates). In spite of considerable technological difficulties associated with a small length ξ in HTSC materials, Josephson structures with quite reproducible properties, such as junctions at edge steps, can be obtained even now by using various artificial approaches. Sometimes, the region of a weak link in such structures is coated by a photoconducting layer (usually CdS) in order to improve the sensitivity of the detector and to prevent the degradation of the sample.[65]

Enomoto *et al.*[68] studied the response of thin ($\sim 0.2\ \mu$m) BaPbBiO films ($T_c = 13$ K) to IR radiation. It is well known that the critical current of JJ is determined by the Ambegaokar–Baratov relation $I_c = \pi\Delta/(2eR)\tanh(\Delta/2k_BT)$, and at $T \ll T_c$ we have $I_c \approx \pi\Delta/2eR$. Irradiation of the superconductor leads to a change in the critical current $\delta I_c \approx (\pi\delta\Delta)/2eR$, where the change in the energy gap is connected with the number of excess quasiparticles through the relation $\delta\Delta = \delta n/N(0)$. Thus, knowing the change in critical current, we can find the change in the energy gap and the number of excess quasiparticles. Figure 11 shows schematically the IVC for a tunnel JJ exposed to radiation and without it. In the RSJ model, the IVC of a weak bond is described by the formula[65]

$$V = R(I^2 - I_c^2)^{1/2}. \tag{21}$$

This leads to the following expression for the photoresponse of the weak coupling:

$$\Delta V = -\frac{RI_c\delta I_c}{(I^2 - I_c^2)^{1/2}} = \frac{-\pi I_c\delta\Delta}{2e(I^2 - I_c^2)^{1/2}} \quad \text{for } I > I_c \tag{22}$$

and

$$(\Delta V)_{I=I_c} = R(2I_c\delta I_c)^{1/2} = \frac{\pi}{e}(\delta\Delta/2)^{1/2} \quad \text{for } I \leqslant I_c. \tag{23}$$

The variation of the IVC for a weak link under radiation is shown in Fig. 12a, and the response as a function of bias current together with the dependence calculated by formulas (21)–(23) is presented in Fig. 12b.

Later, Tanabe *et al.*,[69] who studied the response of bridges made of thin YBaCuO and LaSrCuO films to pulsed optical radiation ($\Lambda \sim 1.3\ \mu$m), detected a fast component in the response. The dependence of the response voltage ΔV on I_b had a peak which became narrower and higher upon cooling. With increasing I_b, the peak on the temperature dependence of the response increased and shifted to lower temperatures. The responsivity for the nonbolometric response associated with pair breaking is described by the formula

$$R_{NE} = \left.\frac{\delta V}{\delta I_c}\right|_{I_c} \left.\frac{\delta I_c}{\delta\Delta}\right|_T \left.\frac{\delta\Delta}{n_{qp}}\right|_T \frac{\delta n_{qp}}{P}, \tag{24}$$

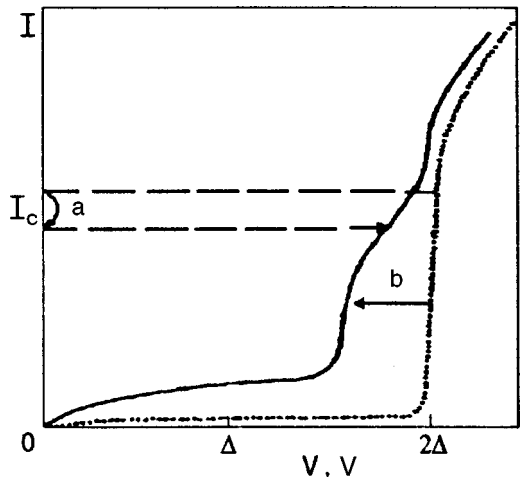

FIG. 11. Typical IVC of a Josephson tunnel junction. Solid and dashed curves represent IVC with irradiation (a) and without it (b) (from Gilabert[65]).

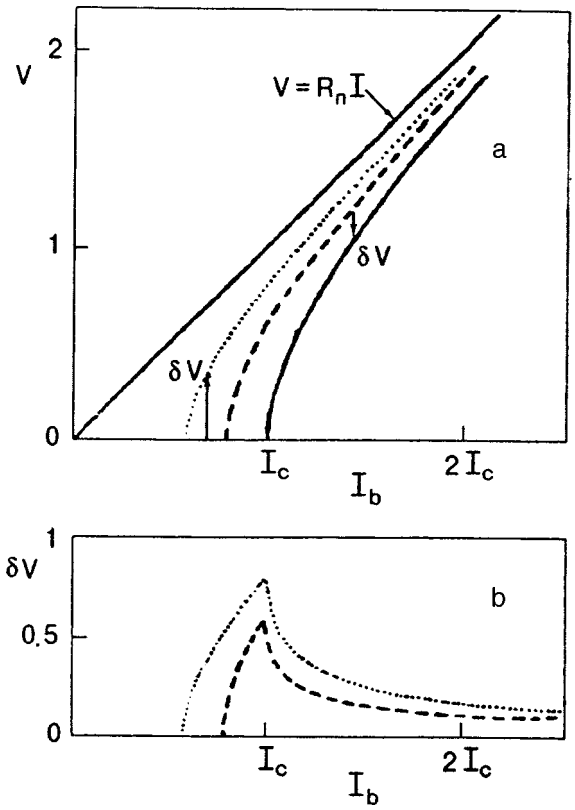

FIG. 12. Effect of radiation on a weak link: the solid curve corresponds to IVC in the absence of radiation, while the dashed and dotted curves correspond to irradiation (a); dependence of the voltage shift δV on the bias current I_b for two characteristics $V(I)$ (dotted and dashed curves) (b) (from Gilabert[65]).

where n_{qp} and P are the number density of quasiparticles and radiation power respectively. The first cofactor in (24) defines the dependence on the bias current I_b, while the temperature dependence is presented by the second and fourth cofactors. The third cofactor can be expressed in terms of the density of states N as $\delta\Delta/\delta n_{qp}=1/2N(0)$. The second cofactor follows the temperature dependence of the critical current, which determines the general temperature dependence of the response. Consequently, the overall temperature dependence is mainly determined by the dependence $I_c(T)$, which was just observed by Tanabe *et al.*[69] According to Tanabe, the value of responsivity is mainly determined by the cofactor $N(0)\Delta/2$. The experiments with YBaCuO and LaSrCuO films give the value of responsivity $\sim$20–30 V/W at low temperatures ($\sim$5 K), while the value of responsivity for similar BaPbBiO films is two orders of magnitude higher. The authors explain this by a considerable difference in the population densities for these two classes of superconductors and assume that the breaking of Cooper pairs by radiation is the basic mechanism of the response.

Johnson[70] studied thin YBaCuO films (20–200 nm) with high values of J_c ($>10^5$ A/cm^2) in quasi-two-dimensional geometry. The response to optical radiation ($\Lambda\simeq 665$ nm) with a pulse duration 0.3 ps and pulse repetition frequency 2 kHz was recorded with the help of ultrahigh-speed oscillograph ($10\ \text{ps}<t<10$ ns). It was found that the response contains two component: in the vicinity of $T_c\pm\Delta T/2$ (where $\Delta T=3$ K is the superconducting transition width), a bolometric signal with a time constant $\sim$3 ns was observed, which increases linearly with the bias current I_b as well as with the radiation power. The second component observed at $T<T_c-\Delta T/2$ has a fall time $\sim$100 ps and is characterized by a steeper than linear dependence on P and I_b with saturation for large values of the argument. In spite of the fact that the position of the peak on the low-temperature component was exactly the same as for the peak of dR/dT, the response was almost two orders of magnitude stronger than the bolometric signal and was virtually independent of temperature at low temperature for which $dR/dT\to 0$. Besides, the response decreased with time much more rapidly ($\sim$100 ps) than the bolometric component ($\sim$3 ns) at $T>T_c-\Delta T/2$. Johnson drew the conclusion that the observed response is associated with photoinduced breaking of Cooper pairs.

A nonbolometric response was also observed by some authors in HTSC epitaxial films.[71] The optical response in the femtosecond range studied with the help of the ''pump–probe'' method (see Sec. 1) demonstrated the avalanche multiplication of quasiparticles following the absorption of a photon.[14] This process is associated with inelastic electron–electron scattering on the time scale $\tau_{ee}\leqslant 1$ ps. Quasiparticles also interact with phonons through inelastic electron–phonon scattering. This loss mechanism is associated with the energy gap suppression as well as with the motion of vortices. A decrease in the number density of Cooper pairs also leads to a change in the kinetic inductance, which also affects temporal characteristics of the response.[72]

Han *et al.*[73] studied the dynamics of a femtosecond response in YBaCuO films of thickness 100–500 nm on a $SrTiO_3$ substrate. They used a laser with a pulse duration $\sim$60 fs, $\Lambda=625$ nm, and the pulse repetition frequency 80 MHz. The typical shape of transient response signal at $T>T_c$ and $T<T_c$ is shown in Figs. 13a and 13b respectively. In the normal state, the response ΔR is positive. It emerges abruptly during the time $\sim$1 ps and decreases slowly over $\sim$3 ns. A comparison of the response with dR/dT revealed its bolometric origin. At the same time, the transient response is negative at $T<T_c$ with a rise time $\sim$300 fs and with a rapid fall to zero over 7–8 ps. After this the response becomes positive due to the thermal effect associated with diffusion of phonons (in analogy with the response at $T>T_c$). It was found that the temperature dependence of the peak height of the response is successfully approximated by the two-fluid model and has the form $[1-(T/T_c)^4]$. Han *et al.*[73] proposed that the optical response mechanism includes the two main processes: (1) avalanche multiplication of quasiparticles following the absorption of a photon, and (2) nonlinear recombination of photogenerated quasiparticles. Han *et al.*[73] also noted that the quasiparticle response is observed only when the system is not saturated. Indeed, the maximum number density of photoinduced quasiparticles estimated from the data on radiation intensity proved to be an order of magnitude smaller than the characteristic density of states in HTSC materials ($N_s\sim 10^{21}$ cm^{-3}). The authors of Ref. 73 also noted that the recombination rate v increases slightly in the interval from 0 to $T_c/2$ and then decreases rapidly. This is explained by the fact that the recombination

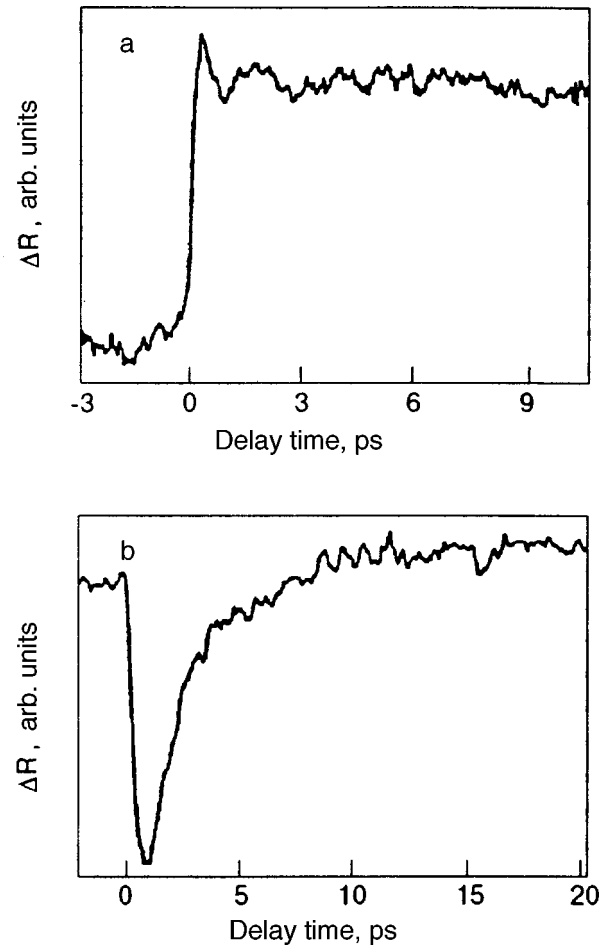

FIG. 13. Transient response ΔR of an epitaxial YBaCuO film at $T=300$ K (a) and 20 K (b) ($T_c=93$ K) (from Han *et al.*[73]).

of quasiparticles is accompanied by the generation of optical phonons that interact resonantly with the gap. The latter circumstance leads to a decrease in the gap width and to softening of this resonant interaction. The decrease in the gap width in turn is manifested directly in a decrease in the recombination rate.

Analyzing the femtosecond dynamics of the optical response, Sobolewski *et al.*[15] proved that the response of YBaCuO epitaxial films of thickness 80–250 nm has a characteristic time ~30 ps and can be explained in the thermomodulation model according to which hot holes are generated by radiation. A redistribution of these holes leads to a displacement (rise) of the Fermi level E_F in copper–oxygen planes, resulting in the emergence of a response. A decrease in the oxygen concentration in the film lowers E_F. If the energy of a probing radiation quantum is lower than the Fermi level (in the initial state), the value of E_F increases upon irradiation. The polarity of the response signal must change at the instant of crossing the energy level corresponding to the energy of the beam, which was actually observed by Sobolewski *et al.*[15] and by Han *et al.*[73] (see Figs. 13a and 13b). If, however, the value of E_F is initially higher than the energy of the beam, the polarity of the response remains unchanged (positive; see Fig. 13a). Sobolewski *et al.*[15] emphasize that the application of the thermomodulation model

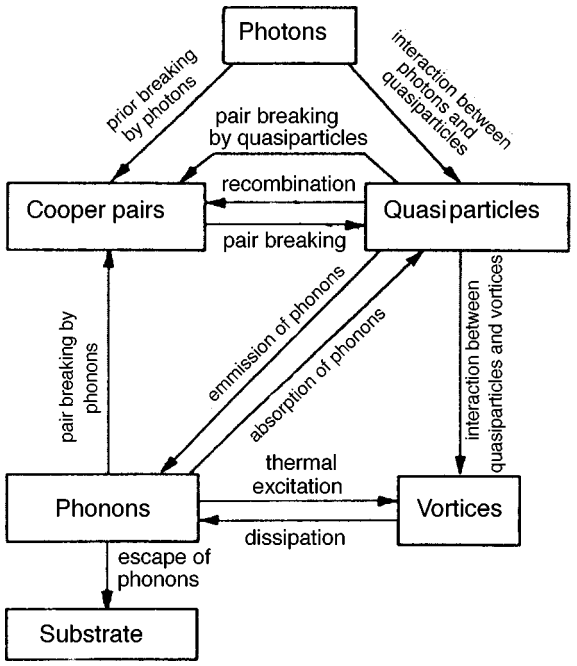

FIG. 14. Nonequilibrium processes in a superconducting film (from Zhang and Frenkel[72]).

is justified only for $YBa_2Cu_3O_{6+x}$ with the oxygen concentration $x>0.4$.

It should be stressed that vortices in type II superconductors, can also be involved in the optical response dynamics in addition to quasiparticles and phonons. The block diagram illustrating all possible types of interactions between these three subsystems is shown in Fig. 14. The processes occurring in the superconductor in this case can be explained as follows[72]: (1) photons interact with Cooper pairs and quasiparticles, generating electrons having a higher energy (the photon–electron interaction occurs during a time ~1 fs); (2) high-energy quasiparticles continuously break new Cooper pairs and generate extra quasiparticles during the time τ_{ee}; (3) quasiparticles interact with phonons through the absorption and emission of phonons ($\tau_{e\mathrm{ph}}$); (4) high-energy phonons break Cooper pairs (τ_B); (5) quasiparticles recombine into Cooper pairs and generate phonons (τ_B); (6) quasiparticles and phonons activate the motion of vortices, leading to dissipation (the corresponding time scales of these processes are denoted by τ_{ev}, $\tau_{\mathrm{ph}v}$, and τ_d); (7) phonons escape from the film to the substrate over the time τ_{es} of the order of nanoseconds.

According to Anisimov *et al.* and Qui and Tien,[74] the electron and phonon subsystems can be assumed to be in equilibrium with each other. The effective temperatures of the electron and phonon gases are given by[75]

$$C_e\frac{dT_e}{dt}=\kappa_e\nabla^2T_e-\gamma_{e\mathrm{ph}}(T_e-T_{\mathrm{ph}})-\gamma_{ev}(T_e-T_0)+q_{ab} \tag{25}$$

and

$$C_{\mathrm{ph}}\frac{dT_{\mathrm{ph}}}{dt}=\kappa_{\mathrm{ph}}\nabla^2T_{\mathrm{ph}}+\gamma_{e\mathrm{ph}}(T_e-T_{\mathrm{ph}})$$

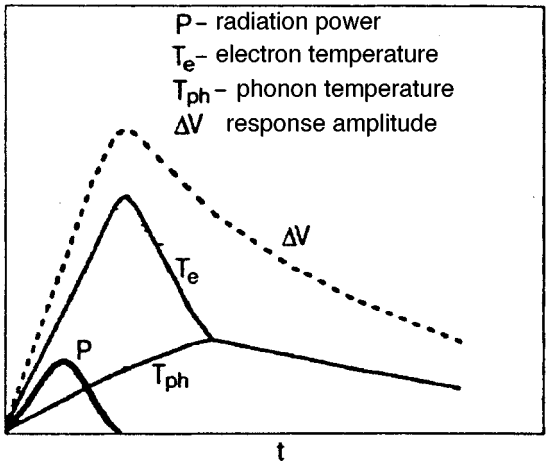

FIG. 15. Time evolution of radiation power P, effective electron (T_e) and phonon ($T_{\rm ph}$) temperatures, and the signal amplitude ΔV of the response of a superconductor to optical radiation (from Zhang and Frenkel[72]).

$$-\gamma_{{\rm ph}v}(T_{\rm ph}-T_0)+q_d\,. \tag{26}$$

where T_e and $T_{\rm ph}$ are effective temperatures of electrons and phonons, T_0 is the equilibrium temperature before irradiation, C_e and $C_{\rm ph}$ are heat capacities per unit volume, and κ_e and $\kappa_{\rm ph}$ the thermal conductivities of the electron and phonon subsystems respectively, $\gamma_{e{\rm ph}}$, γ_{ev}, and $\gamma_{{\rm ph}v}$ are the electron–phonon, electron–vortex, and phonon–vortex coupling constants respectively, and q_{ab} and $q_{\rm d}$ are the absorbed and scattered power densities. The solution of this system of equations makes it possible to calculate the enhancement in the electron temperature relative to the phonon temperature as a result of irradiation. When the duration of radiation pulse is $\tau \geqslant \tau_{e{\rm ph}}$, the electron temperature approaches the phonon temperature. For $\tau \gg \tau_{ee}$ and $\tau_{e{\rm ph}}$, the effective temperatures of electrons and phonons are approximately equal. Figure 15 shows the dynamics of the most important characteristic times as well as the input pulse, when the duration of the latter is shorter than the electron–phonon relaxation time. It can be seen that the value of T_e attains the peak at the end of optical pulse, and the peak of the response corresponds to the peak of T_e. According to Frenkel,[75] the thermal relaxation time determined by the time $\tau_{\rm es}$ during which phonons escape to the substrate can be reduced by eliminating the resistance of the ''film–substrate'' thermal interface by using narrow superconducting microstrips as detectors. The sensitivity in the bolometric mode can be improved by enhancing pinning in operation with large bias currents. However, the mechanisms of interaction between electrons and vortices, phonons and vortices, as well as vortex dissipation have not been studied completely so far.

Gol'tsman *et al.*[7] studied the response of YBaCuO films prepared by laser ablation on various substrates to pulsed ($\tau \sim 20$ ps) optical ($\Lambda = 0.63$ and 1.54 μm) radiation with a pulse repetition frequency 0.5 Hz. The time dependence of transient response has the form of a solitary pulse with steep left slope (of the order of several ps) corresponding to the nonequilibrium component and a ''smeared'' (tens of ps) right slope corresponding to the bolometric component (Fig. 16). The peak of the response amplitude corresponds to the steepest part of the superconducting transition. The shape of the right slope first followed an exponential law, and then a power law identified with a rapid bolometric effect and thermal diffusion to the substrate. Since the time constant corresponding to the exponential decay is proportional to the film thickness, Gol'tsman *et al.*[7] explain this process by the escape of nonequilibrium phonons to the substrate. When nonequilibrium phonons return to the film, a transition from the rapid bolometric effect to diffusion flow with power attenuation takes place. As the temperature decreases ($T = 54$ K), the ratio of the amplitudes of fast and slow components increases, and a signal with negative polarity is formed simultaneously. The response integrated with respect to time is exactly similar to the response in the normal and resistive states, but is characterized by a larger ratio of the amplitudes of the fast and slow components (Fig. 17).

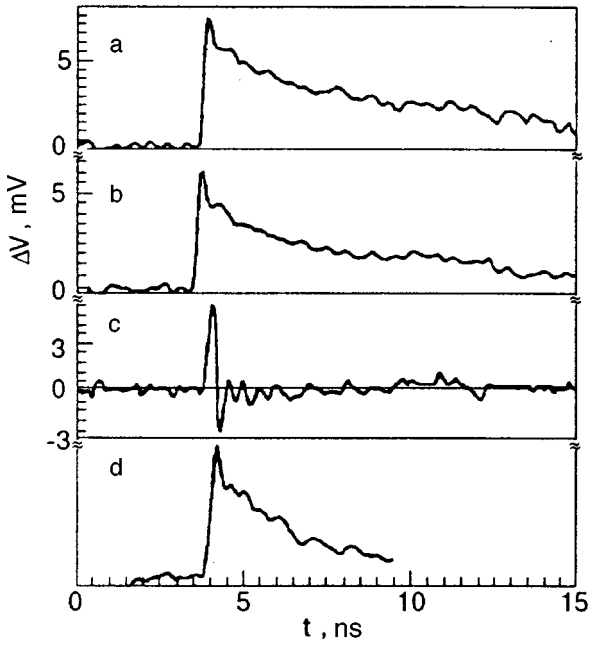

FIG. 16. Transient response of a YBaCuO microbridge at various temperatures (a–c): $T = 100$ K (normal state, $I_b = 7.5$ mA, $E = 40$ μJ/cm^2) (a); $T = 85$ K (near the middle of the junction, $I_b = 1$ mA, $E = 2$ μJ/cm^2) (b); $T = 54$ K (superconducting state, $I_b = 1$ mA, $E = 40$ μJ/cm^2) (c); the integral of the curve in Fig. 16c with respect to time (d) (from Gol'tsman *et al.*[7]).

A similar behavior is observed in the dependence of the response shape in the superconducting state on the displacement current at constant temperature. At first ($I_b = 2$ mA), the negative component decreases, and then vanishes altogether, while the positive component appears. For large values of $I_b (\sim 10$ mA), the wavy shape of the response resembles that in the resistive and normal states. The authors draw the conclusion that a nonequilibrium picosecond component is observed in all the three states. In the normal state, photoexcited charge carriers possess a lower scattering rate than in the equilibrium state, which leads to a decrease in the mobility of charge carriers and hence to an increase in resistance. In the superconducting state, the nonequilibrium response is associated with a change in kinetic inductance. However, in the resistive state (in the superconducting transition region), the inductive and resistive components coex-

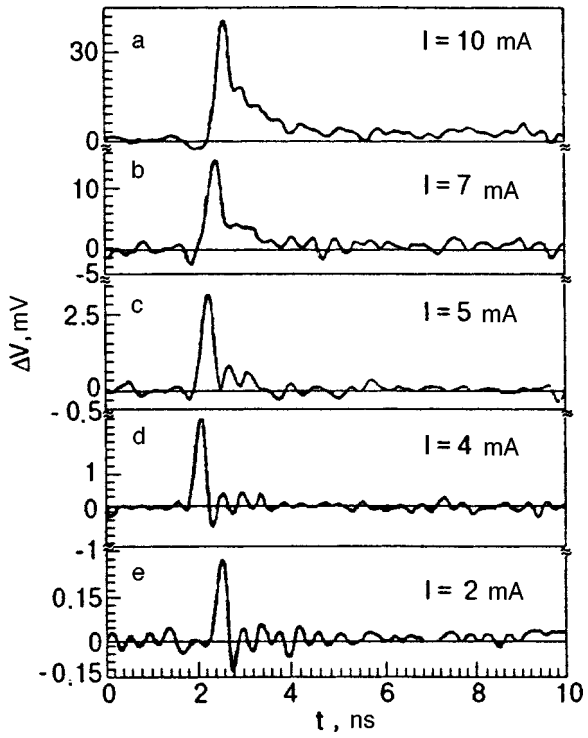

FIG. 17. Transient photoresponse of a YBaCuO microstrip line at $T=4.2$ K, $E=2$ μJ/cm^2 and various bias currents I_b, mA: 10 (*a*), 7 (*b*), 5 (*c*), 4 (*d*), and 2 (*e*) (from Gol'tsman *et al.*[7]).

ist. It was also found that the ratio of the amplitudes of the nonequilibrium and rapid bolometric components virtually does not change during a transition from the normal to the superconducting state. This means that none of superconducting peculiarities affects the shape of a transient pulse, and only the magnitude of the nonequilibrium component commensurate with the bolometric component is affected. This feature is typical of the effect of suppression of the gap by excess quasiparticles generated by irradiation, which results in an increase in resistance in the normal and resistive states or an increase in the kinetic inductance in the superconducting state. This effect is responsible for the coexistence of the nonbolometric and fast bolometric mechanisms in the normal, resistive, and superconducting states of YBaCuO epitaxial films.

Heusinger *et al.*[8] studied NbN films in the form of multistrip structures (having a length of 140 μm and a width of 0.8 μm separated by 3.2 μm on sapphire substrates. Separate strips made of YBaCuO epitaxial films of thickness 80 μm, length 800 μm, and width 80 μm were placed between contact areas. Both types of superconductors in the superconducting state exhibit a bipolar response to pulsed (100 fs) optical radiation with a wavelength of 0.8 μm and a pulse repetition frequency up to 82 MHz. The positive peak of the response for NbN had the rise and fall time $\sim$40 ps and preserved its duration in the entire temperature range 20 K $<T<T_c$. It was followed by a negative peak with a fall time $\sim$190 ps, which broadened with increasing temperature. According to Heusinger *et al.*[8] this peak reflects relaxation processes in the film. For all values of bias current I_b (up to 0.3 mA) and integral power density P_1 (up to 0.6 mJ/cm^2), the photoresponse preserved its shape, and its amplitude was proportional to I_b and P_l. For YBaCuO samples, the duration of the positive and negative peaks of the response was $\sim$25 ps and $\sim$35 ps, respectively. The amplitude of the response on the whole was proportional to the bias current. At the same time, the response in the superconducting transition region was formed by a bi-exponential unipolar voltage peak which is correctly described in the two-temperature model.[71] According to Semenov *et al.*,[71] the mechanism of the response away of the transition is associated with nonequilibrium change in the kinetic inductance of the superconductor under radiation, while the shape and amplitude of the response are determined by the temperature evolution of the number density of Cooper pairs. This is confirmed by good agreement between experimental results and the theory developed in Ref. 71, which gives a relation between the response voltage and the change dN_{sc} in the number density of pairs under irradiation. It is assumed that the working temperature should be maintained below T_c (away from the transition temperature) to optimize the speed of response of a detector based on the given effect since the signal has no slow ''tail'' characteristic of the resistive state at low temperatures.

Salient features and conditions for realization of the mechanism

(1) Depending on temperature, the response is almost constant at low temperatures and decreases abruptly as T_c is approached.
(2) The response associated with the breaking of Cooper pairs appears at lower threshold levels of the signal as compared to the bolometric component, has much higher speed (10–100 ps), and is characterized by clearly manifested saturation as a function of radiation intensity.
(3) The temperature dependence of the response at low temperatures is either exponential, or coincides with the temperature dependence of critical current (for $h\nu>2\Delta$ and for large deviations from equilibrium).
(4) The amplitude of the response increases sharply with the bias current (more steeply than linear dependence) and attains saturation for large I_b.

2.6. Electron heating

The idea of a bolometer based of the effect of electron heating in superconductors was put forth for the first time at the beginning of eighties by Gershenzon *et al.*[76] These authors divide all nonequilibrium effects into two large categories: Josephson and electronic detection mechanisms (JDM and EDM). The idea lies in electron heating by radiation with phonons as a thermostat. Such a mechanism can exist when the heat capacity of the phonon subsystem is higher than that of the electron subsystem: $C_{\rm ph}/C_e>100$.[76] The EDM was realized in practice only in two cases.[77] In one case, it was associated with granular BaPbBiO films at $T \ll T_c(T_c=13.6$ K). The radiation suppresses the order parameter in granules, which is accompanied by a decrease in the critical current of intergranular weak links and the emergence of additional resistance in the resistive state of weak links.[68] The search for this mechanism in HTSC materials

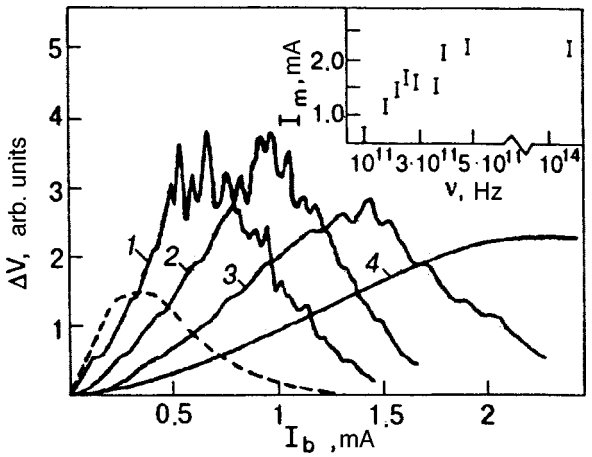

FIG. 18. Dependence of the response ΔV on the bias current I_b for a YBaCuO film for various radiation wavelengths Λ, mm: 2.2 (curve *1*), 1.5 (curve *2*), 1.1 (curve *3*), 0.6 and 8×10^{-4} (curve *4*) and $B=0$ (solid curves) and 3 T (dashed curves), $T=4.2$ K. The inset shows the frequency dependence of the maximum response current I_m (from Aksaev *et al.*[77]).

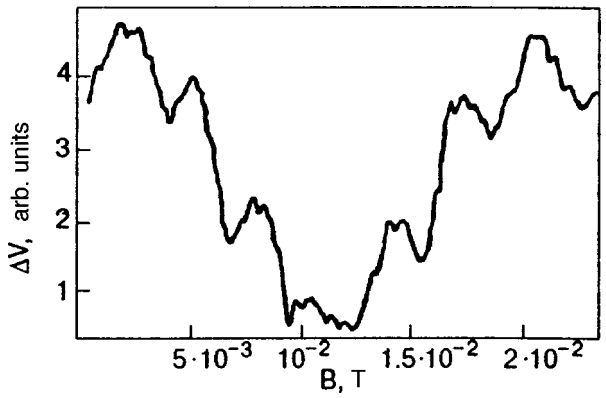

FIG. 19. Field dependence of oscillations of the response ΔV for a granular YBaCuO film at $T=4.2$ K, $\Lambda=2.2$ mm, $I=2\ \mu$A (from Aksaev *et al.*[77]).

did not lead to any positive results by the beginning of the nineties.[77] Another method of realization of EDM was investigated in detail for thin homogeneous Nb, Al, and NbN films.[76] The main difference between these results and those obtained in Refs. 68 is that superconductivity is suppressed considerably in the entire volume of the film, and the resistive state is attained due to transport current and/or magnetic field. The high concentration of quasiparticles as well as their small mean free path (due to scattering by defects) enhance the Coulomb interaction between quasiparticles. The latter is responsible for a lack of selectivity (absence of frequency dependence) of the heating mechanism. Indeed, high-intensity electron–electron interaction leads to an effective redistribution of absorbed energy in the electron subsystem, which is enhanced owing to secondary breaking of Cooper pairs by nonequilibrium quasiparticles and an increase in their number density. Cooling of the electron subsystem as a result of the electron–phonon interaction as well as recombination of quasiparticles turns out to be slower. The resistive state is characterized by a large steepness of dR/dT and serves as a sensitive indicator of electron heating: $\Delta V = I(dR/dT)\Delta\Theta$, where Θ is the effective electron temperature. The condition of phonon thermostat is observed for a small film thickness such that the time $\tau_{\rm es}$ of phonon escape from the film is shorter than the time $\tau_{\rm phe}$ of phonon-electron scattering. The time constant of the effect is determined by the electron–phonon relaxation time $\tau_{e\rm ph}$. In a narrow range in the vicinity of the superconducting transition $[\Delta(T, H)/k_BT \ll 1]$, the response relaxation time τ is associated with the dynamics of superconducting condensate and is equal to the order parameter relaxation time $\tau_\Delta \sim (k_BT/\Delta)\tau_{e\rm ph}$. A characteristic feature of electron heating is the increase in relaxation rate with temperature.

Aksaev *et al.*[77] studied bridges having a length of 0.01–4 mm and a width of 1–500 μm made of YBaCuO granular films of thickness 0.1–1 μm on Al_2O_3 and MgO substrates. All the samples under investigation could be divided into two categories: the films exhibiting typical features of JDM (A) and those in which EDM was manifested (B). The response was studied in a wide spectral range from $\Lambda=2.2$ to $8\cdot10^{-4}$ mm. The dependence of the response ΔV on bias current had the shape of a curve with a peak which was displaced towards higher values of I_b and became lower upon an increase in frequency. The $\Delta V(I_b)$ dependence for samples of group A had quasiperiodic peaks that ''smeared'' with increasing temperature, frequency, and magnetic field (Fig. 18). For radiation wavelengths $\Lambda<0.6$ mm, the $\Delta V(I_b)$ dependences coincides (curve *4* in Fig. 18 corresponds to $\Lambda=0.6$ and $8\cdot10^{-4}$ mm simultaneously). Similar suppression of peaks also took place at a fixed frequency upon an increase in radiation power. A finite voltage appears on the IVC for samples belonging to both groups (A and B) for infinitely small values of $I_b \geqslant 0$, i.e., $I_c \simeq 0$. According to Aksaev *et al.*,[77] this is due to a large spread in the parameter of weak links.

The magnetic field dependence of the response for samples of group A in the field range 10^{-2}–10^{-3} T is oscillating with two characteristic periods $\Delta B=4\cdot10^{-3}$ and $1.9\cdot10^{-2}$ T (Fig. 19). Such oscillations are not observed for samples of group B on $\Delta V(I)$ or $\Delta V(B)$ curves.

The dependence of the response on the amplitude modulation frequency is shown schematically in Fig. 20. It can be seen that at low temperatures, the decrease in response with

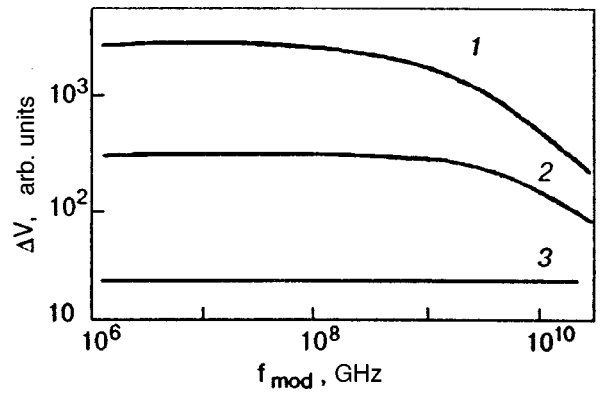

FIG. 20. Dependence of the response ΔV on the modulation frequency $f_{\rm mod}$ for a granular YBaCuO film with a constant impedance at various temperatures T, K: 1.7 (curve *1*), 4.2 (curve *2*) and 77 (curve *3*) (from Aksaev *et al.*[77]).

increasing frequency starts at lower frequencies, while the response at 77 K is constant over the entire frequency range under investigation (0.1–12 GHz). The frequency dependence of the response is described by the formula[77]

$$\Delta V(\nu)=\Delta V(0)[1+(2\pi\nu\tau)^2]^{-1/2}. \quad (27)$$

Using this expression and the experimentally obtained dependence $\Delta V(\nu)$ for various temperatures, the authors obtained the response time $\tau(T)\sim T^{-1}$ over the entire temperature range from 6 to 40 K. It was found that the value of τ does not depend on the substrate material or on the film thickness in the range 0.1–1 μm.

An analysis proved that samples of group A for which oscillations of $\Delta V(I_b)$ and $\Delta V(B)$ are observed display JDM: the peaks on the $\Delta V(I_b)$ curve (see Fig. 18) correspond to Shapiro steps on IVC, which are formed as a result of irradiation of weak intergranular links, while oscillations of ΔV in a magnetic field correspond to oscillations of I_c. The transverse (relative to current) size L of weak links can be estimated from the Josephson interference relation for critical current, i.e., $L=(h/8\pi e)\lambda_L\Delta B$, which gives $L=0.35$ and 1.7 μm (for $\lambda_L=2000$ Å). These values are in good accord with the actual size of microbridges.

As the radiation frequency increases, JDM is replaced by EDM due to electron heating in granules. This can be explained by spectral dependence of JDM sensitivity which varies in proportion to ν^2 for $\nu\sim 2\Delta/h$ in accordance with the theory (see Refs. 11, 24, 77). Since the heating effect remains independent of frequency, upon an increase in temperature, magnetic field, and with decreasing share of granular structure in the films, the frequency of crossover separating these two mechanisms decreases.

Samples of group B were distinguished by a lower degree of granulation and a larger thickness of intergranular junctions. The absence of JDM in group B samples is confirmed by the coincidence of the dependences $\Delta V(I)$ and $dV/dT(I)$, which is typical of the bolometric response. However, the estimates of the EDM time constant give 1–10 ps, which is one or two orders of magnitude smaller than the minimum possible time for a bolometric response defined by the parameter $\tau_{es}=4d/\eta c_s\simeq 10^{-10}$ s, where c_s is the velocity of sound. Besides, the observed response does not depend on the film thickness and the substrate material, which is also typical of a bolometric response. The optimization of EDM is possible for a choice of bias current for which weak links have already been broken, while granules are still in the superconducting state. The resistance at the working point usually amounts to $\sim$10% of the resistance R_n in the normal state. The form of the dependence $\tau(T)\sim T^{-1}$ suggests that the temporal characteristics of EDM are determined by $\tau_{e\text{ph}}$ rather than by the recombination time τ_R of quasiparticles in granules (excluding the temperature region near T_c), which is characterized by an exponential increase upon cooling. A similar dependence for LTS materials has the form $\tau(T)\sim T^{-2}$ corresponding to the temperature dependence of time $\tau_{e\text{ph}}$ in the normal state measured by other methods.[77]

The spectral characteristic of EDM is determined by the frequency dependence of the absorption coefficient α and of the change in the energy gap width $\delta\Delta^*$ ($\delta\Delta^*$ is the mean value of Δ in the resistive state). It is well known that the value of α for YBaCuO changes significantly in the near IR range even in the normal state, leading to a smooth decrease in ΔV with increasing frequency in this range. The absence of singularities in the response for $h\nu=2\Delta$ is associated with considerable inhomogeneity of the resistive state. The ratio of ΔV to the power P_A absorbed by unit volume remains unchanged in a wide frequency range, but was very sensitive to the mechanism of electron energy relaxation. Since the electron–electron interaction dominates in the case of a small mean free path l, energy is redistributed in the electron subsystem, excess quasiparticles are generated, and superconductivity is suppressed effectively for any frequency ν. Besides, the lower value of the Fermi energy in HTSC materials as compared to LTS substances confirms the effectiveness of the electron–electron interaction (along with the electron–phonon interaction), which explained the nonselective nature of the ratio $\Delta V/P_A$.

For $\nu>\tau_{e\text{ph}}^{-1}$, the response under the electron heating conditions is described by the formula[77]

$$\Delta V=(dV/dT)P_A\tau_{e\text{ph}}[1+(2\pi\nu\tau_{e\text{ph}})^2]^{-1/2}C_e^{-1}, \quad (28)$$

which can be used for deriving the temperature dependence of $\tau_{e\text{ph}}$ even in the temperature range inaccessible for measurements. According to (28), $\tau_{e\text{ph}}\sim T\Delta V(dV/dT)^{-1}$ for $\nu\ll(2\pi\tau_{e\text{ph}})^{-1}$ and $C_e=\gamma T$. It was found that the temperature dependences of τ calculated by formula (27) obtained from quasistationary measurements coincide with the dependence of $\tau_{e\text{ph}}$ calculated by formula (28) obtained from nonstationary measurements: both times are proportional to T^{-1}. This confirms the uniform nature of energy relaxation and indicates that diffusion of quasiparticles does not play any significant role in relaxation processes. Moreover, the smallness of the film thickness (as compared to λ_L), which ensures a uniform absorption of radiant energy, is an important condition for realization of electron heating.

Lindgren *et al.*[5,6] studied the response of microbridges made of YBaCuO epitaxial films of thickness 100 nm on $LaAlO_3$ substrates to optical radiation with $\Lambda=790$ nm, pulse duration 100 fs, and pulse repetition frequency 76 MHz. A bridge having the size 5×7 μm was placed at the center of a coplanar waveguide of length 4 mm and width 30 μm through which a bias current of frequency $\sim$18 GHz was supplied via a semirigid coaxial cable. The entire sample was coated with a layer of $LiTaO_3$ insulating crystal to facilitate electro-optical measurements made in the ''pump–probe'' technique (see Sec. 1). The incident beam was focussed in the region of the bridge while the probing beam was focussed at a distance of $\sim$20 μm from the bridge in the region of insulating gap. The sample heating estimated from the absorbed power was $\sim$0.2 K.

The current-voltage characteristics of HTSC samples were measured by the four-probe technique in the temperature range 20–80 K. The IVC were characterized by two clearly distinctive voltage modes: the superconducting state (flux flow with zero/low voltage across the bridge) and the resistive state in which the current is almost constant, while the voltage increases abruptly (Fig. 21). With increasing bias current, a transition occurs from the superconducting state to

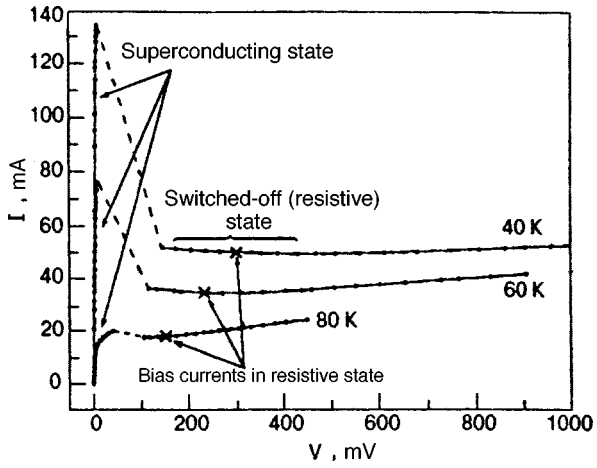

FIG. 21. Current-voltage characteristic of a YBaCuO microbridge measured by the four-probe technique (from Lindgren *et al.*[6]).

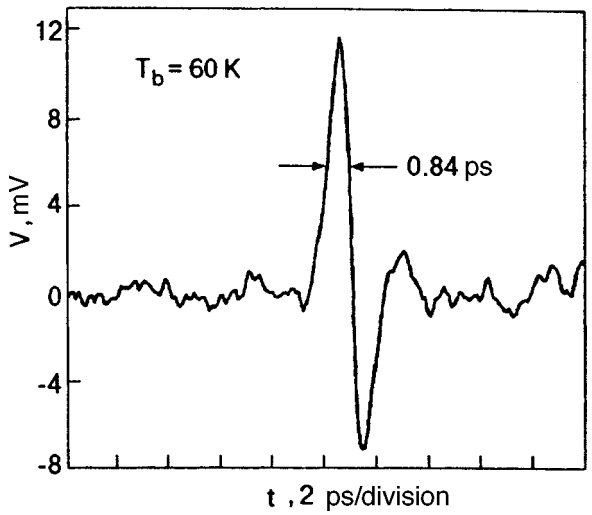

FIG. 23. Transient response of a YbBaCuO bridge in the superconducting state at $T_b = 60$ K (from Lindgren *et al.*[6]).

the flux flow regime in which the bridge becomes dissipative (dissipates heat). The hot spot increasing with a further increase in I_b gradually transforms the bridge to the resistive state with a low and direct current and a high voltage. In the hot spot region, the temperature is maintained at a nearly constant level exceeding T_c. At still higher values of I_b, the bridge goes over to the normal state, and the IVC becomes linear.

In the resistive state, a transient response has the form of a narrow solitary pulse having a width ~ 1.1 ps at half height in the entire temperature range 20–80 K. The response was followed by a voltage plateau (~ 200 μV) associated with a slow bolometric response with a nanosecond fall time (Fig. 22).

According to the model of photoinduced nonequilibrium electron heating, the rise time for a transient pulse is determined by the larger of two time intervals, i.e., the duration of the laser pulse or by the time τ_{et} od electron thermalization. Since the laser pulse in this case is shorter, and hence does not limit the evolution of the nonequilibrium processes under consideration, Lindgren *et al.*[5,6] who used the model of electron heating managed to determine from the results of measurements the two fundamental characteristics of the samples, viz., the electron thermalization time $\tau_{et} \simeq 0.56$ ps and the electron–phonon relaxation time $\tau_{eph} \simeq 1.1$ ps.

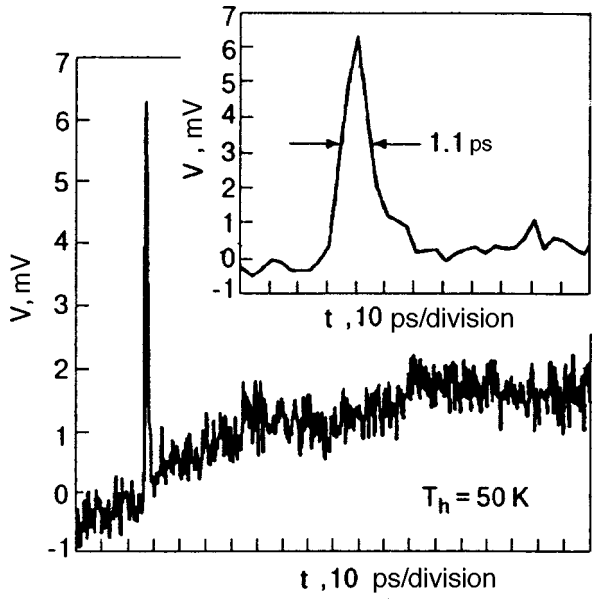

FIG. 22. Transient response of a YbBaCuO bridge in the resistive state at $T_b = 50$ K. Nonzero initial level is due to slow drift of the scanning beam relative to the center of the gap between coplanar waveguides (from Lindgren *et al.*[6]).

In the superconducting state (for small bias currents), a bipolar shape of the response is observed (Fig. 23) with a time constant ~ 1 ps typical of the kinetic inductance mechanism. Additional experiments with the removal of the probing beam to a distance ~ 600 μm from the bridge demonstrated a considerable decrease in amplitude and distortion of the shape of the transient response pulse.[6] Lindgren *et al.*[6] believe that it was the distortion of the shape of a pulse propagating along the transmission line from the bridge to the region of recording, which was observed in early experiments led to erroneous interpretation of the response mechanism as a change in kinetic inductance as a result of uniform heating of the entire region of the bridge. For this reason, the response should be measured as closely to the bridge as possible to reduce pulse distortion effects. Lindgren *et al.*[6] assumed that in this case a nonequilibrium change in the kinetic inductance $L_{\rm kin}$ takes place, in which the variation of the relative fraction of condensate is associated with the electron temperature T_e rather than with the temperature T_b of the thermostat. Lindgren *et al.*[6] attained excellent agreement between the experimental shape of the response in the resistive state and the two-temperature model.[71] The rise time for electron temperature $\tau_{et} = 0.56$ ps and the fall time $\tau_{\rm eph} = 1.1$ ps were extracted from the approximation of experimental data. Since both times exceed the laser pulse duration, they are regarded as intrinsic characteristic times for photoresponse in YBaCuO. The application of the kinetic inductance model described in Ref. 6 leads to an equally good agreement with experimental results in the superconducting state. This made it possible to determine the rise time

of the response $\tau_{et}=0.9\pm0.1$ ps which virtually remains unchanged in the temperature range 20–80 K. This value is much larger than $\tau_{et}=0.56$ ps in the resistive state. The negative component of the response was approximated by using the value of $\tau_{e\text{ph}}=1.1$ ps obtained from measurements in the resistive state and was found to be in satisfactory agreement with experimental data. The linear dependence of the response on I_b also confirmed the effectiveness of the kinetic inductance mechanism.

As regards applications, the kinetic inductance mode is less interesting[6] in view of the oscillatory form of the response. At the same time, the observed effect of optically induced electron heating can be used for developing high-speed detectors and mixers with an intermediate frequency band above 100 GHz in the range from infrared to ultraviolet radiation. Such photodetectors can also be used in fiber optical transmission lines with a data transmission rate >100 Gbit/s. Another region of application can be high-speed optoelectrical transducers using high-speed single flux-quantum circuits and optical fibers for high-speed data transmission.

Salient features and realization conditions for the mechanism

(1) Thin HTSC films can exhibit both Josephson and electronic monitoring mechanisms, a transition from the former to the latter occurring upon an increase in frequency. With increasing temperature, magnetic field, and radiation power, the value of transition frequency decreases. Besides, this frequency is the lower, the smaller the degree of granulation and the larger the grain size in the film. For films with a granule size ~1 μm at 4.2 K and low radiation powers, the transition region lies in the submillimeter range.
(2) For the realization of EDM, the film thickness must be smaller than the radiation penetration depth.
(3) The inertia of the response is determined by the time $\tau_{e\text{ph}}$ of the electron–phonon relaxation, which decreases upon an increase in temperature in proportion to T^{-1}.
(4) The EDM is characterized by the lack of selectivity in a wide frequency range, high values of responsivity (10^3–10^5 V/W), and a low noise level ($P_{\text{eq}}\sim10^{-12}$–$10^{-14}$ $W/\text{Hz}^{1/2}$).[76]

2.7. Percolation superconductivity

This mechanism of response was proposed for the first time by Afanasyev *et al.*[78,79] who studied the interaction between EMR of the millimeter range and thin YBaCuO films. The same authors[80] studied the response of three different YBaCuO films to mm radiation: (1) multiphase granular film (of thickness $d\simeq1$ μm), (2) polycrystalline film with a granule size ~1 μm ($d\simeq1$ μm) and (3) epitaxial film ($d\simeq0.1$ μm). For film 2, two peaks were observed on the temperature dependence of the response, one of which coincided with the dR/dT peak, while the other was manifested in the region of resistive tail. The epitaxial film had only one high-temperature (bolometric) peak, and a weak low-temperature component was observed only for very large bias currents ($I_b\geqslant10$ mA). For film 1, only the low-temperature component was observed for any attainable I_b, which increased in amplitude and was displaced towards low temperatures with increasing I_b. A comparison of the dependences $\Delta V(I_b)$ and $d^2V/dI^2(I_b)$ proved that the response is not associated with an ordinary monitoring mechanism due to nonlinearity of IVC.[79] The low-temperature component for film 2 behaved in the same way as for film 1, while the high-temperature component increased in proportion to I_b. The application of a weak magnetic field caused oscillatory behavior of the resistance $R(H)$ and $\Delta V(H)$ typical of JJ at temperatures corresponding to the low-temperature component of the response. The electrical parameters of film 2 to which a strong magnetic field (of the order of several tens of tesla) was applied were similar to those observed for $I_b\geqslant10$ mA in zero magnetic field.

Afanasyev *et al.*[79,80] concluded that the monitoring mechanism for epitaxial films is either purely bolometric, or is associated with electron heating,[76] while the model of a two-dimensional ($2D$) network of disordered granules connected through weak links with a wide spread of critical currents I_{ci} is more appropriate for granular films. According to Likharev,[60] the energy $E_{ci}=hI_{ci}/4\pi e$ of the ith link at $T\sim T_c$ is comparable with the thermal energy k_BT, and hence the weak link has a finite resistance $R_i=R_{Ni}F(E_{ci}/k_BT)$, where $F(z)\sim\exp(-2z)$ in the case of weak links with strong attenuation in the limit $z\gg1$. The calculation of electrical characteristics of the film is reduced to determining the resistance of the random network of weak links with an exponential spread of resistance.[81] In this case, R is equal to the resistance $R_m=R_{N_m}F(z_m)$ of the weakest link with highest resistance in cluster formed by weak links with $R_i\leqslant R_m$ to within the pre-exponential factor $(E_c/k_BT)^{\tilde{\nu}}$ ($\tilde{\nu}$ is the critical index of correlation length). Here the resistance R_{N_m} is equal to the resistance R_N of an ensemble of weak links in the normal state to within the coefficient of the order of unity. The response of a superconductor in such a system is determined by the variation of I_c under irradiation, i.e.,

$$\Delta V=I\Delta R\simeq I\Delta I_cR_{N_m}\frac{dF}{dI_c}\sim z_m\exp(-2z_m), \tag{29}$$

where $z_m=-hI_b/4\pi ek_BT$, and I_{cm} is the critical current of the mth weak link.[79] Expression (29) shows that the resistance as well as the response of a granular film must decrease exponentially in the region of resistive tail, which was actually observed in experiments.[78] According to this model, the response must have a peak at $z\simeq1$, which corresponds to a temperature T defined by the equation

$$T_c-T=2\pi T_c\overline{R}_Ne^2/h. \tag{30}$$

It follows hence that as the film quality improves (as I_c increases and $\overline{R}_N$ decreases), the low-temperature peak must be shifted to T_c, which was also confirmed in experiments.[78] When the value of I_c is high and comparable with the value of I_c of granules, the bolometric mechanism or electron heating become dominating, and the peak of the response in this case coincides with the dR/dT peak. The responsivity of the low-temperature component was 10^2–10^3 V/W in the temperature range 20–60 K, while that for the bolometric re-

sponse was smaller than 10^2 V/W. These values of responsivity were obtained for a film in the resistive state with a resistance of 1 Ω. These results are compared with the monitoring mechanism observed by Bertin and Rose[82] who studied the films of tin molten into the gold matrix, creating an artificial granular structure. Bertin and Rose[82] emphasized that the *enhanced monitoring* conditions observed by them is typical only of films with a high resistance R_n in the normal state ($\sim$11.4 kΩ). These conditions exist along with the bolometric mode, but differ significantly from the latter in a stronger response. It was assumed that this is a result of a nonlinear response to currents induced in the film by incident EMR.

Finally, according to the percolation model 78, the current flows only through a few channels formed by weak links with the lowest resistance in view of strong spatial inhomogeneity of films. These channels are combined into clusters with a certain characteristic correlation length which is in fact equal to the separation between these clusters. Such a pattern was confirmed by laser probing of the film. The dependence of variation of the voltage across the field due to weak local heating by radiation ($\Delta T \ll T_c$) on the coordinate along the film had the form of nearly periodic peaks having different amplitudes (obviously, due to different resistances of various regions of a cluster) with a characteristic period ~ 100 μm. This value is just the correlation length of the cluster being formed.

Salient features and conditions for realization of the mechanism

(1) The presence of a low-temperature component of the response in the region of resistive tail, which increases in amplitude and which is shifted towards low temperatures upon an increase in I_b and to T_c as a result of improvement of the film quality.
(2) An exponential decrease of the response as well as dc resistance upon cooling.
(3) The presence of a peak at the temperature determined by the relation $hI_{cm}/4\pi e k_B T = 1$.
(4) The high value of responsivity ($\sim 10^2 - 10^3$ V/W) which increases with the film resistance in the normal state.

2.8. Stimulation of superconductivity

An increase in the critical current in thin superconducting bridges induced by EMR was observed for the first time Wyatt *et al.*[83] This was followed by a number of works devoted to this problem (see the review by Dmitriev and Khristenko in Ref. 67). Since stimulation of superconductivity was detected below as well as above T_c, it is often referred to as the effect of stimulation and induction of superconductivity by EMR. For a long time, the effect of stimulation was observed only in weakly coupled superconductors, and was detected much later in narrow, thin, and long films (see Ref. 8 in the literature cited by Dmitriev and Khristenko[67]). Manifestations of the effect in weakly coupled structures and in long homogeneous channels are quite similar, although their mechanisms are different. Besides, the stimulation of superconductivity in bridges is limited by the effective volume of the weak link, while in long channels it is limited by the structure width. The most significant difference between the stimulation in bridges and in long channels is that the superconducting transition temperature and the critical current in the bridge do not exceed corresponding values for the banks. On the contrary, the critical current $I_c(P_\omega)$ in long films exposed to radiation is noticeably larger than the Ginzburg–Landau depairing current. It is appropriate to consider a new state in the MW field with a new energy distribution function for electrons and with the gap $\Delta(P_\omega)$ in the energy spectrum, whose width is larger than that of the unperturbed gap $\Delta(0)$. Long narrow films as well as bridges are characterized by the lower (ω_1) and upper (ω_2) boundary frequencies of the effect. The two boundary frequencies increase upon cooling.

The stimulation effect was initially explained on the basis of phenomenological models (Refs. 5 and 15–18 in the literature cited in Ref. 67) which described its salient features, but failed to explain some peculiarities of the effect (such as the presence of the upper and lower frequency boundaries of the effect, different manifestations of the effect in weakly coupled structures and in long homogeneous superconducting channels, and the coexistence of the Josephson effect with the effect of stimulation and induction of superconductivity in weakly coupled superconductors). The Eliashberg microscopic theory[66] and the Aslamazov–Larkin theory[84] which appeared later described superconductivity stimulation in homogeneous superconductors and in heterogeneous weakly coupled junctions, respectively.

The Eliashberg microscopic theory[66] is based on the assumption that radiation of frequency $\nu < 2\Delta/h$ does not change the total number of excitations in a superconductor, but can lead to a displacement of the ''center of gravity'' of the electron distribution function $f(\varepsilon)$ towards higher energies due to absorption of the MW energy by excitations located near the edge of the gap. According to the basic equation of the BCS theory connecting the energy gap Δ with the electron distribution function $f(\varepsilon)$, this must lead to an increase in Δ, and hence to the enhancement of superconducting properties of the sample.[66]

According to the Aslamazov–Larkin theory,[84] the order parameter Δ in the contact region of heterogeneous junctions carrying a direct current becomes smaller than the order parameter Δ_0 in the banks outside this region. The electrons with energy $\varepsilon < \Delta_0$ become ''trapped'' in the contact and move within the potential well, being reflected by its walls. The application of an ac field causes ''quivering'' of the potential well, and hence to energy diffusion of electrons. As a result, the electron distribution function becomes nonequilibrium, the deviation from equilibrium being most significant at the center of the junction, where the number of electrons decreases as compared to the equilibrium case due to energy diffusion. This is equivalent to effective cooling of the junction. At the same time, electron diffusion may cause the accumulation of electrons in the region of high energies leading to heating of the junction. The resultant effect depends on the radiation power.

The stimulation of superconductivity in HTSC materials by MW radiation was also observed, but it was studied less

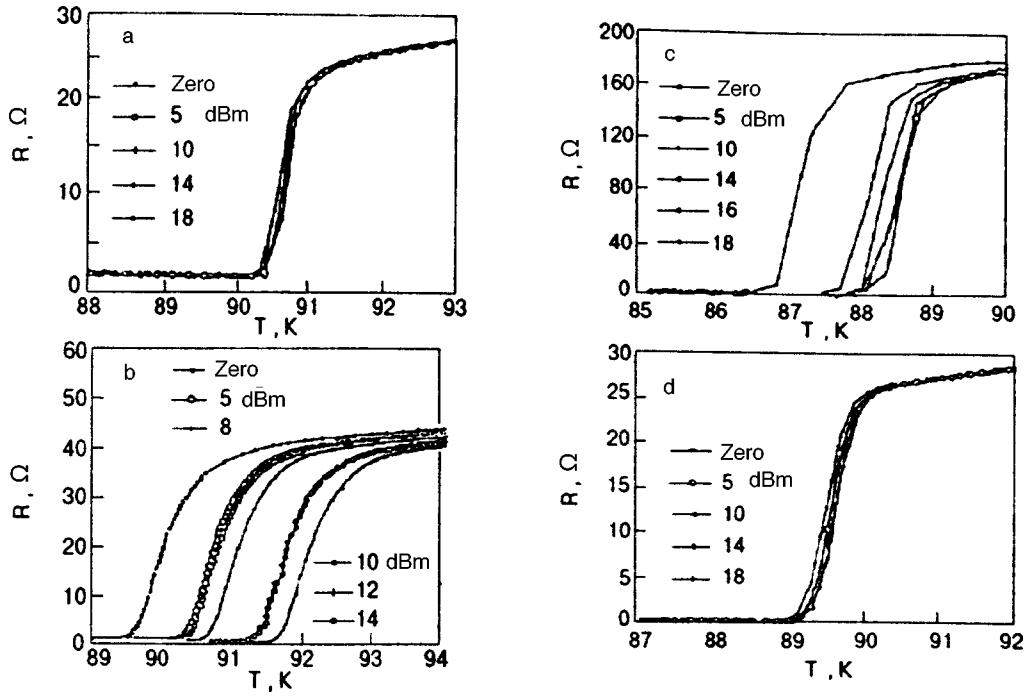

FIG. 24. The $R(T)$ dependence enhanced by microwave radiation for $\theta=24°$ (a), 36.8° (b), and 45° (c). The results for intragranular boundary of a bridge with $\theta=36.8°$ are shown for comparison (d). It can be seen that stimulation is significant for weakly coupled junctions (from Fu *et al.*[86]).

comprehensively than in traditional superconductors. This can be explained, above all, by small number of publications in this field, which is due to some peculiarities of new superconductors. For example, the small value of ξ complicates the preparation of weak links with parameters satisfying the conditions limiting the sample size, which must be satisfied to observe stimulation according to the Aslamazov–Larkin mechanism, while the strong electron–electron interaction associated with the small mean free path l hampers the superconductivity stimulation according to the Eliashberg mechanism.[66,67]

First communications concerning the superconductivity stimulation in HTS samples by MW radiation[85] were purely ''speculative'' and did not lay claims on a detailed description of the observed effect or its analysis. Later, Dmitriev *et al.*[44] reported the observation of nonequilibrium effects in YBaCuO ceramic bridges. Among other things, they observed stimulated excess current in the bridges exposed to MW signal at frequency 13.3 GHz. It was proved that in spite of the emergence of Shapiro steps on IVC as a result of irradiation by MW signal, the dependence of I_c on $P_\omega^{1/2}$ cannot be described by a Bessel function as expected for bridges. On the contrary, this curve consists of two linear regions typical of a long superconducting channel. Dmitriev *et al.*[44] also observed that the passage of direct current for radiation powers higher then the critical value $P_\omega^c(I_c(P_\omega^c)=0)$ leads to a transition from the normal to the resistive state. The transition current I_{tr} increases with the MW power. This effect was observed in HTSC materials for the first time and was attributed to a charge redistribution between ''active'' CuO_2 planes and the ''reservoir'' of chains, which is induced by the direct current. This can lead to an increase in the number density of holes in CuO_2 planes, where the holes form pairs. Detailed measurements and an analysis of the results as well as a comparison with available data for low-temperature superconductor led Dmitriev *et al.*[44] to the conclusion that the stimulation of superconductivity in YBaCuO ceramic bridges occurs according to the Aslamazov–Larkin mechanism due to energy diffusion of electrons localized in the constriction region.

Fu *et al.*[86] studied the response of bridges made of YBaCuO epitaxial films on $SrTiO_3$ bicrystalline substrates to MW radiation ($\nu=12.4$ GHz). The typical size of the bridges was 60 μm×20 μm×120 nm. The response of the intragranular as well as intergranular regions was measured simultaneously by using the four-probe technique. The obtained $R(T)$ dependence shows that the normal resistance in a sample region which does not intersect a weak link is an order of magnitude lower, and the transition width is much smaller than the corresponding values for a region intersecting a weak link. Besides, the measurements of IVC for a region intersecting a weak link revealed the presence of steps satisfying the Josephson relation. Fu *et al.* came to the conclusion that the blurring of the transition for a region with a weak link is associated with the formation of PSC.

An analysis of the $R(T)$ dependences for three different disorientation angles θ for the bicrystalline substrate proved that MW power virtually does not affect $R(T)$ for $\theta=24°$, while the value of T_c increases with radiation power for $\theta=36°$ and 45° (Fig. 24). The maximum effect was observed for $\theta=45°$. Since the entire superconducting transition was shifted by 2–3 K above the equilibrium value of T_c, and the value of T_c increases only for the region of weak link, Fu *et al.*[86] believe that the observed phenomenon may be due not only to fluctuations or effects of redistribution of nonequilibrium quasiparticles. It is proposed that stimulation fol-

lowing the Aslamazov–Larkin mechanism takes place in the given case. The measurements of the $I_c(T)$ dependence for weak links with different disorientation angles θ for substrate crystals revealed that it has the form $I_c \sim (1-T/T_c)^2$ typical of weak links of the SNS type for all three junctions. However, a departure (''bend'') from the theoretical dependence is observed for $\theta = 24°$ in a narrow range of low temperatures. Fu *et al.*[86] believe that this confirms the existence of a stronger intergranular coupling inherent in this junction and assume that the difference in the transport properties of the three boundary weak links is due to their geometrical structure; the differences in these structures are also manifested in the $R(T)$ dependences for different values of P_ω (see Fig. 24).

Choudhury *et al.*[87] studied the MW surface impedance of a suspended strip of YBaCuO epitaxial film in a constant magnetic field up to 1000 Oe. The MW magnetic field was parallel to the (ab) plane of the sample, while the constant field was applied along the **c**-axis. It was found that a weak magnetic field (of the order of several oersteds) leads to a decrease in R_s. The maximum effect ($\sim 20\%$) was observed in a field of 5 Oe. while superconductivity suppression (increase in R_s) was observed in a field above 25 Oe. The measurements of the $R_s(H)$ dependence upon sweeping of H from -100 to $+100$ Oe revealed that a hysteresis of the MW response (i.e., the lack of coincidence in the shape of the magnetic-field dependence with the initial curve upon repeated field sweeping) appears even for low radiation powers (by 21 dB·m below 1 mW). It was concluded[87] that the MW field competes with the constant field, leading to the emergence of vortices in the sample, which are subsequently entangled with lattice defects (pinning). It was proposed that the observed decrease in R_s is due to nonequilibrium redistribution of quasiparticles, which is induced by MW radiation and leads to superconductivity stimulation in the presence of direct current I_{dc}. It was also emphasized that since HTSC materials exhibit a nonmonotonic dependence $R_s(T)$ $(dR_s/dT<0)$, the manifestation of the effect for which $dR_s/dI_{dc}<0$ is not surprising.

Salient features and conditions for the realization of the mechanism

(1) Superconductivity simulation is observed in heterogeneous and long homogeneous superconducting channels and is manifested experimentally in an increase in superconducting transition temperature and critical current and a decrease in the dc or ac resistance. In bridges and other types of spatially inhomogeneous weak links, the stimulation follows the Aslamazov–Larkin mechanism, while in long and narrow channels it is governed by the Eliashberg mechanism.
(2) Both mechanisms are characterized by the existence of the lower and upper boundaries of the effect, the corresponding frequencies increasing upon cooling.
(3) The decisive role in the emergence of the effect in heterogeneous junctions is played by their volume (which must be smaller than a certain value), while for narrow homogeneous channels the leading role is played by their width (which must satisfy the same requirement).
(4) The main difference between superconductivity stimulation in bridges and in long homogeneous channels is that the critical temperature (or critical current) of the former never exceed the same for the ''banks,'' while the critical current for the channels can not only be larger than the value of I_c in the absence of radiation, but can even exceed the equilibrium depairing current.

CONCLUSIONS

Thus, bolometric and nonbolometric mechanisms can obviously be realized in HTSC materials of any quality. The main nonequilibrium mechanism for granular samples exposed to radiation at frequencies $\nu \ll 2\Delta/h$ is the inverse transient Josephson effect for which the peak of the response lies in the region of resistive ''tail'' of the temperature dependence of resistance and is separated by a considerable temperature interval from the peak of the bolometric response. As the sample quality is improved, the peaks of the nonbolometric and bolometric responses become closer and almost coincide for high-quality epitaxial films. The prevailing mechanisms of the nonequilibrium response are either the radiation-induced flow of magnetic flux trapped in weak links or in granules (in the presence of a strong constant magnetic field), or the phase slip at intergranular weak links and Josephson junctions formed by overlapping segments of adjacent copper-oxygen planes. In spite of the fact that the peaks of the response of the above-mentioned ''high-temperature'' mechanisms almost coincide on the temperature scale with the peaks of the bolometric component, they can be analyzed by using contactless methods of recording (which do not lead to strong nonlinear effects and heating due to a large contact resistance), and the incident radiation with a frequency $\gtrsim 10$ kHz can be modulated in order to eliminate the bolometric effect.

At radiation frequencies $\nu > 2\Delta/h$, electron heating and nonequilibrium variation of kinetic inductance are the dominating nonthermal mechanisms over virtually the entire temperature range below T_c. The fundamental parameters typical of these mechanisms can be observed by monitoring the response by the ''pump–probe'' method in which the signal from the same source (laser) is used to act on the sample and to measure the response (after attenuation and delay). This method is rather effective in the case of short (<1 ps) radiation pulses which do not impose limitations on characteristic times of the response of the picosecond scale. The only drawbacks of the ''pump–probe'' method are its technical complexity and the high cost of the precision instruments. For this reason, monitoring with RF or MW displacement as a simpler economical method can be considered an alternative. However, limitations on the response times as well as the inertia of RF monitoring technique must be determined beforehand.

The authors express their gratitude to Prof. V. M. Dmitriev for valuable remarks made while reading the preliminary version of this review. Thanks are also due to M. A. Hein, P. G. Huggard, W. M. Huber, M. Lindgren, D. P. Choudhury, C. M. Fu, Yu. P. Gusev, and A. M. Kadin who

presented copies of their published and unpublished papers.

*E-mail: velichko@ire.kharkov.ua

[1] G. Blatter, M. V. Feigel'man, V. B. Geshkenbein *et al.*, Rev. Mod. Phys. **66**, 1125 (1994).
[2] M. A. Hein, *Studies of High-Temperature Superconductors*, Nova Science Publ., New York (1996).
[3] Gi. Schneider, P. G. Huggard, T. P. O'Bien, and W. Blau, Solid State Commun. **89**, 705 (1994).
[4] P. L. Richards, J. Clarke, R. Leoni *et al.*, J. Appl. Phys. **54**, 283 (1989): J. Clarke, G. I. Hoffer, P. L. Richards, and N. H. Yeh, J. Appl. Phys. **48**, 4865 (1977).
[5] M. Lindgren, M. Currie, C. Williams *et al.*, in *Proc. of ASC'96, ER- 4*.
[6] M. Lindgren, M. Currie, C. Williams *et al.*, J. of Selected Topics in Quantum Electronics **2**, 668 (1996).
[7] G. N. Gol'tsman, P. Kouminov, I. Goghidze, and E. M. Gershenson, IEEE Trans. Appl. Supercond. **5**, 2591 (1995).
[8] M. A. Heusinger, A. D. Semenov, R. S. Nebosis *et al.*, IEEE Trans. Appl. Supercond. **5**, 2595 (1995).
[9] M. W. Johnson, A. M. Domino, and A. M. Kadin, J. Appl. Phys. **79**, 7069 (1996).
[10] M. Leung, P. P. Broussard, J. H. Claassen *et al.*, Appl. Phys. Lett. **50**, 2046 (1987).
[11] N. T. Cherpak, E. V. Izhyk, A. Ya. Kirichenko *et al.*, in *Int. Conf. on HTSC and Localization Phenomena*, Moscow (1991); A. V. Velichko, E. V. Izhyk, A. Ya. Kirichenko *et al.*, in *1st Ukrainian Symp. on Physics and Engineering of mm and submm Waves*, Kharkov (1991); A. V. Velichko, N. T. Cherpak, E. V. Izhyk *et al.*, in *Proc. Int. Symp. on Physics and Engineering of mm and submm Waves*, Kharkov (1994).
[12] A. L. Dorofeev, *Induction Spectroscopy* [in Russian], Energiya, Moscow (1973).
[13] F. F. Mende, I. N. Bondarenko, and A. V. Trubitsyn, *Superconducting and Cooled Resonant Systems* [in Russian], Naukova Dumka, Kiev (1978).
[14] S. G. Han, Z. V. Vardeny, K. S. Wong, and O. G. Symko, Phys. Rev. Lett. **65**, 2708 (1990).
[15] R. Sobolewski, L. Shi, T. Gong *et al.*, Proc. SPIE **2159**, 110 (1990).
[16] P. W. Anderson, Phys. Rev. Lett. **9**, 309 (1962).
[17] E. Zeldov, N. M. Amer, G. Koren, and A. Gupta, Phys. Rev. B **39**, 9712 (1989).
[18] A. Frenkel, E. Clausen, C. C. Chang *et al.*, Appl. Phys. Lett. **55**, 911 (1989); A. Frenkel and C. C. Chang, J. Mater. Res. **5**, 691 (1990).
[19] A. Frenkel, Physica C **180**, 251 (1991).
[20] W. Eideloth, IEEE Trans. Magn. **27**, 2828 (1991).
[21] T. T. M. Palstra, B. Batlogg, R. B. van Dover *et al.*, Phys. Rev. B **41**, 6621 (1990).
[22] M. Tinkham, Phys. Rev. Lett. **61**, 1658 (1988).
[23] V. Ambegaokar and B. J. Halperin, Phys. Rev. Lett. **22**, 1364 (1969).
[24] Y. Yeshurun and P. A. Malozemoff, Phys. Rev. Lett. **60**, 2202 (1988).
[25] M. P. A. Fisher, Phys. Rev. Lett. **62**, 1415 (1989).
[26] P. H. Kes, J. Aarts, J. van der Berg *et al.*, Supercond. Sci. Technol. **1**, 242 (1989).
[27] J. Bardeen and M. J. Stephen, Phys. Rev. A **140**, 1197 (1965).
[28] L. Ji, M. S. Rzchowski, and M. Tinkham, Phys. Rev. B **42**, 4838 (1990).
[29] A. M. Portis, K. W. Blazey, K. A. Müller, and J. G. Bednordz, Europhys. Lett. **5**, 467 (1988).
[30] A. V. Velichko, Ph.D thesis, Kharkov (1996).
[31] Yu. V. Medvedev and A. S. Petrov, Izv. Vuzov. Fizika **10**, 93 (1972); I. I. Eldumiatti and G. A. Haddad, IEEE Trans. Electron Devices **19**, 257 (1972).
[32] A. V. Velichko, N. T. Cherpak, E. V. Izhyk *et al.*, Physica C **261**, 220 (1996); A. V. Velichko, N. T. Cherpak, E. V. Izhyk *et al.*, Physica C **277**, 101 (1997).
[33] A. V. Velichko, N. T. Cherpak, E. V. Izhyk *et al.*, Fiz. Nizk. Temp. **22**, 963 (1996) [Low Temp. Phys. **22**, 533 (1996)]; A. V. Velichko, N. T. Cherpak, E. V. Izhyk *et al.*, Czech. J. Phys. **46**, 1639 (1996).
[34] A. Gurevich and H. Küpfer, Phys. Rev. B **48**, 6477 (1993).
[35] J. Halbritter, J. Appl. Phys. **68**, 6315 (1990).
[36] S. Sridhar, Appl. Phys. Lett. **65**, 1054 (1994).
[37] A. Gurevich, Physica C **243**, 191 (1995).
[38] I. M. Dmitrenko, Fiz. Nizk. Temp. **22**, 849 (1996) [Low Temp. Phys. **22**, 648 (1996)].
[39] V. V. Shmidt, *Introduction to Superconductor Physics* [in Russian], Nauka, Moscow (1982).
[40] H. A. Blackstead, D. B. Pulling, P. J. McGinn, and J. Z. Liu, Physica C **174**, 394 (1991).
[41] W. K. Kwok, U. Welp, G. W. Crabtree *et al.*, Phys. Rev. Lett. **64**, 966 (1990).
[42] J. M. Kosterlitz and D. J. Thouless, J. Phys. C **6**, 1181 (1973).
[43] H. A. Blackstead, J. Supercond. **5**, 67 (1992).
[44] V. M. Dmitriev, I. V. Zolochevskii, and E. V. Khristenko, Fiz. Nizk. Temp. **19**, 249 (1993) [Low Temp. Phys. **19**, 173 (1993)].
[45] J. C. Culbertson, U. Strom, S. A. Wolf *et al.*, Phys. Rev. B **39**, 12359 (1989); A. T. Fiory, A. F. Hebard, P. M. Manikiewich, and R. E. Howard, Phys. Rev. Lett. **61**, 1419 (1988).
[46] A. M. Kadin, M. Leung, and A. D. Smith, Phys. Rev. Lett. **65**, 3162 (1990).
[47] A. M. Kadin, M. Leung, A. D. Smith, and J. M. Murduck, IEEE Trans. Magn. **27**, 1540 (1991).
[48] W. J. Skocpol, M. R. Beasley, and M. Tinkham, J. Low Temp. Phys. **16**, 145 (1974).
[49] A. M. Kadin, M. Leung, A. D. Smith, and J. M. Murduck, Appl. Phys. Lett. **57**, 2847 (1990).
[50] M. W. Johnson, A. M. Domino, and A. M. Kadin, IEEE Trans. Appl. Supercond. **5**, 2587 (1995).
[51] W. J. Skocpol, M. R. Beasley, and M. Tinkham, J. Appl. Phys. **45**, 4054 (1974).
[52] D. N. Langerberg, D. J. Scalapino, B. N. Taylor, and R. E. Eck, Phys. Lett. **20**, 563 (1966).
[53] R. Durny, S. Ducharme, J. Hautala *et al.*, Physica C **162–164**, 1065 (1989).
[54] K. Chang, J. T. Chen, and L. E. Wenger, Physica C **162–164**, 1591 (1989); K. Chang, G. Yong, L. E. Wenger, and J. T. Chen, Appl. Phys. Lett. **59**, 7316 (1991).
[55] J. C. Gallop, W. J. Radcliffe, C. D. Langhman *et al.*, Physica C **162–164**, 1545 (1989).
[56] B. G. Boone, R. M. Sova, K. Moorjani, and W. J. Green, Appl. Phys. Lett. **59**, 2676 (1991).
[57] P. G. Huggard, Gi. Schneider, T. P. O'Brien *et al.*, Appl. Phys. Lett. **58**, 2549 (1991).
[58] P. Russer, J. Appl. Phys. **43**, 2008 (1972).
[59] A. Barone and G. Patterno, *Physics and Application of the Josephson Effect*, Wiley, New York (1986).
[60] K. K. Likharev, *Introduction to the Dynamics of Josephson Junctions* [in Russian], Nauka, Moscow (1985).
[61] Gi. Schneider, P. G. Huggard, T. P. O'Brien *et al.*, Appl. Phys. Lett. **60**, 648 (1992).
[62] L. Ngo Phong and T. Shin, J. Appl. Phys. **74**, 7414 (1993).
[63] A. Irie and G. Oya, IEEE Trans. Appl. Supercond. **5**, 3267 (1995).
[64] D. C. Ling, J. T. Chen, and L. E. Wenger, Phys. Rev. B **53**, 1 (1996).
[65] A. Gilabert, Ann. Phys. (Paris) **15**, 255 (1990).
[66] G. M. Eliashberg, Pis'ma Zh. Éksp. Teor. Fiz. **11**, 186 (1970) [JETP Lett. **11**, 114 (1970)].
[67] V. M. Dmitriev and E. V. Khristenko, Fiz. Nizk. Temp. **4**, 821 (1978) [Sov. J. Low Temp. Phys. **4**, 387 (1978)].
[68] Y. Enomoto, T. Murakami, and M. Suzuki, Physica **B** and C **148**, 408 (1988); Y. Enomoto and T. Murakami, Jpn. J. Electr. Commun. Lab. Tech. **34**, 1597 (1985); M. Suzuki, Y. Enomoto, and T. Murakami, J. Appl. Phys. **56**, 2083 (1984).
[69] H. Tanabe, Y. Enomoto, M. Suzuki *et al.*, Jpn. J. Appl. Phys., Suppl. **29**, L466 (1990).
[70] M. Johnson, Appl. Phys. Lett. **59**, 1371 (1991).
[71] A. D. Semenov, G. N. Gol'tsman, J. G. Gogidze *et al.*, Appl. Phys. Lett. **60**, 903 (1992); N. Bluzzer, Phys. Rev. B **46**, 1033 (1992).
[72] Z. M. Zhang and A. Frenkel, J. Supercond. **7**, 871 (1994).
[73] S. G. Han, Z. V. Vardeny, O. G. Symko, and G. Koren, IEEE Trans. Magn. **27**, 1548 (1991).
[74] S. I. Anisimov, B. L. Kapeliovich, and T. L. Perel'man, Zh. Éksp. Teor. Fiz. **66**, 776 (1974); T. Q. Qiu and C. L. Tien, Int. J. Heat Mass Transf. **35**, 719 (1992).
[75] A. Frenkel, Phys. Rev. B **48**, 9717 (1993).
[76] É. M. Gershenson, M. E. Gershenson, G. N. Gol'tsman *et al.*, Pis'ma Zh. Éksp. Teor. Fiz. **34**, 281 (1981) [JETP Lett. **34**, 268 (1981)]; E. M. Gershenson, M. E. Gershenson, G. N. Gol'tsman *et al.*, Zh. Éksp. Teor. Fiz. **86**, 758 (1984) [Sov. Phys. JETP **59**, 442 (1984)]; E. M. Gershenson, M.

E. Gershenson, G. N. Gol'tsman *et al.*, IEEE Trans. Magn. **27**, 2836 (1991).
[77] È. E. Aksaev, E. M. Gershenzon, G. N. Gol'tsman *et al.*, Sverkhprovodimost': Fiz., Khim., Tekh. **3**, 1933 (1990).
[78] A. S. Afanasyev, V. N. Gubankov, P. M. Shadrin, and A. F. Volkov, in *Proc. of ISEC*, Tokyo (1989).
[79] A. S. Afanasyev, A. F. Volkov, V. N. Gubankov *et al.*, IEEE Trans. Magn. **25**, 2571 (1989).
[80] A. S. Afanasyev, A. F. Volkov, and V. N. Gubankov, Fiz. Nizk. Temp. **15**, 322 (1989) [Sov. J. Low Temp. Phys. **15**, 181 (1989)].
[81] B. I. Shklovskii, *Electronic Properties of Doped Semiconductors*, Springer-Verlag, New York, NY (1984).
[82] C. L. Bertin and K. Rose, J. Appl. Phys. **42**, 631 (1971).
[83] A. F. G. Wyatt, V. M. Dmitriev, V. M. Moore, and F. W. Sheard, Phys. Rev. Lett. **16**, 1166 (1966).
[84] L. G. Aslamazov and A. I. Larkin, Zh. Éksp. Teor. Fiz. **74**, 2184 (1978) [Sov. Phys. JETP **47**, 1136 (1978)].
[85] E. M. Rudenko, I. V. Korotash, I. P. Neverkovets *et al.*, Supercond. Sci. Technol. **4**, 1 (1991); A. Ya. Kirichenko, M. B. Kosmyna, A. B. Levin, and N. T. Cherpak, Pis'ma Zh. Éksp. Teor. Fiz. **50**, 260 (1989) [JETP Lett. **50**, 260 (1989)].
[86] C. M. Fu, J. Y. Juang, M. F. Chen *et al.*, IEEE Trans. Appl. Supercond. **5**, 2196 (1994).
[87] D. P. Choudry, B. A. Willemsen, J. S. Derov, and S. Sridhar, IEEE Trans. Appl. Supercond. **7**, 1260 (1996).

Translated by R. S. Wadhwa

QUANTUM LIQUIDS AND QUANTUM CRYSTALS

On the theory of superfluid Fermi liquid with spin-triplet pairing in a magnetic field

A. N. Tarasov

*National Science Center ''Kharkov Institute of Physics and Technology,'' 320108 Kharkov, Ukraine**
(Submitted December 3, 1997)
Fiz. Nizk. Temp. **24**, 429–437 (May 1998)

The Fermi-liquid approach generalized to superfluid systems is used to derive general formulas for the normal and abnormal distribution functions (DF) for quasiparticles of a superfluid Fermi liquid (SFL) consisting of electrically neutral fermions with spin-triplet pairing (the spin of a pair $s=1$, the orbital angular momentum l of the pair being an arbitrary odd number) in a static uniform magnetic field, taking into account the Landau spin-exchange Fermi-liquid interaction at temperatures $0<T<T_c$ (T_c is the temperature of phase transition from the normal to the superfluid state). In deriving the DF, the explicit form of the energy functional (EF) for SFL is not used. A system of coupled equations is obtained for the order parameter, energy of quasiparticles, and effective magnetic field for the SFL under investigation in the case of an EF quadratic in DF. The obtained DF and the system of equations are applicable for describing both unitary and nonunitary phases of superfluid ^{3}He in a magnetic field, e.g., for determining the magnetization and magnetic susceptibility of these phases. © *1998 American Institute of Physics.* [S1063-777X(98)00205-9]

1. INTRODUCTION

This research is devoted to a theoretical analysis of superfluid Fermi liquids (SFL) with spin-triplet pairing in a magnetic field. We consider a SFL consisting of electrically neutral fermions possessing a magnetic moment. Such SFL include, for example, superfluid phases of ^{3}He as well as neutron liquid in the superfluid state in neutron stars. These objects were studied by many authors by using different methods (see, for example, the reviews,[1–4] monographs,[5–7] and the literature cited therein). We shall not discuss here in detail the large number of publications devoted to SFL with spin-triplet pairing in a magnetic field, but pay attention to the article by Schopohl.[8] In this paper, the solutions of the Gor'kov equations for normal and abnormal Green's temperature functions are given for the general case of SFL with spin-triplet pairing in a uniform static magnetic field. Schopohl[8] confined his analysis to the static B-phase of ^{3}He (one of unitary phases of superfluid ^{3}He) in a magnetic field, which he described by taking into account only the p-pairing of ^{3}He atoms and using the so-called weak-coupling approximation valid under low pressures. He obtained a system of coupled nonlinear equations for the order parameter and effective magnetic field in the bulk of ^{3}He$-B$ and derived an expression for the magnetic susceptibility of ^{3}He$-B$ taking into account Landau exchange amplitudes F_0^a and F_2^a for a normal Fermi liquid (NFL). An analysis of ^{3}He$-B$ in a magnetic field at finite temperatures was complicated in view of the fact that $F_2^a \neq 0$. The obtained system of equations[8] was solved numerically for various values of the magnetic field at temperatures $0<T<T_c$ (T_c is the temperature of phase transition from the normal to the superfluid state). A comparison with experimental data led to the conclusion that the weak-coupling theory does not provide an adequate explanation of the transition from ^{3}He$-B$ to ^{3}He$-A$ in strong magnetic fields. Although the result obtained in Ref. 8 for nonlinear magnetic susceptibility of ^{3}He$-B$ is in good agreement with experiments in the range of weak fields, a noticeable discrepancy with experimental results is observed in strong fields. This was noted by Fishman and Sauls,[9] who took into account the effects associated with f-pairing in ^{3}He$-B$ in addition to p-pairing while calculating nonlinear magnetic susceptibility. The latter quantity was determined by using the perturbation theory to within quadratic terms in the small parameter $\gamma H/\Delta(T)$ (γ is the gyromagnetic ratio of the ^{3}He atom, H the external magnetic field and $\Delta(T)$ the energy gap in the spectrum of quasiparticles) in the weak-coupling approximation in the semiclassical theory.

In view of a certain discrepancy between the predictions of the theory for SFL with spin-triplet pairing and experimental results, it is interesting to consider other theoretical approaches. An alternative method for describing superfluid Fermi systems was developed in Refs. 10–13 on the basis of the Fermi liquid model. In this method, simpler quantities, viz., normal and abnormal ''distribution functions'' (DF) for quasiparticles, which obey a nonlinear self-consistent equation, are used instead of the formalism of Green's temperature functions.

This research mainly aims at the derivation of general expressions for the normal and abnormal DF for quasiparticles in a SFL with spin-triplet pairing (the spin of a pair $s=1$ and its orbital angular momentum l is an arbitrary odd number) in a static uniform magnetic field at $0<T<T_c$ on the basis of the Fermi liquid method developed in Refs. 10–

13. These expressions for DF, which are valid both for unitary and nonunitary phases of SFL with spin-triplet pairing, are interesting as such and are generalizations of the results obtained by Isaev and Peletminskii[14] for the case of applied magnetic field and exchange NFL interactions. It should be emphasized that the specific structure of the functional dependence of the SFL energy on DF is used only at the last stage for obtaining a coupled system of nonlinear self-consistent equations for the order parameter (OP) of SFL, quasiparticle energy, and effective magnetic field $\mathbf{H}_{\rm eff}(\mathbf{p})$ (emerging in the bulk of a SFL due to renormalization of the applied magnetic field $\mathbf{H}$ by exchange NFL interactions). In this research (like in Ref. 14), we derived this system of equations by using the energy functional (EF) of the SFL, which is quadratic in the DF.

In Sec. 2, we present basic equations (equivalent to the self-consistent equation) for normal and abnormal DF of quasiparticles in the SFL (applicable in the case of singlet and triplet pairing) as well as definitions of the quantities used in the following sections for describing SFL with spin-triplet pairing. The general form of the DF for quasiparticles, which is valid for unitary as well as nonunitary phases of SFL with spin-triplet pairing in a magnetic field, is derived in Sec. 3 taking into account the exchange NFL interactions. The same section also contains an expression for magnetization of SFL in a magnetic field in terms of the normal DF as well as a coupled system of equations derived for the vector OP $\mathbf{\Delta}(\mathbf{p})$, quasiparticle energy, and effective magnetic field in the SFL under investigation in the case of EF quadratic in DF. In Sec. 4, general expressions for DF are used for deriving the expressions for DF in particular cases, i.e., for the unitary phases ($|\mathbf{\Delta}(\mathbf{p})\times\mathbf{\Delta}^*(\mathbf{p})|=0$) for $\mathbf{H}_{\rm eff}(\mathbf{p})$ having an arbitrary direction in space and nonunitary phases ($|\mathbf{\Delta}(\mathbf{p})\times\mathbf{\Delta}^*(\mathbf{p})|\neq 0$) of a SFL in the magnetic field $\mathbf{H}_{\rm eff}(\mathbf{p})\| i[\mathbf{\Delta}(\mathbf{p}),\mathbf{\Delta}^*(\mathbf{p})]$. The obtained results are discussed briefly in Conclusion.

2. BASIC EQUATIONS FOR A SUPERFLUID FERMI LIQUID IN A MAGNETIC FIELD

Following Refs. 10–13, we shall describe SFL (both with singlet and triplet pairing) in a static uniform magnetic field $\mathbf{H}$ by introducing the EF $E(f,g,g^+;H)$ depending on the normal $f_{12}\equiv \mathrm{Tr}\,\rho a_2^+ a_1$ and the abnormal $g_{12}\equiv \mathrm{Tr}\,\rho a_2 a_1$, $g_{12}^+\equiv \mathrm{Tr}\,\rho a_2^+ a_1^+$ distribution functions for quasiparticles (ρ is the statistical operator, a_1^+ and a_1 are the creation and annihilation operators for Fermi quasiparticles in the state $1\equiv \mathbf{p}_1, s_1$, where $\mathbf{p}_1$ is the momentum and s_1 the spin component along the quantization axis). Henceforth, we shall assume that the EF for the SFL is invariant to phase transformations and rotations both in the coordinate and spin spaces. Such a rotational invariance indicates that we take into account the strongest exchange EF and disregard weak relativistic interactions in the SFL. For example, for SFL with spin-triplet pairing (like superfluid phases of ^{3}He), we disregard weak magnetic-dipole interaction between fermions (nuclei of ^{3}He atoms possess a magnetic dipole moment), which is justified in strong magnetic fields ($H \gg 30$ G for ^{3}He).[2] The energy functional may have, for example, the form

$$E(f,g,g^+;H)=E_0(f;H)+E_1(f)+E_2(g,g^+). \tag{1}$$

Here $E_0(f;H)$ is the energy of interacting fermions in a magnetic field, which can be written in the form

$$E_0(f;H)=\sum_{1,2}[\varepsilon_0(p_1)\delta_{s_1s_2} - \mu_n H_\alpha(\sigma_\alpha)_{s_1s_2}]f_{s_1s_2}(\mathbf{p}_1)\delta_{\mathbf{p}_1\mathbf{p}_2}, \tag{2}$$

where $\varepsilon_0(p)=p^2/2m$ is the energy of a fermion in the absence of Fermi liquid interactions, m the mass of a free fermion, μ_n the magnetic dipole moment of a fermion, and σ_α are Pauli spin matrices ($\alpha=1,2,3$; the components of vectors in the spin space will be denoted by Greek letters). Expression (1) contains $E_1(f)$, viz., the energy functional possessing the above symmetry properties, which describes NFL interactions:

$$E_1(f)=\frac{1}{2V}\sum_{\mathbf{p}_1\mathbf{p}_2}[f_0(\mathbf{p}_1)F_1(\mathbf{p}_1,\mathbf{p}_2)f_0(\mathbf{p}_2) + f_\alpha(\mathbf{p}_1)F_2(\mathbf{p}_1,\mathbf{p}_2)f_\alpha(\mathbf{p}_2)] \tag{3}$$

(V is the volume occupied by the SFL). In this expression, as well as in (2), we take into account the fact that

$$f_{12}=f_{s_1s_2}(\mathbf{p}_1)\delta_{\mathbf{p}_1\mathbf{p}_2}=[f_0(\mathbf{p}_1)\delta_{s_1s_2}+f_\alpha(\mathbf{p}_1) \times(\sigma_\alpha)_{s_1s_2}]\delta_{\mathbf{p}_1\mathbf{p}_2} \tag{4}$$

in the spatially homogeneous case under investigation. We assume that the superfluid component of the SFL is at rest in thermodynamic equilibrium, i.e., the velocity $v_s=0$ (see Refs. 10–13 for details of the condition of spatial homogeneity in SFL).

Formula (3) for $E_1(f)$ contains NFL functions F_1 and F_2 of interaction between quasiparticles (introduced by Landau),[15,16] which can be simplified in the case of an isotropic Fermi liquid (like ^{3}He). In this case, the functions $F_1(\mathbf{p_1},\mathbf{p_2})$ and $F_2(\mathbf{p_1},\mathbf{p_2})$ for $\mathbf{p}_1$ and $\mathbf{p}_2$ lying on the Fermi surface depend only on the angle θ between $\mathbf{p}_1$ and $\mathbf{p}_2$, and hence can be expanded into a series in Legendre polynomials:

$$F_{1,2}(\theta)=\sum_{l=0}^{\infty}(2l+1)F_{1,2}^{(l)}P_l(\cos\theta).$$

In actual practice, however, the analysis is confined only to a few first terms of this expansion. For example, Schopohl[8] retained only the terms $F_2^{(0)}$ and $F_2^{(2)}$ in the expansion of the exchange interaction function F_2 for quasiparticles (in our notation), putting the remaining exchange NFL Landau amplitudes for ^{3}He equal to zero, i.e., $F_2^{(1)}=0$ for $l>2$.

Finally, the last term $E_2(g,g^+)$ in (1), which satisfies the properties of invariance listed above, can be chosen in a form quadratic in g in the case of singlet as well as triplet pairing in SFL, i.e.,

$$E_2(g,g^+)=\frac{1}{V}\sum_{\mathbf{p}_1\mathbf{p}_2}[g_0^*(\mathbf{p}_1)L_s(\mathbf{p}_1,\mathbf{p}_2)g_0(\mathbf{p}_2) + g_\alpha^*(\mathbf{p}_1)L_t(\mathbf{p}_1,\mathbf{p}_2)g_\alpha(\mathbf{p}_2)], \tag{5}$$

where we take into account the fact that

$$(g_0)_{\mathbf{p}_1\mathbf{p}_2}=g_0(\mathbf{p}_1)\delta_{\mathbf{p}_1,-\mathbf{p}_2},\quad (g_\alpha)_{\mathbf{p}_1\mathbf{p}_2}=g_\alpha(\mathbf{p}_1)\delta_{\mathbf{p}_1,-\mathbf{p}_2},$$

in the spatially homogeneous case. Since $g_{12}=-g_{21}$ for fermions, we have

$$g_0(\mathbf{p})=g_0(-\mathbf{p})=\frac{1}{2}\,\mathrm{Tr}_s g(\mathbf{p})\sigma_2,$$
$$g_\alpha(\mathbf{p})=\frac{1}{2i}\,\mathrm{Tr}_s g(\mathbf{p})\sigma_2\sigma_\alpha=-g_\alpha(-\mathbf{p}). \tag{6}$$

Expression (5) contains abnormal Fermi-liquid (AFL) functions of interaction between quasiparticles (introduced in Refs. 10–13) leading to singlet pairing for $L_s(\mathbf{p_1},\mathbf{p_2})\neq 0$ and to triplet pairing for $L_t(\mathbf{p_1},\mathbf{p_2})\neq 0$.

It should be noted that instead of $E_2(g,g^+)$, we can use in formula (1) another EF, e.g., essentially nonlinear (nonquadratic) functional in abnormal DF (similar to the EF which was used in Ref. 17 for SFL with singlet pairing alone). The choice of a specific EF structure is dictated by the relevant formulation of the problem for SFL. Here (see Introduction) we mainly aim at the derivation of a general expression for the normal and abnormal DF for quasiparticles in SFL with triplet pairing in a magnetic field at temperatures $0<T<T_c$ taking into account Landau exchange amplitudes for NFL. For this purpose, we need not use the explicit form of EF for SFL. The knowledge of the general form of DF allows us to obtain an appropriate system of equations for the vector OP, quasiparticle energy, and effective magnetic field $\mathbf{H}_{\mathrm{eff}}(\mathbf{p})$ for a given choice of EF for the SFL with triplet pairing under consideration. This will be demonstrated in Sec. 3 for an EF of the type (5) with $L_s(\mathbf{p_1},\mathbf{p_2})\equiv 0$.

It was proved in Refs. 10–13 that the distribution functions f_{12} and g_{12} for quasiparticles satisfy the equations (valid for SFL with singlet as well as triplet pairing) which are equivalent to the self-consistent equation, but are more convenient for applications and have the form

$$g=K\tilde{n}X+K(1-n)X, \tag{7}$$

$$f=Kn+X(1-\tilde{n})X^+K, \tag{8}$$

where

$$K=(1+XX^+)^{-1}, \tag{9}$$

$$n=\{\exp[\beta(\xi-X\Delta^+)]+1\}^{-1}\quad(\beta\equiv T^{-1}). \tag{10}$$

Here the matrix X satisfies the equation

$$\xi X+X\tilde{\xi}+\Delta-X\Delta^+X=0,\quad \tilde{X}=-X \tag{11}$$

(the symbol ''tilde'' indicates transposition of the matrix), while the matrix ξ is defined by the formula[10–13,18]

$$\xi_{12}(f;H)=\varepsilon_{12}(f;H)-(\mathbf{v}_n\cdot\mathbf{p}_1+\mu)\delta_{12}, \tag{12}$$

where

$$\varepsilon_{12}(f;H)=\frac{\partial E(f,g,g^+;H)}{\partial f_{21}} =\varepsilon_{\mathbf{p}_1\mathbf{p}_2}(f\,)\delta_{s_1s_2}+[\xi_\beta(f;H)]_{\mathbf{p}_1\mathbf{p}_2}(\sigma_\beta)_{s_1s_2}.$$

In the spatially homogeneous case, we have (in accordance with (4))

$$\xi_{12}=\xi_{s_1s_2}(\mathbf{p}_1)\delta_{\mathbf{p}_1\mathbf{p}_2} =[\xi_0(\mathbf{p}_1)\delta_{s_1s_2}+\xi_\beta(\mathbf{p}_1)(\sigma_\beta)_{s_1s_2}]\delta_{\mathbf{p}_1\mathbf{p}_2}, \tag{13}$$

where

$$\xi_0(\mathbf{p})=\varepsilon(\mathbf{p})-(\mathbf{v}_n\cdot\mathbf{p}+\mu),$$
$$\xi_\beta(\mathbf{p})=\varepsilon_\beta(\mathbf{p})-\mu_n H_\beta\equiv-\mu_n[H_{\mathrm{eff}}(\mathbf{p})]_\beta. \tag{14}$$

Here $\mathbf{v}_n$ is the velocity of the normal component of SFL and μ the chemical potential. Expression (14) contains $\varepsilon(\mathbf{p})=\varepsilon(p)$, viz., the energy of a quasiparticle taking into account nonexchange NFL interaction amplitudes as well as the functions $\varepsilon_\beta(\mathbf{p})$ which take into account the effect of Landau exchange interaction amplitudes for NFL and are associated with the effective magnetic field $\mathbf{H}_{\mathrm{eff}}(\mathbf{p})$ in the bulk of SFL (the functions $\varepsilon_\beta(\mathbf{p})$ were disregarded by Isaev and Peletminskii[14]).

Expressions (10) and (11) contain explicitly the matrix Δ_{12} (which is the OP for SFL). In the spatially homogeneous case and in the presence of only triplet pairing in a SFL $[L_s(\mathbf{p_1},\mathbf{p_2})\equiv 0$; see (5)], this matrix has the form

$$\Delta_{12}=2\frac{\partial E(g,g^+)}{\partial g_{21}^+}=i\Delta_\alpha(\mathbf{p}_1)(\sigma_\alpha\sigma_2)_{s_1s_2}\delta_{\mathbf{p}_1,-\mathbf{p}_2},$$
$$\Delta_\alpha(-\mathbf{p})=-\Delta_\alpha(\mathbf{p}). \tag{15}$$

It should be noted that the choice of the EF $E(g,g^+)$ determines the function $\Delta_\alpha(\mathbf{p})$ but not the spin structure of expression (15) for Δ_{12} which will be used in the following sections.

3. GENERAL FORMULAS FOR QUASIPARTICLE DISTRIBUTION FUNCTIONS AND SELF-CONSISTENT EQUATIONS FOR SFL WITH TRIPLET PAIRING IN A MAGNETIC FIELD

In order to find the general form of the DF g and f from Eqs. (7) and (8), we must first solve Eq. (11) for the matrix X. In accordance with (15), we shall seek the matrix X in the form

$$X_{12}=iX_\alpha(\mathbf{p}_1)(\sigma_\alpha\sigma_2)_{s_1s_2}\delta_{\mathbf{p}_1,-\mathbf{p}_2},\quad X_\alpha(-\mathbf{p})=-X_\alpha(\mathbf{p}) \tag{16}$$

and assume that

$$\xi_\alpha(\mathbf{p})=\xi_\alpha(-\mathbf{p}). \tag{17}$$

Using (11), we obtain the following expression for $\mathbf{X}(\mathbf{p})$:

$$2\Sigma(\mathbf{p})X_\alpha(\mathbf{p})+\Delta_\alpha(\mathbf{p})+\Delta_\alpha^*(\mathbf{p})M(\mathbf{p}) + i2e_{\alpha\beta\gamma}\xi_\beta(\mathbf{p})X_\gamma(\mathbf{p})=0 \tag{18}$$

($e_{\alpha\beta\gamma}$ is an absolutely antisymmetric tensor). We have introduced the quantities

$$\Sigma(\mathbf{p})\equiv z(\mathbf{p})-X_\beta(\mathbf{p})\Delta^*_\beta(\mathbf{p}),$$
$$z(\mathbf{p})\equiv\frac{\xi_0(\mathbf{p})+\xi_0(-\mathbf{p})}{2}=\varepsilon(p)-\mu,\quad M(\mathbf{p})\equiv\mathbf{X}^2(\mathbf{p}). \tag{19}$$

As a result of solution of Eq. (18), we obtain

$$X_\alpha(\mathbf{p})=\frac{\Delta_\beta(\mathbf{p})+\Delta^*_\beta(\mathbf{p})M(\mathbf{p})}{2\Sigma(\mathbf{p})[\xi^2(\mathbf{p})-\Sigma^2(\mathbf{p})]}\times[\,\delta_{\alpha\beta}\Sigma^2(\mathbf{p})-\xi_\beta(\mathbf{p})\xi_\alpha(\mathbf{p})+i\Sigma(\mathbf{p})e_{\alpha\beta\gamma}\xi_\gamma(\mathbf{p})], \tag{20}$$

where, in accordance with (19), we have

$$M=\frac{2\Sigma(\Sigma-z)(\xi^2-\Sigma^2)-\eta(\mathbf{l}\cdot\xi)\Sigma-\Delta_\beta\Delta^*_\gamma(\xi_\beta\xi_\gamma-\delta_{\beta\gamma}\Sigma^2)}{\Delta^*_\lambda\Delta^*_\nu(\xi_\lambda\xi_\nu-\delta_{\lambda\nu}\Sigma^2)}. \tag{21}$$

In order to simplify the form of expression (21), we have omitted the argument $\mathbf{p}$ for all the functions and introduced the real-valued unit vector

$$\mathbf{l}(\mathbf{p})\equiv\frac{i}{\eta(\mathbf{p})}\,[\Delta(\mathbf{p})\times\Delta^*(\mathbf{p})]. \tag{22}$$

It should be noted that the quantity $\eta(\mathbf{p})\equiv|\mathbf{\Delta}(\mathbf{p})\times\mathbf{\Delta}^*(\mathbf{p})|$ differs from zero for nonunitary states of a SFL with triplet pairing.

Proceeding from (19) and taking into account (18), (20), and (21), we can prove that the function $\Sigma^2(\mathbf{p})$ satisfies the quadratic equation whose solutions have the form

$$\Sigma^2_{1,2}(\mathbf{p})=\frac{1}{4}\,[E_+(\mathbf{p})\pm E_-(\mathbf{p})]^2. \tag{23}$$

Here the functions $E_\pm(\mathbf{p})$, which have the physical meaning of the energy of quasiparticles in a SFL (with spin components parallel and antiparallel to the magnetic field), in nonunitary (for $\eta\neq0$) and unitary (for $\eta=0$) phases have the form (cf. formula (4) in Ref. 8)

$$E^2_\pm(\mathbf{p})\equiv\alpha(\mathbf{p})\pm\sqrt{\beta^2(\mathbf{p})+\gamma^2(\mathbf{p})}, \tag{24}$$

where

$$\alpha(\mathbf{p})\equiv|\Delta(\mathbf{p})|^2+z^2(\mathbf{p})+\xi^2(\mathbf{p}),$$
$$\beta^2(\mathbf{p})\equiv[\,\eta(\mathbf{p})1(\mathbf{p})+2z(\mathbf{p})\xi(\mathbf{p})]^2,$$
$$\gamma^2(\mathbf{p})\equiv4|\xi(\mathbf{p})\cdot\Delta(\mathbf{p})|^2.$$

We can now represent the matrix n_{12} [see (10)] in the spatially homogeneous case taking, into account (13), (14) and (16) in the form

$$n_{12}=\delta_{\mathbf{p}_1\mathbf{p}_2}[N^0_{\mathbf{p}_1}\delta_{s_1s_2}+N^\parallel_{\mathbf{p}_1}\hat{h}_\nu(\mathbf{p}_1)(\sigma_\nu)_{s_1s_2}], \tag{25}$$

where

$$N^0_{\mathbf{p}}\equiv\frac{1}{2}\,[N^{(+)}_{\mathbf{p}}+N^{(-)}_{\mathbf{p}}],\quad N^\parallel_{\mathbf{p}}\equiv\frac{1}{2}\,[N^{(+)}_{\mathbf{p}}-N^{(-)}_{\mathbf{p}}], \tag{26}$$

$$N^{(\pm)}_{\mathbf{p}}\equiv\left\{\exp\left[\beta\left(\frac{\xi_0(\mathbf{p})-\xi_0(-\mathbf{p})}{2}+\Sigma(\mathbf{p})\pm\left|\mathbf{h}(\mathbf{p})\right|\right)\right]+1\right\}^{-1}, \tag{27}$$

$$h_\alpha(\mathbf{p})\equiv\xi_\alpha(\mathbf{p})-ie_{\alpha\beta\gamma}X_\beta(\mathbf{p})\Delta^*_\gamma(\mathbf{p}),\quad \hat{h}_\alpha\equiv\frac{h_\alpha}{|\mathbf{h}|}. \tag{28}$$

Under the condition (17), the function h_α possesses the property

$$h_\alpha(-\mathbf{p})=h_\alpha(\mathbf{p}). \tag{29}$$

We also introduce the following quantities:

$$A(\mathbf{p})=\frac{a(\mathbf{p})}{a^2(\mathbf{p})-b^2(\mathbf{p})},\quad \mathbf{B}(\mathbf{p})=-\frac{\mathbf{b}(\mathbf{p})}{a^2(\mathbf{p})-b^2(\mathbf{p})},$$
$$(b\equiv|\mathbf{b}|), \tag{30}$$
$$a(\mathbf{p})\equiv1+X_\alpha(\mathbf{p})X^*_\alpha(\mathbf{p}),\quad b_\alpha(\mathbf{p})\equiv ie_{\alpha\beta\gamma}X_\beta(\mathbf{p})X^*_\gamma(\mathbf{p}).$$

Taking into account formulas (9), (16), and (25)–(30), we obtain the following expression [from (7)] for the abnormal DF for quasiparticles in the spatially homogeneous case (see (6)):

$$\begin{aligned}g_\alpha(\mathbf{p})&=(1-N^0_{\mathbf{p}}-N^0_{-\mathbf{p}})[X_\alpha(\mathbf{p})A(\mathbf{p})-ie_{\alpha\beta\gamma}X_\beta(\mathbf{p})B_\gamma(\mathbf{p})]\\&\quad-(N^\parallel_{\mathbf{p}}+N^\parallel_{-\mathbf{p}})\{-ie_{\alpha\beta\gamma}X_\beta(\mathbf{p})\hat{h}_\gamma(\mathbf{p})A(\mathbf{p})\\&\quad+[X_\alpha(\mathbf{p})B_\beta(\mathbf{p})+X_\beta(\mathbf{p})B_\alpha(\mathbf{p})]\hat{h}_\beta(\mathbf{p})\},\\g_0(\mathbf{p})&=(N^\parallel_{\mathbf{p}}-N^\parallel_{-\mathbf{p}})[e_{\alpha\beta\gamma}X_\alpha(\mathbf{p})B_\beta(\mathbf{p})\hat{h}_\gamma(\mathbf{p})\\&\quad-iA(\mathbf{p})X_\beta(\mathbf{p})\hat{h}_\beta(\mathbf{p})],\end{aligned} \tag{31}$$

while for the normal DF $f_0(\mathbf{p})$ and $f_\alpha(\mathbf{p})$ [see (4)] we obtain from (8)

$$\begin{aligned}f_0(\mathbf{p})&=1-N^0_{-\mathbf{p}}+(N^0_{\mathbf{p}}+N^0_{-\mathbf{p}}-1)A(\mathbf{p})\\&\quad+(N^\parallel_{\mathbf{p}}+N^\parallel_{-\mathbf{p}})B_\alpha(\mathbf{p})\hat{h}_\alpha(\mathbf{p}),\\f_\alpha(\mathbf{p})&=(N^0_{\mathbf{p}}+N^0_{-\mathbf{p}}-1)B_\alpha(\mathbf{p})+N^\parallel_{\mathbf{p}}[A(\mathbf{p})\hat{h}_\alpha(\mathbf{p})\\&\quad-ie_{\alpha\beta\gamma}\hat{h}_\beta(\mathbf{p})B_\gamma(\mathbf{p})]-N^\parallel_{-\mathbf{p}}[W_\alpha(\mathbf{p})A(\mathbf{p})\\&\quad+\{ie_{\alpha\beta\gamma}W_\beta(\mathbf{p})+b_\alpha(\mathbf{p})\hat{h}_\gamma(\mathbf{p})\}B_\gamma(\mathbf{p})],\end{aligned} \tag{32}$$

where

$$W_\alpha(\mathbf{p})\equiv[(a(\mathbf{p})-1)\,\delta_{\alpha\beta}-X_\alpha(\mathbf{p})X^*_\beta(\mathbf{p})-X^*_\alpha(\mathbf{p})X_\beta(\mathbf{p})]\hat{h}_\beta(\mathbf{p}).$$

Thus, formulas (31) and (32) obtained for the normal and abnormal DF for quasiparticles in SFL together with formulas (20) and (21) for $X_\alpha(\mathbf{p})$ and (23) and (24) for $\Sigma(\mathbf{p})$ as well as formulas (26)–(28) and (30) can be used to solve the problem formulated above in the general case of triplet pairing (the spin of a pair $s=1$ and its orbital angular momentum l is an arbitrary odd number) in a magnetic field at temperatures $0<T<T_c$. The distribution functions (31) and (32) are more general than the corresponding results obtained by Isaev and Peletminskii[14] (see also Refs. 12 and 13)

since we have taken into account the effect of the external magnetic field **H** and exchange NFL interactions on SFL [i.e., $\xi(\mathbf{p})\neq 0$; see (17)].

It should be noted that, knowing the form (32) for the DF $f_\alpha(\mathbf{p})$, we can find the magnetization **M** emerging in a SFL in a magnetic field **H** on account of Landau exchange amplitudes for NFL, and hence the magnetic susceptibility $\chi_{\alpha\beta}$ by using the formula

$$M_\alpha=\frac{2\mu_n}{V}\sum_{\mathbf{p}} f_\alpha(\mathbf{p})=\chi_{\alpha\beta}H_\beta. \tag{33}$$

The magnetization and magnetic susceptibility in superfluid phases of ^{3}He at $T\neq 0$ in a magnetic field were determined by Hasegawa[19] using other methods taking into account the p-pairing alone, while Schopohl[8] and Fishman and Sauls[9] obtained these quantities for ^{3}He–B (see Introduction for greater details) taking into account the p- and f-pairing as well as Landau exchange amplitudes for NFL $F_2^{(l)}\neq 0$ for $l=0,2$ and $F_2^{(l)}=0$ for $l>2$ (in our notation; see Sec. 2).

In order to obtain a closed system of equations for the OP $\mathbf{\Delta}(\mathbf{p})$, the quasiparticle energy $\xi_0(\mathbf{p})$ [see (13)], and the effective magnetic field $\mathbf{H}_{\rm eff}(\mathbf{p})$ [see (14)], we must use a specific structure of EF for SFL (see Sec. 2). For this purpose, we choose the EF $E_2(g,g^+)$ in the form (5) for $L_s(\mathbf{p}_1,\mathbf{p}_2)=0$. In view of the odd nature of the DF $g_\alpha(\mathbf{p})$ [see (6)], the AFL interaction function $L_t(\mathbf{p}_1,\mathbf{p}_2)$ possesses the following properties:

$$L_t(-\mathbf{p},\mathbf{p}_1)=-L_t(\mathbf{p},\mathbf{p}_1)=L_t(\mathbf{p},-\mathbf{p}_1)$$

and hence the function $L_t(\mathbf{p},\mathbf{p}_1)=L_t(p,p_1,\cos\theta)$ (θ is the angle between the vectors $\mathbf{p}$ and $\mathbf{p}_1$ lying near the Fermi surface) can be expanded in the Legendre polynomials $P_l(\cos\theta)$, where $l=2n+1$ ($n=0,1,2,\ldots$):

$$L_t(\mathbf{p},\mathbf{p}_1)=\sum_{l=1,3,\ldots}^{\infty}(2l+1)L^{(l)}(p,p_1)P_l(\cos\theta).$$

Taking into account (15) we obtain the following equation for $\Delta_\alpha(\mathbf{p})$ from (5):

$$\Delta_\alpha(\mathbf{p})=\frac{1}{V}\sum_{\mathbf{p}_1} L_t(\mathbf{p},\mathbf{p}_1)g_\alpha(\mathbf{p}_1), \tag{34}$$

where the functions $g_\alpha(\mathbf{p})$ in the general case have the form (31).

Similarly, formulas (12)–(14) and (1)–(3) lead to equations for the energy $\xi_0(\mathbf{p})$ of quasiparticles and for the function $\xi(\mathbf{p})$ associated with the effective magnetic field $\mathbf{H}_{\rm eff}(\mathbf{p})$ in a SFL through formula (14). Namely,

$$\xi_0(\mathbf{p})=\varepsilon_0(p)-(\mathbf{v}_n\cdot\mathbf{p}+\mu)+\frac{1}{2V}\sum_{\mathbf{p}_1} F_1(\mathbf{p},\mathbf{p}_1)f_0(\mathbf{p}_1). \tag{35}$$

$$\xi_\alpha(\mathbf{p})=-\mu_n H_\alpha+\frac{1}{2V}\sum_{\mathbf{p}_1} F_2(\mathbf{p},\mathbf{p}_1)f_\alpha(\mathbf{p}_1), \tag{36}$$

where the DF $f_0(\mathbf{p})$ and $f_\alpha(\mathbf{p})$ satisfy the general formulas (32). While deriving Eqs. (35) and (36), we considered that $F_{1,2}(\mathbf{p},\mathbf{p}_1)=F_{1,2}(\mathbf{p}_1,\mathbf{p})$. It should be noted that the necessary condition for the function $\xi_\alpha(-\mathbf{p})=\xi_\alpha(\mathbf{p})$ to be even [see (17)] is $F_2(\mathbf{p},\mathbf{p}_1)=F_2(-\mathbf{p},\mathbf{p}_1)$, which leads to the expendability of $F_2(\mathbf{p},\mathbf{p}_1)=F_2(p,p_1,\cos\theta)$ in the Legendre polynomials $P_{2n}(\cos\theta)(n=0,1,2,\ldots)$ according to Schopohl.[8]

Thus, Eqs. (34)–(36) (which are valid when the EF is chosen quadratic in DF) together with expressions (31) and (32) for DF allow us to solve the general problem on triplet pairing in SFL (both in unitary and nonunitary phases) in a magnetic field taking into account exchange NFL interactions, and hence generalize the results obtained by Isaev and Peletminskii[14] (as well as the results on triplet pairing in SFL discussed in the reviews by Akhiezer *et al.*[12,13]).

4. DISTRIBUTION FUNCTIONS FOR QUASIPARTICLES FOR UNITARY AND NONUNITARY PHASES OF SFL WITH TRIPLET PAIRING IN A MAGNETIC FIELD

Proceeding from the general formulas (31) and (32), we can find the structure of abnormal and normal DF for quasiparticles in some special cases of SFL with triplet pairing in a magnetic field.

Let us first consider unitary phases of SFL for which $\eta\equiv|\Delta\times\Delta^*|=0$. Let us suppose that $\Delta(\mathbf{p})=\Delta^*(\mathbf{p})$ (the case when $\Delta=-\Delta^*$ is treated similarly). In this case, we obtain from (31)

$$g_\alpha(\mathbf{p})=\frac{1}{2R_{1,2}}\left\{(1-N^0_{\mathbf{p}}-N^0_{-\mathbf{p}})\frac{1}{\Sigma_{1,2}}\times[\xi_\alpha(\xi\cdot\Delta)-\Delta_\alpha\Sigma^2_{1,2}+iz[\xi,\Delta]_\alpha]+(N^{\|}_{\mathbf{p}}+N^{\|}_{-\mathbf{p}})\times\frac{1}{h_{1,2}}[\xi_\alpha(\xi\cdot\Delta)-\Delta_\alpha\Sigma^2_{2,1}+iz[\xi,\Delta]_\alpha]\right\}, \tag{37}$$

$$g_0(\mathbf{p})=(N^{\|}_{\mathbf{p}}-N^{\|}_{-\mathbf{p}})\frac{i(\xi\cdot\Delta)}{2\Sigma_{1,2}h_{1,2}}.$$

Here $N^0_{\pm\mathbf{p}}(\Sigma_{1,2})$ and $N^{\|}_{\pm\mathbf{p}}(\Sigma_{1,2})$ have the form (26) and (27), while the remaining functions, whose abbreviated form contains no argument, depend on **p**. The functions $\Sigma_{1,2}(\mathbf{p})$ are defined by formulas (23); in addition, we introduced in (37) the quantity [see (24)]

$$R_{1,2}(\mathbf{p})=\pm E_+(\mathbf{p})E_-(\mathbf{p})=\pm\sqrt{\alpha^2(\mathbf{p})-\beta^2(\mathbf{p})-\gamma^2(\mathbf{p})}. \tag{38}$$

Expression (37) also contains the function $h_{1,2}(\mathbf{p})\equiv|\mathbf{h}_{1,2}(\mathbf{p})|$ [see (28)] for which the following formula is valid when $\Delta(\mathbf{p})=\Delta^*(\mathbf{p})$:

$$h^2_{1,2}=\Sigma^2_{2,1}-\frac{2(\xi\cdot\Delta)^2(\Sigma^2_{2,1}-\xi^2)}{(\Sigma^2_{1,2}-\xi^2)(\Sigma_{1,2}+z)^2}. \tag{39}$$

Here and in (37) we consider that $\Sigma^2_{1,2}-R_{1,2}=\Sigma^2_{2,1}$ according to (23) and (38).

It should be noted that since $\Sigma_{1,2}(-\mathbf{p})=\Sigma_{1,2}(\mathbf{p})$ [see (19)] and $h_{1,2}(-\mathbf{p})=h_{1,2}(\mathbf{p})$ [see (29)], we have $N^{\|}_{\mathbf{p}}-N^{\|}_{-\mathbf{p}}\neq 0$ only because $\xi_0(\mathbf{p})-\xi_0(-\mathbf{p})=-2\mathbf{p}\cdot\mathbf{v}_n\neq 0$.

It follows from formula (32) for the normal DF with $\Delta(\mathbf{p})=\Delta^*(\mathbf{p})$ that

$$f_0(\mathbf{p})=\frac{1}{2}\,(1+N^0_{\mathbf{p}}-N^0_{-\mathbf{p}})+\frac{z}{2R_{1,2}}\left[(1-N^0_{\mathbf{p}}-N^0_{-\mathbf{p}})\times\frac{\xi^2-\Sigma^2_{1,2}}{\Sigma_{1,2}}+(N^{\|}_{\mathbf{p}}+N^{\|}_{-\mathbf{p}})\,\frac{\xi^2-\Sigma^2_{2,1}}{h_{1,2}}\right],$$

$$f_\alpha(\mathbf{p})=\frac{1}{2R_{1,2}}\left\{(1-N^0_{\mathbf{p}}-N^0_{-\mathbf{p}})\,\frac{1}{\Sigma_{1,2}}\,[\xi_\alpha(z^2-\Sigma^2_{1,2})+\Delta_\alpha(\xi\cdot\Delta)]+(N^{\|}_{\mathbf{p}}+N^{\|}_{-\mathbf{p}})\,\frac{1}{h_{1,2}}\,[\xi_\alpha(z^2-\Sigma^2_{2,1})+\Delta_\alpha(\xi\cdot\Delta)]\right\}+(N^{\|}_{\mathbf{p}}-N^{\|}_{-\mathbf{p}})\,\frac{z\xi_\alpha}{2\Sigma_{1,2}h_{1,2}},\qquad(40)$$

where, as in (37), the argument $\mathbf{p}$ is not written explicitly for all the functions except $N^0_{\pm\mathbf{p}}(\Sigma_{1,2})$ and $N^{\|}_{\pm\mathbf{p}}(\Sigma_{1,2})$. It should be noted that substituting $f_\alpha(\mathbf{p})$ of the form (40) into formula (33), we obtain the magnetization and susceptibility for unitary phases ($\Delta=\Delta^*$) of SFL with triplet pairing in a magnetic field (for ^{3}He–B; see Refs. 8 and 9).

It should also be noted that in the presence of the external magnetic field at temperatures $|T_c-T|\ll T_c$, formulas (37) and (40) lead to expressions for $f^{(0)}_\alpha(\mathbf{p})$ and $g^{(1)}_\alpha(\mathbf{p})$ in the main approximation in perturbation theory in small $\Delta(\mathbf{p})$, which coincide with formulas (27) and (41) from Ref. 18 (for $|\xi|\neq 0$ and $v_n\neq 0$).

In zero external magnetic field [for $\xi(\mathbf{p})=0$] for unitary states of SFL (for $\Delta(\mathbf{p})=\pm\Delta^*(\mathbf{p})$), we obtain from (19)–(21) [cf. (23), (24)]

$$\Sigma^2(\mathbf{p})=E^2(\mathbf{p})=|\Delta(\mathbf{p})|^2+z^2(\mathbf{p}),\qquad(41)$$

while formulas (34) and (37) lead to the following equation for $\Delta_\alpha(\mathbf{p})$:

$$\Delta_\alpha(\mathbf{p})=\frac{1}{2V}\sum_{\mathbf{p}_1}L_t(\mathbf{p},\mathbf{p}_1)\,\frac{\Delta_\alpha(\mathbf{p}_1)}{E(\mathbf{p}_1)}\,(N_{\mathbf{p}_1}+N_{-\mathbf{p}_1}-1),\qquad(42)$$

where

$$N_{\mathbf{p}}=\left\{\exp\left[\beta\left(E(\mathbf{p})+\frac{\xi_0(\mathbf{p})-\xi_0(-\mathbf{p})}{2}\right)\right]+1\right\}^{-1}.$$

Proceeding from (35) and taking into account (40) for $f_0(\mathbf{p})$, we obtain the equation for $\xi_0(\mathbf{p})$:

$$\xi_0(\mathbf{p})=\varepsilon_0(p)-(\mathbf{v}_n\cdot\mathbf{p}+\mu)+\frac{1}{4V}\sum_{\mathbf{p}_1}\frac{F_1(\mathbf{p},\mathbf{p}_1)}{E(\mathbf{p}_1)}\,\{[E(\mathbf{p}_1)+z(\mathbf{p}_1)]N_{\mathbf{p}_1}+[E(\mathbf{p}_1)-z(\mathbf{p}_1)](1-N_{-\mathbf{p}_1})\}.\qquad(43)$$

In other words, expressions (42) and (43) are in accord with the corresponding expressions for unitary states in SFL obtained in Refs. 12–14 [cf. Eqs. (3.47) in Ref. 12].

Let us now consider nonunitary states of SFL with triplet pairing in a magnetic field. For simplicity, we confine our analysis to the case when $\boldsymbol{\xi}=\xi\mathbf{l}$ [see formulas (14) and (22)]. In this case, it follows from (20), (21), and (28) that

$$h_\alpha(\mathbf{p})=h_{1,2}(\mathbf{p})l_\alpha(\mathbf{p})=\frac{l_\alpha(\mathbf{p})}{2\Sigma_{1,2}(\mathbf{p})}\,[\eta(\mathbf{p})+2\xi(\mathbf{p})z(\mathbf{p})],\qquad(44)$$

where

$$\Sigma_{1,2}=\frac{1}{2}\,(\sqrt{|\Delta|^2+(z+\xi)^2+\eta}\pm\sqrt{|\Delta|^2+(z-\xi)^2-\eta}).\qquad(45)$$

Ultimately, the general expressions (31) and (32) lead to the following expressions for the DF of quasiparticles for $\boldsymbol{\xi}=\xi\mathbf{l}[g_0(\mathbf{p})=0]$:

$$g_\alpha(\mathbf{p})=\frac{1-N^0_{\mathbf{p}}(\Sigma_1)-N^0_{-\mathbf{p}}(\Sigma_1)}{2R_1}\,(ih_1[1,\Delta]_\alpha-\Sigma_1\Delta_\alpha)+\frac{1-N^0_{\mathbf{p}}(\Sigma_2)-N^0_{-\mathbf{p}}(\Sigma_2)}{2R_2}\,(ih_2[1,\Delta]_\alpha-\Sigma_2\Delta_\alpha),\qquad(46)$$

$$f_0(\mathbf{p})=\frac{1}{2}\,(1+N^0_{\mathbf{p}}-N^0_{-\mathbf{p}})+[1-N^0_{\mathbf{p}}(\Sigma_1)-N^0_{-\mathbf{p}}(\Sigma_1)]\,\frac{\xi h_1-z\Sigma_1}{2R_1}+[1-N^0_{\mathbf{p}}(\Sigma_2)-N^0_{-\mathbf{p}}(\Sigma_2)]\,\frac{\xi h_2-z\Sigma_2}{2R_2},\qquad(47)$$

$$f_\alpha(\mathbf{p})=\frac{l_\alpha}{2}\left\{N^{\|}_{\mathbf{p}}-N^{\|}_{-\mathbf{p}}+[1-N^0_{\mathbf{p}}(\Sigma_1)-N^0_{-\mathbf{p}}(\Sigma_1)]\,\frac{zh_1-\xi\Sigma_1}{R_1}+[1-N^0_{\mathbf{p}}(\Sigma_2)-N^0_{-\mathbf{p}}(\Sigma_2)]\,\frac{zh_2-\xi\Sigma_2}{R_2}\right\}.\qquad(48)$$

For brevity, the argument $\mathbf{p}$ is not written in formulas (45)–(48) for all the functions (except $N^0_{\pm\mathbf{p}}$ and $N^{\|}_{\pm\mathbf{p}}$). We have also taken into account the fact that

$$N^0_{\mathbf{p}}(\Sigma_1)-N^0_{-\mathbf{p}}(\Sigma_1)=N^0_{\mathbf{p}}(\Sigma_2)-N^0_{-\mathbf{p}}(\Sigma_2),\qquad N^{\|}_{\mathbf{p}}(\Sigma_1)-N^{\|}_{-\mathbf{p}}(\Sigma_1)=N^{\|}_{\mathbf{p}}(\Sigma_2)-N^{\|}_{-\mathbf{p}}(\Sigma_2).\qquad(49)$$

The functions $R_{1,2}(\mathbf{p})$ are now defined by the formulas

$$R_{1,2}(\mathbf{p})=\pm R(\mathbf{p}),\qquad R(\mathbf{p})=\sqrt{[|\Delta|^2+(z+\xi)^2+\eta[|\Delta|^2+(z-\xi)^2-\eta]}.\qquad(50)$$

Formulas (46)–(48) for DF together with Eqs. (34)–(36) generalize the results obtained in Ref. 14 for nonunitary phases of SFL to the case when the magnetic field $\mathbf{H}$ is applied, and exchange NFL interactions are present (provided that $\boldsymbol{\xi}=\xi\mathbf{l}$) and are in accord with the results obtained in Ref. 14 for $\xi=0$ and $\eta\neq 0$.

It should be noted that for $\mathbf{H}_{\text{eff}}\|\mathbf{H}$ for $F^{(l)}_2=0$ ($l\geqslant 2$; (see Ref. 8), and the SFL under investigation with $\mathbf{H}_{\text{eff}}\|\mathbf{l}$ [see (14)] can be reduced, for example, in the case of p-wave pairing, to the nonunitary $2D$-phase (planar phase) of ^{3}He

(existence of the unitary $2D$-phase in superfluid ^{3}He was predicted in Refs. 1, 5, and 20) and also to A_1- and A_2-phases of ^{3}He (see Ref. 6 and Chapters 1 and 2 in Ref. 7). However, it may be important to take into account the strong coupling effects in ^{3}He to describe the last two phases.[21–24]

5. CONCLUSION

The main result of this research is the derivation of the general formulas (31) and (32) (which are valid at temperatures $0<T<T_c$) for DF of quasiparticles in SFL with triplet pairing (the spin of a pair $s=1$ and its orbital angular momentum l is an arbitrary odd number) in a static uniform magnetic field taking into account exchange NFL interactions. Formulas (31) and (32) together with Eqs. (34)–(36) (for the OP, quasiparticle energy, and effective magnetic field in SFL) derived with the help of EF quadratic in DF make it possible to solve the general problem on triplet pairing in SFL (both in unitary and nonunitary phases) in a magnetic field. Formulas (32) and (33) can be used for determining the magnetization and magnetic susceptibility of SFL.

It should be emphasized that formulas (31) and (32) for DF lead to a complete system of equations (similar to Eqs. (34)–(36)) in the case of a different choice of EF for SFL in a magnetic field also. For example, we can use an EF which is essentially nonlinear (nonquadratic) in abnormal DF for SFL with triplet pairing. This case is interesting and can be the subject of independent investigations in connection with so-called strong coupling effects[21–24] manifested in SFL of the type of ^{3}He under comparatively high pressures.

The author is grateful to S. V. Peletminskii for his interest in this work and for fruitful discussions of the results.

This research was partly financed by the Ukrainian State Foundation for Fundamental Studies (Project No. 2.4/378).

*E-mail: antarasov@kipt.kharkov.ua

[1] A. J. Leggett, Rev. Mod. Phys. **47**, 331 (1975).
[2] V. P. Mineev, Usp. Fiz. Nauk **139**, 303 (1983) [Sov. Phys. Usp. **26**, 160 (1983)].
[3] J. W. Serene and D. Rainer, Phys. Rep. **101**, 221 (1983).
[4] D. M. Sedrakyan and K. M. Shakhabasyan, Usp. Fiz. Nauk **161**, 3 (1991) [Sov. Phys. Usp. **34**, 555 (1991)].
[5] P. N. Brusov and V. N. Popov, *Superfluidity and Collective Properties of Quantum Liquids* [in Russian], Nauka, Moscow (1988).
[6] D. Vollhardt and P. Wölfle, *The Superfluid Phases of Helium 3*, Taylor and Francis, London (1990).
[7] W. P. Halperin and L. P. Pitaevskii (eds.), *Helium Three*, North-Holland, Amsterdam (1990).
[8] N. Schopohl, J. Low Temp. Phys. **49**, 347 (1982).
[9] R. S. Fishman and J. A. Sauls, Phys. Rev. B **33**, 6068 (1986).
[10] V. V. Krasil'nikov, S. V. Peletminskii, A. A. Yatsenko, and A. A. Rozhkov, Fiz. Elem. Chast. At. Yadra **19**, 1440 (1988) [*sic*].
[11] V. V. Krasil'nikov, S. V. Peletminskij, and A. A. Yatsenko, Physica A **162**, 513 (1990).
[12] A. I. Akhiezer, V. V. Krasil'nikov, S. V. Peletminskii, and A. A. Yatsenko, Usp. Fiz. Nauk **163**, 1 (1993) [Phys. Usp. **36**, 5 (1993)].
[13] A. I. Akhiezer, V. V. Krasil'nikov, S. V. Peletminskii, and A. A. Yatsenko, Phys. Rep. **245**, 1 (1994).
[14] A. A. Isaev and S. V. Peletminskii, Ukr. Fiz. Zh. **37**, 952 (1992).
[15] D. Pines and Ph. Noziere, *The Theory of Quantum Liquids*, New York (1967).
[16] E. M. Lifshitz and L. P. Pitaevskii, *Statistical Physics. Part 2. The Theory of Condensed State* [in Russian], Nauka, Moscow (1978).
[17] A. P. Ivashin, V. V. Krasil'nikov, and S. V. Peletminskii, Fiz. Nizk. Temp. **19**, 1295 (1993) [Low Temp. Phys. **19**, 917 (1993)].
[18] A. N. Tarasov, Fiz. Nizk. Temp. **21**, 24 (1995) [Low Temp. Phys. **21**, 17 (1995)].
[19] Y. Hasegawa, Prog. Theor. Phys. **63**, 1040 (1980).
[20] V. Alonso and V. N. Popov, Zh. Éksp. Teor. Fiz. **73**, 1445 (1977) [Sov. Phys. JETP **46**, 760 (1977)].
[21] P. W. Anderson and W. F. Brinkman, Phys. Rev. Lett. **30**, 1108 (1973).
[22] W. F. Brinkman, J. W. Serene, and P. W. Anderson, Phys. Rev. A **10**, 2386 (1974).
[23] J. W. Serene and D. Rainer, in *Quantum Fluids and Solids* (ed. by S. B. Trickey, E. D. Adams, and J. W. Dufty), Plenum, New York (1977).
[24] J. A. Sauls and J. W. Serene, Phys. Rev. B **24**, 183 (1981).

Translated by R. S. Wadhwa

SUPERCONDUCTIVITY, HIGH-TEMPERATURE SUPERCONDUCTIVITY

Electrical properties of a normal contact to HTSC Josephson media

V. I. Omelchenko and A. A. Sukhanov

*Institute of Radioengineering and Electronics, Russian Academy of Sciences, 141120 Fryazino, Moscow distr., Russia**

(Submitted July 14, 1997; revised November 12, 1997)
Fiz. Nizk. Temp. **24**, 438–444 (May 1998)

Electrical properties of normal metal contacts to percolation Josephson HTSC systems are studied by computer simulation. The current and voltage distributions, current–voltage characteristics (IVC), and temperature dependences $R_c(T)$ of the resistance of the Josephson network with a limited contact are calculated. It is shown that macroheterogeneity of current distribution leads to broadening of the IVC and $R_c(T)$ dependences of the contact in comparison with the bulk characteristics. In the vicinity of critical currents and temperatures, the contact IVC and $R_c(T)$ obey the ''3/2'' law. A peak on the current and temperature dependences of the spreading resistance is observed. The applicability of the effective medium model for describing contact characteristics of the Josephson network is substantiated. The computer simulation results are in accord with experimental temperature dependences of the contact resistance. © *1998 American Institute of Physics.* [S1063-777X(98)00305-3]

1. INTRODUCTION

It is well known that ceramics and (as a rule) HTSC films possess strongly heterogeneous granular structure in which individual superconducting granules are connected through weak links. The concept of such a granular system as a percolation Josephson medium with a wide spread of parameters of Josephson junctions is generally accepted at present.[1]

Bulk electrical and magnetic characteristics of such HTSC media were investigated by several authors[1–3] on the basis of percolation theory and computer calculations. For example, the bulk current–voltage characteristics (IVC) for model Josephson systems and magnetic-field dependences of IVC and critical current were calculated in Refs. 2 and 3. It was proved that, in accordance with experimental data, the bulk IVC have the form $V\sim(I-I_c)^m$, $m=1.5$–2.1 for currents I close to critical current I_c, and the critical current $I_c\propto B$ in strong magnetic fields B.

We believe that an analysis of the characteristics of normal contacts to percolation HTS media is interesting as such and, besides, is important in connection with experimental investigation of contact IVC and temperature dependences $R_c(T)$ of the contact resistance.[4–7]

Obviously, the characteristics of ''point'' contacts must differ significantly from the corresponding ''bulk'' characteristics of a Josephon medium in view of macroheterogeneity of the current distribution in the contact region. Among other things, the former characteristics display considerable broadening of IVC and temperature dependence of resistance (TDR), strong effect of transport current and magnetic field on the $R_c(T)$ dependence, and a large spread in their critical parameters and characteristics.

The results of computer simulation of IVC and TDR for a model Josephson medium, viz., a square network of weak SC bonds with a limited (''point'') contact are presented below.

2. COMPUTATIONAL METHOD

The computation of electrophysical parameters of disordered systems of weak links is a very complicated problem since it involves taking into account the spread in critical currents as well as phase correlation of the order parameters of adjacent links. However, the problem can be simplified significantly when the phase coherence is broken, for example, due to ''thermal'' or ''magnetic field-induced'' fluctuations.[1,8]

''Thermal'' fluctuations destroy the coherent state (CS) for $kT\gg E_c=\Phi_0 i_c/(2\pi)$, where E_c is the binding energy, i_c the critical current of Josephson junctions, and $\Phi_0=2\times10^{-15}$ V·s the magnetic flux quantum. This condition is satisfied for $T\gg0.25$ K for Josephson bonds with $i_c\leqslant10^{-8}$ A, for example junctions with critical current density $j_c\leqslant10$ A/cm^2 and contact area $S\leqslant10^{-9}$ cm^2.

''Magnetic field-induced'' fluctuations disturb the CS in external fields with induction $B\gg\Phi_0/a^2$, where a is the granule size, as well as in ''intrinsic'' fields when the condition $2\pi L i_c\gg\Phi_0$ is satisfied, where the inductance $L=\mu_0 a l_n$, l_n being the geometrical factor weakly depending on a. The former condition can be satisfied in systems with large granules of size $a>6$ μm in the Earth field $B_E=7\times10^{-5}$ T, while the second condition is observed in systems with large critical currents $i_c\gg\Phi_0/(2\pi a\mu_0 l_n)\approx10^{-5}$ A for $a=10^{-5}$ m and $l_n=2$. It should be noted that $i_c\approx10^{-9}$–10^{-2} A in real granular HTSC materials.

Thus, there exists a wide range of critical currents, temperatures, and external magnetic field in which no phase cor-

relation of the order parameter in a system of weak links takes place, and the problem of determining the resistance of the system is reduced to the calculation of current and voltage distributions in a network of independent nonlinear resistors.[1,8] This approach was used by us for calculating contact characteristics.

We considered an $N\times N$ square network of superconducting weak links with a wide spread of critical currents i_c as a simple model of a granular superconductor. We chose a chain of N_c sites on a network face, which formed a ''point'' contact to the HTSC sample, assuming that the links of this face that do not belong to the contact are ruptured.

The electrical properties of a Josephson medium (JM), including the IVC and TDR in the bulk and in the contact region, are determined by individual IVC $v_n(i_n, i_{cn})$ of weak links, where v_n is the voltage across the nth link, temperature dependences $i_{cn}(T, i_{cn0})$ of critical currents, and the function $f(i_{cn0})$ of distribution of weak bonds over critical currents at $T=0$.

In accordance with Refs. 1 and 2, the IVC of weak links were defined by the following expressions typical of Josephson junctions:

$$v_n=\begin{cases}0, & \text{for } i_n\leqslant i_{cn}\\ \rho_0\sqrt{i_n^2-i_{cn}^2}, & \text{for } i_n>i_{cn}\end{cases}, \tag{1}$$

while the temperature dependences $i_{cn}(T)$ of critical currents were specified in a form typical of insulating Josephson junctions:

$$i_{cn}(T)=i_{cn0}(1-T/T_c)^2. \tag{2}$$

The function $f(i_{cn0})$ of distribution of weak links over critical currents was regarded as constant on the interval $[0, i_{cm}]$: $f=1/i_{cm}$. For convenience of calculations, the unit of current density was chosen equal to the maximum critical current in the system of weak links; i.e., $i_{cm}=1$; it was also assumed that $\rho_0=1$.[1)]

Contact and bulk IVC and temperature dependences of resistance were calculated mainly for a network of the size $N\times N=50\times 50$ and for a contact of the size $N_c=7$. The choice of the values of $N=50$ was dictated by the condition of small spread in ''bulk'' characteristics from realization to realization, while the size N_c of the contact was determined by the condition $1\ll N_c\ll N$.

The calculations involved the numerical solution of the Kirchhoff equations consecutively for each elementary loop of the network taking into account the values of currents in links, determined at the previous step for the neighboring loop. The computational procedure consisted of the following steps:

(1) A random realization of bonds in critical currents i_{cn0} was specified.
(2) For each temperature T, the critical currents i_{cn} were calculated by formula (2), and transition temperature for all links was assumed to be $T_c=100$ K.
(3) The lower face of the network and the contact were assumed to be equipotential surfaces.
(4) The initial distribution of currents flowing through the network links was chosen in the form of current distribution in a network of unit resistors. For such a distribution, the Kirchhoff first law is observed for each node of the network: $\Sigma_{l=1}^4 i_{lm}=0$, where l is the number of the link of the mth junction.
(5) The Kirchhoff nonlinear equation for voltages

$$\sum_{k=1}^{4} v_k(i_k\pm\Delta i)=0,$$

where v_k is the voltage across the kth link of an elementary loop and i_k the value of its current determined earlier, was solved numerically in the current variation Δi for each elementary loop, viz., a square formed by four weak links, consecutively, starting from the chosen loop. The sign of the current increment Δi was chosen so that the current balance at junctions was not violated.

Similar calculations for an adjacent loop were made taking into account new values of currents in their common link.

After the calculations were made for all from $N\times N$ elementary loops of the network, the above procedure was repeated from the very beginning.
(6) The calculations were terminated when the variation of currents in the network became relatively small, i.e., for $\Sigma_n|\Delta i_n/i_n|<10^{-5}$.

In addition, another criterion for the termination of iterative procedure was also used. It was based on the variational principle proposed in Refs. 1 and 2, according to which the distribution of currents and voltages in a nonlinear system consisting of elements with individual IVC $v_n=v_n(i,i_{cn})$ corresponds to the minimum of the functional

$$W=\sum_n \int_0^{i_n} v_n(i, i_{cn})di, \tag{3}$$

where the summation is carried out over all n elements of the network, and i_n are the values of currents in links. Accordingly, functional (3) was calculated after each iteration step described in item 5, and the iterative procedure was terminated either after the attainment of its minimum value, or at a low rate of its variation $\Delta W/W<10^{-5}$.

It was pointed out by Gurevich *et al.*[2] that the value of functional (3) calculated for one loop (and hence its total value also) decreases as a result of such a recalculation of currents.

It should be noted that the quantity W has the meaning of dissipated power only in the case of a linear system.
(7) We calculated the potential difference V between the contact and the lower face of the network as well as value of ''integral'' contact resistance $R_c=V/I$, where I is the total current flowing through the network. It should be noted that in order to verify the obtained results, the calculations were also made for various other initial distributions of currents for which the balance of currents at the junctions is preserved. The obtained distributions of corresponding values of currents and potentials proved to be identical, which indicates the uniqueness of the obtained solutions.

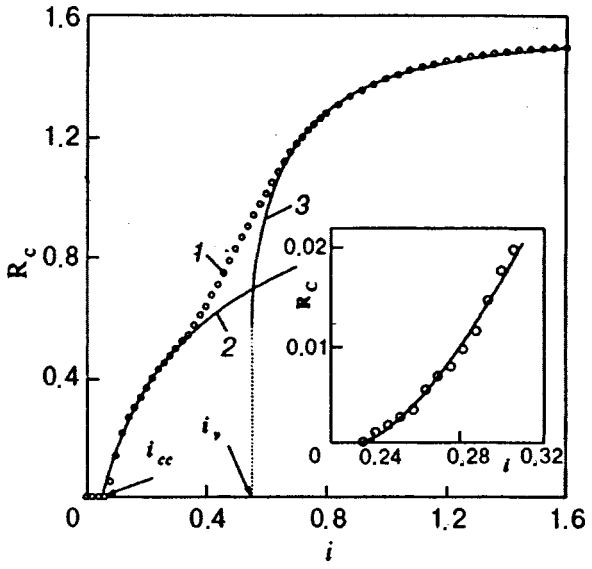

FIG. 1. Current dependence of normalized contact resistance $R_c(i)$ at $T=0$: calculated dependence $R_c(i)$ (curve *1*), approximations of the low- and high-temperature segments of curve *1* by functions (6) and (7) (curves *2* and *3*), $i=I/N$ is the average current in the links, I the normalized current, $N=50$, and the contact size $N_c=7$. The inset shows the initial segment of the $R_c(i)$ dependence for a model medium with $N=85$, $N_c=35$, and the curve describing function (8).

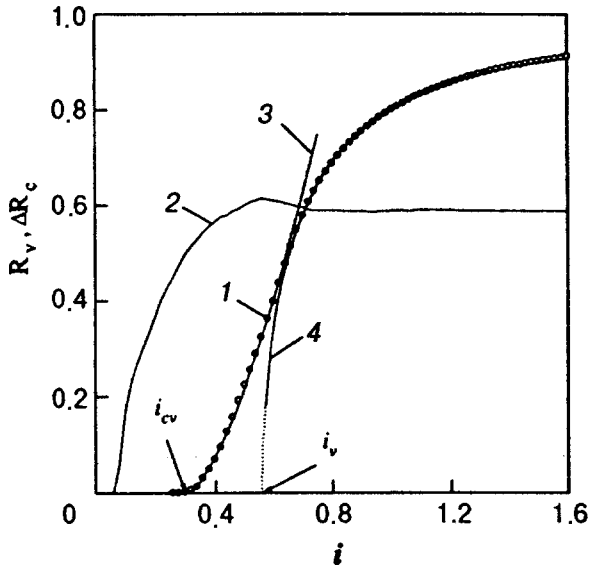

FIG. 2. Current dependences of volume resistance $R_v(i)$ (curve *1*) and spreading resistance $\Delta R_c(i)$ (curve *2*) at $T=0$. Curves *3* and *4* describe the functions (4) and (5).

(8) The procedure was repeated for various currents and temperatures for determining IVC and TDR.

3. DISCUSSION OF COMPUTATIONAL RESULTS

Current–voltage characteristics

For better visualization, curve *1* in Fig. 1 shows a typical IVC of a structure with a ''point'' contact ($N_c=7$) calculated at $T=0$ in the form of the dependence $R_c(i)$, where R_c is the normalized contact resistance, $i=I/N$ the average current in the system of links, I the normalized total current, and $N=50$ the ''linear size'' of the network. It can be seen that the $R_c(i)$ dependence has two segments with sublinear increase in current for $i \geqslant i_{cc} \approx 0.07$ and $i \geqslant i_v \approx 0.56$ separated by a region of inflection.

Figure 2 shows for comparison the current dependences of the volume resistance $R_v(i)$ (curve *1*) and the spreading resistance equal to the difference between the total resistance of the system with a limited contact and the volume resistance, $\Delta R_c(i)=R_c(i)-R_v(i)$ (curve *2*). The dependence $R_v(i)$ has a segment of sharp increase in resistance and tends to saturation for $i>3i_v$. Thus, it is clear that the segment corresponding to sharp increase in the resistance of the medium with a ''point'' contact in the range of ''small'' currents is determined by the spreading region, while the second segment with $i \geqslant i_{cv}$ is determined by the volume of the Josephson network.

It should be noted that the current dependence of spreading resistance $\Delta R_c(i)$ has a typical peak in the range of current $i \approx i_v \approx 0.56$.

The initial segment of the dependence $R_v(i)(i_{cv}<i<2i_{cv})$ is approximated by the power function

$$R_v=k_1(i-i_{cv})^{3/2}, \quad k_1=2.55, \quad i_{cv}=0.3 \tag{4}$$

(curve *3* in Fig. 2), which is associated in Refs. 1–3 with the percolation type of conductivity near the percolation threshold. In the region of ''high'' current densities ($i>i_v$), the volume IVC is correctly described by the effective medium model according to which the characteristics of a JM with a random distribution of critical currents coincide with the characteristics of a homogeneous medium with the averaged value of critical current:

$$R_v=R_2\sqrt{1-(i_v/i)^2}, \quad i>0.6, \tag{5}$$

where $i_v=0.56$, and the value of $R_2=0.98$ is determined by the size of the model network containing 49 longitudinal and 50 transverse links. Dependence (5) is shown in Fig. 2 (curve *4*).

The current dependence of the resistance of a system with a ''point'' contact (see Fig. 1) is also described correctly by the effective medium model and can be approximated by the function

$$R_c=\frac{1}{I}\int_{r_c}^{\infty}\sqrt{(I/\pi r)^2-i_{cc}^2}\,dr$$

$$=\frac{1}{\pi}\left[\ln\left(\frac{ai}{i_{cc}}+\sqrt{(ai/i_{cc})^2-1}\right)-\sqrt{1-(i_{cc}/ai)^2}\right],$$

$$i<i_v, \tag{6}$$

where the total current $I=iN$, the contact radius $r_c=N_c/\pi$, $a=N/N_c(N=50, N_c=7)$, while the effective critical current $i_{cc}=0.07$, and

$$R=R_{c0}+R_2\sqrt{1-(i_{cv}/i)^2}, \quad i>i_v, \tag{7}$$

where $R_{c0}\approx 0.56$, $R_2=0.98$, and $i_v=0.54$.

Formula (6) describes the spreading resistance of a semicircular contact to a conducting half-plane with a nonlinear resistivity $\rho=[1-(i_c/i)^2]^{1/2}$, while expression (7) describes the volume contribution to the resistance of a Josephson me-

dium with a ''point'' contact, for which R_{c0} is a correction to the contact resistance value, which weakly depends on current for $i > i_v$. The critical currents i_{cv} and i_{cc} appear in (6) and (7) as fitting parameters.

For large contacts ($N_c > 20$), the contact IVC $R_c(i)$ for $i - i_{cc} \ll i_{cc}$ obeys the ''3/2'' law (see the inset to Fig. 1):

$$R_c = k(i - i_{cc})^{3/2}, \quad k = 1.05, \quad i_{cc} = 0.235. \tag{8}$$

This dependence follows from the effective medium model for two- and three-dimensional cases and can be explained physically by the fact that the size of the resistive region near the threshold increases linearly with $i - i_c$, while its resistivity increases in proportion to $(i - i_c)^{1/2}$. In our opinion, the ''3/2'' law can be of the same nature for volume IVC of JM near the percolation threshold also.

The emergence of a peak on the current dependence of spreading resistance $\Delta R_c(i)$ is due to the macroheterogeneity of the current distribution and nonlinearity of the Josephson medium and has a simple physical meaning. Let us suppose, for example, that all links are characterized by the same critical current i_c for which their resistance changes abruptly from 0 to 1. In view of spreading, local currents having the mean value $i = i_c - \delta i (\delta i \to 0)$ become stronger than the critical current virtually in all longitudinal current-carrying links of the percolation network (down to the last layer), and hence they all are already in the resistive state. At the same time, the volume resistance is still equal to zero, but increases abruptly for $i = i_c + \delta i$. As a result, the difference $\Delta R_c = R_c - R_v$ decreases abruptly at $i = i_c$ by $R_{vm} = 1$, i.e., has a peak at $i = i_c$.

Temperature dependences of resistance

Temperature dependences $R_c(T)$ of the contact resistance of a model HTSC medium are shown in Fig. 3 for various current densities and in Fig. 4 for volume resistance $R_v(T)$ for $i = 0.02$.

The dependence $R_v(T)$ (curve *1* in Fig. 4) obeys the ''3/2'' law ($R_v(T) \sim (T - T_{cv})^{3/2}$) near the temperature of volume resistive transition $T_{cv} \approx T_{c0}(1 - 1.8i^{1/2})$ ($T_{c0} = 100$ K), while at high temperatures ($T > T_v$) it is successfully described by the effective medium model, i.e., is determined by expressions (5) for $R_v(i, i_v)$ and (2) for $i_v \equiv i_v(T)$ with the effective critical current $i_{v0} = 0.51$ which is close to the average value $i_{c0} = 0.5$ of the critical current of the network links, and attains saturation at $T > T_{c0}(1 - 0.5i^{1/2})$.

The temperature dependences $R_c(T)$ of contact resistance (see Fig. 3) have two clearly distinguishable segments. At relatively high temperatures ($T > T_v$), the shape of the $R_c(T)$ curves is similar to that of temperature dependences of volume resistance. An analysis of distributions of potential and current density shows that this is associated with the spreading of the contact region having normal conductivity to the boundaries of the model network at high temperatures, and hence the $R_c(T)$ curves at these temperatures reflect volume properties of the network rather than its contact properties.

At $T_{cc} < T < T_v$, the $R_c(T)$ curves have low-temperature ''tails'' whose length increases with current. A comparison

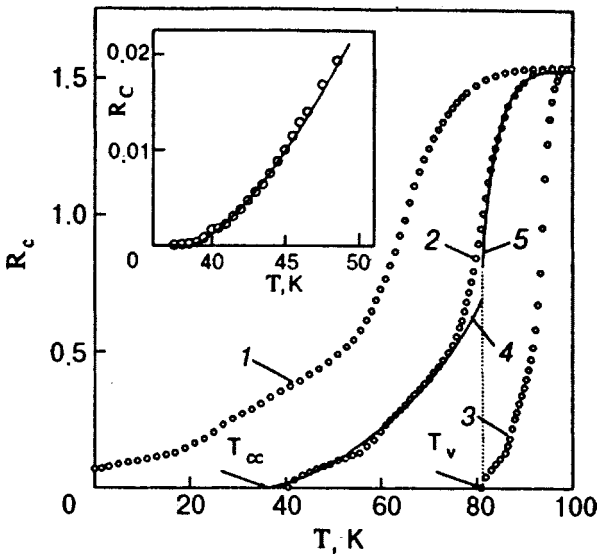

FIG. 3. Temperature dependences of the contact resistance $R_c(T)$ for various average current i in the links: 0.07 (curve *1*), 0.02 (curve *2*), and 0.002 (curve *3*); curve *4* approximates the low-temperature segment of curve *2* by the functions (5) and (2), while curve *5* is the approximation of the high-temperature segment of curve *2* by the functions (6) and (2). The inset shows the initial segment of the $R_c(T)$ dependence for a model medium with $N = 85$, $N_c = 35$, and the curve describing the function (9).

of the numerically calculated dependence $R_c(T)$ for $i = 0.02$ (curve *2* in Fig. 3) with curve *4* approximating its low-temperature segment by the functions (6) and (2) shows that the low-temperature segment of the $R_c(T)$ dependence is correctly described by the effective medium model.

In the temperature range $(T - T_{cc}) \ll (T_{c0} - T_{cc})$ close to the threshold, the $R_c(T)$ dependence can be written in the form

$$R_c(T) = R_3\left(\frac{T - T_{cc}}{T_{c0} - T_{cc}}\right)^{3/2}, \tag{9}$$

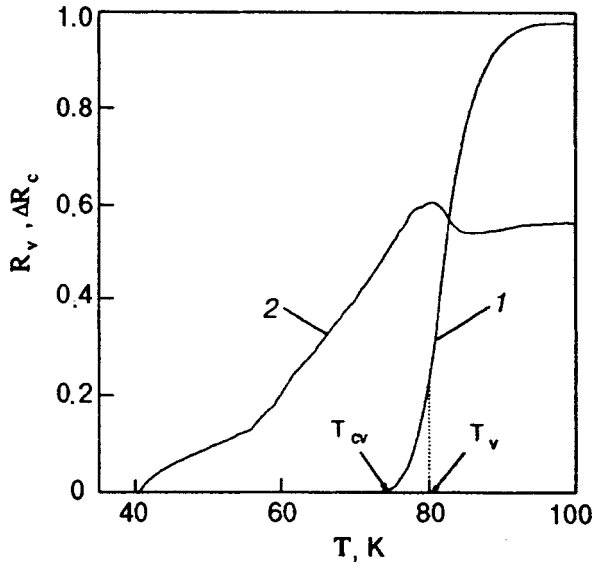

FIG. 4. Temperature dependences of the volume resistance $R_v(T)$ (curve *1*) and spreading resistance $\Delta R_c(T)$ (curve *2*) for $i = 0.02$.

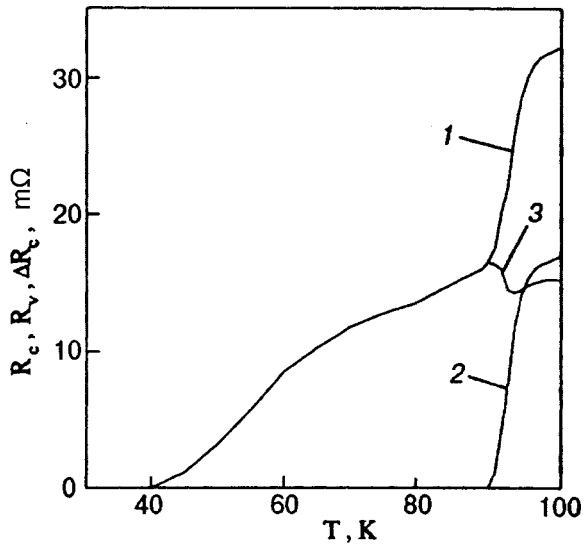

FIG. 5. Temperature dependences of the breakjunction resistance ((curve *1*), volume resistance (curve *2*) and spreading resistance (curve *3*) for 1–2–3 ceramics. The current $I=1$ mA.

where $R_3=0.3$, $T_{cc}(i)\approx T_{c0}(1-(i/i_{cc}))$, $i_{cc}=0.07$ ($T_{cc}=38.5$ K). Dependence (9) is presented in the inset to Fig. 3.

It should be emphasized that the temperature dependence of spreading resistance $\Delta R_c(T)$ has a peak at $T=T_v$ (curve *2* in Fig. 4), whose nature is the same as for the peak on the $\Delta R_c(i)$ dependence.

We obtained an experimental confirmation of the basic predicted peculiarities of contact resistive characteristics mainly from an analysis of temperature dependences of the resistance of normal contacts to $Y_1Ba_2Cu_3O_{7-x}$ ceramics. The shift and broadening of the resistive transition in temperature and their current dependences were studied by us in detail earlier.[7]

The ''3/2'' law was observed by us for low-resistivity Au contacts in 1–2–3 ceramics, as well as for junctions obtained after breaking the ceramics (curves *1* and *2* in Fig. 5).

A peak on the temperature dependence of the spreading resistance was also observed for breakjunctions (curve *1* in Fig. 5) which can be regarded as a model system for studying spreading effects in HTSC media.

CONCLUSIONS

Using computer simulations of normal contacts to a Josephson medium, we proved that

(1) contact IVC and TDR are broadened in the vicinity of critical current and superconducting transition temperature of the system;
(2) the IVC and TDR obey the ''3/2'' law near the percolation threshold;
(3) in the region of critical currents and temperatures corresponding to superconducting transition in the bulk, the spreading resistance has a peak due to macroheterogeneity of current distribution in the nonlinear medium.

The applicability of the effective medium model for describing spreading effects in HTSC media is substantiated.

The obtained results make it possible to explain experimental data on temperature dependences of contact resistance, including the broadening and shift of the SC transition and the peak on the temperature dependences of spreading resistance of granular Y-based HTSC ceramics.

*E-mail: aas195@ire216.msk.su

[1)]The values of resistance given below are normalized to the resistance of a solitary link, while all currents are normalized to the maximum critical current i_{cm} in the system of links.

[1] E. Z. Meilikhov, Usp. Fiz. Nauk **163**, 27 (1993) [Phys. Usp. **36**, 129 (1993)].
[2] M. I. Gurevich, E. Z. Meilikhov, O. V. Tel'kovskaya, and V. V. Yan'kov, Sverkhprovodimost': Fiz., Khim., Tekh. **1**, 80 (1988).
[3] E. Z. Meilikhov and Yu. V. Gershanov, Sverkhprovodimost': Fiz., Khim., Tekh. **1**, 55 (1988).
[4] J. Van der Maas, V. A. Gasparov, and D. Pavuna, Nature (London) **328**, 603 (1987).
[5] S. Yoshihiko, K. Tadaoki. A. Takahiro *et al.*, Appl. Phys. Lett. **54**, 666 (1989).
[6] Y. Enomoto and K. Moriwaki, Jpn. J. Phys. **29**, L1445 (1990).
[7] V. I. Omelchenko and A. A. Sukhanov, Sverkhprovodimost': Fiz., Khim., Tekh. **7**, 100 (1994).
[8] K. K. Likharev and B. T. Ul'rikh, *Systems with Josephson Junctions* [in Russian], Izd. MGU, Moscow (1978).

Translated by R. S. Wadhwa

Resistive state of HTSC film in a varying magnetic field

A. M. Palti and A. I. Ruban

Institute of Metal Physics, National Academy of Sciences of the Ukraine, 242142 Kiev, Ukraine

A. A. Snarskii

*National Technological University of the Ukraine ''KPI,'' 252056 Kiev, Ukraine**

(Submitted August 7, 1997)
Fiz. Nizk. Temp. **24**, 445–448 (May 1998)

The frequency dependence of dissipation in a varying external magnetic field perpendicular to a HTSC film is calculated by using the percolation model. The dependence is linear at low frequencies and has a peak at high frequencies. The linear frequency dependence of dissipation in the low-frequency region is confirmed by the results of experimental studies of current–voltage characteristics. © *1998 American Institute of Physics.* [S1063-777X(98)00405-8]

The application of a varying magnetic field to a sample is an effective method of studying dynamic properties of the vortex structure of type II superconductors. Cryogenic power devices, even those intended for operation with direct transport current, are generally located in a medium of varying electromagnetic fields such as fields induced by pulse sources of accelerators of charged particles or generator parts of electric power plants. For this reason, the study of the effect of these fields on the transport properties of superconductors is of independent interest.

Let us consider the problem on the resistive state of an HTSC film in a transverse varying magnetic field $H_a < H_{c1}$.

As in Ref. 1, the object of our investigations is a thin film of type II superconductor (whose thickness is much smaller than the London penetration depth λ_L; in a layered crystal, λ_L corresponds to the depth of penetration of the magnetic field H parallel to the **c**-axis in the plane of the layer). Pinning centers in the film are distributed at random, while their intensity distribution (over the force F_p) is continuous. This means that for any fixed value of $F_p < F_{pm}$, the entire film can be divided into two phases: the conditionally ''black'' phase in which $F_L > F_p$ (F_L is the Lorentz force) and the conditionally ''white'' phase in which $F_L < F_p$. Since the values of F_p are different for different pinning centers, there must be a critical value F_{pc} for which the ''black'' phase forms a connected structure of channels piercing the entire sample in a direction perpendicular to the transport current for $F_p < F_{pc}$.[1]

If in this case the equality

$$F_p + F_\eta = F_L, \tag{1}$$

is satisfied, where $F_\eta = \eta v$ is the ''viscous friction'' force of a vortex,[2] a steady-state flow of vortices is possible at a velocity

$$v = \frac{F_L - F_p}{\eta} = \left(\frac{j\varphi_0}{c} - F_p \right) \eta, \tag{2}$$

where η is the viscosity, φ_0 the magnetic flux quantum, j the transport current density, and c the velocity of light. We assume that if the force F_η is strong enough for as to neglect the contribution from the regions of vortex acceleration and deceleration in their interaction of vortices with pinning centers. In addition, we consider a weak magnetic field ($H \ll H_{c2}$) so that the forces of interaction between vortices can be neglected (''one-particle'' pinning mode).

The magnitude of the critical current I_c is determined by the critical pinning force:

$$I_c = c \frac{F_{pc}}{\varphi_0}. \tag{3}$$

Let us analyze the behavior of vortices for a transport current close to critical, for which the following condition is satisfied:

$$\tau_j = \frac{I - I_c}{I_c} \ll 1. \tag{4}$$

According to general concepts of percolation theory, the resistance of a two-phase (''black-and-white'') medium near the percolation threshold (in the region whose size is of the order of correlation length ξ) is mainly determined by simply connected percolation channels which are bridges of ''black'' phase of various lengths. Here ξ is the length over which the values of physical quantities are self-averaged so that $\xi \sim \tau^{-\nu}$,[3] where ν is the critical index of correlation length ($\nu = 4/3$ in $2D$ systems), and τ the parameter of proximity to the percolation threshold:

$$\tau = \frac{p - p_c}{p_c} \ll 1. \tag{5}$$

Here p is the concentration of the ''black'' phase and p_c the critical concentration for which an infinite ''black'' percolation cluster is formed.

In our model, the value of p is determined by the relation

$$p = \int_0^{F_p} D(F_p) dF_p, \tag{6}$$

where $D(F_p)$ is the function of pinning center distribution over F_p. In particular, the parameters τ and τ_j coincide for a uniform distibution $D(F_p)=1/F_{pm}=\text{const}$.

A large number of bridges exist near the percolation threshold, when an infinite cluster has not formed yet, in which vortices can move in the forward and backward direction due to field reversal in a varying field. In this case, we can introduce two characteristic times (or frequencies)

$$t_{01}\sim\frac{\xi}{v}\quad\text{and}\quad t_{02}\sim\frac{L}{v},\tag{7}$$

where ξ is the correlation length and L the maximum possible length of a cluster in the indicated structure of the order of ξ. Let us estimate the time intervals t_{01} and t_{02} assuming that the closeness to the percolation threshold is given by $\tau\approx 0.1$. Suppose that $v=0.1$ mm/s and $a_0=10$ Å; in this case, we obtain $\xi=a_0\tau^{-\nu}=22$ nm.[4] Similarly, $L=a_0\tau^{-1.263}=18$ nm[5] and $t_{01}=0.22$ ms$(\omega_{01}=4.6$ kHz$)$, $t_{02}=0.18$ ms$(\omega_{02}=5.5$ kHz$)$. For definiteness, we assume that the modulating field varies according to a periodic law with a period t (frequency ω). We consider an element of the film of size $\xi\times\xi$ for two qualitatively different cases.

1. $t\gg t_0(\omega\ll\omega_0)$. For the cluster length l, we can write the inequalities

$$l\leqslant vt_{01}\sim\xi\leqslant L\sim vt_{02}\ll l_0=vt\sim v/\omega.$$

A vortex crossing a cluster of such a length comes to a halt and remains stationary over a time $t-l/v\equiv t-t_1$. In other words, the vortex is in motion for only a part of the period t of the order of $t_1/t\sim l/tv$. The dissipation power for all the vortices located in a cluster of length l is given by

$$W_1=nF_\eta v\,\frac{l}{tv}=la_0\,\frac{B}{\varphi_0}\,\eta v^2\,\frac{l}{tv}=\frac{a_0B\eta v}{\varphi_0 t}\,l^2,\tag{8}$$

where n is the number of vortices in a cluster of length l and B the magnetic induction in the film element under consideration.

The dissipation in clusters of various lengths is given by

$$W_n=\frac{A}{ta_0}\int_{a_0}^{L}l^2n_l\,dl,\tag{9}$$

where $A\equiv\eta Bv/\varphi_0$ and n_l the cluster length distribution function in the percolation structure above the percolation threshold.[5] Introducing the dimensionality of space under the condition $a_0\ll l\ll L_c=a_0s_c\sim\xi^{1/\nu d}\sim\xi^{1/2\nu}\sim(\tau^{-\nu})^{1/2\nu}\sim\tau^{-1/2}\sim\xi^{3/8}$ we obtain

$$n_l\cong\left(\frac{l}{a_0}\right)^{-\tau_p}\equiv x^{-\tau_p}.\tag{10}$$

If relation (9) is valid for all lengths in the range $a_0<l<L$, the total dissipated power for lengths other than L has the form

$$W_n=\frac{Aa_0^2}{t}\int_{l}^{L/a_0}x^{-\tau_p+2}dx\sim\frac{Aa_0^2}{t}\left(\frac{L}{a_0}\right)^{3-\tau_p}.$$

Dissipation in a cluster of length L forms a special case. After crossing such a cluster, a vortex leaves the superconductor and is replaced by a new vortex emerging at the beginning of the cluster. Thus, dissipation is continuous in this case and is given by

$$W_{BK}=\frac{\eta a_0Bv^2L}{\varphi_0}=Aa_0v\left(\frac{L}{a_0}\right).\tag{11}$$

Since $\tau_p=187/91$,[5] the total dissipation has the form

$$W=W_n+W_{BK}=A\left(\frac{a_0L}{t}+vL\right)=Aa_0v\left(\frac{L}{l_0}+\frac{L}{a_0}\right)$$
$$=Aa_0v\left(\frac{\omega}{\omega_{02}}+\frac{v}{a_0\omega_{02}}\right)=\frac{Av^2}{\omega_{02}}\left(1+\frac{\omega a_0}{v}\right).\tag{12}$$

Estimation of the contribution from finite clusters gives $\omega a_0/v\ll\omega_0a_0/v\sim a_0/vt\sim 0.05$.

2. Let us now consider the case when $t\ll t_0(\omega\gg\omega_0)$. We shall distinguish between clusters of two types with different lengths:

(a) $l\leqslant vt\equiv l_0$

In such clusters, dissipation occurs in analogy to the case considered above, and accordingly is given by

$$W_{1n}=\left(\frac{A}{ta_0}\right)\int_{a_0}^{l_0}l^2n_l\,dl=\left(\frac{Aa_0^2}{t}\right)\left(\frac{l_0}{a_0}-1\right)=Aa_0\left(v-\frac{a_0}{t}\right)$$
$$=Aa_0v\left(1-\frac{a_0}{l_0}\right)=Aa_0v\left(1-\frac{a_0\omega}{v}\right);\tag{13}$$

(b) $l_0\leqslant l\leqslant vt_0$

In clusters whose length is greater than l_0, dissipation occurs continuously, and

$$W_{2n}(l<L)\approx\left(\frac{\eta a_0Bv^2}{\varphi_0}\right)\int_{l_0}^{l\leqslant L}ln_1d\left(\frac{l}{a_0}\right)$$
$$=Aa_0v\,\ln\left(\frac{\omega}{\omega_{02}}\right),\tag{14}$$

while in an infinite cluster of length L, dissipation is defined, as before, by the expression

$$W_{BK}=AvL=Aa_0v\left(\frac{v}{a_0\omega_0}\right).\tag{15}$$

Denoting $W_0\equiv Aa_0v$ and taking into account relations (13)–(15), we can write the total dissipated power in the form

$$W=W_0\left[1-\frac{a_0}{l}+\ln\left(\frac{L}{l_0}\right)+\frac{L}{a_0}\right]$$

and then the ratio $Wa_0\omega_{02}/W_0v$ (dimensionless dissipation) has the form

$$\omega=\frac{Wa_0\omega_{02}}{W_0v}=1+\frac{a_0\omega_{02}}{v}\left[1-\frac{a_0\omega}{v}+\ln\left(\frac{\omega}{\omega_{02}}\right)\right].\tag{16}$$

This gives

(1) for $\omega\ll\omega_0$, $w_{lf}=1+\dfrac{a_0\omega}{v}=1+\dfrac{\omega}{\omega_1}$

(2) for $\omega \gg \omega_0$, $w_{hf} = 1 + \frac{a_0\omega_0}{v}\left[1 - \frac{a_0\omega}{v} + \ln\left(\frac{\omega}{\omega_0}\right)\right] = 1 + \frac{\omega_0}{\omega_1}\left[1 - \frac{\omega}{\omega_1} + \ln\left(\frac{\omega}{\omega_{02}}\right)\right]$.

Thus, there exist two regions with different frequency dependences of dissipated power, which can be desctribed on the basis of the model of percolation structure of pinning regions.

In one region $\omega_0 \ll \omega \ll \omega_1$ (according to our estimates, 5 kHz$\ll\omega\ll$100 kHz), dissipated power increases according to a linear law, while dissipation in the other region has a peak (at $\omega \sim 2$ MHz) and then decreases apparently due to the inertial nature of the vortex system (vortices have no time to respond to variation of the applied magnetic field).

In order to verify the proposed model, experiments were made on thin epitaxial YBCO films of thickness 100 nm on MgO substrates. Microbridges of width 50 μm and length 1 mm were created on the films by scribing. The films had the superconducting transition temperature $T_{c0} = 85$ K and the critical current $I_c(4.2\text{ K}) = 10^6 - 10^7$ A/cm^2 in liquid He. All the measurements were made in an applied electromagnetic field at 4.2 K. The external field was created by a superconducting solenoid connected to a source of ac voltage. The sample was placed into the solenoid. The measurements were made by using the four-probe technique. Potential contacts were connected to a constant-voltage filter followed by a voltage amplifier. The filter was intended to prevent the penetration of the varying emf induced by the varying external field. The sensitivity of the measuring circuit in the given sample geometry was 20 nV/cm. Under the action of the varying field, YBCO microbridges go over to the resistive state at currents $I < I_c$. Figure 1 shows for comparison the current–voltage characteristics in a constant external field ($\omega = 0$) and for different frequencies. No resistive losses were observed in a constant field for currents below critical. This is due to the fact that for $H \ll H_{c2}$ and at $T \ll T_{c0}$, thermally activated flux flow plays an insignificant role in comparison with the observed resistive losses. The losses increased both with amplitude and with the frequency of the applied varying field. A nearly linear shape of the curves for $I < I_c$ allowed us to determine the bridge resistance averaged over the segment and to calculate the frequency dependence of losses. To within the error of measurements at low frequencies, dissipation is a linear function of frequency, which is in qualitative agreement with the constructed model.

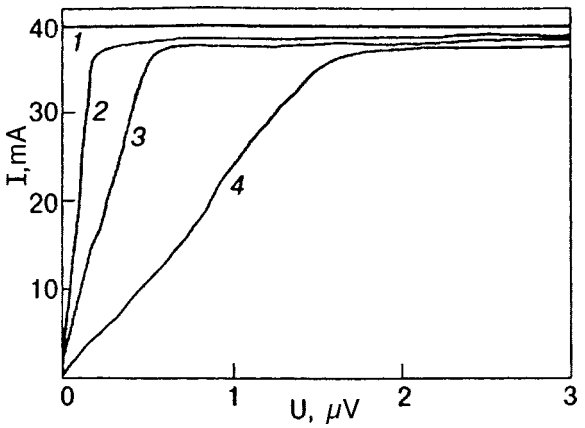

FIG. 1. Current–voltage characteristics of a bridge formed by an YBCO thin film at various frequencies ω of the applied varying field (in Hz): 0 (*1*), 20 (*2*), 40 (*3*), and 200 (*4*). In a constant external field ($\omega = 0$), resistive losses are not observed.

This research was partly supported by the Russian Foundation of Fundamental Studies, Project No. 97-02-18397.

*E-mail: asnar@phys.carrier.kiev.ua

[1] A. A. Snarskii, E. A. Pashitskii, and A. M. Palti, Fiz. Nizk. Temp. **21**, 917 (1995) [Low Temp. Phys. **21**, 706 (1995)]; A. A. Snarskii, E. A. Pashitskii, A. M. Palti, and A. E. Morozovskii, Pis'ma Zh. Eksp. Teor. Fiz. **61**, 112 (1995) [JETP Lett. **61**, 119 (1995)].
[2] A. V. Gurevich, R. G. Mints, and A. L. Rakhmanov, *Physics of Composite Superconductors* [in Russian], Nauka, Moscow (1987).
[3] A. L. Efros and B. I. Shklovskii, Phys. Status Solidi B **76**, 475 (1976).
[4] V. V. Shmidt, *Introduction to Superconductor Physics* [in Russian], Nauka, Moscow (1980).
[5] D. Stauffer and A. Aharony, *Introduction to Percolation Theory*, Taylor and Francis, London, Washington (1992).
[6] P. Clerc, G. Giraud, J. M. Laugier, and J. M. Luck, Adv. Phys. **39**, 191 (1990).

Translated by R. S. Wadhwa

Critical current in a granular superconductor

V. K. Ignatjev

*Volgograd State University, 400062 Volgograd**

(Submitted September 30, 1997; revised November 20, 1997)
Fiz. Nizk. Temp. **24**, 449–456 (May 1998)

The mechanism of hypervortex pinning in a granular superconductor at intergranular contacts and intragranular defects is proposed for describing the field dependence of the critical current density and pinning potential. The results are in good agreement with those obtained experimentally. The proposed model describes the peak effect and the percolation mechanism of conductivity in ceramic superconductors. © *1998 American Institute of Physics.* [S1063-777X(98)00505-2]

INTRODUCTION

A significant factor restricting the technical application of high-temperature superconductors (HTSC) is a comparatively low value of the critical transport current density which is mainly determined by their structure like other electromagnetic properties of HTSC. A superconductor prepared by using ceramic technology is a heterogenous system consisting of two phases, viz., granules with a strong superconductivity and a weakly superconducting intergranular phase. The splitting of a superconductor into superconducting regions separated by thin normal layers is a topological effect associated with the structure of oxides and not with the mechanism of high-temperature superconductivity.[1] The main question concerns the origin of the critical current, i.e., whether it is associated with pinning of some vortex structures, or with the critical current of weak intergranular links. Both mechanisms may participate simultaneously in the formation of the critical current. Thus, Gaidukov *et al.*[2] proposed that the critical current is determined by vortex movement in bulk samples and by the critical current for contacts in films. Using the model of a Josephson medium, Belevtson *et al.*[3] obtained the field dependence of the critical current density in a superconducting ceramic in the form $j_c(H) = j_c(0)(1-H/H_0)$, which is in good agreement with the experimental results.

Intergranular (Josephson) and intragranular currents cannot be excited independently in a superconducting ceramic since the two current subsystems interact mutually. A characteristic feature of a ceramic superconductor is that the critical current densities of these subsystems differ from each other by three orders of magnitude. Experiments devoted to the study of magnetization curves of finely dispersed powders of superconducting ceramics show that the intragranular critical current density is close to the critical current density of monocrystalline samples and amounts to about 10^5 A/cm^2 in zero magnetic field at 77 K.[4] Under identical conditions, the critical density of transport current in a bulk superconducting ceramic sample is found to be about 10^2 A/cm^2 and depends strongly on the technology of sample preparation.[5]

Experiments on visualization of magnetic field in single crystals and magnetization of finely dispersed HTSC powders show that the intragranular critical current is associated with pinning of Abrikosov vortices at the granule boundaries and intragranular twinning planes,[6] i.e., we can apply Bean's model[7] for the critical state of hard superconductors to granules. The origin of critical transport current in bulk ceramic superconductors remains unclear so far. On one hand, the experimental dependences of critical transport current on temperature, applied magnetic field,[8] and pressure[9] are in good agreement with the model of weakly linked granules in which the critical current is associated with Josephson currents of weak links. On the other hand, the hysteresis curves of magnetization of a ceramic[10] and the characteristic triangular distribution of magnetic field in the critical state[11] can be explained only by vortex pinning. Brandt *et al.*[12] measured directly the pinning force in bulk ceramic superconductors, and attributed its small value in comparison with single crystals to the role of weak intergranular links. But since the pinning of Abrikosov vortices in granules is independent of the critical current of intergranular junctions, it can be assumed naturally that the pinning force measured by the authors corresponds to Josephson's hypervortices.[13]

1. PINNING OF HYPERVORTICES

The mechanism of pinning of hypervortices in a ceramic superconductor remains unclear so far. Pinning of Abrikosov vortices in type II superconductors occurs at inhomogeneities and inclusions as a result of interaction of vortices with the interface,[14,15] and the dimensions of the pinning centers must be considerably larger than the vortex size. A hypervortex, which embraces hundreds and thousands of granules in a ceramic superconductor, cannot be trapped effectively at the defects of the material. It was shown in Ref. 16 that a two-dimensional distributed Josephson vortex (hypervortex) in a regular cubic lattice of Josephson junctions may undergo considerable pinning under certain conditions. Such a vortex has two equilibrium positions, viz., a stable position when the vortex center lies in the middle of a cell, and an unstable position when the vortex center lies on a weak link. The difference in the energies between these positions constitutes the pinning potential. In a real ceramic, however, the Josephson junctions form a disordered system and the hypervortex

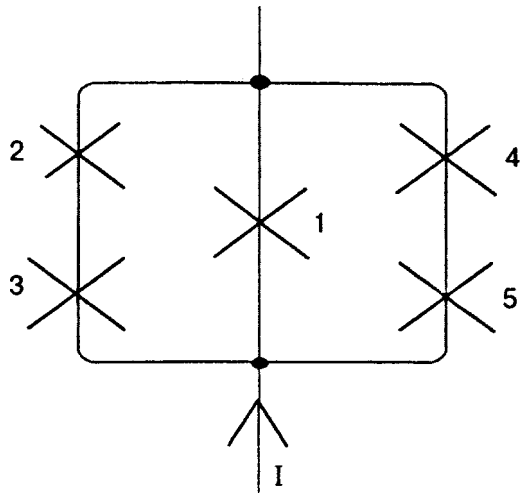

FIG. 1. Intergranular junctions at the center of a hypervortex.

axis passing through the vortex center in one section may pass through a weak link in another section. Hence the total average vortex energy of a hypervortex will not depend on the position of its center, which indicates that there is no pinning. Moreover, the Josephson network model is oversimplified since it does not take into account penetration of Abrikosov vortices into granules.

In order to analyze the pinning force, we must consider the fact that the model of a hypervortex as a system of coaxial solenoids with a continuous distribution of the order parameter phases is obtained as a result of averaging over a large number of vortices in the network.[17] A solitary vortex in a Josephson medium is described by a discrete values of the phase difference in individual junctions. The phase and magnetic field distribution in a hypervortex adjusts itself to the ceramic structure in each section in such a way that the vortex energy is minimum. Any deviation of the hypervortex axis from equilibrium under the action of transport current leads to an increase in the total vortex energy, i.e., to the emergence of a pinning force.

Let us consider two adjacent cells in a Josephson network formed by contacts of three granules at the vortex center (Fig. 1). Let the hypervortex center be located in the left cell 1–2–3. In analogy with one- and two-contact SQUIDS,[18] we can write the quantization condition for the 1–2–3 loop in the form

$$\varphi_1+\varphi_2+\varphi_3+2\pi\Phi/\Phi_0=2\pi, \tag{1}$$

where φ_i is the phase difference at the ith Josephson junction, Φ the magnetic flux embraced by the loop, and Φ_0 the magnetic flux quantum. Note that $\Phi \leqslant L_0 I_J$, where L_0 is the inductance of the circuit and I_J is the critical current of Josephson junctions. The volume fraction of normal phase in a ceramic superconductor is $\approx 10\%$, hence the inductance L_0 of a circuit formed by three granules of size $a \simeq 10$ μm is approximately equal to $\mu\mu_0\pi a \approx 4\times 10^{-12}$ H. Putting the average critical current I_J of Josephson junctions equal to 10 μA, we find that the maximum magnetic flux Φ embraced by the loop is about $0.02\Phi_0$, i.e., we can disregard the last term on the left-hand side of formula (1) and write the quantization condition for loops 1–2–3 and 1–5–4, respectively, in the form

$$\varphi_1+\varphi_2+\varphi_3=2\pi, \quad \varphi_1-\varphi_4-\varphi_5=0. \tag{2}$$

For we shall assume that critical currents for Josephson junctions are identical. If a transport current does not pass through a ceramic, the phase difference for the junctions in the 1–2–3 loop will be identical, which is in accord with the position of the hypervortex axis at the center of the cell: $\varphi_1=\varphi_2=\varphi_3=2\pi/3$ and $\varphi_4=\varphi_5=\varphi_1/2=\pi/3$ (circumvention of the loop in counterclockwise direction is assumed to be positive). In this case, a superconducting current $i_s \simeq 0.85 I_J$ flows through the loop 1–2–3, and the total current I in the cell is equal to zero.

Let us now suppose that a transport current of density j flows through the ceramic, increasing the current i_1 through junction 1 and decreasing the current through junctions 2 and 3, respectively. Such a current redistribution indicates that the center of the hypervortex is displaced to the right. The limiting stable steady state of the vortex corresponds to the case when the current i_1 through junction 1 is equal to the critical Josephson current I_J of the junction. According to Eq. (2),

$$\varphi_1=\pi/2, \quad \varphi_2=\varphi_3=3\pi/4, \quad \varphi_4=\varphi_5=\pi/4,$$

$$i_2=i_3=I_J\sqrt{2}/2,$$

and the total current through the junction is $I_C=i_1-i_2 \approx 0.3 I_J$. Upon a further increase in the transport current, the junction 1 goes over to the resistive state and a voltage $u=R\sqrt{i_1^2-I_J^2}$ appears in it, R being the normal resistance of the junction,[18] and the phase differences in the junctions begin to vary according to the law

$$\dot{\varphi}_2=\dot{\varphi}_3=-\dot{\varphi}_4=-\dot{\varphi}_5=-\dot{\varphi}_1/2=-u/(2\Phi_0).$$

An increase in the phase difference for junctions 4 and 5 upon a decrease in its value for junctions 2 and 3 corresponds to a displacement of the hypervortex center to the cell 1–5–4.

An analytic description of the transient process is quite complex, since redistribution of magnetic flux over cells induces a vortex electric field which in turn affects the rate of variation of phase difference in the junctions. The passage of the vortex center through junction 1 corresponds to excitation of microwave vibrations in this junction, which are not described by the resistive model of the junction.[19] Here we simply observe that a transition of the hypervortex center from 1–2–3 cell to 1–5–4 cell is analogous to the switching of a tunnel cryotron.[18] If we decrease the transport current, the new position of the hypervortex with its center in the 1–5–4 cell will be stable. The displacement of a hypervortex is a dissipative process associated with energy losses at the normal resistance of Josephson junctions. If transport current flowing through 1–5–4 and subsequent cells exceeds the value I_C, the vortex continues its motion to the right, i.e., the flux-flow regime is realized.

In order to find the critical transport current density j_{C1} for which hypervortices start their movement without Abri-

kosov vortex pinning in granules, we observe that the current flowing through each junction belongs simultaneously to two cells. Hence we obtain

$$j_C = I_C/2a_0^2 = 0{,}15 I_J(B_0)/a_0^2, \tag{3}$$

where a_0 is the mean separation between Josephson junctions and B_0 is the magnetic field in the gap between granules at the vortex center.

It follows from formula (3) that the field dependence of the critical transport current is associated with the dependence of the critical current of Josephson junctions on the intergranular magnetic field. In order to analyze this dependence, we consider Meilikhov's model of deformed granules,[20] the weak link between which is formed in the region of plane segments. In this case, the banks of an intergranular Josephson junction are in the form of a circle whose radius r is proportional to the granule size $r=ka$. Suppose that d is the junction thickness. The following relation is valid for the field dependence of the critical current in the junction[18]:

$$I_J(B_0) = j_J \pi r^2 \Phi_0 \left|\sin(\pi r d B_0/\Phi_0)/(\pi r d B_0)\right|, \tag{4}$$

where j_J is the critical density of the Josephson current in the junction.

Equation (4) should be averaged over the random junction radius r which naturally obeys the Maxwell distribution[17]:

$$\omega(r) = \frac{32r^2}{\pi^2 k^3 a^3} \exp\left(-\frac{4r^2}{\pi k^2 a^2}\right),$$

where a is the average granule size. Since it is quite difficult to average the modulus in Eq. (4), we calculate the mean square critical current of the junctions:

$$\begin{aligned}\langle I_J^2(B_0)\rangle &= \frac{32 j_J^2 \Phi_0^2}{\pi^2 k^3 a^3 d^2 B_0^2} \\ &\times \int_0^\infty r^4 \sin^2\left(\frac{\pi d B_0 r}{\Phi_0}\right) \exp\left(-\frac{4r^2}{\pi k^2 a^2}\right) dr \\ &= \frac{\pi k^2 a^2 j_J^2 \Phi_0^2}{16 d^2 B_0^2}\left[3-\left(3-\frac{\pi^3 d^2 B_0^2 k^2 a^2}{4\Phi_0^2}\right.\right. \\ &\left.\left.\times\left(3-\frac{\pi^3 d^2 B_0^2 k^2 a^2}{4\Phi_0^2}\right)\right)\exp\left(-\frac{\pi^2 d^2 B_0^2 k^2 a^2}{4\Phi_0^2}\right)\right].\end{aligned}$$

This is a quite cumbersome expression and can be approximated quite well by the dependence

$$\begin{aligned}\langle I_J^2(H)\rangle &= \frac{I_{J0}^2}{1+H^2/H_J^2}, \quad H_J = \frac{\Phi_0}{2\pi d k a\sqrt{3}}, \\ I_{J0} &= \frac{\sqrt{3\pi}}{8}\,\pi a^2 k^2 j_J.\end{aligned} \tag{5}$$

While deriving this relation, we have assumed that the magnetic field induction for a hypervortex lattice in the intergranular gaps at the vortex center is about double the mean value of this induction, which is equal to the external magnetic field strength, i.e., $B_0 = 2H$. Formulas (3) and (5) lead to the following expression for the critical transport current density associated with the hypervortex pinning:

$$j_{C1}(H) = \frac{j_{C0}}{\sqrt{1+H^2/H_J^2}}, \quad j_{C0} = j_C(0) = \frac{0{,}15 I_{J0}}{a^2}. \tag{6}$$

2. PEAK EFFECT IN A GRANULAR SUPERCONDUCTOR

The displacement of a hypervortex to the adjoining cell as a result of an increase in the transport current beyond the critical current density j_{C1} (6) indicates that the Lorentz force acting on a hypervortex for such a transport current density exceeds the maximum force confining a vortex to the cell, i.e., the pinning force. The equation for the balance of forces[21] can be used easily to obtain the modulus of the pinning force at the intergranular junctions per unit length of hypervortex: $f_1 = j_{C1}\Phi/c$, where Φ is the magnetic flux in the hypervortex. However, the displacement of hypervortex changes the magnetic field in the vicinity of granules, i.e., the concentration of Abrikosov vortices in granules also, which move in the granules and perform work against intragranular pinning forces. The total energy dissipation associated with the motion of Abrikosov vortices upon displacement of a hypervortex to the adjacent cell divided by the separation between cells is the additional pinning force f_2.

Suppose that the magnetic field in the vicinity of a granule of radius R^g varies periodically from its maximum value B_1 to the minimum value $B_1 - \Delta B_1$ during uniform movement of a hypervortex. In this case, the concentration n^g of Abrikosov vortices and the magnetic induction B^g in granules also vary periodically, and the amplitude of variation decreases linearly into the bulk of the granule according to the law

$$\begin{aligned}\Delta B^g(x<l) &= \Delta B_1 - \frac{8\pi j_C^g x}{c}, \\ \Delta B^g(x\geqslant l) &= 0, \quad l = \min\left(\frac{c\Delta B_1}{8\pi j_C^g}, \quad R^g\right),\end{aligned} \tag{7}$$

where j_C^g is the intragranular critical current density.

If the concentration of Abrikosov vortices changes by $\Delta n^g(x)$ over a distance x from the granule surface, the vortices under question are displaced by a distance x under the action of Lorentz force and enter or leave the granule. The total dissipation energy in the granule is then defined as

$$\begin{aligned}q &= \frac{2\pi}{c}\int_0^l \Delta n^g(x) R^g (R^g - x) x \Phi_0 j_C^g dx \\ &= \frac{2\pi R^g j_C^g}{c}\int_0^l \Delta B^g(x)(R^g - x)x\, dx.\end{aligned}$$

Substituting the relation (7) into this equation and averaging over random radii R^g with Maxwell distribution, we obtain

$$\begin{aligned}q(\Delta B_1 < 2H_K) &= \frac{\pi a^3}{512 H_K}(\Delta B_1)^3, \\ q(\Delta B_1 \geqslant 2H_K) &= \frac{\pi a^3}{192} H_K \Delta B_1.\end{aligned} \tag{8}$$

Here $H_K=2\pi a j_C^g/c$ is the magnetic field in which the penetration depth is equal to the mean granule radius a.

Let us consider the uniform motion of a square vortex lattice with a period L along the x-axis with a velocity v. Suppose that the center of the hypervortex moves along the line $y=0$, B_0 is the magnetic field at the center of the hypervortex in the gap between granules, and $B_0-\Delta B_0$ the field at the boundary of a hypervortex for $y=\pm L/2$. In this case, the amplitude of variation of magnetic field in the vicinity of a granule with coordinates $y=y_0<L/2$ will be $\Delta B_1(y_0)=\Delta B_0[1-2y_0/L]$. Since the magnetic field varies twice in the vicinity of a granule (increases and decreases) during one lattice period $\tau=v/L$, we obtain the following expression for the loss power in a hypervortex of unit length:

$$p=\frac{2}{\tau}\int_{-L/2}^{L/2}\int \frac{q(y)}{a^3}\,dxdy=4v\int_0^{L/2}\frac{q(y)}{a^3}\,dy.$$

Substituting the expression for q from formula (8) into the integral, we obtain

$$p(\Delta B_0<2H_K)=\frac{Lv\pi(\Delta B_0)^3}{1024H_K},$$

$$p(\Delta B_0\geqslant 2H_K)=\frac{Lv\pi H_K\Delta B_0}{192}.$$

These formulas can be approximated by a single dependence of the type

$$p=\frac{Lv\pi H_K(\Delta B_0)^3}{1024H_K^2+192(\Delta B_0)^2}. \tag{9}$$

For the same values of magnetic field, when Abrikosov vortices start penetrating the granules and the losses associated with the entry or removal of these vortices become significant, the difference ΔB_0 in magnetic fields at the center of a hypervortex and at its boundary is of the order of the mean field B. Formula (9) allows us to determine the additional frictional force acting on a unit length of a moving hypervortex in a granular superconductor. Taking into account the relation between the average induction and the hypervortex lattice period $L=\sqrt{\Phi/B}$, we obtain

$$f_2=-\frac{H_KB^2\sqrt{\Phi B}}{64\mu(5\mu^2H_K^2+B^2)}\frac{\mathbf{v}}{v}, \tag{10}$$

where $\mu=B/H$ is the permeability of a superconductor in the mixed state. This additional force $\mathbf{f}_2$ is independent of the modulus of velocity, i.e., is analogous to static friction and can be treated as additional pinning of hypervortices associated with intragranular pinning of Abrikosov vortices. Since the magnetic flux Φ embraced by a hypervortex depends on the average magnetic field B in the superconductor,[17,22] the additional pinning force also depends on the magnetic field.

The total pinning force of a hypervortex is obtained by supplementing the force $f_1=j_{C1}\Phi/c$ of pinning at the intergranular junctions with the static frictional force f_2 associated with intragranular pinning of Abrikosov vortices (10):

$$f_P=f_1+f_2=\frac{j_{C1}\Phi}{c}+\frac{H_KB^2\sqrt{\Phi B}}{64\mu(5\mu^2H_K^2+B^2)}.$$

The total critical current at which hypervortices start moving can be presented in the final form after taking into account the intragranular pinning of Abrikosov vortices:

$$j_{C2}(H)=\frac{cf_P}{\Phi}=j_{C1}(H)+\frac{cH_KH^2\sqrt{H/(\mu\Phi)}}{64(5H_K^2+H^2)}. \tag{11}$$

It follows from formula (6) that the first term in this formula decreases[11] with increasing magnetic field strength H in the ceramic, while the second term is inversely proportional to the vortex lattice period and increases due to an increase in the bulk intragranular pinning of Abrikosov vortices. However, it was shown in Refs. 17 and 24 that the density of nondissipative current in a superconductor is limited to the value $j_J/\sqrt{2e}$, where the Josephson current density $j_J=3I_J\sqrt{\pi}/(2a)^2$ depends on the critical Josephson current I_J of junctions in the form (4). In this case, we can write the critical current density of a granular superconductor in the form

$$j_C(H)=\min\left(j_{C1}(H)+\frac{cH_KH^2\sqrt{H/(\mu\Phi)}}{64(5H_K^2+H^2)},\ \times 10\sqrt{\pi}j_{C1}(H)\right). \tag{12}$$

The field dependence of the critical current density, calculated by using formula (12) for $I_J=0.1c\Phi_0/a$ and $H_K=10B_J$ is presented in Fig. 2. The values of the magnetic field h are normalized by the characteristic field $B_J=\sqrt{12\Phi_0I_J/(ca^3)}$ of a Josephson medium.[17,22] For an average grain size $a=3\ \mu$m and an average critical current $I_J\approx 300\ \mu$A of intergranular junctions (which corresponds to a critical transport current density of a bulk superconducting ceramic of the order of 100 A/cm^2),[5] the field $B_J\simeq 3$ G. The permeability of the ceramic in the mixed state is assumed to be equal to 0.3, and the dependence of the magnetic flux Φ on the applied magnetic field is calculated by using equations presented by us earlier.[22] On the initial segment, the field dependence is described by formula (4) which is in good agreement with the experimental result obtained by Kugel *et al.*[24] who found that the critical current must decrease more slowly than $1/H^2$, but more rapidly than $1/H$. The characteristic local extremum on the field dependence, which is called the peak effect, is also observed for low-temperature metallic superconductors,[21,25] although it is manifested much more strongly for high-temperature superconductors.[26,27]

The model considered above connects the peak effect with intergranular pinning of Abrikosov vortices. Naturally, it is assumed that the lower critical field H_{C1}^g for granules is much lower than the field H_p corresponding to the maximum in the peak effect (Fig. 2). Hence formulas (10) and (11) are also valid under the condition $H>H_{C1}^g$. For the case depicted in Fig. 2, $H_p\approx H_K\approx 30$ Oe, and the peak effect will be observed for $H_{C1}^g\approx 3$ Oe, which corresponds to a temperature 85–90 K for a yttrium-based ceramic. At nitrogen temperatures, $H_{C1}^g\approx 100$ Oe, and the peak effect (for an appropriate increase in I_J) may be less strongly manifested, and even suppressed altogether for a small critical current in in-

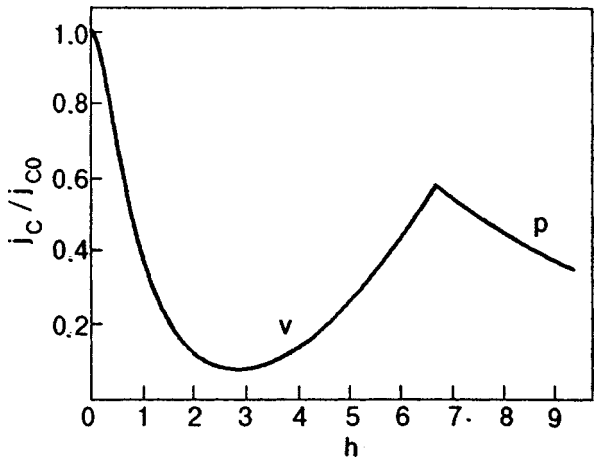

FIG. 2. Field dependence of critical current.

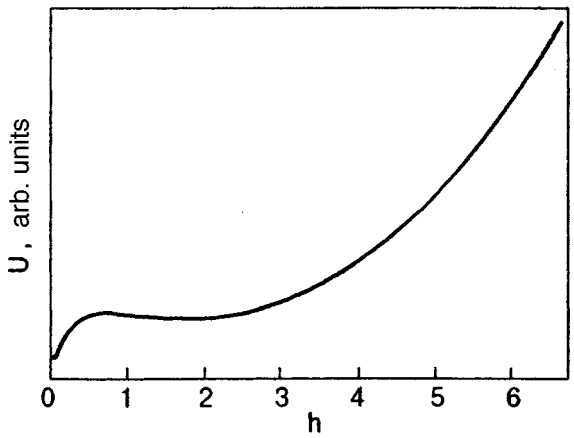

FIG. 3. Field dependence of the hypervortex pinning potential.

tergranular junctions if the transition to the percolation regime sets in before Abrikosov vortices penetrate the granules.

For magnetic fields higher than the maximum field H_p corresponding to the peak effect (line p in Fig. 2), the transport current is confined not by the pinning of hypervortices, but by the limiting nondissipative current in intergranular Josephson junctions. If the transport current exceeds the critical value, the Josephson junctions go over to the resistive state and hypervortices are not formed. This regime of current flow is close to the percolation model[28] since weak links are practically ruptured. Abrikosov vortices inside the granules can be assumed to be stationary in this case since the intragranular critical current density is much higher than the intergranular one. The branch of the field dependence of critical current for $H>H_p$ (Fig. 2) can naturally be called percolation branch, while the branch $H<H_p$ on which the critical current is determined by pinning of hypervortices and is described by formula (11) is termed the vortex branch (shown by curve v in Fig. 2).

According to the model constructed by us, the pinning centers of a hypervortex are Josephson unit cells, and the critical current corresponds to displacement of a hypervortex by a distance of the order of intergranular separation. In this case, the pinning potential can be represented in the form

$$U(H)=j_C(H)\Phi a/c, \tag{13}$$

where the critical current density on the vortex segment is defined by formula (11). Figure 3 shows the field dependence of the pinning potential described by formula (13) in arbitrary units. Such a theoretical dependence is in good agreement with the results of investigation of the magnetic flux creep in superconducting ceramics.[30] It is shown by numerical simulation that the specific form of the field dependence of the pinning potential depends strongly on the average grain size, average critical current in intergranular junctions, and the critical density of the intragranular current in the superconductor, which explains a considerable spread of the experimental data over pinning potentials in superconducting ceramics.

CONCLUSIONS

The model of the field dependence of the critical transport current density in superconducting ceramics takes into consideration both possible mechanisms, viz., the pinning of hypervortices at intergranular Josephson junctions and intragranular defects, and the rupture of weak links between granules. The percolation nature of conductivity observed in a superconducting ceramic in relatively strong magnetic fields has been confirmed experimentally.[29] On the other hand, measurements made by Brandt *et al.*[12] provide an equally convincing evidence in favor of the pinning model. The model proposed by us describes the ability of a granular conductor to display the percolation as well as characteristic Bean type of electrical conductivity as a function of the external magnetic field and the field created by a transport current. It also attributes the contradictory experimental results to different conditions under which measurements were made.

Note that the pinning force f_2 associated with intragranular pinning of Abrikosov vortices depends rather weakly on temperature. The critical current of intergranular Josephson junctions, and hence the Josephson current density j_J, decreases exponentially with increasing temperature. Consequently, an increase in temperature also leads to a decrease in the magnetic field H_p for which a transition to the percolation curve takes place. This explains the fact that the experiments on temperature dependence of the electric conductivity of HTSC are described more correctly by the percolation model.

It should also be observed that the division of charge carriers into bound and free (and hence of current into molecular (magnetization) and conduction (transport)) categories, used in the description of electrodynamics of magnets is quite arbitrary when applied to superconductors. The Bose condensate of Cooper pairs in a superconductor participates in the formation of vortex currents as well as in transport current. The current transport can be treated as laminar flow of a superconducting condensate in a vortex-free regime, and as a turbulent flow in the presence of vortices. Under the same approach, a hypervortex can be treated as a quasiparticle (elementary excitation) in analogy with a roton in super-

fluid helium, which solves the problem concerning the physical observability of hypervortices.

This research was carried out under project 96015 of the State program on ''Physics of the Condensed State.''

*E-mail: ivanov@physic.vgu.tsaritsyn.su

[1] L. Civale, H. Pastoriza, F. Crus, *et al.*, Solid State Commun. **72**, 341 (1989).
[2] M. M. Gaidukov, E. F. Gatsura, E. K. Goltsman, *et al.*, Sverkhprovodimost': Fiz., Khim., Tekh. **3**, 62 (1990).
[3] L. V. Belevtson, S. S. Shevchenko, and V. N.Tulupenko;, Physica C **271**, 235 (1996).
[4] E. Shimizu and D. Ito, Phys. Rev. B **39**, 2921 (1989).
[5] A. D. Kikin, A. G. Peresada, Yu. S. Karimov, and M. D. Nersesyan, Zh. Tekh. Fiz. **59**, No. 8 29 (1989).
[6] L. Ya. Vinnikov, I. V. Grigor'eva, L. A. Gurevich, and A. E. Koshelev, Sverkhprovodimost': Fiz., Khim., Tekh. **3**, 50 (1990).
[7] C. P. Bean, Phys. Rev. Lett. **8**, 250 (1962).
[8] H. Kupfer, I. Apfelsteadt, R. Flukiger *et al.*, Cryogenics **28**, 650 (1988).
[9] E. Z. Meilikhov, Sverkhprovodimost': Fiz., Khim., Tekh. **2**, 91 (1989).
[10] Yu. I. Kuz'min and I. V. Pleshakov, Pis'ma Zh. Éksp. Teor. Fiz. **49**, 30 (1989) [JETP Lett. **49**, 34 (1989)].
[11] S. Gotoh, N. Koshizuka, and M. Yoshida, Jpn. J. Appl. Phys., Suppl. **29**, L1083 (1990).
[12] N. B. Brandt, L. M. Kovba, V. V. Moshchalkov *et al.*, Zh. Éksp. Teor. Fiz. **95**, 2021 (1989) [Sov. Phys. JETP **68**, 1168 (1989)].
[13] É. B. Sonin, Pis'ma Zh. Éksp. Teor. Fiz. **47**, 415 (1988) [JETP Lett. **47**, 496 (1988)].
[14] G. S. Mkrtchan, F. V. Shakirzanova, E. A. Shapoval, and V. V. Shmidt, Zh. Éksp. Teor. Fiz. **63**, 667 (1972) [Sov. Phys. JETP **36**, 352 (1972)].
[15] G. S. Mkrtchan and V. V. Shmidt, Zh. Éksp. Teor. Fiz. **68**, 186 (1975) [Sov. Phys. JETP **41**, 90 (1975)].
[16] M. A. Zelikman, Sverkhprovodimost': Fiz., Khim., Tekh. **7**, 946 (1994).
[17] V. K. Ignatjev, Sverkhprovodimost': Fiz., Khim., Tekh. **7**, 215 (1994).
[18] V. V. Shmidt, *Introduction to Superconductor Physics* [in Russian], Nauka, Moscow (1982).
[19] K. K. Likharev, *Introduction to the Dynamics of Josephson Junctions* [in Russian], Nauka, Moscow (1995).
[20] E. Z. Meilikhov, Sverkhprovodimost': Fiz., Khim., Tekh. **2**, 91 (1989).
[21] A. Campbell and J. Evetts, *Critical currents. Superconductors*, Taylor and Francis, London (1972).
[22] V. K. Ignatjev, Fiz. Nizk. Temp. **23**, 686 (1997) [Low Temp. Phys. **23**, 514 (1997)].
[23] H. Dersch and G. Blatter, Phys. Rev. B **38**, 11391 (1988).
[24] K. I. Kugel', T. Yu. Lisovskaya, and R. G. Mints, Sverkhprovodimost': Fiz., Khim., Tekh. **4**, 2263 (1991).
[25] J. B. Kim, C. F. Hempstead, and A. R. Strand, Phys. Rev. **131**, 2486 (1963).
[26] J. W. Ekin, T. M. Larson, A. M. Hermann, *et al.*, Physica C **160**, 489 (1989).
[27] L. M. Fisher, N. V. Il'in, N. A. Podlevskikh, and S. I. Zakharchenko, Solid State Commun. **73**, 687 (1990).
[28] V. M. Pan, V. G. Prokhorov, G. G. Kaminskii *et al.*, Fiz. Nizk. Temp. **13**, 861 (1987) [Sov. J. Low Temp. Phys. **13**, 493 (1987)].
[29] H. Kupfer, I. Apfelsteadt, R. Flukiger *et al.*, Cryogenics **28**, 650 (1988).
[30] T. I. Arbuzova, I. B. Smolyak, N. M. Chebotaev, *et al.*, Fiz. Nizk. Temp. **17**, 1431 (1991) [Sov. J. Low Temp. Phys. **17**, 775 (1991)].

Translated by R. S. Wadhwa

LOW-TEMPERATURE MAGNETISM

Giant magnetoresistance in $La_{0.7}Pb_{0.3}MnO_3$ thin film

S. I. Khartsev

*A. Galkin Physicotechnical Institute, National Academy of Sciences of the Ukraine, Ukraine, 340114, Donetsk, R. Luxemburg st., 72**

(Submitted November 3, 1997; revised January 8, 1998)
Fiz. Nizk. Temp. **24**, 457–461 (May 1998)

Epitaxial thin films of $La_{0.7}Pb_{0.3}MnO_3$ have been grown on (100) $LaAlO_3$ and (110) $SrTiO_3$ substrates by dc magnetron sputtering. The magnetic-field and temperature-dependent resistivity of as-deposited and post-annealed films was examined. At $H=10$ kOe the maximum observed magnetoresistance ratio $(R_0-R_H)/R_0$ was 62%. The bolometric response to 0.94-μm low-frequency modulated radiation in the film with the temperature coefficient of resistance $d\ \ln R/dT=14\%$ was studied. The transport properties are described using Zhang's spin-polaron theory. An unusual approach to stabilizing the film temperature at the point corresponding to the maximum of the magnetoresistance ratio and responsivity is discussed. © *1998 American Institute of Physics.* [S1063-777X(98)00605-7]

Perovskite metal-oxide manganites with the formula $La_{1-x}A_xMnO_3$, where A=Ca, Sr, Ba, Pb, have attracted interest[1–4] in recent years due to presence of the semiconductor-metal (SM) transition coupled with the paramagnetic-ferromagnetic one and the demonstration of a giant magnetoresistance (MR) in the vicinity of the transitions. Epitaxial thin films of the above-mentioned compositions are more attractive for an application due to greater MR ratio in comparison with the bulk and due to the possibility of controlling the transition temperature (T_c) by changing the oxygen contents.[3–4] Abrupt character of the temperature dependence of the resistivity allows us to use such films as a bolometric detector, as has been shown recently.[5]

The transport and bolometric optical response measurements were performed on series of $La_{0.7}Pb_{0.3}MnO_3$ epitaxial films of thickness 300 nÅ *in situ* grown by dc magnetron sputtering. The target of nominal composition was fabricated by reaction of the high-purity component oxides at 900 °C (36 h), followed by grinding, pressing into disk form (40×1 mm^2), and conglomerating at 1150 °C (10 h). X-ray diffraction measurements indicate orthorhombically distorted, single-phase, perovskite structure.

All films were made in 15-mTorr argon-oxygen mixture (1:1). Deposition rate was $\sim$0.1 nm/s at a plasma current of 100 mA and substrate-target distance of 5 cm. Film 1 was grown on a (100)-oriented $LaAlO_3$ (LAO) substrate at temperature $T_{sub}=575$ °C. Film 2 was grown on a (110)-oriented $SrTiO_3$ (STO) substrate at $T_{sub}=625$ °C. After the deposition films were cooled to room temperature in 250-Torr oxygen at the rate of 5 K/min. Their crystal orientation was determined by X-ray diffraction measurements. Film 1 was found to be ⟨100⟩-oriented, while film 2 had ⟨110⟩-orientation. All films had epitaxial in-plane alignment.

Magnetoresistance and electrical resistance of the films were measured by standard four-probe dc technique in an electromagnet with a field of up to 10 kOe. The sensing current varied from 1 μA to 100 μA. The MR ratios were defined as

$$\Delta R/R\equiv(R_0-R_{10\ \mathrm{kOe}})/R_0.$$

All as-deposited films demonstrate a sharp drop of $\rho(T)$ below T_c and activated behavior above T_c (Fig. 1). The MR effect reaches its maximum at a point close to the temperature at which the maximum value of dR_0/dT occurs (inflection point). The film grown on STO substrate shows the highest $T_c=256$ K, while the films deposited on LAO substrates have $T_c=225$ K. These transition temperatures are too far from $T_c=326$ K obtained by Searle and Wang[6] for a single crystal of $La_{0.7}Pb_{0.3}MnO_3$. The decrease in the oxygen content, as we know, could also decrease the SM transition temperature in the La–Pb–Mn–O system,[3] because oxygen deficiency leads to a decrease in Mn^{4+} concentration. That was the reason for carrying out the series of post-deposition annealings in oxygen flow. Each film was subsequently annealed at different temperatures for 0.5 h. The results of treatments are shown in Fig. 1. The increase in the annealing temperature (T_a) leads to a monotonic increase of T_c only for an STO deposited film 2, while film 1 demonstrates the increase of T_c only to $T_a=800$ °C. Note that the sharpness of the $\rho(T)$ peak, which can be correlated with the film quality, increases only for film 1 after annealing at 600 °C, in contrast with the other cases which lead to a degradation of this characteristic. Such development of film 1 results in improving the MR ratio from 58.8% for as-deposited film to 62%. Finally, an attempt to attain bulk single-crystal T_c has not been successful. It can be suggested that a possible reason could be elastic stress that arises in film clamped to substrate from substrate-film lattice mismatch. In general, epitaxial film must be considered as complex with the substrate, particularly when we face sharp phase transition with

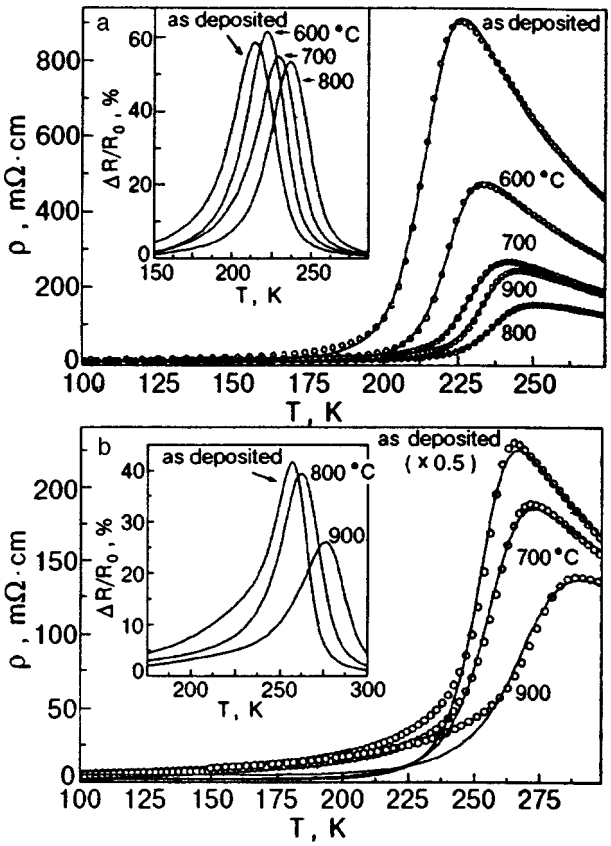

FIG. 1. Resistivity vs. temperature for $La_{0.7}Pb_{0.3}MnO_3$ films deposited on a $LaAlO_3$ substrate (a) and $SrTiO_3$ substrate (b) annealed at different temperatures. The open circles are representative data points and the lines are a least-squares fit of Eq. (1) to the data. The inset shows 10-kOe magnetoresistance.

a discontinuity in the lattice parameters.[7] The different behavior of transport properties of the films under study grown on LAO and STO substrates is argument in favor of such conclusions.

For interpretation of the obtained $\rho(T)$ behavior it is convenient to use Zhang's spin-polaron theory[8] based on a Hamiltonian which consists of a single-electron kinetic energy term, a term represents a magnetic interaction between localized spins, and a term of the interaction between mobile carriers and localized spins. By this model the current carriers are magnetic polarons in the entire temperature range under consideration. There are two independent processes of the carrier scattering: elastic and inelastic. The first process dominates at low temperatures the transport by coherent elastic electron hopping leads to decreasing of conductivity as the temperature increases. The second process (high temperatures) corresponds to incoherent, inelastic, thermally activated hopping, where the resistivity decreases with increasing temperature. Using an approximation of a single optical magnon frequency ω_0, we can describe these processes by a simple formula[8]:

$$\frac{\rho(0)}{\rho(T)} = \exp[-\alpha N(\omega_0)] + \frac{b^2}{E_a k_B T}\exp\left(-\frac{E_a}{k_B T}\right), \qquad (1)$$

where $N(\omega_0)=[\exp(\omega_0/k_BT)-1]^{-1}$ is the number of thermal magnons, E_a is the activation energy of the spin polaron, α is the structure factor, and b is the function of the basic Hamiltonian. Using E_a, ω_0, b, and α as the fitting parameters, we can fit Eq. (1) to the experimental $\rho(T)$ data. The solid lines in Fig. 1 represent the results of least-squares fitting. Table I contains our parameters.

TABLE I. Parameters of the least-squares fit of Eq. (1) to the resistivity data.

Film	ω_0, K	E_a, meV	b, K	α
Film 1 as deposited	1399±20	114±1	636±15	3976±361
Film 1 (T_a=600 °C)	1664±22	105±0.9	451±13	10247±720
Film 1 (T_a=700 °C)	1600±25	100±0.9	427±12	5862±440
Film 1 (T_a=800 °C)	1846±30	91±0.8	396±11	11733±804
Film 1 (T_a=900 °C)	1764±41	104±0.8	431±17	10619±973
Film 2 as deposited	1943±180	98±10	369±57	13240±345
Film 2 (T_a=700 °C)	2009±120	80±7.9	316±67	11555±172
Film 2 (T_a=900 °C)	2098±137	77±11.7	435±56	6360±215

Reasonable agreement between theory and resistivity data for the temperature region close to the peak of resistivity (especially in case of film 1) is evident. It is appropriate to mention here that Zhang's model omits well-knowns binding[9,10] between the low-temperature conductivity of ferromagnetic perovskite structures and magnetization. Apart from the basic Hamiltonian of the theory ignores the term that describes the film—substrate stress. Neglect of these factors may introduce the observed disparity between predicted and experimental low-temperature resistivity. Nevertheless, good prediction of resistivity transformations and acceptable values of the phenomenological parameters (particularly, polaron hopping energy E_a is close similar to reported in[11]) allows the observed $\rho(T)$ dependences to be described as a cross-over from metallic conduction at low temperatures to the hopping-type conduction at high temperature in accordance with the model under discussion.

The resistivity as a function of applied magnetic field as well as $T_H(H)$ and $T_\Delta(H)$ dependences (where T_H and T_Δ are temperatures of the resistivity and MR peaks) were measured. The results are shown in Fig. 2. The behavior of $R(H)$ curves is too far from saturation up to a field of 10 kOe and completely isotropic in regard to the field orientation in the film plane. The MR ratio for the field perpendicular to the film plane is close to the ratio for the field parallel to the film plane for $H=10$ kOe, but there is sufficient difference for a weak field due to the shape factor. The question of full MR isotropy in the films under study is unanswerable without magnetization versus field measurements. Unfortunately, no such measurements can be carried out by us. The fact that the temperature of the MR ratio maximum for a perpendicular field orientation is always higher than T_Δ for parallel orientation has been established. For example, this difference is above 3 K for film 1 at $H=3$ kOe. The $T_H(H)$ dependences are almost linear, in contrast with $T_\Delta(H)$, which demonstrates threshold character. In our opinion, such difference can be accounted for by possible indirect magnetization dependence: magnetic state is ferromagnetic when we measure $T_\Delta(T<T_c)$ and paramagnetic with $M\to 0$ at $T>T_c$ ($T_H>T_c$).

Annealing of film 1 at 600 °C improves the sharpness of

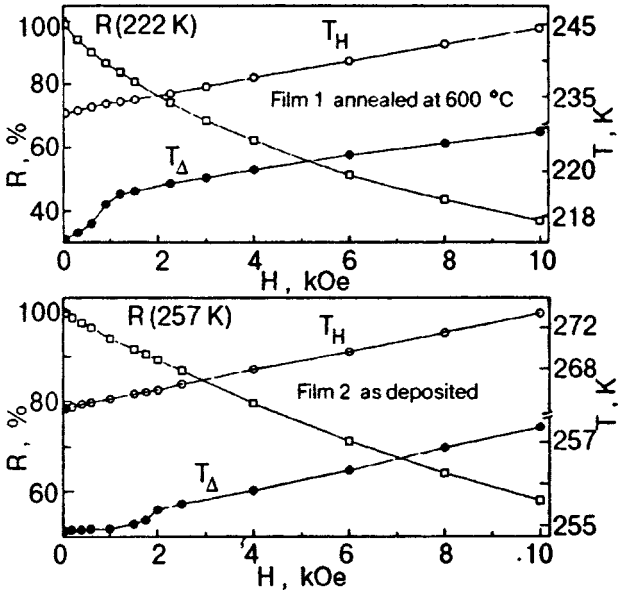

FIG. 2. Resistivity (□), temperatures of the magnetoresistance (T_Δ) and resistivity (T_H) peaks as a function of the magnetic field for film 1 (a) and for film 2 (b).

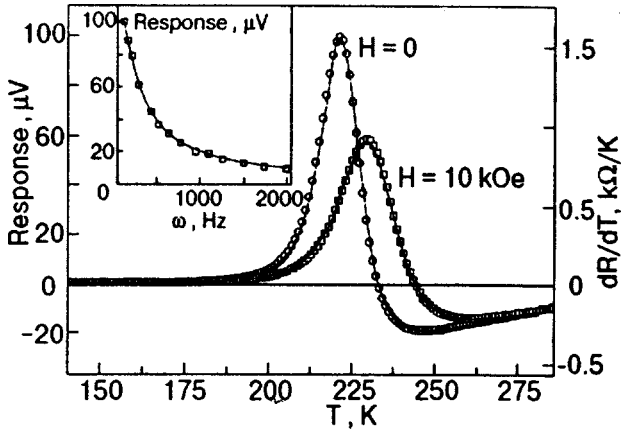

FIG. 3. Infrared response of film 1 with modulation frequency 20 Hz and bias current 100 μA for $H=0$ (○) and $H=10$ kOe (□). Solid lines are corresponding temperature derivatives dR/dT. The inset shows modulation angular frequency dependence of the response at 222 K. Here the solid line is the best fit of Eq. (3) to the data.

semiconductor-metal transition, as was indicated above. The value of the temperature coefficient of resistivity (TCR $=d\ \ln R/dT$) is about 12–14% K^{-1} in the vicinity of the phase transition. As is well known, the voltage of the optical response caused by the resistance modulation due to radiation-induced temperature modulation in the presence of a bias current is proportional to the temperature derivative of the electrical resistance[12]

$$\Delta V = I \frac{dR}{dT} \Delta T, \tag{2}$$

where I is the bias current, R is the electrical resistance of the sensor (MR film), and ΔT is the temperature difference between the film-substrate composite and the heat sink. Hence, the value of TCR is a key factor of the detector performance. The responsivity S of the radiation detector (the ratio output voltage to the incident power) can be calculated from the equation

$$S = \frac{\alpha I (dR/dT)}{G_{\text{eff}}(1+\omega^2\tau^2)^{1/2}}, \tag{3}$$

where α is the absorptance of the detector, G_{eff} is the effective thermal conductance, ω is the modulation angular frequency, and τ is the thermal time constant of the detector.

Infrared response measurements were performed in a thermostat cooled by liquid nitrogen flow. The film was clamped to sapphire plate mounted on the cooper holder. Four-probe technique was used with a direct 100-μA bias current. A 500-μW infrared diode with $\lambda = 0.94$ μm served as a radiation source. The distance from the output diode window to the film surface was 5 mm. The response was metered by a lock-in amplifier. The modulation voltage and reference signal were taken from a low-frequency oscillator. The temperature dependence of the response voltage is shown in Fig. 3 for zero applied magnetic field at $H=10$ kOe. The solid curves correspond to data obtained by differentiating $R_0(T)$ and $R_{10\,\text{kOe}}(T)$ (see Fig. 1). The strong correlation between the response voltage and corresponding derivative of $R(T)$ is apparent. This correlation signifies the bolometric character of infrared response. Using Eq. (2), we found the amplitude of the temperature modulation to be ~ 0.6 mK.

The inset in Fig. 3 represents the best fit of Eq. (3) to the modulation angular frequency dependence of the response. The fitting parameter τ was found to be ~ 6 ms. Preliminary studying shows that the detector is suitable even at room temperature (but with the responsivity only 10% of the maximum) and with long-wave infrared radiation such as hand heat. We hope to obtain a set of data concerning the thermal properties of films and substrates in our future research.

The practical application of MR films for magnetic field as well as radiation detection demands a reliable temperature stabilization of the operating point (T_{op}). Under this condition the maximum possible detectivity can be reached. The exponential character of a $R(T)$ dependence promises to facilitate the solution of this problem. The solution is possible when a film has $T_{\text{op}} > T_s$, where T_s is the surrounding temperature. In such a situation T_{op} can be reached at the expense of Joule power U^2/R, where U is the voltage applied to a film. In so doing, a film temperature would be relatively independent of T_s and stabilized due to the positive value of dR/dT. On the one hand, increasing T_s leads to an increase of the film temperature and resistance and, on the other hand, a higher R causes the Joule power to decrease. Such a feed back is valid for the opposite case in which T_s starts to decrease. In order to check this speculation the following experiment was carried out. Film 1 was situated in a thermostat and clamped to the holder with low thermal conductance. The holder temperature was controlled by a thermocouple, while for the film temperature control its resistance was used as a resistive thermometer. The operating point of the $R(T)$ dependence (at which MR ratio and optical response reach the maximum value) was estimated to be 222 K. A thermostat was cooled to 200 K, while film was

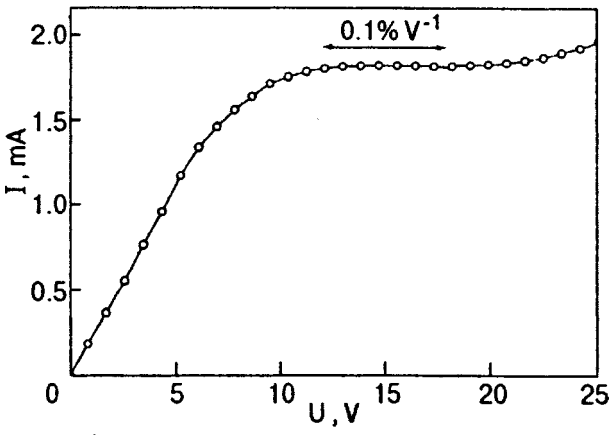

FIG. 4. The current–voltage characteristic demonstrates the heating of film 1 at the start temperature of 200 K.

heated to 222 K by increasing the bias current. The corresponding voltage was fixed. Then the thermostat temperature was changed to 215 K ($\Delta T_s = 15$ K). Under this condition the film temperature variation did not exceed 4.5 K, which is ~ 3 times less than ΔT_s. The $I-V$ characteristic corresponding to the Joule heating of the film 1 at the rate of 0.2 V/s is shown in Fig. 4. The ending of the linear part of the $I-V$ characteristic indicates the beginning of heating the film. Of special interest is the plateau in the vicinity of the operating point with $d \ln I/dU < 0.1\%\ V^{-1}$ within the interval $\Delta U \sim 5$ V. In this case the film works as a low-frequency stable current device.

In conclusion, $La_{0.7}Pb_{0.3}MnO_3$ epitaxial thin films were grown on LAO and STO substrates at different substrate temperatures. The film properties, including transition temperature, resistivity and MR ratio, depend on the type of substrate, deposition regime and oxygen content. Using Zhang's magnetic polaron theory, we established the phenomenological relation describing the temperature dependence of the film resistivity. An essential value of temperature coefficient of resistivity allows to use these films as an infrared bolometric detector as well as a low-frequency stable current device.

I wish to thank Yu. Medvedev and A. Martinovich for fruitful discussions and V. Kamenev for help in the x-ray measurements. Special thanks are to V. Krivoruchko for helpful suggestions.

*E-mail: khartsev@host.dipt.donetsk.ua

[1] K. Chahara, T. Ohno, M. Kasai, and Y. Kozono, Appl. Phys. Lett. **63**, 1990 (1993).
[2] G. Srinivasan, V. Suresh Babu, and M. S. Seehara, Appl. Phys. Lett. **67**, 2090 (1995).
[3] K. M. Satyalakshmi, S. S. Manoharan, M. S. Hedge, V. Prasad, and S. V. Subramanyam, J. Appl. Phys. **78**, 6861 (1995).
[4] H. L. Ju, C. Kwon, Qi Li, R. L. Greene, and T. Vekatesan, Appl. Phys. Lett. **65**, 2108 (1994).
[5] M. Rajeswari, C. H. Chen, A. Goyal, C. Kwon, M. C. Robson, R. Ramesh, T. Venkatesan, and S. Lakeou, Appl. Phys. Lett. **68**, 3555 (1996).
[6] C. W. Searle and S. T. Wang, Can. J. Phys. **47**, 2706 (1969).
[7] A. M. Grishin, S. I. Khartsev, and K. V. Rao, Appl. Phys. Lett. **68**, 2008 (1996).
[8] S. Zhang, J. Appl. Phys. **79**, 4542 (1996).
[9] F. M. Hundley, J. J. Neumeier, R. H. Heffner, Q. X. Jia, X. D. Wu, and J. D. Thompson, J. Appl. Phys. **79**, 4535 (1996).
[10] J. Fontcuberta, B. Martinez, A. Seffer, S. Pinol, J. L. Garcia-Munoz, and X. Obrador, Phys. Rev. Lett. **76**, 1122 (1996).
[11] M. Rubinstein, D. J. Gillespie, and J. E. Snyder, Phys. Rev. B **56**, 5412 (1997).
[12] Z. M. Zhang and A. Frenkel, J. Supercond. **7**, 871 (1994).

This article was published in English in the original Russian Journal. It was edited by S. J. Amoretty.

Critical behavior of small magnetic particles in Cr_2O_3

A. K. Murtazaev, Kh. K. Aliev, I. K. Kamilov, and K. Sh. Khizriev

Institute of Physics, Dagestan Science Center, Russian Academy of Sciences, 367003 Makhachkala, Russia
(Submitted December 9, 1997)
Fiz. Nizk. Temp. **24**, 462–467 (May 1998)

The critical behavior of small magnetic particles of the real antiferromagnet Cr_2O_3 is investigated by the Monte Carlo method. The critical exponents α,β,γ and the corresponding critical amplitudes for particles containing from 286 to 2502 spins are calculated. It is found that the presence of superficial spins extends the temperature range with the Heisenberg critical behavior and displaces the crossover temperature to the critical point. © *1998 American Institute of Physics.* [S1063-777X(98)00705-1]

INTRODUCTION

Quantitative description of critical phenomena in various lattice systems remains one of the most difficult problems in the contemporary theory of condensed state. It involves various methods of theoretical physics such as the renormalization group method and ε expansion, high- and low-temperature expansions, and Pade's method of approximants.[1–3] Usually, the critical behavior of lattice systems which undergo a second-order phase transition is described by the Ising and Heisenberg models as well as their various modifications. On the basis of these models, detailed information on the behavior of various thermodynamic quantities was obtained by using the above methods in a wide range of temperatures and other physical parameters. These models were also studied intensely by the Monte Carlo (MC) methods.[4,5] Experiments were made for lattices of various types in spatial dimensions, as well as by varying a large number of various parameters, which simultaneously provided a good deal of relevant information. In recent years, MC methods were are also successfully used for studying the critical region, including calculations of critical exponents (CE) and critical amplitudes (CA) to a high degree of accuracy.[6–8]

Until now, simple ferromagnetic model systems with interaction between nearest neighbors were mainly investigated.[4] Real antiferromagnetic systems with a specific crystallographic structure and with weak relativistic interactions of various types are studied much less comprehensively.

METHOD OF CALCULATIONS AND RESULTS

In this paper, the Monte Carlo method is used to study small magnetic particles in a real antiferromagnet Cr_2O_3 with a rhombohedral lattice. All the crystallographic, exchange, and other quantities correspond to real Cr_2O_3 samples and are taken from experimental studies.

The Hamiltonian of the system can be written in the form[9]

$$H=-\frac{1}{2}\sum_{i,j} J_1(\mu_i\mu_j)-\frac{1}{2}\sum_{k,l} J_2(\mu_k\mu_l)-D_0\sum_i (\mu_i^z)^2,$$
$$|\mu_i|=1. \qquad (1)$$

Here μ_i are unit vectors with continuous orientations, according to the results on neutron scattering and the theory of spin waves presented by Samuelson *et al.*,[10] J_1 the parameter of interaction of each spin with a nearest neighbor separated by the distance $r_{ij}=2.65$ Å, and J_2 is the parameter of interaction with three next neighbors separated by a distance $r_{ij}=2.89$ Å$(J_2=0.45J_1,\ J_1<0,\ J_2<0)$. The constants of interaction with more remote neighbors are much smaller and are disregarded. The Z-axis coincides with the direction of spatial diagonal of a rhombohedral cell [1,1,1]. Relativistic interactions of various types were approximated by the effective one-ion anisotropy $D_0>0$. The ratio of anisotropy to exchange was assumed to be $D_0/|J_1|=0.025$.[11]

The calculations were made for spherical particles of diameter $d=24.0$, 28.4, 32.8, 34.8, 41.82, 46.4, and 48.64 Å, and the number N of spins in particles was 286, 508, 760, 908, 1602, 2170, and 2502, respectively. Markov chains generated on a computer had lengths from 2×10^4 to 10^5 MCsteps/spin. In order to bring the system to equilibrium, a nonequilibrium region consisting of $5\times10^3-2\times10^4$ MC steps/spin (depending on the closeness to the critical region) was cut off.

In an analysis of critical phenomena by MC methods, the effect of the surface should be reduced, and various periodic boundary conditions are imposed on the system.[4] In our case, we consider systems with open surfaces since the problems associated with critical phenomena in small particles[12] as well as the dependence of CE and CA on the presence of a fraction of surface spins that are under conditions differing from those in the bulk are also of independent interest.[13] The fraction of surface spins for the particles under investigation varied from 46.8% for the smallest particle to 22.8% for a particle with $N=2502$. Since the total number of surface spins in particles is quite large, their influence on various thermodynamic parameters must be significant.

The conventional Hamiltonian in the isotropic Heisenberg model was studied in detail by various methods, and the values of critical exponents and amplitudes have been calculated to a high degree of accuracy.[14] In the case of Cr_2O_3, the results of experimental investigations of the critical behavior of heat capacity are also available. According to different authors and the results obtained by different methods of mea-

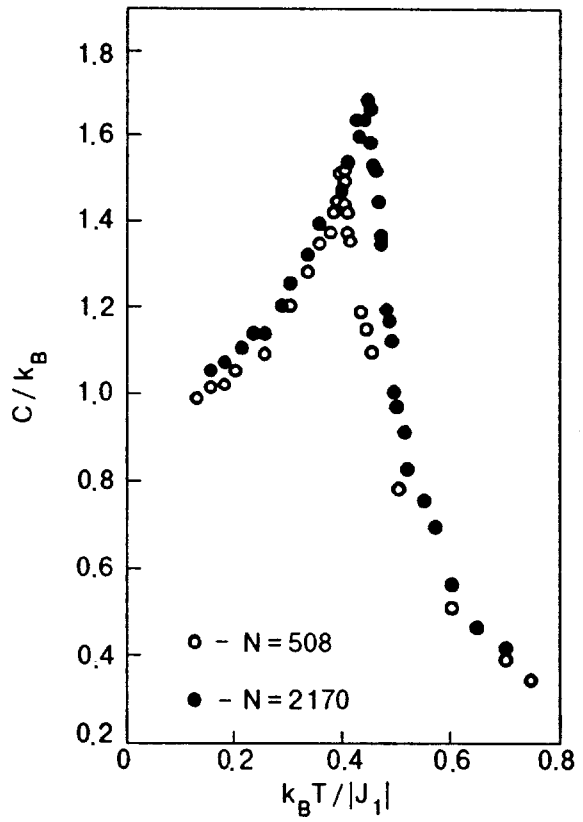

FIG. 1. Dependence of the heat capacity C/k_B on temperature $k_B/T/|J_1|$.

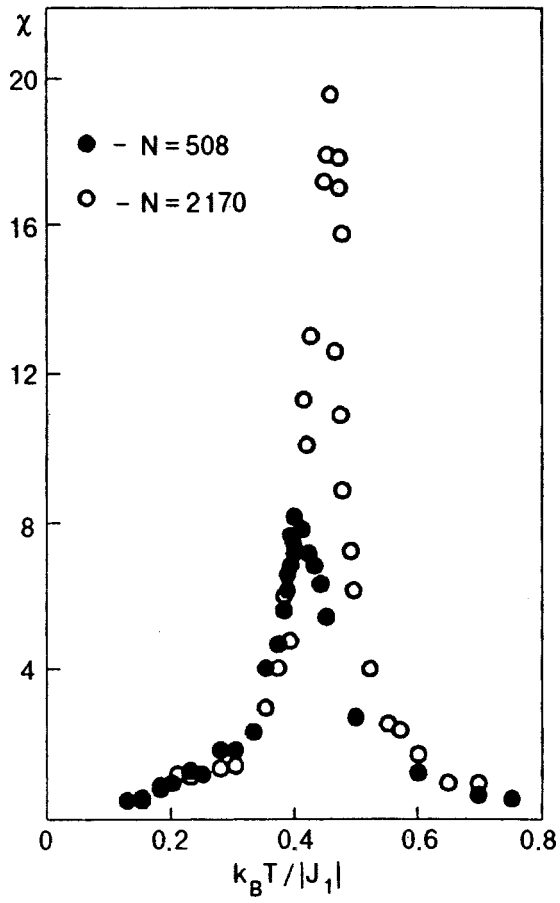

FIG. 2. Dependence of the susceptibility χ on temperature $k_B T/|J_1|$.

surements of heat capacity, the critical exponent α varies from 0.14 to -0.12.[15]

In order to trace the temperature variation of heat capacity and susceptibility, we used the following expressions:[7]

$$C=(NK^2)(\langle U^2\rangle-\langle U\rangle^2), \tag{2}$$

$$\chi=(NK)(\langle m^2\rangle-\langle m\rangle^2), \tag{3}$$

where $K=|J_1|/k_BT$, U is the internal energy, and m the sublattice magnetization.

The temperature dependences of C and χ have clearly manifested peaks in the critical region. It is well known that T_N for small systems is shifted towards low temperatures as compared to ''macrosystems.'' In our experiments, a clearly manifested displacement of the C and χ peaks upon the variation of N is also observed (Figs. 1 and 2). Figure 3 shows the dependences T^C and T^χ of critical temperatures on the radius R of particles, which were determined from the peaks of heat capacity C and susceptibility χ. It can be seen from Fig. 3 that, as the size of particles increases, the temperatures corresponding to heat capacity and susceptibility peaks are displaced to the high-temperature region, indicating an increase in the ''phase transition'' temperature.

The critical behavior of heat capacity was approximated by the formula[16]

$$C=\left[\frac{A}{\alpha}(|t|^{-\alpha}-1)+D|t|^x\right]+B+Et, \tag{4}$$

in which only the terms in brackets are retained for our Hamiltonian. In this expression, $t=(T-T_N)/T_N$, α, A, and D are the critical exponents of heat capacity, the critical amplitude, and the amplitude of correction to scaling, respectively. The same quantities with primes correspond to $T<T_N$. The value of x was put equal to 0.55.[14] The MC data were processed by using a nonlinear least squares method. The values minimizing the standard deviation were used as optimal values of α, A, and D. In operation with formula (4), the values corresponding to heat capacity peaks were used for T_N.

Table I contains the results obtained for α and A. All the values of α for $T>T_N$ are negative (which is typical of the Heisenberg critical behavior) and are virtually independent

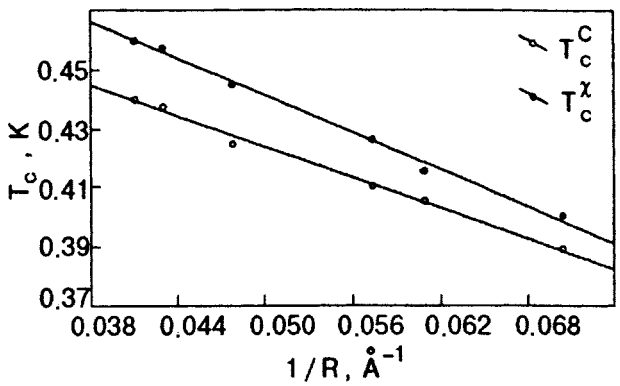

FIG. 3. Dependence of the critical temperature on the particle radius.

TABLE I. Critical exponents α and critical amplitudes A for particles with different numbers of pins N. The values of A' are obtained by putting $\alpha'=\alpha$.

	α	A	A'	α'	A	A'
N	$5\times10^{-3}\leqslant t\leqslant 7.5\times10^{-1}$			$2.5\times10^{-2}\leqslant t\leqslant 7.5\times10^{-1}$		
286	−0.20(3)	0.61	0.61	−0.19(3)	0.60	0.59
508	−0.18	0.57	0.55	−0.17	0.56	0.56
760	−0.20	0.67	0.67	−0.20	0.65	0.66
908	−0.17	0.57	0.58	−0.16	0.55	0.57
1 602	−0.19	0.66	0.60	−0.19	0.64	0.59
2 170	−0.17	0.61	0.64	−0.17	0.60	0.63
2 502	−0.21	0.63	0.68	−0.20	0.62	0.67

of the particle size. The absolute values of α are slightly smaller than the theoretical value $\alpha=-0.126(28)$ obtained for the Heisenberg isotropic model with short-range forces.[14] The values of A' for $T<T_N$ were calculated in the course of data processing under the assumption that $\alpha'=\alpha$ in accordance with predictions of static scaling.[1–3] The relations between the critical amplitudes A and A' determined according to this algorithm for all the particles belong to the interval $0.95\leqslant A/A'\leqslant 1.10$. Most of the laboratory studies of the heat capacity of Cr_2O_3[15,17] indicate that $\alpha<0$, but the absolute value varies over wide limits depending on the range of t and on the choice of T_N and some other parameters. It should be noted that, since the Hamiltonian (1) contains the term describing single-ion anisotropy, the critical behavior of Cr_2O_3 must display a crossover from the Heisenberg to Ising behavior.[2,18] In our calculations, the crossover temperature is $t_{cr}\approx 0.052$. However, the values of α obtained in the temperature range $5\times10^{-3}\leqslant t\leqslant 7.5\times10^{-1}$ do not indicate the crossover. This is probably due to the fact that the surface spins in Cr_2O_3 particles reorient themselves freely even at temperatures much lower than T_N (this was established by us earlier in Ref. 9). Such a behavior extends the region with the Heisenberg critical behavior and leads to a shift of the crossover temperature t_{cr} to the Néel point. Consequently, the entire range of reduced temperatures under investigation can correspond entirely to the Heisenberg critical behavior.

The obtained values of α, which are slightly smaller than those predicted by the theory[14] and laboratory experiments,[15,17] are also associated with the presence of a considerable fraction (22.8%–46.8%) of weakly trapped superficial spins. It should be noted that, according to the results of data processing in the low temperature phase $T<T_N$ without taking into account the scaling assumption $\alpha'=\alpha$, $\alpha'\approx 0.03(3)$ for all particles in the temperature intervals studied by us. The ratio of A to A' in this case belongs to the interval $2.0\leqslant A/A'\leqslant 5.0$.

In order to clarify the details of the critical behavior of a particle, we must consider the temperature dependence of sublattice magnetization and susceptibility. It should be noted at the very outset that these quantities are inconvenient for studying by the MC technique since the magnetization **m** near T_N has high-temperature ''tails,'' and χ is a strongly fluctuating quantity.

The temperature dependences of sublattice magnetization for two particles with $N=508$ and 2170 are shown in Fig. 4. It is worth noting that the magnetization curves have high-temperature ''tails'' decreasing with increasing N, which are typical of MC results.

In order to approximate the critical behavior of m, we used the formula

$$m=B|t|^{\beta}(1+a_m|t|), \tag{5}$$

where B and a_m are the critical amplitude and the amplitude of correction to scaling.

Table II contains the data obtained for β for $a_m=0$ in a certain temperature range $t_{min}\leqslant t\leqslant t_{max}$. It should be noted that, contrast to other critical indices (α and γ) considered by us, the value of β depends on the number of spins in the particle and increases with N. We observed one more peculiarity for β: the value of β increases with t_{min}. These peculiarities are apparently associated with short-range order effects which are clearly manifested in the high-temperature magnetization ''tails'' shown in Fig. 4. The dependences of m on t presented on double logarithmic scale display a kink at $T_B=0.08$. A typical pattern with two values of $\beta\approx 0.27$ at $t\leqslant t_B$ and $\beta\approx 0.38$ at $T>t_B$ is shown in Fig. 5 for a particle with $N=1602$. These data probably indicate a crossover from the Heisenberg behavior with $\beta\approx 0.38$ (in the Heisenberg model, $\beta=0.367$)[14] to the Ising behavior with $\beta\approx 0.27$ ($\beta=0.326$ in the Ising model),[14] which is not observed in the behavior of heat capacity.

Typical results for susceptibility determined on the basis of formula (3) are shown in Fig. 2. For the processing of

TABLE II. Effective values of the critical exponent β. For all temperature intervals, $t_{min}\leqslant t\leqslant t_{max}$, $t_{max}=0.75$.

	β						
	t_{min}, $a_m=0$				t_{min}, $a_m\neq 0$		
N	5×10^{-3}	1×10^{-2}	3×10^{-2}	8×10^{-2}	1×10^{-2}	3×10^{-2}	8×10^{-2}
286	0.18	0.21	0.26	0.31	-	-	-
508	0.22	0.25	0.29	0.32	0.23	0.28	0.34
760	0.25	0.27	0.30	0.33	0.25	0.30	0.36
908	0.25	0.31	0.32	0.36	0.26	0.31	0.38
1 602	0.29	0.31	0.33	0.36	0.28	0.32	0.38
2 170	0.33	0.37	0.39	0.41	0.30	0.35	0.39
2 502	0.33	0.37	0.40	0.43	0.30	0.34	0.40

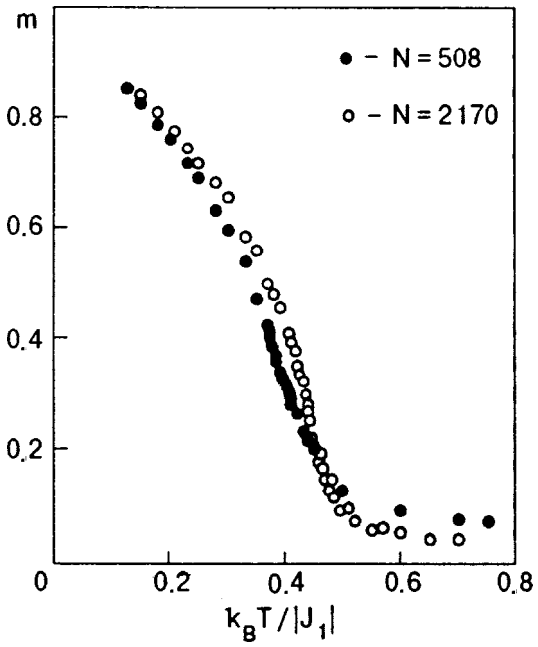

FIG. 4. Dependence of the sublattice magnetization **m** on the reduced temperature t.

these results, we used a simple power dependence of χ on t:

$$\chi = \Gamma |t|^{-\gamma}, \tag{6}$$

where γ and Γ are the critical exponent and amplitude of susceptibility. Table III contains the values of γ obtained on the basis of formula (6). The values of critical exponents γ and γ' were determined above and below T_N independently. The value of T_N was determined from the peak of the temperature dependence of χ. The critical exponents γ and γ' as well as α display no dependence on the number of spins in the particle. The values of γ and γ' strongly depend on $t_{\min}$ and increase with $t_{\min}$. It should be noted that the absolute values of γ and γ' cannot be used to classify the critical

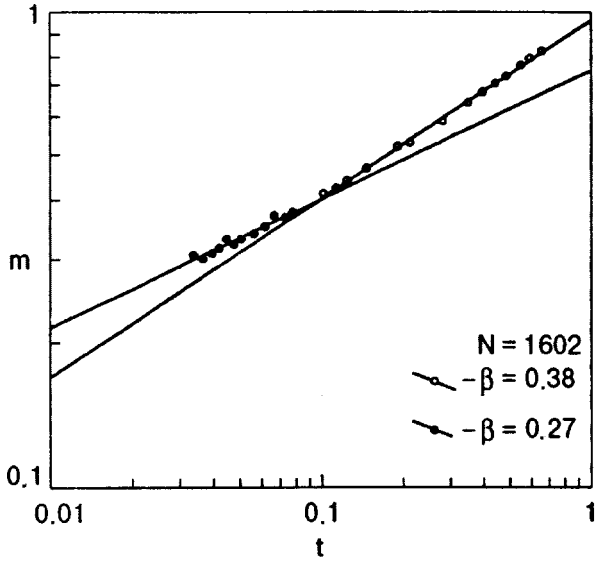

FIG. 5. Double logarithmic dependence of the sublattice magnetization **m** on the reduced temperature t.

TABLE III. Effective values of the critical exponents γ and γ'. For all temperature intervals, $t_{\max}=0.75$.

	γ			γ'		
			$t_{\min}$			
N	4×10^{-2}	8×10^{-2}	1×10^{-1}	4×10^{-2}	8×10^{-2}	1×10^{-1}
508	0.96(3)	1.14(3)	1.22(3)	0.90(3)	1.15(3)	1.33(3)
760	0.94	1.15	1.20	0.93	1.14	1.30
908	1.02	1.14	1.18	0.91	1.22	1.31
1 602	1.01	1.15	1.19	0.90	1.21	1.30
2 170	1.00	1.13	1.20	0.95	1.20	1.28
2 502	0.98	1.13	1.22	0.96	1.18	1.29

behavior of susceptibility as the Ising behavior ($\gamma=1.24$)[14] of the Heisenberg behavior ($\gamma=1.39$).[14] Concluding the section, we note that all the data were processed in the same temperature intervals for various values of $T_N'=T_N\pm\Delta T$, where ΔT was varied from 1.5 to 2.5% of T_N. The results obtained for α, A, A', γ, and γ' varied only within experimental error. The results obtained for β varied more strongly, decreasing and increasing with T_N, which was also attributed by us to the fact that the sublattice magnetization depends on the short-range order effects and on the presence of a free surface more strongly than other quantities.

CONCLUSION

The critical behavior of the heat capacity of small particles of Cr_2O_3 is of the Heisenberg nature and does not show a crossover to the Ising scenario. Susceptibility data can hardly be used for determining the nature of the critical behavior. It should be noted that the values of α as well as γ in the same temperature range do not depend on the number N of spins in a particle. On the contrary, the exponent β depends on N quite strongly, displaying a tendency to increase with N. The critical behavior of the sublattice magnetization **m** exhibits crossover effects typical of a transition from the Heisenberg critical behavior to the Ising behavior. A certain discrepancy between the theoretical[14] and experimental[15,17] values of critical indices is apparently associated with the presence of a large fraction of weakly trapped superficial spins, while the behavior of **m** and β is also determined by the peculiarities typical of MC method as applied to investigations of this type.

[1] A. Z. Patashinskii and V. L. Pokrovskii, *Fluctution Theory of Phase Transitions*, Pergamon, Oxford, 1979.
[2] S. Ma, *Modern Theory of Critical phenomena*, Benjamin/Cummings, Reading, Mass. (1976).
[3] H. Stanley, *Introduction to Phase Transitions and Critical Phenomena*, Pergamon Press, Oxford (1971).
[4] K. Binder (Ed.), *Monte Carlo Methods in Statistical Physics*, Springer-Verlag, Heidelberg (1979).
[5] K. Binder and D. V. Heerman, *Simulation by Monte Carlo Methods in Statistical Physics* [Russian Translation], Nauka, Moscow (1995).
[6] P. Peczak and D. P. Landau, Phys. Rev. B **43**, 1048 (1991).
[7] P. Peczak and D. P. Landau, Phys. Rev. B **43**, 6087 (1991).
[8] P. Peczak and D. P. Landau, Phys. Rev. B **47**, 14260 (1993).
[9] A. K. Murtazaev and I. A. Favorskii, Fiz. Nizk. Temp. **19**, 160 (1993) [Low Temp. Phys. **19**, 113 (1993)].
[10] E. J. Samuelson, M. T. Hutchings, and G. Shirane, Physica **48**, 13 (1970).
[11] J. O. Altman, J. C. Murphly, and S. Fones, Phys. Rev. A **138**, 912 (1965).

[12] Yu. I. Petrov, *Physics of Small Particles* [in Russian], Nauka, Moscow (1982).
[13] K. Binder and P. C. Hohenberg, Phys. Rev. B **9**, 2194 (1974).
[14] J. C. Le Guilio and J. Zinn-Justin, J. Phys. (France) Lett. **45**, L137 (1985).
[15] M. Marinelli, F. Mercuri, V. Zammit *et al.*, Phys. Rev. B **49**, 9523 (1994).
[16] G. Bednorz, D. J. W. Geldart, and M. A. White, Phys. Rev. B **47**, 14247 (1993).
[17] R. H. Bruce and D. S. Cannel, Phys. Rev. B **15**, 4451 (1977).
[18] I. K. Kamilov and Kh. K. Aliev, *Static Critical Phenomena in Magnetically Ordered Crystals* [in Russian], Dag. Sci. Center, Russ. Acad. Sci., Makhachkala (1993).

Translated by R. S. Wadhwa

LOW-DIMENSIONAL AND DISORDERED SYSTEMS

Backward helical waves in spatially disordered magnetic media

E. A. Ivanchenko

*National Science Center ''Kharkov Institute of Physics and Technology,'' 310108 Kharkov, Ukraine**

(Submitted November 4, 1997; revised December 19, 1997)
Fiz. Nizk. Temp. **24**, 468–473 (May 1998)

A nonlinear evolution system of hydrodynamic-type equations describing a three-dimensional multisublattice magnet is studied. An explicit expression is obtained for the energy density function of magnetic systems whose energy density is invariant to right- and left-spin rotations. Exact solutions for spin density are obtained in the form of helical waves for quadratic–biquadratic dependence of the energy density (in terms of Cartan's invariant functions) in three-dimensional case. Solutions are also obtained for magnon fields inducing such waves. The existence of backward helical waves is predicted. © *1998 American Institute of Physics.* [S1063-777X(98)00805-6]

1. INTRODUCTION

In spatially disordered media like the multisublattice magnets, superfluid phases of He-3, spin glasses, etc., spin-excitation investigations are carried out by using the hypothesis of spontaneous symmetry violation of the statistical equilibrium state.[1,2] Using this hypothesis, Halperin and Hohenberg[3] proposed a hydrodynamic approach which was used for formulating dynamic equations for magnetic media with a spontaneously broken symmetry relative to spin rotations. Linear dynamic equations were obtained by Halperin and Saslow,[4,5] while nonlinear dynamics was considered in the phenomenological Lagrangian approach by Volkov and Zheltukhin[6] and by Andreev and Marchenko.[7] Dzyaloshinskii and Volovik[8] used the Hamiltonian formalism for this purpose. The systems mentioned above have a number of interesting properties. The present communication is devoted to the prediction of one of them.

The dynamic variables describing the nonequilibrium state of magnets with a spontaneously broken symmetry include the spin density $s_\alpha(\mathbf{x})$ $(\alpha=x,y,z)$ and the order parameter, i.e., orthogonal rotational matrix $a_{\alpha\beta}(\mathbf{x})$ $(a^T a=1)$, for which the set of Poisson's brackets has the form

$$\begin{aligned}
&\{s_\alpha(\mathbf{x}),s_\beta(\mathbf{x}')\}=e_{\alpha\beta\gamma}s_\gamma(\mathbf{x})\,\delta(\mathbf{x}-\mathbf{x}'),\\
&\{s_\alpha(\mathbf{x}),a_{\beta\gamma}(\mathbf{x}')\}=e_{\alpha\gamma\rho}a_{\beta\rho}(\mathbf{x})\,\delta(\mathbf{x}-\mathbf{x}'),\\
&\{a_{\alpha\beta}(\mathbf{x}),a_{\gamma\rho}(\mathbf{x}')\}=0.
\end{aligned}\tag{1}$$

In the longwave limit where spatial inhomogeneities of dynamic variables are small, we shall investigate the dynamics and take into consideration the possible nonlinear interactions of spin waves, using the concept of spontaneous breaking of SO(3)-symmetry of spin rotations that leave the exchange interactions invariant. We shall assume that the energy density is a function of the quantities s, a, and ∇a or, which is the same, of the quantities $s,a,\omega_{ak}(a)$ $=(1/2)e_{\alpha\beta\gamma}a_{\lambda\gamma}\nabla_k a_{\lambda\beta}$ (Cartan's left form):

$$\varepsilon[\mathbf{x},s_\alpha(\mathbf{x}'),a(\mathbf{x}')]=\varepsilon[s_\alpha(\mathbf{x}),\omega_{\alpha k}(a),a],\quad k=x,y,z.\tag{2}$$

Since the energy density of exchange interactions is invariant relative to uniform rotations

$$\{S_\alpha,\varepsilon\}=0,\tag{3}$$

where

$$S_\alpha=\int d^3x s_\alpha(\mathbf{x}),$$

we obtain

$$\varepsilon(s,a,\omega_k)=\varepsilon(bs,ba,b\omega_k)=\varepsilon(\underline{s},\underline{\omega}_k).\tag{4}$$

Here, b is an arbitrary orthogonal matrix, $s\equiv as$; $\underline{\omega}_{\alpha k}=(1/2)e_{\alpha\beta\gamma}a_{\beta\lambda}\nabla_k a_{\gamma\lambda}$ is Cartan's right form. Using Poisson's brackets (1), we can write the equations of motion for a spatially disordered magnet in the Hamiltonian form without taking dissipation into account:

$$\begin{aligned}
&\dot{s}_\alpha=\{s_\alpha,H\}=-\nabla_k\partial_{\omega_{\alpha k}}\varepsilon,\\
&\dot{a}_{\alpha\beta}=\{a_{\alpha\beta},H\}=a_{\alpha\rho}e_{\rho\beta\gamma}\partial_{s_\gamma}\varepsilon,\\
&H=\int d^3x\,\varepsilon(\mathbf{x})
\end{aligned}\tag{5}$$

being the Hamiltonian of the system. The dot indicates partial derivative with respect to time.

Poisson's brackets for the variables $\underline{s}_\alpha\equiv a_{\alpha\beta}s_\beta$, $\underline{\omega}_{\alpha k}\equiv a_{\alpha\beta}\omega_{\beta k}$ have the form

$$\begin{aligned}
&\{\underline{s}_\alpha(\mathbf{x}),\underline{s}_\beta(\mathbf{x}')\}=-e_{\alpha\beta\gamma}\underline{s}_\gamma(\mathbf{x})\,\delta(\mathbf{x}-\mathbf{x}'),\\
&\{\underline{\omega}_{\alpha k}(\mathbf{x}),\underline{\omega}_{\beta i}(\mathbf{x}')\}=0,\\
&\{\underline{s}_\alpha(\mathbf{x}),\underline{\omega}_{\beta k}(\mathbf{x}')\}=e_{\alpha\nu\beta}\underline{\omega}_{\nu k}(\mathbf{x})\,\delta(\mathbf{x}-\mathbf{x}')\\
&\qquad\qquad+\delta_{\alpha\beta}\nabla'_k\delta(\mathbf{x}-\mathbf{x}').
\end{aligned}\tag{6}$$

Hence the evolution equations (5) in variables $\underline{s}_\alpha$, $\underline{\omega}_{\alpha k}$ assume the form of equations with Maurer-Cartan constraints[8,9]:

$$\dot{\underline{s}}_\alpha = -\nabla_k \partial_{\underline{\omega}_{\alpha k}} \varepsilon + e_{\alpha\beta\gamma}(\underline{s}_\beta \partial_{\underline{s}_\gamma} \varepsilon + \underline{\omega}_{\beta k} \partial_{\underline{\omega}_{\gamma k}} \varepsilon),$$

$$\dot{\underline{\omega}}_{\alpha k} = -\nabla_k \partial_{\underline{s}_\alpha} \varepsilon + e_{\alpha\beta\gamma} \underline{\omega}_{\beta k} \partial_{\underline{s}_\gamma} \varepsilon,$$

$$\nabla_k \underline{\omega}_{\alpha i} - \nabla_i \underline{\omega}_{\alpha k} = e_{\alpha\beta\gamma} \underline{\omega}_{\beta k} \underline{\omega}_{\gamma i}. \tag{7}$$

In these equations, $\underline{\omega}_\alpha = (1/2) e_{\alpha\beta\gamma} (\dot{a} a^T)_{\gamma\beta}$ is the right form associated with the time derivative, and $\underline{\omega}_\alpha \equiv -\partial_{\underline{s}_\alpha} \varepsilon$.

It follows from the system of equations (7) that the energy density ε and the momentum components π_i are conserved locally:

$$\dot{\varepsilon} = -\nabla_k \partial_{\underline{s}_\alpha} \varepsilon \, \partial \underline{\omega}_{\alpha k} \varepsilon, \quad \dot{\pi}_\alpha = -\nabla_k t_{ik}, \tag{8}$$

where $\pi_i = \underline{s}_\alpha \underline{\omega}_{\alpha i}$, and

$$t_{ik} = -\delta_{ik}(\varepsilon - \underline{s}_\alpha \partial_{\underline{s}_\alpha} \varepsilon) + \underline{\omega}_{\alpha i} \partial_{\underline{\omega}_{\alpha k}} \varepsilon \tag{9}$$

is the momentum flux density tensor.

The general system of equations (7) was studied by us in an earlier work.[11] In the present work, we shall obtain the analytic expressions describing helical spin density waves in a three-dimensional anisotropic magnet taking into account biquadratic contributions to the energy density. The existence of backward helical spin waves is predicted. Ivanov[12] used the Lagrangian approach for the quadratic dependence of the energy density (amorphous magnet) to obtain the soliton solutions. Sukstanskii and Ivanov[13] studied the nonlinear dynamics of multisublattice noncollinear antiferromagnets with a modulated magnetic structure in an external magnetic field.

MODEL ENERGY DENSITY

Let us study a disordered magnet whose energy density is invariant to left- and right-spin rotations. In this case, the energy density function ε satisfies the overdetermined system of partial differential equations[10]:

$$e_{\alpha\beta\gamma}(\underline{s}_\beta \partial_{\underline{s}_\gamma} \varepsilon + \underline{\omega}_{\beta k} \partial_{\underline{\omega}_{\gamma k}} \varepsilon) = 0. \tag{10}$$

The general solution of this system has the form

$$\varepsilon = G(\underline{s}_\alpha^2, \underline{\omega}_{\alpha x}^2, \underline{\omega}_{\alpha y}^2, \underline{\omega}_{\alpha z}^2, \pi_x, \pi_y, \pi_z), \tag{11}$$

where G is an arbitrary function of the above-mentioned arguments. Since the system of equations (10) is invariant to the group of transpositions of the subscript k, it is expedient to go over to symmetric variables. After this, we can use the following expression for energy density for practical calculations:

$$\varepsilon = \varepsilon_i + \varepsilon_a,$$

where

$$\varepsilon_i = \frac{1}{2\chi} \underline{s}_\alpha^2 + \frac{\rho}{2} \underline{\omega}_{\alpha k}^2 + \frac{1}{4\chi_1} \underline{s}_\alpha^4 + \frac{\rho_1}{4} \underline{\omega}_{\alpha k}^4 + \frac{q}{2} \pi_i^2 \tag{12}$$

is the isotropic and

$$\varepsilon_a = \frac{\rho_2}{4} (\underline{\omega}_{\alpha x}^2 \underline{\omega}_{\alpha y}^2 + \underline{\omega}_{\alpha x}^2 \underline{\omega}_{\alpha z}^2 + \underline{\omega}_{\alpha y}^2 + \underline{\omega}_{\alpha z}^2) \tag{13}$$

the anisotropic component of energy (without taking into account the differential equations of coupling between $\underline{\omega}_{\alpha x}, \underline{\omega}_{\alpha y}, \underline{\omega}_{\alpha z}$), χ is the magnetic susceptibility, ρ the ''rigidity'' constant, $\chi_1, \rho_1, \rho_2, q$ are phenomenological coupling constant. The model under consideration can be interpreted as the continual limit of the system of distributed symmetric tops.

SOLUTION OF EQUATIONS

Let us now determine the exact nonlinear solutions of stationary profile, i.e., for the case when the required functions $\underline{s}_\alpha(\mathbf{x},t), \underline{\omega}_{\alpha k}(\mathbf{x},t)$ depend on the self-simulating variable $\mathbf{q}\cdot\mathbf{x} - et$ (the parameter e determines the possible velocities of propagation of perturbations in the system, and the vector $\mathbf{q}$ is associated with the direction of wave propagation, see below). Owing to Maurer–Cartan differential constraints, the system of equations (7) in the three-dimensional case is reduced to the one-dimensional case considered in Ref. 14. This follows from the fact that if the variables $\underline{\omega}_{\alpha x}, \underline{\omega}_{\alpha y}, \underline{\omega}_{\alpha z}$ depend on $\mathbf{q}\cdot\mathbf{x} - et$, the constraints

$$\nabla_k \underline{\omega}_{\alpha i} - \nabla_l \underline{\omega}_{\alpha k} = e_{\alpha\beta\gamma} \underline{\omega}_{\beta k} \underline{\omega}_{\gamma i} \tag{14}$$

are holonomic, i.e., integrable:

$$\underline{\omega}_{\alpha y} = \frac{q_y}{q_x} \underline{\omega}_{\alpha x},$$

$$\underline{\omega}_{\alpha z} = \frac{q_z}{q_x} \underline{\omega}_{\alpha x}. \tag{15}$$

The initial system (7) now assumes the form

$$-e(\underline{s}_\alpha)' = -q_x(\partial_{\underline{\omega}_{\alpha x}} \varepsilon)',$$

$$-e(\underline{\omega}_{\alpha x})' = -q_x(\partial_{\underline{s}_\alpha} \varepsilon)' + e_{\alpha\beta\gamma} \underline{\omega}_{\beta x} \partial_{\underline{s}_\gamma} \varepsilon, \tag{16}$$

$$f' \equiv \frac{df}{d(\mathbf{q}\cdot\mathbf{x} - et)}.$$

It follows directly from the above system that

$$-\overline{e}\,\underline{s}_\alpha + \overline{\rho}\,\underline{\omega}_{\alpha x} = C_\alpha,$$

$$\overline{e} \equiv e - q_x l q \pi,$$

$$\overline{\rho} \equiv q_x l \rho + q_x \left(l^2 \rho_l + \frac{q_x^2 q_y^2 + q_x^2 q_z^2 + q_y^2 q_z^2}{q_x^4} \rho_2 \right) \underline{\omega}_{\alpha x}^2, \tag{17}$$

$$l \equiv \frac{\mathbf{q}^2}{q_x^2}, \quad \pi \equiv \underline{s}_\alpha \underline{\omega}_{\alpha x},$$

where C_α are integration constants. Using Eq. (17), we can easily eliminate the unknown functions $\underline{\omega}_{\alpha x}$ in the system (16). It should also be noted that the quantities π and $\underline{\omega}^2{}_{\alpha x}$ are functions of $\underline{s}_\alpha^2$ and $C_\alpha \underline{s}_\alpha$ (see Appendix).

Finally, using the gauge transformation

$$\xi = \frac{(\mathbf{q}\cdot\mathbf{x} - et)|\mathbf{C}|}{-\overline{e}^2 \overline{\chi} + \overline{\rho}}, \tag{18}$$

in which the susceptibility $\overline{\chi}$ is now equal to

$$\frac{1}{\overline{\chi}} \equiv \frac{1}{\chi} + \frac{1}{\chi_1} \underline{s}_\alpha^2, \tag{19}$$

we arrive at a linear system of Euler equations for the right form $\underline{s}_\alpha$:

$$\frac{d}{d\xi} \underline{s}_\alpha = e_{\alpha\beta\gamma} n_\beta \underline{s}_\gamma, \quad n_\alpha \equiv \frac{C_\alpha}{|\mathbf{C}|}. \tag{20}$$

The solution of this system of equations has the form

$$\underline{s}_\alpha(\xi) = g_{\alpha\beta} \underline{s}_\beta(\xi_0), \tag{21}$$

where the orthogonal rotation matrix $g(g^T g = 1)$ is defined as

$$g_{\alpha\beta} = \cos\,\xi \delta_{\alpha\beta} + (1 - \cos\,\xi) n_\alpha n_\beta - \sin\,\xi e_{\alpha\beta\gamma} n_\gamma, \tag{22}$$

$\underline{s}_\beta(\xi_0)$ being the integration constant.

Using the obtained solution for the right form (21), we can define the spin density as follows:

$$s_\alpha = a_{\beta\alpha} \underline{s}_\beta. \tag{23}$$

The orthogonal rotation matrix $a_{\alpha\beta}$ satisfies the overdetermined system of equations

$$\begin{aligned} \underline{\omega}_\alpha &= \frac{1}{2} e_{\alpha\beta\gamma} a_{\beta\lambda} \dot{a}_{\gamma\lambda}, \\ \underline{\omega}_{\alpha k} &= \frac{1}{2} e_{\alpha\beta\gamma} a_{\beta\lambda} \partial_k a_{\gamma\lambda}, \\ k &= x, y, z, \end{aligned} \tag{24}$$

as well as relations (15).

While solving the system (24) relative to the matrix $a_{\alpha\beta}$, we use the parametrization of Euler's angles[15]:

$$a = \begin{pmatrix} \cos\,\psi \cos\,\varphi - \cos\,\theta \sin\,\psi \sin\,\varphi & \cos\,\theta \sin\,\psi \cos\,\varphi + \cos\,\psi \sin\,\varphi & \sin\,\theta \sin\,\psi \\ -\sin\,\psi \cos\,\varphi - \cos\,\theta \cos\,\psi \sin\,\varphi & \cos\,\theta \cos\,\psi \cos\,\varphi - \sin\,\psi \sin\,\varphi & \sin\,\theta \cos\,\psi \\ \sin\,\theta \sin\,\varphi & -\sin\,\theta \cos\,\varphi & \cos\,\theta \end{pmatrix}. \tag{25}$$

In terms of the variables ψ,θ,φ, the system of equations (24) assumes the form

$$\begin{aligned} \underline{\omega}_1 &= -\dot{\theta} \cos\,\psi - \dot{\varphi} \sin\,\theta \sin\,\psi, \\ \underline{\omega}_2 &= \dot{\theta} \sin\,\psi - \dot{\varphi} \sin\,\theta \cos\,\psi, \\ \underline{\omega}_3 &= -\dot{\psi} - \dot{\varphi} \cos\,\theta, \\ \underline{\omega}_k &= -\theta_k \cos\,\psi - \varphi_k \sin\,\theta \sin\,\psi, \\ \underline{\omega}_{2k} &= \theta_k \sin\,\psi - \varphi_k \sin\,\theta \cos\,\psi, \\ \underline{\omega}_{3k} &= -\psi_k - \varphi_k \cos\,\theta, \\ \underline{\omega}_{\alpha y} &= \frac{q_y}{q_x} \underline{\omega}_{\alpha x}, \quad \underline{\omega}_{\alpha z} = \frac{q_z}{q_x} \underline{\omega}_{\alpha x}. \end{aligned} \tag{26}$$

Let us now consider the case when $\mathbf{n} = (0,0,-1)$, i.e., $C_3 < 0$ and $\mathbf{s}(\xi_0) = (c_1, 0, c_3)$. The exact solution of the overdetermined system (26) can easily be obtained for $\varphi = \varphi_0 = \text{const}$. Under these conditions, if we take into account Eqs. (16) and (21), the system of equations (26) contains the integral subsystem

$$\begin{aligned} -\dot{\theta} \cos\,\psi &= -\left(\frac{1}{\overline{\chi}} + q l \pi z\right) c_1 \cos\,\xi, \\ \dot{\theta} \sin\,\psi &= \left(\frac{1}{\overline{\chi}} + q l \pi z\right) c_1 \sin\,\xi, \\ -\dot{\psi} &= -(q l \pi) \frac{C_3}{\overline{\rho}} - \left(\frac{1}{\overline{\chi}} + q l \pi z\right) c_3, \\ -\theta_x \cos\,\psi &= z c_1 \cos\,\xi, \\ \theta_x \sin\,\psi &= -z c_1 \sin\,\xi, \\ -\psi_x &= \frac{C_3}{\overline{\rho}} + z c_3, \\ z &\equiv \frac{\overline{e}}{\overline{\rho}}. \end{aligned} \tag{27}$$

Hence the solution for the function $\psi(\mathbf{x},t)$ in the R^3-space can obviously be represented in the form

$$\psi(\mathbf{x},t) = -\left(\frac{C_3}{\overline{\rho}} + z c_3\right) \mathbf{q}\mathbf{x} + \left[\left(\frac{1}{\overline{\chi}} + q l \pi z\right) c_3 + q l \pi \frac{C_3}{\overline{\rho}}\right] t + \psi_0, \tag{28}$$

where ψ_0 is a constant.

The overdetermination of the differential system (27) with respect to the function $\theta(\mathbf{x},t)$ can be removed easily when the equality of functions $\xi(\mathbf{x},t) = \psi(\mathbf{x},t)$ is observed, i.e., under the conditions

$$\begin{aligned} -\left(\frac{C_3}{\overline{\rho}} + z c_3\right) &= q_x k_1, \\ \left(\frac{1}{\overline{\chi}} + q l \pi z\right) c_3 + q l \pi \frac{C_3}{\overline{\rho}} &= -k_1 e, \\ k_1 &\equiv \frac{|C_3|}{-\overline{e^2 \chi} + \underline{\rho}}, \quad \underline{\rho} \equiv q_x \overline{\rho}. \end{aligned} \tag{29}$$

These relations define an overdetermined system of algebraic equations in the parameter $\overline{e}$ whose compatibility equation has the form

$$\overline{e}^2 - \frac{|C_3|}{c_3}\,\overline{e} - \frac{\underline{\underline{\rho}}}{\underline{\underline{\chi}}} = 0. \tag{30}$$

Hence the function $\theta(\mathbf{x},t)$ can be defined on the set $\{\mathbf{x},t:\xi \neq \pi/2m,\ m=0,\pm 1,\pm 2,...\}$ as follows:

$$\theta(\mathbf{x},t) = \omega t - \mathbf{k}\cdot\mathbf{x} + \theta_0, \tag{31}$$

where

$$\mathbf{k} = \frac{c_1}{\underline{\rho}}\left(\frac{|C_3|}{2c_3} \pm \left(\frac{C_3^2}{4c_3^2} + \frac{\underline{\underline{\rho}}}{\underline{\underline{\chi}}}\right)^{1/2}\right)\mathbf{q},$$

$$\omega = \frac{1}{\underline{\underline{\chi}}}c_1 + q\pi l q_x \frac{\overline{e}}{\underline{\rho}}\,c_1 = \frac{\underline{\rho}}{c_1\mathbf{q}^2}\,\mathbf{k}^2 - \frac{|C_3|}{c_3}\,\frac{\mathbf{k}\cdot\mathbf{q}}{\mathbf{q}^2} + ql q_x \frac{\mathbf{k}\cdot\mathbf{q}}{q^2}\left(\frac{-|C_3|c_3}{\overline{\rho}} + \frac{c_1^2+c_3^2}{c_1}\,q_x\,\frac{\mathbf{k}\cdot\mathbf{q}}{\mathbf{q}^2}\right), \tag{32}$$

and θ_0 is a constant.

The solutions for parameters φ,θ,ψ define the rotation matrix (25) and, in accordance with formula (23), the spin density s_α:

$$\begin{aligned} s_1 &= c_3 \sin\varphi_0 \sin\theta + c_1 \cos\varphi_0, \\ s_2 &= -c_3 \cos\varphi_0 \sin\theta + c_1 \sin\varphi_0, \\ s_3 &= c_3 \cos\theta. \end{aligned} \tag{33}$$

The obtained exact solutions are helical waves with helical vector $\mathbf{k}$ and dispersion relation (32) for ω, and satisfy the initial system (5). Putting $\mathbf{q}=(1,0,0)$ and replacing e by $-e$, we arrive at the result obtained by us earlier in Ref. 14.

The effective magnetic field h_α forming a helical spin-density wave s_α (33) is determined from the relation $h_\alpha \equiv \partial_{s_\alpha}\varepsilon$ and is defined as

$$h_\alpha = \left(\frac{1}{\chi} + \frac{1}{\chi_1}\,(c_1^2+c_3^2)\right)s_\alpha + ql\left(\frac{C_3c_3}{\overline{\rho}} + (c_1^2+c_3^2)\,\frac{q_x}{\mathbf{q}^2}\,\mathbf{k}\cdot\mathbf{q}\right) \times\left(\frac{a_{3\alpha}C_3}{\overline{\rho}} + \frac{q_x}{c_1\mathbf{q}^2}\,\mathbf{k}\cdot\mathbf{q}s_\alpha\right). \tag{34}$$

BACKWARD SPIN DENSITY WAVES

By definition, the backward spin waves describe a wave process in which the energy can be transported at an angle larger than $\pi/2$ relative to the direction of wave propagation.

According to formula (8), the energy flux density is defined as

$$j_k = \partial_{\underline{s}_\alpha}\varepsilon\,\partial_{\omega_{\alpha k}}\varepsilon. \tag{35}$$

For the helical spin waves obtained by us, this vector assumes the form

$$\begin{aligned} \mathbf{j} &= \left(\left[\frac{\underline{\underline{\rho}}}{\underline{\underline{\chi}}} + ql\underline{\rho}\,\underline{\omega}_{\alpha x}^2 + \left(\frac{1}{\underline{\underline{\chi}}}\right)ql\underline{s}_\alpha^2 + (ql\pi)^2\right]\pi, 0, 0\right), \\ \pi &= \frac{C_3c_3 + \overline{e}(c_1^2+c_3^2)}{\overline{\rho}}. \end{aligned} \tag{36}$$

Let us now determine the cosine of the angle between the direction of wave propagation $\mathbf{k}$ and the direction of energy flux density $\mathbf{j}$:

$$\cos w = \frac{\mathbf{k}\cdot\mathbf{j}}{|\mathbf{k}||\mathbf{j}|}. \tag{37}$$

It can easily be shown that for $\overline{e}$ defined by Eq. (30), the expression $[C_3c_3 + \overline{e}(c_1^2+c_3^2)]\overline{e}$ is positive. As a result, formula (37) assumes the form

$$\cos w = \frac{|q_x|}{\sqrt{q_x^2+q_y^2+q_z^2}} \times \operatorname{sgn}\left\{\left[\frac{\underline{\underline{\rho}}}{\underline{\underline{\chi}}} + ql\underline{\rho}\,\underline{\omega}_{\alpha x}^2 + \frac{1}{\underline{\underline{\chi}}}ql\underline{s}_\alpha^2 + (ql\pi)^2\right]c_1\right\}. \tag{38}$$

Since the constant c_1 can be positive as well as negative in the model under consideration, we arrive at the conclusion that helical waves in a heterogeneous magnet can propagate in a direction opposite to the energy transportation direction. For example, formula (38) assumes a simple form for all positive phenomenological coupling constants:

$$\cos w = \frac{|q_x|}{\sqrt{q_x^2+q_y^2+q_z^2}}\operatorname{sgn} c_1. \tag{39}$$

Processes with a negative group velocity were studied experimentally[16] and theoretically[17] in connection with waves in a rotating liquid. Such an effect can be observed in disordered magnets.

CONCLUSION

A stepwise solution of systems of first-order equations is a characteristic feature of the Hamiltonian formalism. Hence the form of the solution (21) at the intermediate stage is entirely responsible for the choice of parametrization (25) which considerably simplifies integration.

According to (33), the exact nonlinear solutions presented here are helical waves. The contribution of biquadratic terms to the energy density (12) increases with the initial spin density distribution in the system. The dependence on the coupling constant q is contained only in the frequency ω of the spin density helical wave (32), and the wave vector $\mathbf{k}$ is independent of this constant. Energy transport may occur at an angle larger than $\pi/2$ relative to the direction of propagation of the helical spin wave.

The author is obliged to S. V. Peletminskii for stimulating discussions.

This research was supported by the Ukrainian Foundation for Fundamental Research (project No. 2.4/378).

APPENDIX

Using the compatibility condition

$$\underline{\omega}_{\alpha x}^2 = \frac{C_\alpha^2 + 2\overline{e}C_\alpha\underline{s}_\alpha + \overline{e}^2\underline{s}_\alpha^2}{\overline{\rho}^2} \tag{A1}$$

we can eliminate ρ from formula

$$\overline{e}^2 - i\overline{e} - \frac{\rho}{\overline{\chi}} = 0. \tag{A2}$$

As a result, we obtain a sixth-degree equation:

$$\begin{aligned} &\overline{e}^6 - 3i\overline{e}^5 + (3i^2 - p_1)\overline{e}^4 + (2ip_1 - i^3)\overline{e}^3 \\ &\quad - \left(i^2 p_1 + \frac{c_1^2 + c_3^2}{c_3^2}\, p \right) \overline{e}^2 + 2ip\overline{e} - i^2 p = 0, \\ &i \equiv \frac{|C_3|}{c_3}, \quad p_1 \equiv \frac{\mathbf{q}^2 \rho}{\overline{\chi}}, \\ &p \equiv \frac{c_3^2}{\overline{\chi}^3} \left[\mathbf{q}^4 \rho_1 + (q_x^2 q_y^2 + q_x^2 q_z^2 + q_y^2 q_z^2) \rho_2 \right]. \end{aligned} \tag{A3}$$

Under the constraint $c_1 = \pm c_3$, we can represent the above equation in the form

$$(\overline{e}^2 - i\overline{e} - r_1)(\overline{e}^2 - i\overline{e} - r_2)(\overline{e}^2 - i\overline{e} - r_3) = 0, \tag{A4}$$

where r_1, r_2, r_3 are the roots of the cubic equation

$$r^3 - p_1 r^2 - 2pr - pi^2 = 0, \quad r \equiv \frac{\rho}{\overline{\chi}}. \tag{A5}$$

Thus, we have proved that r depends on $C_\alpha \underline{s}_\alpha, \underline{s}_\alpha^2$ under the condition $c_1 = \pm c_3$. Hence $\underline{\omega}_{\alpha x}^2$ and π also depend on $C_\alpha \underline{s}_\alpha, \underline{s}_\alpha^2$, i.e., do not depend on the self-simulating variable $\mathbf{q}\cdot\mathbf{x} - et$. Note that the constraint $c_1 = \pm c_3$ is imposed by taking into consideration only biquadratic terms proportional to ρ_1 and ρ_2, without which we obtain $r = p_1$.

*E-mail: yevgeny@kipt.kharkov.ua

[1] N. N. Bogolubov, Physica **26**, 1 (1960).
[2] J. J. Goldstone, Nuovo Cimento **19**, 154 (1961).
[3] B. I. Halperin and P. C. Hohenberg, Phys. Rev. **188**, 898 (1969).
[4] B. I. Halperin and W. M. Saslow, Phys. Rev. B **16**, 2154 (1977).
[5] W. M. Saslow, Phys. Rev. B **22**, 1174 (1980).
[6] D. V. Volkov and A. A. Zheltukhin, Izvestiya Akad. Nauk SSSR, ser. Fiz. **44**, 1487 (1980) [Izv. Akad. Nauk SSSR, Ser. Fiz. (1980)].
[7] A. F. Andreev and V. I. Marchenko, Usp. Fiz. Nauk **130**, 39 (1980) [Sov. Phys. Usp. **23**, 21 (1980)].
[8] I. E. Dzyaloshinskii and G. E. Volovik, Ann. Phys. **125**, 67 (1980).
[9] M. Yu. Kovalevskii, S. V. Peletminskii, and A. L. Shishkin, Ukr. Fiz. Zh. **36**, 245 (1991).
[10] M. Yu. Kovalevskii and S. V. Peletminskii, Teor. Mat. Fiz. **100**, 59 (1994).
[11] E. A. Ivanchenko, Fiz. Nizk. Temp. **20**, 158 (1994) [Low Temp. Phys. **20**, 127 (1994)].
[12] B. A. Ivanov, Solid State Commun. **34**, 437 (1980).
[13] A. L. Sukstanskii and B. A. Ivanov, Zh. Éksp. Teor. Fiz. **108**, 914 (1995) [JETP **81**, 502 (1995)].
[14] E. A. Ivanchenko, Fiz. Nizk. Temp. **23**, 830 (1997) [Low Temp. Phys. **23**, 623 (1997)].
[15] H. Goldstein, *Classical Mechanics*, Addison-Wesley, Reading, MA, 1980.
[16] A. Ibbetson and N. Phillips, Tellus **19**, 81 (1967).
[17] M. S. Longuet-Higgins, J. Fluid Mech. **31**, 417 (1968).

Translated by R. S. Wadhwa

Low-temperature properties of two *XY* spin chains with a point contact

E. V. Ezerskaya

*Kharkov State University, 310077 Kharkov, Ukraine**

(Submitted December 2, 1997)
Fiz. Nizk. Temp. **24**, 474–480 (May 1998)

The energy spectrum of a one-dimensional, exactly solvable spin model formed by two semi-infinite *XY* spin chains with spin $s=1/2$ with a point-contact interaction in a longitudinal magnetic field is calculated. It is shown that the spectrum of such a system can contain one or two local energy levels apart from two bands overlapping in weak fields. Local thermodynamic parameters of the chains can have singularities at zero temperature. © *1998 American Institute of Physics.* [S1063-777X(98)00905-0]

1. INTRODUCTION

Consistent interest to theoretical studies of various models of spin chains is due to a large number of anisotropic magnets whose properties are correctly described by such models over a wide temperature range. On the other hand, exact solutions can often be obtained for one-dimensional systems. For example, a one-dimensional *XY* model in which only transverse components of the spin ($s=1/2$) are coupled through the exchange interaction is used for explaining the properties of the compounds $PrCl_3$,[1] $Pr(C_2H_5SO_4)_3\cdot 9H_2O$,[2] and Cs_2CoCl_4.[3] This model is exactly solvable since its Hamiltonian can be transformed to the Hamiltonian of an ideal gas of spinless fermions not only for a system with a simple unit cell,[4,5] but also for a chain with two sublattices.[6] The introduction of an impurity site into the chain does not obstruct the exact diagonalization of the Hamiltonian either. For definite relations connecting the parameters of the impurity and the host matrix, localized states can appear in the spectrum of elementary excitations, which affects significantly the resonant and thermodynamic properties at low temperatures.[7–12]

Here we consider a model system formed by two semi-infinite *XY* chains with different exchange interaction constants and with different magnetons interacting as a point contact. This model is exactly solvable, and the presence of a ''phase boundary'' leads to a number of nontrivial effects. The point contact can operate as a potential wall leading to scattering of elementary excitations and to solutions with exponential attenuation of the wave function in one of the chains. In the case of a strong interaction between the chains, the contact exhibits the properties of a potential well, which leads to the emergence of localized states. The presence of such states can affect significantly the behavior of local thermodynamic parameters of the chains.

2. ENERGY SPECTRUM OF TWO *XY* CHAINS WITH A POINT CONTACT

Let us consider two interacting semi-infinite *XY* chains described by the Hamiltonian

$$\begin{aligned}\mathscr{H}=&-2H\mu_1\sum_{n\leqslant 0}S_n^z-J_1\sum_{n<0}(S_n^xS_{n+1}^x+S_n^yS_{n+1}^y)\\&-2H\mu_2\sum_{n\geqslant 1}S_n^z-J_2\sum_{n\geqslant 1}(S_n^xS_{n+1}^x+S_n^yS_{n+1}^y)\\&-J_0(S_0^xS_1^x+S_0^yS_1^y),\end{aligned}\tag{1}$$

where $J_1>0$ and $J_2>0$ are the constants of exchange interaction along *XY*-chains, J_0 is the constant of exchange interaction at the contact, μ_1 and μ_2 are magnetons of the chains, and H is the magnetic field. Using the well-known Jordan–Wigner transformation[4–6,13]

$$S_n^{\pm}=S_n^x\pm iS_n^y;\quad S_n^z=1/2-S_n^-S_n^+;$$

$$S^+=\prod_{m<n}(1-2a_m^+a_m)a_n;\quad S^-=a_n^+\prod_{m<n}(1-2a_m^+a_m)$$

we can write Hamiltonian (1) in the form that is quadratic in the operators a_n^+ and a_n with the Fermi commutation relations

$$\begin{aligned}\mathscr{H}=&E_0+2\mu_1H\sum_{n\leqslant 0}a_n^+a_n-\frac{1}{2}J_1\sum_{n<0}(a_n^+a_{n+1}+a_{n+1}^+a_n)\\&+2\mu_2H\sum_{n\geqslant 1}a_n^+a_n-\frac{1}{2}J_2\sum_{n\geqslant 1}(a_n^+a_{n+1}+a_{n+1}^+a_n)\\&-\frac{1}{2}J_0(a_0^+a_1+a_1^+a_0).\end{aligned}\tag{2}$$

Here $E_0=-(\mu_1+\mu_2)NH$ is the energy of the ''ferromagnetic'' state for which $a_n|0\rangle=0$ for any value of n, and N is the number of atoms in each chain, which will henceforth be regarded as infinitely large.

Let us calculate the spectrum of elementary excitations (2). The corresponding vector of state satisfying the Schrödinger equation

$$(\mathscr{H}-E_0)|1\rangle=\varepsilon|1\rangle,$$

can be conveniently written in the form

$$|1\rangle=\sum_n W_na_n^+|0\rangle=\sum_{n\leqslant 0}U_na_n^+|0\rangle+\sum_{n\geqslant 1}V_na_n^+|0\rangle.\tag{3}$$

The wave function components U_n, V_n in the lattice site representation are defined by the system of finite-difference equations

$$U_n(\varepsilon-2\mu_1 H)+\frac{1}{2}J_1(U_{n+1}+U_{n-1})=0, \quad n\leqslant -1,$$

$$V_n(\varepsilon-2\mu_2 H)+\frac{1}{2}J_2(V_{n+1}+V_{n-1})=0, \quad n>1 \qquad (4)$$

with the boundary conditions

$$U_0(\varepsilon-2\mu_1 H)+\frac{1}{2}J_1U_{-1}+\frac{1}{2}J_0V_1=0;$$

$$V_1(\varepsilon-2\mu_2 H)+\frac{1}{2}J_0U_0+\frac{1}{2}J_2V_2=0. \qquad (5)$$

It can be seen from relations (4) and (5) that U_n and V_n are connected only through the boundary conditions. We shall seek the solution in the form

$$W_n=\begin{cases} U_n=A_1x_1^n+B_1x_1^{-n}, & n\leqslant 0,\\ V_n=A_2x_2^n+B_2x_2^{-n}, & n\geqslant 1. \end{cases} \qquad (6)$$

The relation between the parameters x_1 and x_2 with the energy ε can be determined from Eqs. (4):

$$\varepsilon=2\mu_1 H-\frac{1}{2}J_1(x_1+x_1^{-1})=2\mu_2 H-\frac{1}{2}J_2(x_2+x_2^{-1}), \qquad (7)$$

while the relation between the coefficients A_1, B_1, A_2, and B_2 is determined from the boundary conditions (5). Obviously, only one of the parameters x_1 or x_2 is independent, while the second is determined from relations (7). The quantities $x_{1,2}$ themselves can be either complex-valued with unit modulus, or real-valued. Since the values of $x_{1,2}$ and $x_{1,2}^{-1}$ are simultaneously solutions of Eq. (7), we shall assume for definiteness that x_1 and x_2 are real-valued with a modulus smaller than unity. Then the requirement of the boundedness of the wave function for $n\to\pm\infty$ indicates that the coefficient of a negative power of the corresponding real-valued parameter is equal to zero. If any of the parameters x_1 and x_2 (or both of them) is complex valued, Eqs. (6) with conditions (5) are satisfied in the energy intervals corresponding to energy bands in each of the XY chains:

$$\varepsilon_{1,2}=2\mu_{1,2}H-J_{1,2}\cos k_{1,2}. \qquad (8)$$

Here the quasiwave vector k_1 or k_2 plays the role of independent parameter. In weak fields $H<|J_1-J_2|/(2|\mu_1-\mu_2|)$, the band corresponding to the smaller exchange interaction constant is completely within the band with the larger value of exchange interaction constant.

In fields $|J_1-J_2|/(2|\mu_1-\mu_2|)<H<|J_1+J_2|/(2|\mu_1-\mu_2|)$, the bands overlap partially, while no band overlapping is observed for $H>|J_1+J_2|/(2|\mu_1-\mu_2|)$. Obviously, energy levels are doubly degenerate in the overlap region. The normalized wave functions satisfying the orthogonality condition in this case have the form

$$W_n^{(1)}(k_1)=\begin{cases} U_n^{(1)}(k_1)=A[\exp(ik_2)\sin k_1n-\alpha_1\alpha_2\sin k_1(n-1)];\\ V_n^{(1)}(k_1)=A\alpha_1\exp(ik_2n)\sin k_1; \end{cases}$$

$$W_n^{(2)}(k_2)=\begin{cases} U_n^{(2)}=-A\alpha_2\exp(-ik_1n)\sin k_2;\\ V_n^{(2)}=A[\sin k_2(n-1)-\alpha_1\alpha_2\exp(ik_1)\sin k_2n], \end{cases} \qquad (9)$$

where

$$A=\{\pi/2[1+\alpha_1^2\alpha_2^2-2\alpha_1\alpha_2\cos(k_1+k_2)]\}^{-1/2},$$

$$\alpha_{1,2}=J_{1,2}/J_0.$$

Outside the band overlapping region, we have either

$$W_n(k_1)=\begin{cases} U_n(k_1)=B_1[x_2\sin k_1n-\alpha_1\alpha_2\sin k_1(n-1)]\\ V_n(k_1)=B_1\alpha_1\sin k_1x_2^n \end{cases}, \qquad (10)$$

or

$$W_n(k_2)=\begin{cases} U_n(k_2)=B_2\alpha_2x_1^{|n|+1}\sin k_2\\ V_n(k_2)=B_2[\alpha_1\alpha_2\sin k_2n-x_1\sin k_2(n-1)], \end{cases} \qquad (11)$$

where

$$B_{1,2}=\left\{\frac{\pi}{2}[x_{2,1}^2+\alpha_1^2\alpha_2^2-2\alpha_1\alpha_2x_{2,1}\cos k_{1,2}]\right\}^{-1/2}$$

for ε_1 and ε_2 respectively. In all cases, the relation between k_1 and k_2 and $k_{1,2}$ and $x_{2,1}$ is determined by Eqs. (7). Thus, the point contact in this case plays the role of a potential wall, leading to scattering of excitations in the band overlapping region and to solutions with exponential attenuation of the wave function of one of the chains outside the overlap region. In the case of a strong interaction between the chains in the contact region ($J_0^2>J_1J_2$), energy levels corresponding to wave functions decreasing exponentially with increasing $|n|$ (the parameters x_1 and x_2 are real-valued) can split from band boundaries. The contact in this case can be regarded as a potential well. When the inequalities

$$J_2[2-\alpha_1^2-1/\alpha_2^2]<4(\mu_1-\mu_2)H<J_1[-2+1/\alpha_1^2+\alpha_2^2],$$

$$\alpha_1\alpha_2<1 \qquad (12)$$

are satisfied, an energy level exists above the bands, while for

$$J_1[2-1/\alpha_1^2-\alpha_2^2]<4(\mu_1-\mu_2)H<J_2[-2+\alpha_1^2+1/\alpha_2^2],$$

$$\alpha_1\alpha_2<1 \qquad (13)$$

an energy level is located below the bands. The corresponding energies can be determined from (7) by taking into account the additional condition

$$x_1x_2=\alpha_1\alpha_2, \qquad (14)$$

ensuring the boundedness of the wave function and following from (5). This gives

$$\varepsilon_{\pm}=(\mu_1+\mu_2)H+\frac{1}{(1-\alpha_1^2)(1-\alpha_2^2)}\times\left\{(\alpha_1^2-\alpha_2^2)(\mu_1-\mu_2)H\pm(1-\alpha_1^2\alpha_2^2)\times\left[(\mu_1-\mu_2)^2H^2+\frac{J_0^2}{4}(1-\alpha_1^2)(1-\alpha_2^2)\right]^{1/2}\right\}. \quad (15)$$

Bounded states correspond to the wave functions

$$U_n=\alpha_2 C x_1^n;\quad V_n=C x_2^n,\qquad C=\left\{\frac{(1-x_1^2)(1-x_2^2)}{2\alpha_2[\beta x_2+\alpha_2(1-\alpha_1^2)]}\right\}^{1/2}. \quad (16)$$

Here $\beta=2(\mu_1-\mu_2)H/J_0$, and $x_{1,2}$ are determined from (7) taking into account (14). For $J_1=0$ (or $J_2=0$), formulas (12) and (13) are transformed into the formulas determining the conditions for the existence of local energy levels in the spectrum of a semi-infinite XY chain with a substitutional impurity,[7,9] while for $\mu_1=\mu_2$ and $J_1=J_2$ these formulas are transformed into expressions corresponding to an infinite XY chain with an interstitial impurity[7] in the special case of equality of magnetons of the impurity and of the chain. An interesting feature of the point contact is that for $\mu_1\neq\mu_2$, local levels emerge only in a finite range of fields [see inequalities (12) and (13)], while the condition for the existence of an energy level for an XY chain with an impurity is determined by a single inequality.

3. CRITICAL BEHAVIOR OF LOCAL THERMODYNAMIC PARAMETERS AT ZERO TEMPERATURE

Let us consider the behavior of the z-component of average local magnetic moments of atoms in the contact ($\langle m_0^z\rangle$ and $\langle m_1^z\rangle$) and at the sites of the chains ($\langle m_n^z\rangle$, $n\neq 0,1$):

$$\langle m_n^z\rangle=2\mu_n\left(\frac{1}{2}-\langle a_n^+ a_n\rangle\right)=2\mu_n\left(\frac{1}{2}-\sum_{\lambda}\left|W_n\right|^2 f(\varepsilon_\lambda)\right), \quad (17)$$

where μ_n stands for μ_1 or μ_2, while W_n is equal to U_n or V_n for $n\leqslant 0$ and $n\geqslant 1$ respectively, and $f(\varepsilon_\lambda)=[\exp(\varepsilon_\lambda/T+1]^{-1}$ is the Fermi distribution function, as well as the behavior of the pair correlator of transverse spin components for atoms in the contact:

$$\langle S_0^x S_1^x+S_0^y S_1^y\rangle=\frac{1}{2}(\langle a_0^+ a_1\rangle+\langle a_1^+ a_0\rangle)=\frac{1}{2}\sum_{\lambda}(U_0^* V_1+U_0 V_1^*)f(\varepsilon_\lambda). \quad (18)$$

The summation over λ in (17) and (18) includes integration with respect to $k_{1,2}$ for the states in the continuous spectrum and the contribution of local levels if they exist.

Let us analyze the behavior of the above thermodynamic parameters at $T=0$, when $f(\varepsilon)=\theta(-\varepsilon)$ ($\theta(-\varepsilon)$ is a step function, and the contribution to (17) and (18) comes only from the states with negative energy values. The limits of integration with respect to $k_{1,2}$ in (17) and (18) in this case are now determined by the relation between the parameters of the chains as well as by the applied field. For example, for $J_1/J_2>\mu_1/\mu_2$ and $J_1>J_2$, we have

$$\langle m_n^z\rangle=2\mu_n\begin{cases}\left[\frac{1}{2}-\int_0^{k_{01}}\left|W_n(k_1)\right|^2 dk_1-\int_{k_{01}}^{k_{c1}}\left(\left|W_n^{(1)}\right|^2+\frac{J_1\sin k_1}{J_2\sin k_2}\left|W_n^{(2)}\right|^2\right)dk_1-W_n^2\Theta\right], & 0\leqslant H\leqslant J_2/2\mu_2,\\ \left[\frac{1}{2}-\int_0^{k_{c1}}\left|W_n(k_1)\right|^2 dk_1-W_n^2\Theta\right], & J_2/2\mu_2\leqslant H\leqslant J_1/2\mu_1,\\ \left[\frac{1}{2}-W_n^2\Theta\right], & H\geqslant J_1/2\mu_1,\end{cases} \quad (19)$$

where

$$\Theta=\theta(-\varepsilon)\,\theta[2\beta-\alpha_1(2-1/\alpha_1^2-\alpha_2^2)]\times\theta[2\beta+\alpha_2(2-\alpha_1^2-1/\alpha_2^2)]\,\theta(1-\alpha_1\alpha_2),$$

$$\theta(x)=\begin{cases}1, & x>0,\quad k_{01}=\arccos\{[2(\mu_1-\mu_2)H+J_2]/J_1\},\\ 0, & x<0,\quad k_{c1}=\arccos(2\mu_1/J_1),\end{cases}$$

and the quantity ε_- is defined by formula (15). The limits of integration for $\langle S_0^x S_1^x+S_0^y S_1^y\rangle$ are the same.

It is well known that a homogeneous XY chain exhibits a second-order phase transition on the field dependence of the average magnetic moment at zero temperature with a root singularity of the susceptibility at this point, which is associated with the disappearance of the gap in the spectrum of one-magnon states.[5] Since local magnetic moment at all the sites of a homogeneous chain are identical and coincide with the average moment, they possess the above-mentioned singularity. In the given case, such singularities associated with the lower boundaries of energy bands for each of the XY

chains (7) are not observed as in an XY chain with an impurity (see Refs. 8 and 10–12) except in the special case in which the critical field for the lower band coincides with the field in which a local level emerges or vanishes. In addition, relations (19) show that the existence of the local level (15) with the energy ε_- can lead to the emergence of new singular points. As the energy of the local level (15) passes through zero value in the critical field

$$H_c=\frac{1}{4}\,J_0(1-\alpha_1^2\alpha_2^2)[(\mu_1-\mu_2\alpha_1^2)(\mu_2-\mu_1\alpha_2^2)]^{-1/2}, \tag{20}$$

existing under the condition

$$2\alpha_1^2/(1+\alpha_1^2\alpha_2^2)<\mu_1/\mu_2<0.5(1+\alpha_1^2\alpha_2^2)/\alpha_2^2, \tag{21}$$

the local magnetic moment $\langle m_n^z\rangle$ abruptly attains its maximum value μ_n, the pair correlator $\langle S_0^xS_1^x+S_0^yS_1^y\rangle$ vanishes abruptly, and local susceptibilities have a δ-function singularity. For $\langle m_n^z\rangle$, the magnitude of the jump obviously decreases exponentially with increasing $|n|$. If, however, inequalities (21) are not satisfied, the energy of the level ε_- is either only negative, or only positive in the entire interval of the fields (13), and this singularity is not observed. When one of the inequalities in (21) is satisfied, the susceptibility acquired the above-mentioned root singularity in the stronger of the fields $H_c=J_1/2\mu_1$ or $H_c=J_2/2\mu_2$ for the left and right inequalities respectively. In the expression for local susceptibility $\chi_n=\partial\langle m_n^z\rangle/\partial H$, the emergence of this singularity is determined by the term

$$\Delta\chi_n=2\mu_n|W_n(k_{c1,2})|^2\,\frac{dk_{c1,2}}{dH}\sim\frac{\sin k_{c1,2}}{x_{2,1}^2+\alpha_1^2\alpha_2^2-2\alpha_1\alpha_2x_{2,1}\cos k_{c1,2}},\qquad k_{c1,2}=\arccos(2\mu_{1,2}/J_{1,2}). \tag{22}$$

This nonintegral term emerging as a result of differentiation of the integral

$$\int_0^{k_{c1,2}}|W_n(k_{1,2})|^2dk_{1,2}$$

in the expression for $\langle m_n^z\rangle$ with respect to the field has a singularity only if $k_{c1,2}\to 0$ simultaneously with $x_{2,1}\to\alpha_1\alpha_2$. The splitting or vanishing of a local level with a negative energy is accompanied by a jump in the local susceptibility for a given finite value of n:

$$\Delta\chi_n=\begin{cases}\dfrac{16\mu_n(\mu_2-\mu_1)}{J_0}\,\dfrac{\alpha_1}{1-\alpha_1^2\alpha_2^2}\quad\begin{cases}1, & n\leqslant 0\\ \alpha_1^{2n}\alpha_2^{2(n-1)}, & n\geqslant 1\end{cases} & \text{if } J_1/J_2>\mu_1/\mu_2;\\[2ex] \dfrac{16\mu_n(\mu_1-\mu_2)}{J_0}\,\dfrac{\alpha_2}{1-\alpha_1^2\alpha_2^2}\quad\begin{cases}\alpha_1^{2|n|}\alpha_2^{2(|n|+1)}, & n\leqslant 0\\ 1, & n\geqslant 1\end{cases} & \text{if } J_1/J_2<\mu_1/\mu_2.\end{cases} \tag{23}$$

It can be seen from (23) that the sign of $\Delta\chi_n$ is determined by the relation between magnetons of the chains. Corresponding critical fields $H_{1,2}$ can be determined from (13) with the boundary values of the field regions containing a local level if the condition

$$0<H_{1,2}\leqslant\max(J_1/2\mu_1,J_2/2\mu_2)$$

is satisfied. These are the points at which the field dependences of $\langle m_n^z\rangle$ and $\langle S_0^xS_1^x+S_0^yS_1^y\rangle$ have kinks.

The following combinations of these singularities are possible for various relations between the parameters of the chains and the contact (see Fig. 1). The inequalities given below are written for definiteness for $\mu_1>\mu_2$.

If the inequalities

$$\alpha_1\alpha_2<1,\quad 0.5(1+\alpha_1^2\alpha_2^2)/\alpha_2^2\leqslant 1 \tag{24}$$

or

$$\alpha_1\alpha_2<1,\quad \mu_1/\mu_2<2\alpha_1^2/(1+\alpha_1^2\alpha_2^2) \tag{25}$$

are satisfied, no singularities are observed (regions 1 and 6 in Fig 1).

Under the condition

$$2\alpha_1^2/(1+\alpha_1^2\alpha_2^2)\leqslant 1<0.5(1+\alpha_1^2\alpha_2^2)/\alpha_2^2<\mu_1/\mu_2 \tag{26}$$

(region 2), the susceptibility experiences a finite jump in the critical field

$$H_1=\frac{J_1}{4(\mu_1-\mu_2)}\,[2-1/\alpha_1^2-\alpha_2^2]. \tag{27}$$

Two finite susceptibility jumps (region 3) correspond to the relations

$$\alpha_1\alpha_2<1,\quad 1<2\alpha_1^2/(1+\alpha_1^2\alpha_2^2),\qquad 0.5(1+\alpha_1^2\alpha_2^2)/\alpha_2^2<\mu_1/\mu_2. \tag{28}$$

In this case, the first singularity emerges as a result of energy level splitting in the critical field (27), while the second is formed when the energy level vanishes in the field

$$H_2=\frac{J_2}{4(\mu_1-\mu_2)}\,[2+1/\alpha_2^2+\alpha_1^2]. \tag{29}$$

One jump of local magnetization, i.e., the δ-function singularity of susceptibility in the critical field (20), corresponds to region 4 in Fig. 1:

$$2\alpha_1^2/(1+\alpha_1^2\alpha_2^2)\leqslant 1<\mu_1/\mu_2<0.5(1+\alpha_1^2\alpha_2^2)/\alpha_2^2. \tag{30}$$

In region 5, we have

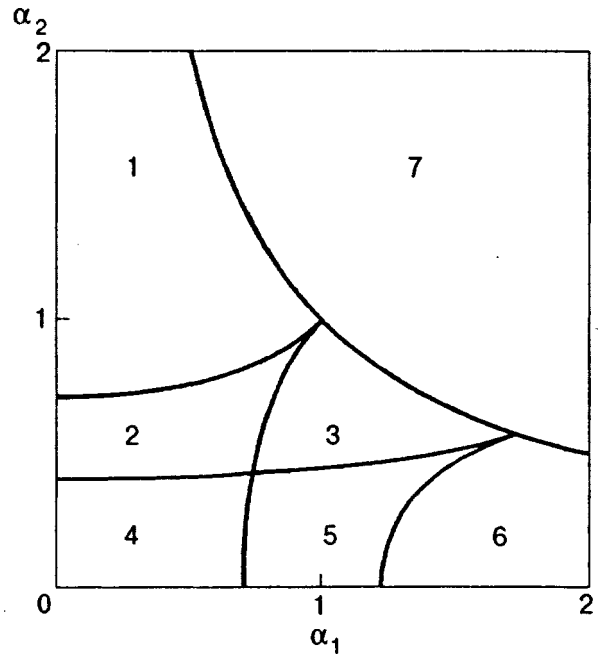

FIG. 1. Ranges of parameters $\alpha_1=J_1/J_0$, $\alpha_2=J_2/J_0$ for $\mu_1/\mu_2=3$ with various types of singularities of local thermodynamic parameters. Region 7 and its boundaries with regions 1, 3, and 6 display no energy levels, and hence no singularities. Region 1 (including its boundary with region 2) and region 6 (inequalities (24) and (25) respectively) also contain no singularities in spite of the presence of local energy levels. Region 2 and its boundary with region 3 displays one finite jump in susceptibility [see (26)], region 3 has two finite susceptibility jumps (see (28)), region 4 (including its boundary with 5) [see (30)] exhibit a local moment jump, while region 5 [see (31)] a susceptibility jump followed by a moment jump. The boundaries between regions 2 and 4, 5 and 6 correspond to root singularities, while the boundary between regions 3 and 5 to a finite jump and a root singularity of susceptibility [curves (32) and (33)].

$$1<2\alpha_1^2/(1+\alpha_1^2\alpha_2^2)<\mu_1/\mu_2<0.5(1+\alpha_1^2\alpha_2^2)/\alpha_2^2. \quad (31)$$

As the field increases, a susceptibility jump is first observed in the critical field (27) as a result of formation of a local level, followed by a jump in magnetic moment observed in the field (20) when the energy of this level passes through the zero value. The curves

$$\mu_1/\mu_2=0.5(1+\alpha_1^2\alpha_2^2)/\alpha_2^2, \quad (32)$$

$$\mu_1/\mu_2=2\alpha_1^2/(1+\alpha_1^2\alpha_2^2) \quad (33)$$

for $\alpha_1\alpha_2<1$ correspond to a root singularity of susceptibility. It should be noted that if $\mu_1<\mu_2$, it is sufficient to change places of the subscripts 1 and 2 in formulas (24)–(31). In the absence of a local level, field dependences have no singularities. An analysis of relation (19) shows that the average local moments of the contact and atoms close to it can decrease and even assume negative values for certain values of parameters of the chains near H_c. This decrease is subsequently compensated by a positive jump in the field H_c. A similar behavior is also typical of the impurity moment in an XY chain.[10]

4. CONCLUSIONS

The energy spectrum of the model one-dimensional, exactly solvable spin system formed by two semi-infinite XY chains interacting as a point contact is studied. The one-particle spectrum consists of two energy bands typical of each chain, and the presence of a ''phase boundary'' in weak external fields leads to scattering of excitations in the band overlapping region and to solutions with decreasing wave functions on one of the chains outside the overlap region. In strong fields, in the absence of band overlapping, only the second-type solutions are left. In the case of a strong interaction between the chains, local levels split from the bottom of the lower band and the top of the upper band in certain ranges of applied fields. Thus, the contact exhibits the properties of a potential wall for states from the continuous spectrum as well as the properties of a potential well, leading to the formation of bound states. The presence of an impurity level below the bands can cause either a jump in the average moments of chain sites at zero temperature and in transverse pair correlator of the contact, or jumps in the local susceptibility at sites or consecutive jumps in susceptibility as well as in moment and correlator upon an increase in the applied longitudinal field depending on the relation between the parameters of the chains and of the contact. The existence of local levels must also be manifested in the resonant properties of the system at low temperatures.

The author takes the opportunity to thank A. A. Zvyagin for fruitful discussions of the results and valuable advice.

*E-mail: elena.v.ezerskaya@univer.kharkov.ua

[1] J. P. Harrison, J. P. Hessler, and D. R. Taylor, Phys. Rev. B **14**, 2979 (1976).
[2] L. L. Gonsalves and R. J. Elliot, J. Phys. C **12**, 1703 (1979).
[3] P. M. Duxbury *et al.*, Phys. Rev. B **24**, 5149 (1981).
[4] E. Lieb, T. Schultz, and D. Mattis, Ann. Phys. **3**, 407 (1961).
[5] S. A. Pikin and V. M. Tsukernik, Zh. Éksp. Teor. Fiz. **50**, 1377 (1966) [Sov. Phys. JETP **23**, 914 (1966)].
[6] V. M. Kontorovich and V. M. Tsukernik, Zh. Éksp. Teor. Fiz. **53**, 1167 (1967) [Sov. Phys. JETP **26**, 687 (1967)].
[7] I. A. Vinikovetskii, A. M. Frishman, and V. I. Khokhlov, Ukr. Fiz. Zh. **18**, 810 (1973).
[8] I. A. Vinikovetskii, A. M. Frishman, and V. M. Tsukernik, Ukr. Fiz. Zh. **19**, 1966 (1974).
[9] V. Z. Kleiner and V. M. Tsukernik, Fiz. Met. Metalloved. **39**, 947 (1975).
[10] V. Z. Kleiner and V. M. Tsukernik, Fiz. Nizk. Temp. **6**, 322 (1980) [*sic*].
[11] J. A. Tjon, Phys. Rev. B **2**, 2411 (1970).
[12] A. A. Zvyagin and Ya. Segal, Fiz. Nizk. Temp. **21**, 1068 (1995) [Low Temp. Phys. **21**, 822 (1995)].
[13] P. Jordan and E. Wigner, Z. Phys. **47**, 631 (1928).

Translated by R. S. Wadhwa

PHYSICAL PROPERTIES OF CRYOCRYSTALS

Electron diffraction studies of mechanisms of crystal structure formation in N_2 clusters

S. I. Kovalenko, D. D. Solnyshkin, E. A. Bondarenko, É. T. Verkhovtseva, and V. V. Eremenko

Special Design Bureau, B. Verkin Institute for Low Temperature Physics and Engineering, National Academy of Sciences of the Ukraine, 310164 Kharkov, Ukraine)*
(Submitted December 26, 1997; revised January 28, 1998)
Fiz. Nizk. Temp. **24**, 481–484 (May 1998)

The structure of N_2 clusters is studied by the electron diffraction method over a wide range of their mean sizes $\overline{N}$. It is found that, as the value of $\overline{N}$ increases, the structure of the clusters is transformed in the sequence quasi-crystal (icosahedron) $\rightarrow \alpha$-N_2 (cubic) phase with stacking faults $\rightarrow \beta$-N_2 (hcp) phase. The formation of the cubic phase from the icosahedral structure follows a mechanism typical of rare gases, while the transition $\alpha \rightarrow \beta$ is due to an increase in the cluster temperature with the size. © *1998 American Institute of Physics.* [S1063-777X(98)01005-6]

INTRODUCTION

The realization of quasi-crystalline (icosahedral) structure in small clusters has been established beyond any doubt at present. However, the mechanism through which quasi-crystalline aggregates are transformed into a structure typical of bulk materials remains unclear. For this reason, the theoretical studies[1,2] in which the importance of kinetic processes in the formation of a crystalline structure in rare gases is emphasized are of special interest. According to the concepts developed by van de Waal,[1,2] coalescence or mutual intergrowth of icosahedral clusters creates fcc regions with stacking faults ensuring the subsequent rapid and defect-free growth of the crystalline phase. The proposed growth mechanism was confirmed by electron diffraction studies on cluster beams of rare gases.[3,4]

This research is devoted to the formation of the crystalline phase in nitrogen clusters. We expect that the mechanism of formation of the crystalline phase in nitrogen clusters is similar to that operating in rare gas clusters in view of a nearly spherical shape of the N_2 molecule and a weak noncentral component of intermolecular interaction of particles.

It should be noted that the structure of N_2 clusters was studied in Refs. 5 and 6. However, the mechanism of formation of the crystalline phase was not considered. Further, the reason behind the formation of a low-temperature cubic phase in clusters with $\overline{N}=4000$,[5] and of a high-temperature hcp phase in clusters with $\overline{N}\geqslant 8000$[6] was not established either.

EXPERIMENT

The experimental setup included a generator of a supersonic cluster beam and an electron diffractometer for high-energy electrons. The setup and the experimental geometry are described in Ref. 6. A supersonic cluster beam was formed by a conical nozzle with a throat diameter of 0.34 mm, a cone angle of 8.6°, and the ratio of the outlet cross sectional area to the throat area equalling 36.7. The mean size of clusters ($\overline{N}$) was varied by changing gas pressure P_0 at the nozzle inlet at a constant temperature $T_0 = 120 \pm 2$ K. The value of P_0 changed from 0.1 to 0.8 MPa. The characteristic size of clusters δ($\delta \sim N^{1/3}$) was determined from the broadening of diffraction peaks taking into account the broadening (in the cubic phase) due to stacking faults (SF). The method of estimating δ for an fcc structure is described in detail in Refs. 3 and 4. The temperature of the crystalline N_2 clusters was determined from experimental lattice parameters and from available data on the linear expansion coefficient for nitrogen.[7] Diffraction patterns were recorded by the electrometric as well as photographic technique. In most experiments, the former method was preferred. Photographic recording was used only for determining the positions of diffraction peaks with the best accuracy. In this case, the diameters D of diffraction rings were measured with the help of the precise optical comparator IZA-2 (the scale factor was 1 μm). The diameter of each ring was measured at least 10 times, while allowed us to process the obtained results statistically. The relative error in determining the interplanar distance d varied from 4×10^{-2}% to 8×10^{-2}% depending on the crystalline cluster size.

DISCUSSION OF RESULTS

The diameters of diffraction rings and the corresponding interplanar distances are given in Tables I and II for β and α phases of nitrogen. Typical diffraction patterns illustrating their variation with the cluster size are depicted in Figs. 1a and 1b. For convenience of analysis, the curves are displaced along the vertical. In the case of large clusters (curve *2* in Fig. 1b, Table I, $P_0=0.6$ MPa, $\overline{N}=24000$), the positions of diffraction peaks correspond to the hcp structure of the high-

TABLE I. Interplanar distances for β-N_2 phase ($P_0=0.6$ MPa, $T_0=120$ K). $2L\lambda=64.128$ mm·Å is the instrument constant (L is the distance from the sample to the photographic plate in mm, and λ the electron wavelength).

D, mm	d_{hkl}, Å	(hk.l)
18.30(1)	3.504	(10.0)
19.41(5)	3.303	(00.2)
20.72(0)	3.095	(10.1)
31.69(9)	2.023	(11.0)
36.60(3)	1.752	(20.0)
37.17(6)	1.725	(11.2)

$a=(4.046\pm0.005)$ Å, $c=(6.606\pm0.005)$Å, $c/a=1.633\pm0.003$

temperature phase of nitrogen. A certain anomaly is observed, however, in the intensity distribution of diffracted beams: the peak (00.2) is unusually high, while the descending slope of the peak (10.1) has a bend in the vicinity of the (200) peak for the cubic α-N_2 phase. These peculiarities are due to a broad size distribution function of clusters and the presence of a small number of α-phase clusters in addition to β-phase clusters of nitrogen in the beam. The most intense peak (111) of the α-phase coincides with the (00.2) peak of the β-phase. Precise measurements of diffraction ring diameters D on electron diffraction patterns and appropriate calculations give the following values of the lattice parameter in the β-phase: $a=(4.046\pm0.005)$ Å, $c=(6.606\pm0.005)$ Å, $c/a=1.633\pm0.003$. The obtained values correspond to the cluster temperature $T=(38\pm3)$K.

As the mean size of the clusters decreases, the peaks of the hcp phase become lower, while those in the cubic phase become higher (see curve *1* in Fig. 1b and curve *2* in Fig. 1a as well as Table II). The analysis of the positions of diffraction peaks in the size range $\bar{N}=3000$–15000 molecules/cluster made it possible to detect deformation-type SF in the cubic phase. It should be noted that the temperature of the cubic phase clusters for $\bar{N}=9000$ molecules/cluster amounts to $T=(35\pm3)$K. A further decrease in $\bar{N}$ leads to vanishing of the (200) peak in the cubic phase and to an anomalously strong broadening of the remaining peaks (see curve *1* in Fig. 1a).

In order to establish the dependence of the SF density ρ in cubic phase clusters on their characteristic size, we first determined the mean size of clusters for different values of pressure P_0. The results are shown in Fig. 2 on the logarithmic scale: the values of $\delta/2$ are laid along the ordinate scale

TABLE II. Interplanar distances for α-N_2 phase ($P_0=0.3$ MPa, $T_0=120$ K).$2L\lambda=64.128$ mm·Å.

D, mm	d_{hkl}, Å	(hk.l)
19.51(6)	3.286	(111)
22.53(3)	2.846	(200)
31.87(3)	2.012	(220)
37.37(1)	1.716	(331)
39.03(1)	1.643	(222)

$a=(5.691\pm0.005)$Å

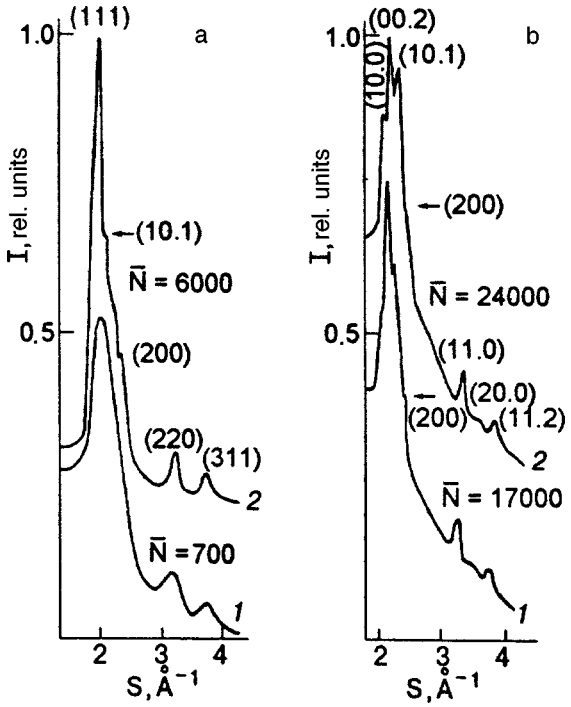

FIG. 1. Diffraction patterns for nitrogen clusters with different mean sizes $\bar{N}$. The curves are shifted along the vertical for convenience of visualization. $S=4\pi\sin\theta/\lambda$ is the diffraction vector, θ being the Bragg angle. (a) Diffraction patterns for clusters with relatively small $\bar{N}$. Curve *1* ($\bar{N}=700$ molecules/cluster) corresponds to the icosahedral structure, curve *2* ($\bar{N}=6000$ molecules/cluster) to the low-temperature cubic α-phase of N_2. The arrow indicates the traces of the peak of the high-temperature β-phase. (b) Diffraction patterns for clusters with relatively large clusters. Curves *1* ($\bar{N}=17000$ molecules/cluster) and *2* ($\bar{N}=24000$ molecules/cluster) correspond to the high-temperature β-phase of N_2. The arrows indicate the traces of the peak of the cubic α-phase.

and P_0 on the abscissa scale. It can be seen that the values of δ fall on the straight line corresponding to the dependence $\delta\propto P_0^{0.67}$ for all pressures higher than 0.25 MPa for which the

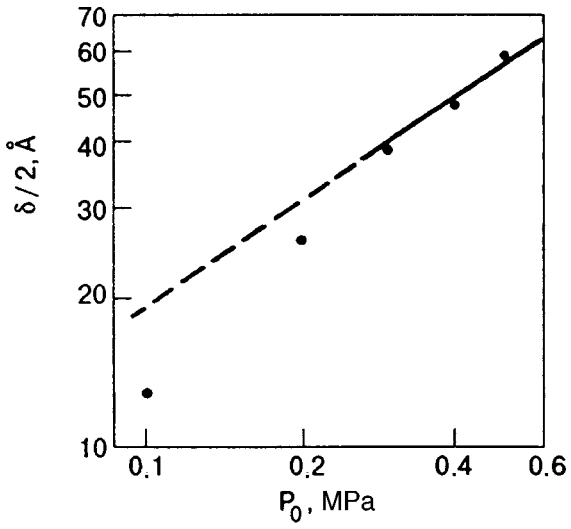

FIG. 2. Dependence of the cluster radius $\delta/2$ on the gas pressure P_0 at the nozzle inlet at a constant temperature $T_0=120$ K. The straight line corresponds to the dependence[8] $\delta\sim P_0^{0.67}$ and our previous results.[6]

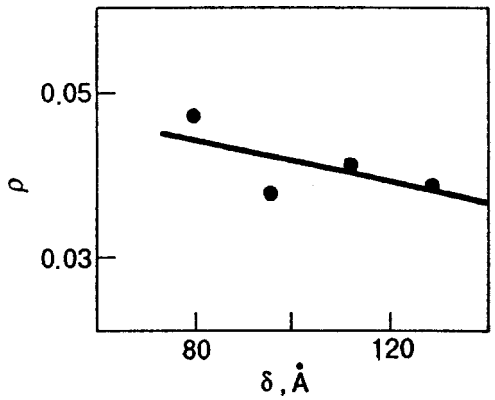

FIG. 3. Dependence of the SF density ρ in the cubic N_2 phase on the characteristic size δ of a cluster.

peaks in the cubic phase are still distinct. The obtained dependence is in good agreement with the theory of ''corresponding'' jets[8] and our previous results.[6] The departure of the value of δ from the found regularity for $P_0<0.25$ MPa correlates with the data obtained in Ref. 6 according to which the peak broadening is faster under low pressures. According to the calculations of the interference function made by Lee and Stein,[9] this effect indicates the predominance of clusters with a quasi-crystalline (icosahedral) structure in the beam.

Figure 3 shows the dependence of the SF density on the characteristic size of crystalline clusters of the low-temperature phase of nitrogen. The plot does not show the values of ρ corresponding to $P_0 \leqslant 0.2$ MPa and $P_0 > 0.6$ MPa since clusters of quasi-crystalline (icosahedral) phase dominate in the former case, while clusters of the high-temperature β-N_2 phase prevail in the latter case. It can be seen that an increase in the size of α-N_2 clusters, and hence the total number n of densely packed plates leads to a monotonic decrease in the SF density. Since $\rho = n_{SF}/n$, where n_{SF} is the number of stacking faults, the observed regularity suggests the constancy or insignificant change in n_{SF} during the cluster growth.

According to calculations based on formulas (5)–(7) in Ref. 3, α-N_2 clusters contain the same number (four) of stacking faults irrespective of their size. This result indicates that SF appear in N_2 clusters, as in rare gases, at early stages of formation of the α-N_2 structure. Such a number of intersecting SF piercing the entire cluster is optimal since it leads to the formation of a nonvanishing step (of the same type as those appearing as a result of emergence of a screw dislocation) on each of the densely packed planes facing the cubooctahedron. Further cluster growth does not require the formation of new nuclei on densely packed faces since it occurs due to trapping of newly arriving atoms by the formed steps. In this case, the regularity in the packing of atoms is not violated, and hence no new SF appear. This leads to a decrease in the SF density being measured with increasing size of the cluster.

Thus, our study proved that an increase in the mean cluster size $\bar{N}$ leads to transformations of the structure of N_2 clusters in the following sequence: quasi-crystal (icosahedron) $\rightarrow \alpha$-N_2 (cubic phase with SF) $\rightarrow \beta$-N_2 (hcp) phase. The formation of the cubic phase of nitrogen from icosahedral phase is governed by the mechanism typical of rare gas clusters.[1–4] The transformation α-$N_2 \rightarrow \beta$-N_2 is apparently associated with an increase in the cluster temperature with the size.

*)E-mail: sktb@ilt.kharkov.ua

[1] B. W. van de Waal, J. Cryst. Growth **158**, 153 (1996).
[2] B. W. van de Waal, Phys. Rev. Lett. **76,** 1083 (1996).
[3] S. I. Kovalenko, D. D. Solnyshkin, E. T. Verkhovtseva, and V. V. Eremenko, Chem. Phys. Lett. **250**, 309 (1996).
[4] S. I. Kovalenko, D. D. Solnyshkin, E. A. Bondarenko, and E. T. Verkhovtseva, Fiz. Nizk. Temp. **23**, 190 (1997) [Low Temp. Phys. **23**, 140 (1997)].
[5] J. Farges, M. F. de Feraudy, B. Raoult, *et al.*, Phys. Chem. **88**, 211 (1984).
[6] S. I. Kovalenko, D. D. Solnyshkin, E. T. Verkhovtseva, and V. V. Eremenko, Fiz. Nizk. Temp. **20**, 961 (1994) [Low Temp. Phys. **20**, 758 (1994)].
[7] I. N. Krupskii, A. I. Prokhvatilov, and A. I. Èrenburg, Fiz. Nizk. Temp. **1**, 359 (1975) [Sov. J. Low Temp. Phys. **1**, 178 (1975)].
[8] O. F. Hagena and W. Obert, J. Chem. Phys. **56**, 1793 (1972).
[9] J. W. Lee and J. D. Stein, J. Phys. Chem. **91**, 2450 (1987).

Translated by R. S. Wadhwa

LATTICE DYNAMICS

Contribution of surface roughness of an isotropic solid to low-temperature surface heat capacity

V. V. Kosachev, V. L. Sorokin, and A. V. Brantov

*Moscow State Institute of Engineering Physics, 115409 Moscow, Russia**
(Submitted November 12, 1997)
Fiz. Nizk. Temp. **24**, 485–492 (May 1998)

The effect of roughness of the free surface of a semi-infinite isotropic solid on the low-temperature surface heat capacity is studied. The method of modified Green's function (as compared with that used by Maradudin, Wallis, and Equiluz (1977) and perturbation theory are used for deriving an analytic expression for the contribution of weak roughness to the low-temperature surface heat capacity, which is a correction to the well-known result obtained by Dupuis, Mazo, and Onsager (1960) for the surface heat capacity of a semi-infinite isotropic solid with a plane free boundary. It is proved that the inclusion of roughness of isotropic crystals with optical surfaces increases the surface heat capacity in a wide temperature range (of the order of several kelvins). © *1998 American Institute of Physics.* [S1063-777X(98)01105-0]

1. INTRODUCTION

An analysis of the effect of the surface of a solid on the low-temperature heat capacity is an important theoretical and applied problem in view of the need in reliable information on the structure of the surface and surface layers of solids. The first publication in this field appeared in 1946.[1] Brager and Schuchowitzky[1] who calculated the heat capacity of an elastic isotropic plate under the assumption of incompressible liquid and cyclic boundary conditions for displacement field proved that the free surface increases the low-temperature heat capacity of the solid and makes a contribution proportional to the area of the surface and the square of temperature. Similar results were obtained for an elastic isotropic rectangular parallelepiped with fixed faces[2] and for a more realistic model, viz., an isotropic elastic plate with cyclic boundary conditions and free surface.[3] The most general analytic expression for the low-temperature surface heat capacity of an isotropic solid with a free surface was derived for the first time by Dupuis, Mazo, and Onsager[4]:

$$\Delta C_V(T)=3\pi\,\frac{k_B^3}{h^2}\,\zeta(3)\,\frac{2c_t^4-3c_t^2c_l^2+3c_l^4}{c_t^2c_l^2(c_l^2-c_t^2)}\,ST^2, \qquad (1)$$

where c_l and c_t are the velocities of propagation of longitudinal and transverse waves in the solid, k_B is Boltzmann's constant, $h=2\pi\hbar$ Planck's constant, T the absolute temperature, S the surface area, and $\zeta(x)$ is the Riemann zeta function.

Burt[5] was the first to use Green's functions for calculating the low-temperature surface heat capacity of a semi-infinite isotropic solid with a free boundary and obtained the result coinciding with formula (1). Subsequent publications[6,7] also confirmed the validity of this expression.

The experimental verification[4] carried out for MgO and NaCl powders revealed, however, that the values calculated by formula (1) are smaller than experimental results approximately by a factor of four for MgO powders and 1.5–2 for NaCl powders. It was proposed in this connection that the discrepancy can be due to the lattice structure of the crystal as well as the roughness of the surface and anisotropy of solids.

The inclusion of the lattice structure in theoretical publications[8–10] improves the agreement with experiments.[11,12]

The contribution of the surface of anisotropic crystals to the low-temperature heat capacity was considered for a hexagonal medium[6] as well as for cubic[7] and strongly anisotropic crystals.[13,14] It was proved that the inclusion of anisotropy leads to an increase in the contribution of the surface to the low-temperature heat capacity.

Maradudin *et al.*[15] constructed the theory of the contribution of the roughness of the free surface of an isotropic solid to the low-temperature surface heat capacity on the basis of the method of Green's functions. In Refs. 16, however, the method of Green's functions was developed further by taking into account the roughness of the free boundary more correctly. This research is devoted to an analysis of the effect of roughness of the free surface of a semi-infinite isotropic solid to the low-temperature surface heat capacity taking into account important corrections introduced into the method of Green's functions.[16]

2. CALCULATION OF AVERAGED GREEN'S FUNCTIONS. CONTRIBUTION OF ROUGHNESS TO LOW-TEMPERATURE HEAT CAPACITY

Let us consider a semi-infinite isotropic solid bounded by a free statistically rough surface $x_3=\xi(x_1,x_2)$ and occupying the half-space $x_3\geqslant\xi(x_1,x_2)$ in the approximation of elastic continuum. The elastic medium is characterized by

the density ρ and the tensor of elastic moduli $C_{\alpha\beta\mu\nu}$. We assume that the function $\xi(x_1,x_2)$ of the surface profile describes a steady-state stochastic process characterized by the following properties:

$$\begin{aligned}&\langle\xi(x_1,x_2)\rangle=0,\\&\langle\xi(x_1,x_2)\xi(x_1',x_2')\rangle=\delta^2W(|\mathbf{x}_\parallel-\mathbf{x}_\parallel'|),\end{aligned}\tag{2}$$

where $\delta=\sqrt{\langle\xi^2\rangle}$ is the root-mean-square roughness amplitude, $W(|\mathbf{x}_\parallel|)$ the surface self-correlation function, $\mathbf{x}_\parallel=x_1\mathbf{i}+x_2\mathbf{j}$, $\mathbf{i}$ and $\mathbf{j}$ being the unit vectors along the axes x_1 and x_2, and the angle brackets denote averaging over the ensemble of realizations of the surface profile function $\xi(\mathbf{x}_\parallel)$. We assume that the surface self-correlation function has the Gaussian form

$$W(|\mathbf{x}_\parallel|)=\exp\left\{-\frac{(\mathbf{x}_\parallel)^2}{a^2}\right\},\tag{3}$$

where a is the roughness correlation length. We must find the contribution of roughness to the low-temperature surface heat capacity.

Following the method developed by Maradudin *et al.*[15] for studying the contribution of the free surface of an isotropic crystal to low-temperature heat capacity, we can present the contribution of the surface in the form

$$\Delta C_V(T)=\frac{k_B(\beta\hbar)^2}{\pi i}\sum_{n=1}^{\infty}n\int_{-\infty}^{+\infty}dy y^3\Omega(y)\mathrm{e}^{-in\beta\hbar y},\tag{4}$$

where $\beta=1/(k_BT)$. The function $\Omega(y)$ in (4) can be expressed in terms of the difference between the frequency Fourier transform of Green's functions $D_{\alpha\beta}(\mathbf{x},\mathbf{x}';\omega)$ for a semi-infinite medium with weakly rough surface and $D^{(\infty)}_{\alpha\beta}(\mathbf{x},\mathbf{x}';\omega)$ for an infinite medium:

$$\begin{aligned}\Omega(y)=-\int dx_1dx_2\int_{\xi(x_1,x_2)}^{+\infty}\\\times dx_3\sum_\alpha\left[D_{\alpha\alpha}(\mathbf{x},\mathbf{x};iy)-D^{(\infty)}_{\alpha\alpha}(\mathbf{x},\mathbf{x};iy)\right].\end{aligned}\tag{5}$$

Using formulas (4) and (5), we can calculate the contribution of a rough as well as a plane surface to the low-temperature heat capacity of a semi-infinite solid bounded by a free surface. Thus, the contribution of the rough surface of an isotropic crystal to its heat capacity is determined by Green's function $D_{\alpha\beta}(\mathbf{x},\mathbf{x}';\omega)$.

In order to calculate Green's function taking into account the correction introduced to the method of Green's function developed in Ref. 16, we write the equations of motion for a semi-infinite solid with a free rough boundary in the form

$$\rho(\mathbf{x})\frac{\partial^2u_\alpha}{\partial t^2}=\frac{\partial}{\partial x_\beta}C_{\alpha\beta\gamma\delta}(\mathbf{x})\frac{\partial u_\gamma}{\partial x_\delta}+C_{\alpha\beta\gamma\delta}(\mathbf{x})\frac{\partial^2u_\gamma}{\partial x_\beta\partial x_\delta},\tag{6}$$

where the elastic moduli and the density of the medium are functions of spatial coordinates:

$$\begin{cases}C_{\alpha\beta\gamma\delta}(\mathbf{x})=C_{\alpha\beta\gamma\delta}\theta(x_3-\xi(x_1,x_2))\\\rho(\mathbf{x})=\rho\,\theta(x_3-\xi(x_1,x_2))\end{cases}.\tag{7}$$

In this expression, $C_{\alpha\beta\gamma\delta}$ and ρ are ordinary elastic moduli and mass density of the solid, which do not depend on coordinates, and $\theta(x)$ is the unit step Heaviside function.

Assuming that the roughness is small, we expand $C_{\alpha\beta\gamma\delta}(\mathbf{x})$ and $\rho(\mathbf{x})$ into a Taylor series to within terms of the order of ξ^2:

$$\begin{cases}C_{\alpha\beta\gamma\delta}(\mathbf{x})=C_{\alpha\beta\gamma\delta}\theta(x_3)-C_{\alpha\beta\gamma\delta}\xi(x_1,x_2)\,\delta(x_3)\\\qquad+\frac{1}{2}C_{\alpha\beta\gamma\delta}\xi^2(x_1,x_2)\,\delta'(x_3)\\\rho(\mathbf{x})=\rho\,\theta(x_3)-\rho\xi(x_1,x_2)\,\delta(x_3)\\\qquad+\frac{1}{2}\rho\xi^2(x_1,x_2)\,\delta'(x_3).\end{cases}\tag{8}$$

It should be noted that the dependence of the density ρ of the medium on spatial coordinates along with $C_{\alpha\beta\gamma\delta}(\mathbf{x})$ is just the correction of principal importance, that has been introduced in the method of Green's function in Ref. 16.

Substituting expansion (8) into the equations of motion (6) and assuming that the displacement field is a harmonic function of time, i.e., $u_\alpha(\mathbf{x},t)=u_\alpha(\mathbf{x},\omega)\exp(-i\omega t)$, we obtain

$$\sum_\beta\left[L^{(0)}_{\alpha\beta}(\mathbf{x};\omega)+\delta L_{\alpha\beta}(\mathbf{x};\omega)\right]u_\alpha(\mathbf{x},\omega)=0,\tag{9}$$

$$\begin{aligned}L^{(0)}_{\alpha\gamma}(\mathbf{x};\omega)=\omega^2\delta_{\alpha\gamma}\theta(x_3)+\frac{\theta(x_3)}{\rho}\sum_{\beta\delta}C_{\alpha\beta\gamma\delta}\frac{\partial^2}{\partial x_\beta\partial x_\delta}\\+\frac{\delta(x_3)}{\rho}\sum_\delta C_{\alpha3\gamma\delta}\frac{\partial}{\partial x_\delta},\end{aligned}\tag{10}$$

$$\delta L_{\alpha\beta}(\mathbf{x};\omega)=L^{(1)}_{\alpha\beta}(\mathbf{x};\omega)+L^{(2)}_{\alpha\beta}(\mathbf{x};\omega),\tag{11}$$

$$\begin{aligned}L^{(1)}_{\alpha\gamma}(\mathbf{x};\omega)=-\omega^2\delta_{\alpha\gamma}\xi\delta(x_3)-\frac{1}{\rho}\sum_{\beta\delta}C_{\alpha\beta\gamma\delta}\\\times\left[\delta(x_3)\xi\frac{\partial^2}{\partial x_\beta\partial x_\delta}+\frac{\partial}{\partial x_\beta}(\delta(x_3)\xi)\frac{\partial}{\partial x_\delta}\right],\end{aligned}$$

$$\begin{aligned}L^{(2)}_{\alpha\gamma}(\mathbf{x};\omega)=\frac{1}{2}\omega^2\delta_{\alpha\gamma}\xi^2\delta'(x_3)+\frac{1}{2\rho}\sum_{\beta\delta}C_{\alpha\beta\gamma\delta}\\\times\left[\delta'(x_3)\xi^2\frac{\partial^2}{\partial x_\beta\partial x_\delta}\right.\\\left.+\frac{\partial}{\partial x_\beta}(\delta'(x_3)\xi^2)\frac{\partial}{\partial x_\delta}\right].\end{aligned}$$

We introduce Green's function $D_{\alpha\beta}(\mathbf{x},\mathbf{x}';\omega)$ as the solution of the system of equations

$$\begin{aligned}\sum_\beta\left[L^{(0)}_{\alpha\beta}(\mathbf{x};\omega)+\delta L_{\alpha\beta}(\mathbf{x};\omega)\right]\\\times D_{\beta\gamma}(\mathbf{x},\mathbf{x}';\omega)=\delta_{\alpha\gamma}\delta(\mathbf{x}-\mathbf{x}'),\end{aligned}\tag{12}$$

satisfying the conditions of leaving or exponentially attenuating waves for $x_3,x_3'\to+\infty$.

Since the surface of the crystal is regarded as statistically rough, we need Green's function averaged over the rough-

ness of the surface. In order to calculate this function, we use the Dyson equation written to within ξ^2 in the first Born approximation:

$$\langle D\rangle = D^{(0)} + \langle D^{(1)}\rangle + \langle D^{(2)}\rangle, \tag{13}$$

where we have taken into account the fact that $\langle L^{(1)}\rangle = 0$ and

$$\langle D^{(1)}\rangle = -D^{(0)}\langle L^{(2)}\rangle D^{(0)},$$

$$\langle D^{(2)}\rangle = D^{(0)}\langle L^{(1)}D^{(0)}L^{(1)}\rangle D^{(0)}.$$

In order to calculate $\langle D^{(1)}\rangle$ and $\langle D^{(2)}\rangle$, we integrate by parts, thus excluding the derivatives of the δ-function, carry out two-dimensional Fourier transform of Green's function, average over the surface roughness by using the Gaussian correlation function (3), and go over from the functions $D^{(0)}_{\alpha\beta}(\mathbf{k}\omega|x_3x_3')$ to the functions $d_{\alpha\beta}(\mathbf{k}\omega|x_3x_3')$ defined in the basis with $\mathbf{k} = k_1\mathbf{i} + k_2\mathbf{j}$ directed along the x_1-axis:

$$D^{(0)}_{\alpha\beta}(\mathbf{k}\omega|x_3x_3') = \sum_{\gamma\delta} S_{\gamma\alpha}(\mathbf{k}) d_{\gamma\delta}(\mathbf{k}\omega|x_3x_3') S_{\delta\beta}(\mathbf{k}), \tag{14}$$

where

$$S(\mathbf{k}) = \frac{1}{k}\begin{pmatrix} k_1 & k_2 & 0 \\ -k_2 & k_1 & 0 \\ 0 & 0 & k \end{pmatrix}, \quad k = \sqrt{k_1^2 + k_2^2}. \tag{15}$$

As a result, we obtain for $\langle D^{(1)}\rangle$ and $\langle D^{(2)}\rangle$

$$\begin{aligned}\langle D^{(1)}_{\alpha\beta}(\mathbf{x},\mathbf{x}';\omega)\rangle = {}& \frac{\delta^2}{2\rho}\sum_{\gamma\delta}\sum_{\rho\sigma}\int \frac{d^2k}{(2\pi)^2}\, e^{-i\mathbf{k}(\mathbf{x}_\parallel - \mathbf{x}'_\parallel)} \\ & \times S_{\gamma\alpha}(\mathbf{k}) S_{\sigma\beta}(\mathbf{k}) \int d^3x''\,\delta(x_3'') \\ & \times \left\{ \frac{\partial}{\partial x_3''}\, d_{\gamma\delta}(x_3x_3'') A_{\delta\rho}(x_3'') \right. \\ & \left. + d_{\gamma\delta}(x_3x_3'') B_{\delta\rho}(x_3'') \right\} d_{\rho\sigma}(x_3''x_3') \\ & + \frac{\delta^2\omega^2}{2}\sum_{\delta}\int \frac{d^2k}{(2\pi)^2}\, e^{-i\mathbf{k}(\mathbf{x}_\parallel - \mathbf{x}'_\parallel)} \\ & \times \int d^3x''\,\delta(x_3'')\, \frac{\partial}{\partial x_3''}\,(d_{\alpha\delta}(x_3x_3'') d_{\delta\beta}(x_3x_3'')),\end{aligned} \tag{16}$$

$$\begin{aligned}\langle D^{(2)}_{\alpha\beta}(\mathbf{x},\mathbf{x}';\omega)\rangle = {}& \frac{\delta^2}{\rho^2}\int \frac{d^2k}{(2\pi)^2}\int \frac{d^2k'}{(2\pi)^2}\sum_{\gamma\delta}\sum_{\rho\sigma}\sum_{\mu\nu} \\ & \times g(|\mathbf{k}-\mathbf{k}'|) e^{-i\mathbf{k}(\mathbf{x}_\parallel - \mathbf{x}'_\parallel)} S_{\mu\alpha}(\mathbf{k}) \\ & \times d_{\mu\nu}(x_3,0) Q_{\nu\rho}(\mathbf{k}|\mathbf{k}';\omega) d_{\rho\sigma}(0,0) \\ & \times Q_{\sigma\delta}(\mathbf{k}|\mathbf{k}';\omega) d_{\delta\gamma}(0,x_3') S_{\gamma\beta}(\mathbf{k}).\end{aligned} \tag{17}$$

Here the operators $A_{\alpha\beta}(k|x_3)$, $B_{\alpha\beta}(k|x_3)$, $Q_{\alpha\beta}(\mathbf{k}|\mathbf{k}';\omega)$ are functions of the density of the medium and the velocity of propagation of longitudinal and transverse waves in an isotropic solid (see Appendix), while $g(|\mathbf{k}|) = \pi a^2 \exp(-a^2k^2/4)$ is the Fourier transform of the surface self-correlation function (3).

According to formula (4), the contribution of roughness to the low-temperature surface heat capacity is determined by singularities of the function $\Omega(y)$ (5) (with averaged Green's function) for $|y| \to 0$, which can be written in the form

$$\Omega(y) = \Omega_0(y) + \Omega_1(y) + \Omega_2(y), \tag{18}$$

$$\begin{aligned}\Omega_0(y) = {}& -S\sum_{\mu}\int_0^{+\infty} dx_3 \int \frac{d^2k}{(2\pi)^2}\,[d_{\mu\mu}(k,iy|x_3x_3) \\ & - d^{(\infty)}_{\mu\mu}(k,iy|x_3x_3)],\end{aligned}$$

$$\Omega_{1,2}(y) = -\sum_{\mu}\int_0^{+\infty} d\mathbf{x}\langle D^{(1,2)}_{\mu\mu}(\mathbf{x},\mathbf{x};iy)\rangle.$$

Here $\Omega_0(y)$ is responsible for the contribution of a plane free surface to the low-temperature heat capacity of a solid, which was calculated in Ref. 4, while the singularities of the functions $\Omega_1(y)$ and $\Omega_2(y)$ give the contribution of the roughness to surface heat capacity.

In order to determine the singular behavior of $\Omega_1(y)$, we introduce polar coordinates and truncate the integration domain in order to estimate the integral with respect to the magnitude of the vector $\mathbf{k}$: $0 \leqslant k \leqslant k_D$, where $1/k_D$ is of the order of atomic spacing. If the magnitude of the vector $\mathbf{k}$ in the lattice theory is confined to the first Brillouin zone, such a truncation should be used in the limit of the theory of elasticity. It will be clear from subsequent calculations that the final result does not depend on k_D since $\Omega_{(1,2)}(y)$ has a logarithmic singularity. We introduce the dimensionless variables

$$k = \frac{u|y|}{c_t}, \quad k_\alpha = \frac{u|y|}{c_t}\,\hat{k}_\alpha, \quad x_3 = \frac{c_t}{u|y|}\,z,$$

$$\hat{k}_1 = \cos\theta, \quad \hat{k}_2 = \sin\theta$$

and also define Green's function

$$d_{\alpha\beta}(u\mathbf{k}|zz') = c_t u|y| d_{\alpha\beta}\left(\frac{u|y|}{c_t}, iy\middle|\frac{zc_t}{u|y|}, \frac{z'c_t}{u|y|}\right). \tag{19}$$

In this case, the function $\Omega_1(y)$ can be written in the form

$$\begin{aligned}\Omega_1(y) = {}& -\frac{\delta^2 S}{2}\frac{y^2}{c_t^4}\int \frac{d^2\hat{k}}{(2\pi)^2}\int_0^{c_tk_D/|y|}\frac{du}{u}\int_0^{\infty} dz\, d^{(1)}_{\mu\mu} \\ & \times(u,\hat{k}|z,z),\end{aligned} \tag{20}$$

where

$$\begin{aligned}& d^{(1)}_{\mu\mu}(u,\hat{k}|z,z) \\ & = \left[-\frac{\partial}{\partial z''}\, d_{\mu\alpha}(u,\hat{k}|z,z'') d_{\alpha\mu}(u,\hat{k}|z'',z) \right. \\ & + u^2\left(\frac{\partial d_{\mu\alpha}(u,\hat{k}|z,z'')}{\partial z''} A_{\alpha\beta}(z'') \right. \\ & \left.\left. + d_{\mu\alpha}(u,\hat{k}|z,z'') B_{\alpha\beta}(z'') \right) d_{\beta\mu}(u,\hat{k}|z'',z) \right]_{z''=0},\end{aligned} \tag{21}$$

$$A(z)=\rho u^2 y^2 A\left(\frac{u|y|}{c_t},\frac{c_t}{u|y|}z\right)=\begin{pmatrix} -\frac{c_l^2}{c_t^2}-\frac{d^2}{dz^2} & 0 & i\frac{c_l^2-3c_t^2}{c_t^2}\frac{d}{dz} \\ 0 & \frac{c_l^2-c_t^2}{2c_t^2}-\frac{d^2}{dz^2} & 0 \\ -i\frac{c_l^2-3c_t^2}{c_t^2}\frac{d}{dz} & 0 & -1-\frac{c_l^2}{c_t^2}\frac{d^2}{dz^2} \end{pmatrix},$$

$$B(z)=\frac{\rho u^3|y|^3}{c_t}B\left(\frac{u|y|}{c_t},\frac{c_t}{u|y|}z\right)=\begin{pmatrix} -\frac{c_l^2}{c_t^2}\frac{d}{dz} & 0 & i\frac{c_l^2-2c_t^2}{c_t^2}\frac{d}{dz} \\ 0 & -\frac{c_l^2-c_t^2}{c_t^2}\frac{d}{dz} & 0 \\ -i\frac{d^2}{dz^2} & 0 & -\frac{d}{dz} \end{pmatrix}.$$

Using the boundary conditions for the function $d_{\alpha\mu}(u,\hat{k}|z'',z)$, i.e.,

$$\begin{pmatrix} \frac{d}{dz} & 0 & i \\ 0 & \frac{d}{dz} & 0 \\ i\frac{c_l^2-2c_t^2}{c_t^2} & 0 & \frac{c_l^2}{c_t^2}\frac{d}{dz} \end{pmatrix}\begin{pmatrix} d_{11}(u,k|z'',z) & 0 & d_{13}(u,k|z'',z) \\ 0 & d_{22}(u,k|z'',z) & 0 \\ d_{31}(u,k|z'',z) & 0 & d_{33}(u,k|z'',z) \end{pmatrix}_{z''=0}=0$$

and the symmetry conditions, we obtain

$$d_{\mu\mu}^{(1)}(u,\hat{k}|z,z)=8iu^2\left(\frac{c_t^2-c_l^2}{c_l^2}\right)(d_{11}(z0)d_{13}(z0)-d_{33}(z0)d_{31}(z0)). \tag{22}$$

In formula (20), we can integrate with respect to angular variables, after which the problem of integration with respect to u comes into play. Since we are interested only in singular terms in $\Omega(y)$ for $|y|\to 0$, and the upper limit of integration $k_D c_t/|y|\to\infty$ in this case, we can divide the integration into two parts: $0\leqslant u\leqslant u_0$ and $u_0\leqslant u\leqslant k_D c_t/|y|$, where $u_0\gg 1$ and independent of y. In this case, $\int_0^{u_0}du$ is a polynomial in y and has no singularities at zero, while a singularity affects the upper limit of integration in $\int_{u_0}^{k_D c_t/|y|}du$. Such a division makes it possible to expand the integrand function into a power series in $1/u$. Using the explicit form of the functions $d_{\alpha\beta}(\mathbf{k}\omega|x_3x_3')$ calculated in Ref. 15, we can immediately integrate with respect to u, retaining the terms with a singularity for $|y|\to 0$. This gives

$$\Omega_1(y)=\frac{\delta^2 S}{8\pi c_t^4}y^2\ln|y|\ \frac{5c_l^8-7c_l^6c_t^2+4c_l^4c_t^4+c_l^2c_t^6-c_t^8}{c_t^4(c_l^2-c_t^2)^2}. \tag{23}$$

The function $\Omega_2(y)$ can be calculated similarly.

As a result we obtain for $\Omega^{(1)}(y)$

$$\Omega^{(1)}(y)=\Omega_1(y)+\Omega_2(y)=\frac{S}{4\pi}\left(\frac{\delta^2}{a^2}\ln|y|\ \frac{3c_l^6-8c_l^4c_t^2+7c_l^2c_t^4+2c_t^6}{c_l^2c_t^2(c_l^2-c_t^2)^2}+\delta^2y^2\ln|y|\ \frac{c_l^4+c_t^4}{c_l^2c_t^2(c_l^2-c_t^2)^2}\right). \tag{24}$$

Substituting this expression into formula (4) for heat capacity and considering that

$$\int_{-\infty}^{+\infty}dy\ y^n\ \mathrm{e}^{-ixy}\ln|y|=-\pi i\frac{n!}{(ix)^{n+1}}\operatorname{sgn}(x), \tag{25}$$

we can write the final expression for the contribution from slightly rough surface to the low-temperature surface heat capacity in the form

$$\Delta C_S(T)=-6\pi\frac{k_B^3}{h^2}\zeta(3)\frac{(3c_l^6-8c_l^4c_t^2+7c_l^2c_t^4+2c_t^6)}{c_l^2c_t^2(c_l^2-c_t^2)^2}\frac{\delta^2}{a^2}\times ST^2+240\pi^3\frac{k_B^5}{h^4}\zeta(5)\frac{c_l^4+c_t^4}{c_l^2c_t^2(c_l^2-c_t^2)^2}\delta^2ST^4. \tag{26}$$

3. CONCLUSION

In order to compare the result obtained for $\Delta C_S(T)$ with that from Ref. 15, we write expression (26) in the form used by Maradudin *et al.*[15] and also taking into account the expression (1) for a plane surface:

$$\Delta C_V(T)=3\pi\frac{k_B^3}{h^2}\zeta(3)\left\{\frac{2c_t^4-3c_t^2c_l^2+3c_l^4}{c_t^2c_l^2(c_l^2-c_t^2)}\right.$$
$$\times S\left(1+\frac{2\delta^2}{a^2}T^2-\frac{2(3c_l^4-7c_l^2c_t^2+6c_t^4)}{c_t^2(c_l^2-c_t^2)^2}\right.$$
$$\left.\left.\times S\frac{2\delta^2}{a^2}T^2\right\}+240\pi^3\frac{k_B^5}{h^4}\zeta(5)\right.$$
$$\times\frac{c_l^4+c_t^4}{c_l^2c_t^2(c_l^2-c_t^2)^2}\delta^2ST^4. \qquad (27)$$

The first term in this formula coincides with the corresponding expression (5.42) derived in Ref. 15. The first term in the braces proportional to ST^2 is just the result (1) obtained by Dupuis *et al.*,[4] in which the area S of a plane surface is replaced by the area of a rough surface. Maradudin *et al.*[15] interpret this term as the contribution of phonons adiabatically tuned to the surface changed as compared to the plane. The second term in the braces, which is proportional to $(\delta^2/a^2)ST^2$ is associated with phonon scattering at the roughness of the surface. As regards the second term in (27), which is proportional to $S\delta^2T^4$, it differs from the corresponding term in Ref. 15 in sign, numerical coefficient, and a factor depending on c_l and c_t. It was mentioned above that this difference is associated with a more appropriate account of roughness in the Green's function method.[16] Physically, this term is also connected with phonon scattering at the rough surface. In the local theory of elasticity, however, we cannot find the contribution of a plane surface to heat capacity, which is proportional to ST^4. Consequently, the second term in (27), which is proportional to δ^2ST^4, is a roughness correction to the contribution to heat capacity of a plane surface proportional ST^4 to be determined.

A comparison of the absolute values of the first and second terms in formula (26) gives a qualitative pattern of roughness contribution to the low-temperature surface heat capacity. For example, if the correlation length a of roughness is smaller than the phonon thermal wavelength λ_T, the first term in (26), which is proportional to $(\delta^2/a^2)ST^2$, makes the main contribution to the surface heat capacity due to roughness. Since this term is negative, the contribution of roughness to heat capacity is also negative. In the opposite limiting case when a is larger than λ_T, the main contribution to heat capacity comes from the second term proportional to δ^2ST^4. This term appears with the plus sign, and hence roughness increases the surface heat capacity as compared to the case of a plane boundary. Physically, this can be explained as follows. In the case of a roughness with a large correlation length $a>\lambda_T$, potential forces acting between the atoms of the surface are suppressed to the maximum extent as compared to such forces in the bulk, and hence such a surface can be regarded as ''soft.'' In this case, a plane surface is the surface obtained by an appropriate processing (grinding and polishing) of a rough soft surface. Such a surface, which is more logical to be referred to as weakly rough, is characterized by correlation lengths $a\sim\lambda_T$ and is considerably more rigid since broken potential bonds are entangled during processing. It follows from formula (26) that the contribution of roughness to the surface heat capacity for $a\sim\lambda_T$ is very small, i.e., such a weakly rough surface is actually close to a true plane (smooth) surface. As a result of further processing, correlation lengths decrease ($a<\lambda_T$), and the surface becomes much more rigid than the plane surface. Such a surface will be referred to as a rigid surface. As compared to the velocity of sound at a plane surface, it is smaller at a soft surface and larger at a rigid surface. It follows from the phonon energy–momentum relation at a fixed temperature than soft phonons make a positive contribution to the surface heat capacity, increasing it as compared to the case of a plane surface, while rigid phonons reduce the surface heat capacity. It should be noted that the results obtained by Maradudin *et al.*,[15] according to which the inclusion of roughness only reduces the thermal heat capacity, are not confirmed in the qualitative pattern considered above.

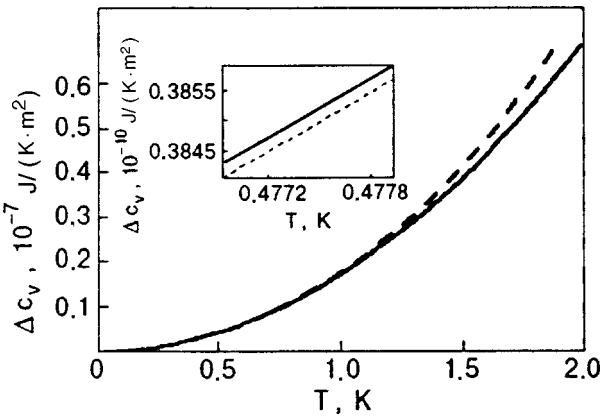

FIG. 1. Temperature dependence of low-temperature surface heat capacity of isotropic molten quartz ($\sigma=0.17$) for roughness parameters $\delta=2$ nm, $a=10^2$ nm (dashed curve). The solid curve corresponds to the plane surface (1).

The obtained contribution of roughness of the surface of an isotropic solid to the low-temperature surface heat capacity (26) is a small correction to the result (1) obtained for a plane boundary. The smallness of this correction allows us to estimate the range of applicability of the obtained results. For example, in the case of optical surfaces of isotropic crystals obtained as a result of polishing (with typical roughness parameters $\delta=2$ nm and $a=10^2$ nm), the temperature range in which our calculations remain correct is $T\leqslant1.9$ K for molten quartz (Poisson's coefficient $\sigma=0.17$),[17] $T\leqslant2.5$ K for aluminum ($\sigma=0.355$), $T\leqslant1$ K for bismuth ($\sigma=0.33$), $T\leqslant1.4$ K for silver ($\sigma=0.38$), and $T\leqslant1.4$ K for cold-drawn gold ($\sigma=0.42$). In the case of optical surfaces obtained at the stage of fine diamond grinding ($\delta=10$ nm, $a=5\times10^2$ nm), the range of attainable temperatures decreases significantly and amounts, for example, only to 0.4 K for molten quartz. Conversely, at the stage of superfinish polishing by an ultradisperse particle flow ($\delta\leqslant0.5$ nm, $a=50$ nm), the temperature range increases significantly and amounts to 7.5 K for the same molten quartz.

Numerical calculations based on formula (27) were used to analyze the behavior of the obtained correction to heat capacity as a function of temperature for various values of roughness parameters. Figure 1 shows the temperature de-

pendence of surface heat capacity per unit surface area, $\Delta c_V(T)=\Delta C_V(T)/S$, for isotropic molten quartz. It can be seen that in the temperature range $T<0.15$ K, the contribution of roughness to the surface heat capacity is negative. However, roughness makes a positive contribution to heat capacity attaining $\sim 10\%$ at $T=1.9$ K in a much wider temperature range (of the order of 1.5 K). A similar pattern of the behavior of surface heat capacity taking into account roughness is observed for all the isotropic materials mentioned above, and not only for polished surfaces, but also for surfaces obtained at the stage of fine diamond grinding and superfinish polishing. This suggests that the contribution of slight roughness of optical surfaces of isotropic crystals to the low-temperature surface heat capacity is positive in the overwhelming part of the temperature range attainable according to the perturbation theory.

The authors are grateful to A. A. Maradudin and V. N. Sobakin for fruitful discussions and valuable remarks.

APPENDIX

$$A_{11}(k|x_3)=-\rho c_l^2 k^2-\rho c_t^2\,\frac{d^2}{dx_3^2};$$

$$A_{22}(k|x_3)=-\rho c_t^2 k^2-\rho c_t^2\,\frac{d^2}{dx_3^2};$$

$$A_{33}(k|x_3)=-\rho c_t^2 k^2-\rho c_l^2\,\frac{d^2}{dx_3^2};$$

$$A_{13}(k|x_3)=-i\rho(c_l^2-3c_t^2)k\,\frac{d}{dx_3}=-A_{31}(k|x_3).$$

$$B_{11}(k|x_3)=-\rho c_l^2 k^2\,\frac{d}{dx_3};$$

$$B_{22}(k|x_3)=-\rho c_t^2 k^2\,\frac{d}{dx_3};$$

$$B_{33}(k|x_3)=-\rho c_t^2 k^2\,\frac{d}{dx_3};$$

$$B_{13}(k|x_3)=i\rho(c_l^2-2c_t^2)k\,\frac{d^2}{dx_3^2};$$

$$B_{31}(k|x_3)=i\rho c_t^2 k\,\frac{d^2}{dx_3^2}.$$

$$Q_{11}=\left(\frac{c_{11}^2-c_{12}^2}{c_{11}}\right)\frac{k_1^2k_1'^2+k_2^2k_2'^2}{kk'}+\left(\frac{c_{12}(c_{11}-c_{12})}{c_{11}}\right)\frac{k_1^2k_2'^2+k_2^2k_1'^2}{kk'}+4c_{44}\,\frac{k_1k_2'k_2k_1'}{kk'}-\frac{\rho\omega^2}{kk'}\,(k_1k_1'+k_2k_2');$$

$$Q_{12}=2c_{44}\left[(k_2^2-k_1^2)\,\frac{k_2'k_1'}{kk'}+(k_1'^2-k_2'^2)\,\frac{k_2k_1}{kk'}\right]-\frac{\rho\omega^2}{kk'}\,(-k_1k_2'+k_2k_1');$$

$$Q_{21}=2c_{44}\left[(k_2'^2-k_1'^2)\,\frac{k_2k_1}{kk'}+(k_1^2-k_2^2)\,\frac{k_2'k_1'}{kk'}\right]-\frac{\rho\omega^2}{kk'}\,(k_1k_2'-k_2k_1');$$

$$Q_{22}=4c_{44}\,\frac{k_1k_2'k_2k_1'}{kk'}+c_{44}\,\frac{(k_2'^2-k_1'^2)(k_2^2-k_1^2)}{kk'}-\frac{\rho\omega^2}{kk'}\,(k_1k_1'+k_2k_2').$$

Here, the following notation has been used: $c_{11}=\rho c_l^2$, $c_{44}=\rho c_t^2$, $c_{12}=c_{11}-2c_{44}$.

*E-mail: kosachev@theor.mephi.msk.su

[1] A. Kh. Brager and A. A. Schuchowitzky, J. Chem. Phys. **14**, 569 (1946).
[2] E. W. Montroll, J. Chem. Phys. **18**, 183 (1950).
[3] R. Stratton, J. Chem. Phys. **37**, 2972 (1962).
[4] M. Dupuis, R. Mazo, and L. Onsager, J. Chem. Phys. **33**, 1452 (1960).
[5] M. G. Burt, J. Phys. C **6**, 855 (1973).
[6] L. Dobrzynski and A. A. Maradudin, Phys. Rev. B **14**, 2200 (1976).
[7] K. Portz and A. A. Maradudin, Phys. Rev. B **16**, 3535 (1977).
[8] D. Patterson, Can. J. Chem. **33**, 1079 (1955).
[9] A. A. Maradudin and R. E. Wallis, Phys. Rev. **148**, 945 (1966).
[10] T. S. Chen, G. P. Alldredge, F. W. de Wette, and R. E. Allen, J. Chem. Phys. **55**, 3121 (1971).
[11] J. H. Barkman, R. L. Anderson, and T. E. Brackett, J. Chem. Phys. **42**, 1112 (1965).
[12] N. Steinmetz, H. Menges, J. Dutri, and H. von Lohneysen, Phys. Rev. B **39**, 2838 (1989).
[13] I. A. Gospodarev and E. S. Syrkin, Fiz. Nizk. Temp. **7**, 1467 (1981) [Sov. J. Low Temp. Phys. **7**, 712 (1981)].
[14] Yu. A. Kosevich and E. S. Syrkin, Fiz. Nizk. Temp. **9**, 624 (1983) [Sov. J. Low Temp. Phys. **9**, 317 (1983)].
[15] A. A. Maradudin, R. E. Wallis, and A. Equiluz, in *Statistical Mechanics and Statistical Methods in Theory and Applications* (ed. by U. Landman), Plenum Publ. Co., N. Y. (1977).
[16] V. V. Kosachev, Yu. N. Lokhov, and V. N. Chukov, Zh. Éksp. Teor. Fiz. **94**, 162 (1988) [Sov. Phys. JETP **67**, 1825 (1988)].
[17] S. Kino, *Acoustic Waves. Devices, Imaging, and Analog Signal Processing*, Cambridge Univ. Press, Cambridge (1987).

Translated by R. S. Wadhwa

BRIEF COMMUNICATIONS

On anomalies of optical exciton reflection spectra of crystals at low temperatures

P. S. Kosobutskii

*''L'vovskaya Polytekhnika'' University, 290646, L'vov, Ukraine**

(Submitted October 21, 1997; revised November 9, 1997)
Fiz. Nizk. Temp. **24**, 493–494 (May 1998)

The anomalies in the optical exciton reflection spectra of crystals at low temperatures are interpreted. It is shown that the amplitude of the reflection minima increases upon an increase in damping. © *1998 American Institute of Physics.* [S1063-777X(98)01205-5]

The exciton reflection spectra of direct-band semiconducting crystals reveal a number of anomalies at low temperatures, which have been described extensively in the literature (see, for example, Ref. 1). An interesting effect was reported in earlier publications:[2–4] starting from the liquid helium temperature ($T=4.2$ K), the amplitude of the minimum in the resonance reflection contour increases with temperature, i.e., the resonance minimum becomes ''brighter.'' Ruckman *et al.*[2] attributed this effect to quasilocal excitons in the surface layer of the crystal, while Pevtsov *et al.*[3] used computer simulation to show that the above-mentioned temperature dependence of the reflection spectrum $R(\omega)$ can be due to the nondispersive layer on the crystal surface.

In this report, we analyze theoretically the reflection of light by a three-layer interface vacuum–nonresonance layer–bulk crystal in the resonant excitation region of excitons. It is shown that irrespective of the nature of dispersion of resonance permittivity, the amplitude of the minimum in the resonance reflection contour increases upon an increase in damping in the exciton system, i.e., upon an increase in temperature. This is associated not with the nature of dispersion of the permittivity, but with the phase relations at the layer boundaries, taking into account the fact that the minimum of the reflection contour is formed at the phase compensation frequency.

Let us consider the normal reflection of light in a three-layer vacuum–nonresonance layer–bulk crystal system. According to Born and Wolf,[5] the complex reflection amplitude is defined as

$$\tilde{r}=\frac{\tilde{r}_1+\tilde{r}_2\,\exp(-i\delta)}{1+\tilde{r}_1\tilde{r}_2\,\exp(-i\delta)}, \tag{1}$$

where the subscripts 1 and 2 correspond to the first and second interface respectively, $\delta=4\pi nd/\lambda$ is the phase shift of the wave in the exciton-free layer having a thickness d and a refractive index n.

According to formula (1), the energy coefficient of light reflection is given by the relation

$$R=(\mathrm{Re}\,\tilde{r})^2(1+\tan^2\varphi), \tag{2}$$

where φ is the resultant phase of the reflected light ($\tan\varphi=\mathrm{Im}\,\tilde{r}/\mathrm{Re}\,\tilde{r}$, $\mathrm{Re}\,\tilde{r}$ *and* $\mathrm{Im}\,\tilde{r}$ being the real and imaginary parts of $\tilde{r}$. At the phase compensation frequency ω_m, the condition

$$\delta+\varphi_2=2\pi \tag{3}$$

is satisfied,[6] and the minimum of the reflection contour is formed since the following conditions are fulfilled:

$$\mathrm{Re}\,\tilde{r}\neq 0, \quad \mathrm{Im}\,\tilde{r}=0, \tag{4}$$

φ_2 being the phase shift of the wave reflected at the layer–crystal interface. Hence, at the frequency corresponding to the minimum, the waves reflected at the opposite faces of the layer oscillate in antiphase, and the amplitude $\mathrm{Re}\,\tilde{r}$ is defined as

$$\mathrm{Re}\,\tilde{r}\Big|_{\omega=\omega_m}=\frac{(\rho_1-\rho_2)}{(1-\rho_1\rho_2)}. \tag{5}$$

With increasing temperature, the damping γ increases due to an enhancement of the exciton-phonon interaction, i.e., the amplitude ρ_2 decreases and hence $\rho_2\to\rho_1$, and $R_{\min}\to 0$.

If the hodograph of $\tilde{r}$ passes through the origin of coordinate axes $\mathrm{Re}\,\tilde{r}$ and $\mathrm{Im}\,\tilde{r}$, we obtain $R_{\min}=0$, and the crystal becomes transparent at this frequency. The phase spectra also undergo significant variation in this case. If $\mathrm{Re}\,\tilde{r}=0$ and $\mathrm{Im}\,\tilde{r}=0$ simultaneously, the phase spectra display the familiar ''N''↔''S''-type transformations in the contour.[7]

*E-mail: petkosob@polynet.lviv.ua

[1] V. A. Kiselev, B. V. Novikov, and A. E. Cherednichenko, *Exciton Spectroscopy in the Surface Layer of Semiconductors* [in Russian], Iz-vo LGU, Leningrad (1987).
[2] I. Ruckman, V. May, and J. Voigt, Phys. Status Solidi B **102**, 97 (1980).
[3] A. B. Pevtsov, S. A. Permogorov, and A. V. Sel'kin, Pis'ma Zh. Éksp. Teor. Fiz. **39**, 261 (1984) [JETP Lett. **39**, 312 (1984)].
[4] U. Arimoto, M. Tachiki, and K. Nakamura, J. Phys. Soc. Jpn. **60**, 4356 (1991).
[5] M. Born and E. Wolf, *Principles of Optics* 4th ed., Pergamon, Oxford, 1969.
[6] P. S. Kosobutskii, Ukr. Fiz. Zh. **28**, 1090 (1983).
[7] S. B. Moskovskii, L. E. Solov'ev, and M. O. Chaika, Fiz. Tverd. Tela (Leningrad) **23**, 3618 (1981) [Sov. Phys. Solid State **23**, 2102 (1981)].

Translated by R. S. Wadhwa

Point contact studies of the superconducting gap of $CeRu_2$

Yu. G. Naidyuk, A. V. Moskalenko, and I. K. Yanson

B. Verkin Institute for Low Temperature Physics and Engineering, National Academy of Sciences of Ukraine, 47, Lenin Ave., 310164, Kharkov, Ukraine

C. Geibel

Institut für Festkörperphysik, TU Darmstadt, D-64289 Darmstadt, Germany
(Submitted December 25, 1997)
Fiz. Nizk. Temp. **24**, 495–497 (May 1998)

The measured $dV/dI(V)$ curves of point contacts between the intermetallic compound $CeRu_2$ in the superconducting state and the normal metal Cu correspond fairly well to the Blonder–Tinkham–Klapwijk model. It is used to obtain temperature and magnetic field dependence of the superconducting gap Δ. The $\Delta(T)$ dependence corresponds well to the BCS theory with $2\Delta(0)/k_BT_c^*=3.1\pm0.1$. Additionally, a region of gapless superconductivity between $T_c^*\simeq 4.4-5.4$ K and $T_c^{\rm bulk}\simeq 6.2$ K is found. The gap decreases approximately linearly in a magnetic field and vanishes in a field $B_c^*\simeq 3.5$ T, which is well below the upper critical field $B_{c2}\simeq 6$ T and close to the irreversibility field. © *1998 American Institute of Physics.* [S1063-777X(98)01305-X]

1. INTRODUCTION

The recently renewed interest in the intermetallic compound $CeRu_2$ is attributable to its anomalous magnetic and transport properties in the superconducting (SC) mixed state. As one of the possible reasons for this the generalized Fulde–Ferrell–Larkin–Ovchinnikov state[1] is discussed with a spatially modulated SC order parameter (OP), which could have planar nodes aligned perpendicularly to the vortices. Until now, however, only a few direct investigations of the OP have been reported. From Shottky tunneling experiments[2] the SC gap was estimated to be $2\Delta(0)/k_BT_c=11-12$. Subsequent attempts by using metallic point contacts (PC)[3] revealed a rather low value (less than 2). Recent break-junction tunneling measurements[4] yielded $2\Delta(0)/k_BT_c=4.2$, quite different from the former results, indicating specific difficulties of the aforementioned methods. In the latter investigation a BCS-type temperature dependence of the gap peculiarities was ascertained. Unfortunately, no magnetic field behavior of SC gap features was established in any of the studies, although magnetic field is one of the sensitive probes of superconductivity.

The aim of this paper is to study the temperature and the magnetic-field dependences of the SC gap in $CeRu_2$ using a metallic PC between the $CeRu_2$ and the normal metal. We obtained $dV/dI(V)$ characteristics, which correspond well to the Blonder–Tinkham–Klapwijk (BTK) model,[5] taking into account the well-known mechanism of the Andreev reflection (AR) at a normal metal-superconductor (N-S) interface. The gap value was determined directly from a fit according to this BTK model.

2. EXPERIMENT AND RESULTS

We used $CeRu_2$ polycrystals with $RRR\simeq 14$ and $T_c=6.2$ K. The PC's were prepared by touching the $CeRu_2$ crystal with the edge of a Cu electrode. The freshly broken $CeRu_2$ surface gave the best dV/dI curves with a pronounced minimum (or double minimum). The sample was immersed in liquid ^{4}He to ensure good thermal coupling. The differential resistance dV/dI was recorded vs. bias voltage V using a standard lock-in amplifier technique, modulating the direct current I with a small ac component. The applied magnetic field B was approximately parallel to the contact axis.

Figures 1 and 2 show the dV/dI curves vs. V of the $CeRu_2$–Cu contacts at various temperatures and magnetic fields. The double-minimum structure of about $V=0$ is clearly seen. This feature is a strong indicator of the Andreev reflection in the presence of weak quasiparticle reflection at the N-S interface, as described by the phenomenological barrier strength parameter Z.[5] The $I-V$ characteristic in this case is

$$I(V)\sim\int_{-\infty}^{\infty}T(E)[f(E-eV)-f(E)]dE, \tag{1}$$

$$T(E)=\frac{2\Delta^2}{E^2+(\Delta^2-E^2)(2Z^2+1)^2},\quad |E|<\Delta,$$

$$T(E)=\frac{2|E|}{|E|+(E^2-\Delta^2)^{1/2}(2Z^2+1)},\quad |E|>\Delta,$$

where $f(E)$ is the Fermi distribution function and Δ is the superconducting gap. In the modified BTK theory the broadening of the quasiparticle density of states $N(E,\Gamma)$ in the superconductor for the finite quasiparticle lifetime τ is taken into account. According to the Dynes *et al.*,[6]

$$N(E,\Gamma)=\mathrm{Re}\left\{\frac{E-i\Gamma}{[(E-i\Gamma)^2-\Delta^2]^{1/2}}\right\},$$

where the broadening parameter is $\Gamma=\hbar/\tau$.

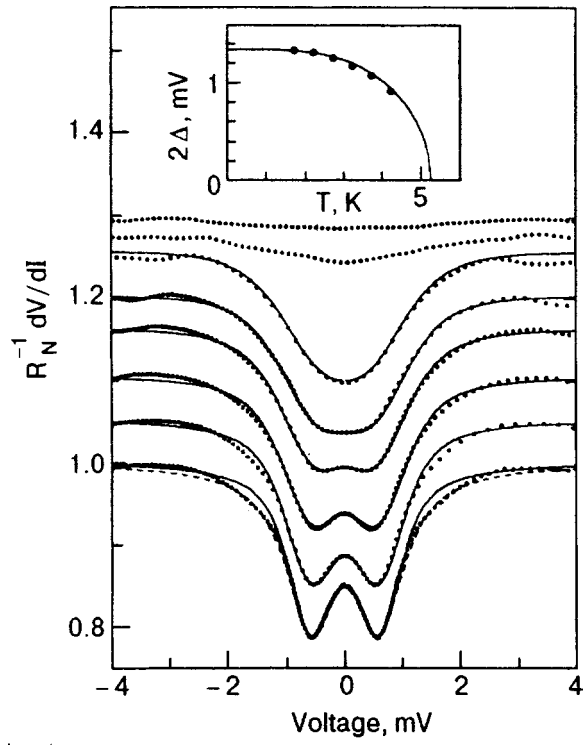

FIG. 1. The temperature dependence of the reduced dV/dI curves vs. bias V (points) for a $CeRu_2$–Cu contact with $R_N=1.4\Omega$ along with a fit using Eq. (1) with $\Gamma=0$ (solid lines) and $\Gamma/\Delta=0.25$ (dashed line). The left scale corresponds to the experimental curves and to the dashed line. The curves are offset vertically for clarity. The temperatures from top curve to bottom curve T, K: 6.2, 5.2, 4.2, 3.7, 3.2, 2.7, 2.2, and 1.7 K. Inset: reduced gap Δ vs. temperature from the fit with $\Gamma=0$. The solid line is BCS curve with $2\Delta(0)/k_BT_c^*\simeq 3$.

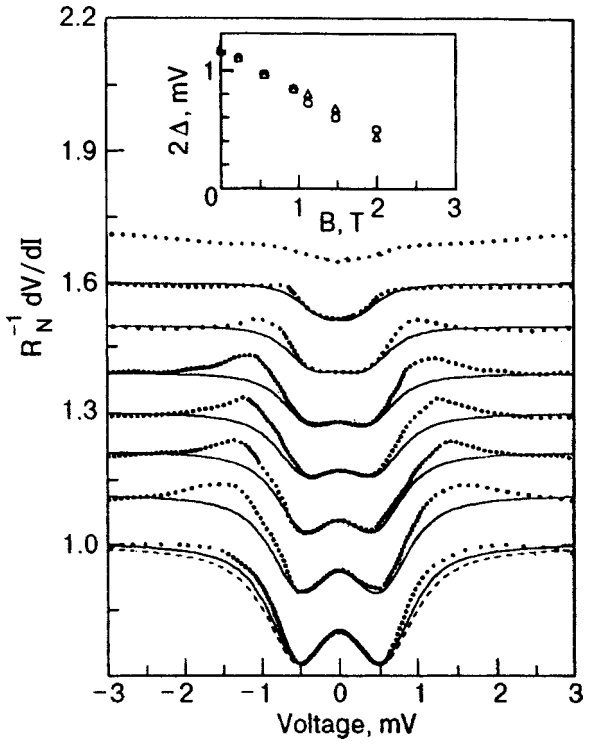

FIG. 2. The magnetic field dependence of the reduced dV/dI curves vs. bias V (points) for $CeRu_2$–Cu contact at $T=1.8$ K with $R_N=1.1\Omega$ along with the fit using Eq. (1) with $\Gamma=0$ (solid lines) and $\Gamma/\Delta=0.1$ (dashed line). The left scale corresponds to the experimental curves and to the dashed line. The curves are offset vertically for clarity. The magnetic fields from top curve to bottom curve B, T: 2.8, 2, 1.5, 1.13, 0.94, 0.56, 0.22, and 0. Inset: 2Δ vs. magnetic field using the fit with $\Gamma=0$ (triangles) and $\Gamma\neq 0$ (circles).

In order to obtain the temperature and magnetic field dependences of Δ we fitted the measured dV/dI curves according to Eq. (1) for $\Gamma=0$ and $\Gamma\neq 0$. The parameter Z was kept fixed, independent of the temperature and magnetic field. The plots of $\Delta(T)$ and $\Delta(B)$ of different $CeRu_2$ contacts are shown in the insets in Figs. 1–3. The original BTK theory, i.e., with $\Gamma=0$, usually fitted better the behavior of dV/dI near the double-minimum (see Figs. 1 and 2), especially compared to the fit with large $\Gamma/\Delta>0.1$ ratio, but it does not reproduce the relative change of dV/dI between $V=0$ and large biases. On the average, we obtained a reduced gap of $2\Delta(0)/k_BT_c^*=3.1\pm 0.1$. Using the modified BTK fit, we see that the $2\Delta(0)/k_BT_c^*$ ratio decreases (by about 10–30%) with increasing Γ/Δ value (correspondingly from 0.25 to 0.75).

As can be seen from Fig. 1, the dV/dI curve at $T=5.2$ K still exhibits a broad and shallow SC minimum, but it is not possible to fit it reasonably to any Δ. Since for this contact BCS $\Delta(T)$ behavior (see the inset in Fig. 1) extrapolates to $T_c^*\simeq 5.25$ K, we conclude that the small SC features above T_c^* and below $T_c^{\text{bulk}}=6.2$ K correspond to a gapless state. For different contacts T_c^* is between 4.4 and 5.25 K probably because of the local superconducting properties in the contact region.

The magnetic field dependence $\Delta(B)$ is almost linear (see the insets in Figs. 2 and 3b), with a critical field B_c^*

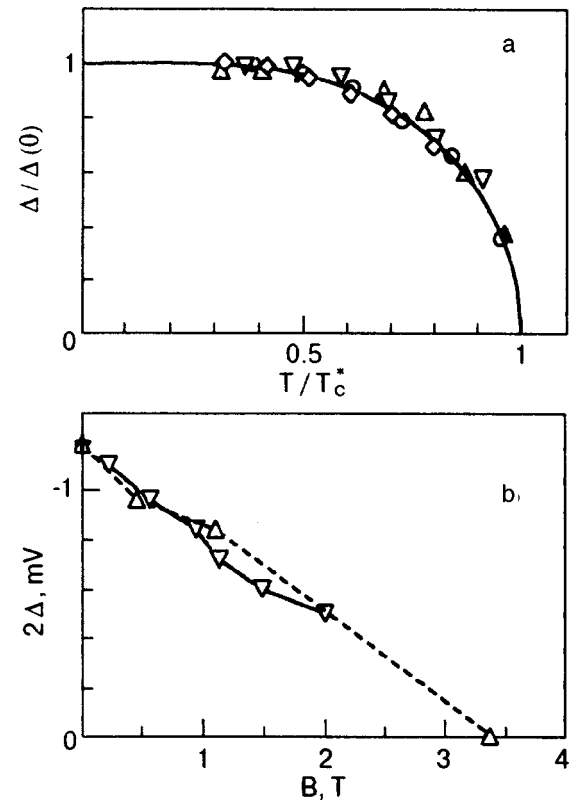

FIG. 3. a) Reduced Δ vs. temperature of different PC along with the BCS curve, b) 2Δ vs. magnetic field of different PC. The lines connect the symbols for clarity.

about 3.4 T. This is quite different to what is expected for a type-II superconductor.[7]

3. DISCUSSION AND CONCLUSIONS

The other possibility of yielding a maximum at $V=0$ and similar double-minimum structure on dV/dI is Kondo scattering superimposition with SC minimum, which was recently discussed in detail in Ref. 8. However, in a magnetic field this maximum vanishes (see Fig. 2) without the splitting characteristic of the Kondo effect.[9] Moreover, the fit according to BTK theory, obeys the measured characteristics quite well, thus making the magnetic scattering unlikely to occur in the observed structure.

According to our findings, $CeRu_2$ is a BCS-like superconductor. The relatively small $2\Delta(0)/k_BT_c^*$ value (corresponding to weak-coupling superconductivity) and the region of gapless superconductivity close to T_c^{bulk} are possibly related to the pair-breaking effect caused, e.g., by the Ce local magnetic moments which are distributed randomly in the contact region. This pair-breaking effect may also contribute to the small value of the reduced gap.[10] For the reason mentioned above it seems reasonable to include Kondo scattering in the BTK theory for a better understanding of the point contact characteristics and the relationship between superconductivity and magnetism in the point contacts.

The gradually decreasing gap in the magnetic field makes the transition to the Fulde–Ferrell–Larkin–Ovchinnikov state unlikely, which should be of the first order. The linear decrease of $\Delta(B)$ and the low magnetic field at which the superconducting gap vanishes remains an enigma. The close coincidence of B^* with the irreversibility field[11] points to a change of the vortex dynamics as a possible reason. To solve these puzzles it is necessary to carry out further experiments on the temperature and magnetic field $dV/dI(V)$ dependences of the same point contact much closer to T_c^* and B_c^* using a more perfect $CeRu_2$ single crystal.

This work was carried out, in part, thanks to the support of A. V. Humboldt Stiftung. We are indebted to K. Gloos for a useful discussion, R. Häussler for BTK fit program, and R. Clemens for preparing the samples. I. K. Yanson acknowledges the financial support under INTAS Project No.94-3562.

[1] M. Tachiki *et al.*, Z. Phys. B **100**, 369 (1996).
[2] W. Schmitt and G. Guntherodt, J. Magn. Magn. Mater. **47–48**, 542 (1985).
[3] M. E. Solanki-Moser, Ph. D. Thesis, ETH Zürich (1987).
[4] T. Ekino, H. Fujii, T. Nakama, and K. Yagasaki, Czech. J. Phys. **46**, 783 (1996); Phys. Rev. **56**, 7851 (1997).
[5] G. E. Blonder, M. Tinkham, and T. M. Klapwijk, Phys. Rev. **25**, 4515 (1982).
[6] R. C. Dynes, V. Narayanamurti, and J. P. Garno, Phys. Rev. Lett. **21**, 1509 (1978).
[7] K. Maki, in Superconductivity, R. D. Parks (Ed.), Marcel Dekker, New York (1969).
[8] Yu. G. Naidyuk, K. Gloos, and A. A. Menovsky, J. Phys.: Condens. Matter **9**, 6279 (1997).
[9] A. G. M. Jansen, A. P. van Gelder, and P. Wyder, J. Phys. C **13**, 6073 (1980).
[10] M. Tinkham, *Introduction to Superconductivity*, McGraw-Hill, New York (1980).
[11] A. D. Huxley *et al.*, J. Phys.: Condens. Matter **5**, 7709 (1993).

This article was published in English in the original Russian journal. It was edited by S. J. Amoretty.

LETTERS TO THE EDITOR

Thermal transport through Luttinger liquid constriction

I. V. Krive

*B. I. Verkin Institute for Low Temperature Physics and Engineering, National Academy of Sciences of Ukraine, 47, Lenin Ave., 310164, Kharkov, Ukraine**

(Submitted February 23, 1998)
Fiz. Nizk. Temp. **24**, 498–500 (May 1998)

The heat transport through one-dimensional quantum wire is considered in the frameworks of the inhomogeneous Tomonaga–Luttinger liquid model. It is shown that even for perfect (impurity free) wire thermal transport is suppressed due to multiple scattering of plasmons on the boundaries that connect quantum wire to the leads of noninteracting electrons. In the presence of impurity inside the Luttinger liquid constriction resonant enhancement of thermal conductivity at certain conditions is predicted. © *1998 American Institute of Physics.* [S1063-777X(98)01405-4]

Recently Kane and Fisher[1] studied the heat transport in a Luttinger liquid (LL). They claimed that: (i) in pure LL thermal conductance $K(T)$ does not depend on electron-electron interaction and it coincides with the one of Fermi liquid (FL) $K_0(T)=(\pi^2/3)T/h$ (h is the Planck constant, T is the temperature); (ii) in the presence of single impurity $K(T)\propto T^3$ at low temperatures and for strong repulsive interaction $g<1/2$ (g is the correlation parameter of LL).

Both above results were obtained for infinitely long LL. In this case it is known[2] that the dc electrical conductance $G(T)$ (formally defined as response function to the change in chemical potential) is renormalized by interaction. For pure LL $G_0=ge^2/h$ and in the presence of single impurity $G(T)\propto T^{2/g-2}$. So the authors of Ref. 1 concluded that the ratio of thermal to electrical conductance $L_g=K/TG$ is modified by interaction. In FL this quantity, known as the Lorentz number, is universal $L_0=(\pi^2/3)(k_B/e)^2$ (k_B is the Boltzman constant). In infinite perfect LL wire $L_g=L_0/g$ and in the presence of impurity the Lorentz ''number'' diverges as $T\to 0$ for $g<1/2$.[1]

The predictions obtained for homogeneous infinite LL cannot be applied directly to the realistic situation when the LL wire is connected to the reservoirs of noninteracting electrons (source and drain leads). In this case it was proved[3] that the dc electrical conductance is not renormalized by interaction in the absence of electron backscattering.

The purpose of the present communication is to reconsider the Kane–Fisher problem[1] for a realistic experimental setup. We study thermal transport through a LL *constriction* in the framework of the inhomogeneous Tomonaga–Luttinger liquid (ITLL) model.[3] For simplicity we consider here only the case of spinless electrons.

If electrons are not backscattered by inhomogeneities, the entropy is totally carried by plasmons. The simplest way to visualize charge and heat transport in a repulsively interacting electron system is to consider the motion of a $1D$ Wigner solid (WS) through the constriction. At zero temperature the rigid shift of WS results in the interaction independent conductance e^2/h. It is evident that at finite temperatures thermally activated sound waves in WS (plasmons) cannot affect electrical transport through perfect LL constriction. However the scattering of plasmons on the interfaces LL-FL will suppress heat transport.

The heat transport associated with plasmons can be expressed in terms of transmission probability, $T_t(\varepsilon)$, of plasmons through LL constriction. The corresponding formula for thermal conductance is readily derived in Landauer–Buttiker formalism for transport coefficients (see, e.g., [Ref. 4])

$$K(T)=\frac{1}{Th}\int_0^\infty d\varepsilon\,\varepsilon^2\left(\frac{-\partial f_B}{\partial\varepsilon}\right)T_t(\varepsilon), \tag{1}$$

where $f_B(\varepsilon)=(e^{\varepsilon/T}-1)^{-1}$ is the distribution function of plasmons. In ITLL model it is assumed[3] that the transition from interacting to noninteracting electrons is smooth (the characteristic length $\lambda_F\ll\xi\ll L$, where λ_F is the Fermi wavelength and L is the length of LL wire). Therefore Eq. (1) determines the exact thermal conductance for perfect (impurity free) LL when the Lagrangian of LL is quadratic in terms of boson variables (the leads are modeled by $1D$ noninteracting electrons which correspond to $g=1$ LL). In the presence of electron backscattering inside the LL constriction Eq. (1) for $g<1/2$ determines the main contribution to heat transport at low temperatures.

So our problem is reduced to the calculation of the plasmon transmission coefficient. Here we consider the special case when the scattering potential is placed exactly in the middle of an LL wire (in this case one could expect the enhancement of heat transport due to resonant tunneling of plasmons through the impurity).

Backscattering of electrons causes the appearance of nonlinear local term in bosonic form of LL Lagrangian $\delta L=-V_p\delta(x)\cos\varphi$. For our problem this term describes the scattering of plasmons, $\varphi\ll 1$, on a δ-function potential and we immediately find the desired transmission coefficient for

infinite LL wire $T_t(\varepsilon)=\varepsilon^2/(\varepsilon^2+\varepsilon_0^2)$, where $\varepsilon_0=2\pi g V_p/\hbar$. The heat conductance Eq. (1) reads

$$K_\delta(T)=K_0[1+3z+6z^2-6z^3\Psi'(z)],\quad z=\frac{gV_p}{T}. \qquad (2)$$

Here $\Psi(z)=d\ \ln\Gamma(z)/dz$, $\Gamma(z)$ is the gamma-function. At low temperatures, $T\ll gV_p$, Eq. (2) reproduces T^3-behavior of heat conductance found in Ref. 1.

To calculate the transmission probability of plasmons through LL constriction we should additionally take into account the scattering of plasmons on LL-FL boundaries. For adiabatic contact (ITLL model) it can be done by matching the wave functions of plasmons at the boundaries. The straightforward calculations yield

$$T_t^g(\varepsilon)=\left(\frac{\varepsilon}{\varepsilon_0}\right)^2\left\{\left[g_- - g_+\left(\cos\frac{\varepsilon}{\Delta}+\frac{\varepsilon}{\varepsilon_0}+\sin\frac{\varepsilon}{\Delta}\right)\right]^2 + \left(\sin\frac{\varepsilon}{\Delta}+\frac{\varepsilon}{\varepsilon_0}\cos\frac{\varepsilon}{\Delta}\right)^2\right\}^{-1}, \qquad (3)$$

where $\Delta=\hbar s/L$, $g_\pm=1/2(g^{-1}\pm g)$, $g=s/v_F$, s is the plasmon velocity.

At first we consider the case of pure LL constriction ($\varepsilon_0\to 0$). In this limit the transmission coefficient $T_t(\varepsilon)=[\cos^2(\varepsilon/\Delta)+g_+^2\sin^2(\varepsilon/\Delta)]^{-1}$ is a periodic function of plasmon energy with the period $\varepsilon_n=n\pi\Delta$ (n is an integer). This property is the manifestation of quantization of plasmons in LL constriction.[5] Plasmon transport through LL wire is resonant at energies in the vicinity of $\varepsilon_n(T_t(\varepsilon_n)=1)$ and is suppressed (strongly suppressed $T_t\ll 1$ for strong interaction $g\ll 1$) at off-resonance energies.

At low temperatures $T\ll\Delta$ thermal conductance $K(T)$ is determined by the contribution of long wavelength plasmons ($n=0$ resonance to integral Eq. (1). Low energies of plasmons correspond to the region of noninteracting electrons and therefore thermal transport is not affected by interaction.[1] Notice however that for long wires the corresponding temperature interval is contracted to a point. On contrary at temperatures $T>\Delta$ heat conductance is strongly (for $g\ll 1$) renormalized by interaction $K(T)/K_0\simeq 2g\ll 1$. The dependence of Lorentz ''number'' on temperature for pure LL constriction is shown on Fig. 1. It clearly demonstrates the violation of Wiedemann–Franz law for LL wires (the effect is pronounced for the case of strong interaction $g\ll 1$).

We now proceed to the transport properties of LL wire with impurity. Electrical conductance for the problem under study was calculated in Ref. 6. As it was expected from physical considerations,[2] the conductance of *finite* LL wire at $T\ll\Delta$ is temperature independent $G\simeq(e^2/h)(\Delta/gV_p)^{2/g-2}$ and the infinite LL-like behavior[2] is restored only at $T\gg\Delta$. The behavior of thermal conductance can be found from Eqs. (1) and (3). At low temperatures one can neglect the quantization of plasmons and T^3 dependence of infinite LL wire, Eq. (2), $K(T)\simeq K_0(T)(T/gV_p)^2$ could be expected. However in exactly the same manner as for electrical conductance, the factor $(T/gV_p)^2$ caused by interaction effects is replaced by $(\Delta/gV_p)^2$. With the increase of temperature the quantization of plasmons comes into play. For our geometry when the impurity is placed in the middle of LL wire resonant tunneling of plasmons through impurity occurs and thermal conductance at $T\gg\Delta$ attains its maximum for the perfect LL constriction value $K(T)\simeq 2gK_0(T)$ ($g\ll 1$). Therefore the Lorentz ''number'' of LL constriction is an inverse function of the temperature as it was predicted in Ref. 1. For the resonance case studied above the ''high'' temperature ($T>\Delta$) behavior of L_g is determined by the temperature dependence of conductance of LL constriction[6] and hence $L_g/L_0\propto g(gV_p/T)^{2/g-2}$. Moreover, unlike the case an infinite homogeneous LL in a finite LL wire the Lorentz number for $g<1/2$ saturates at value $L_g\simeq L_0(gV_p/\Delta)^{2/g-4}$ for $T\to 0$.

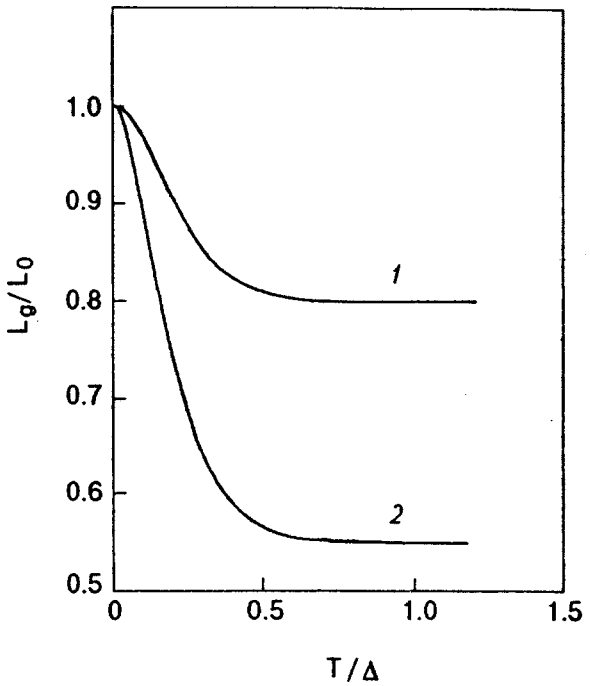

FIG. 1. The dependence of Lorentz ''number'' of perfect LL constriction on temperature at different values of g: 0.5 *(1)* and 0.3 *(2)*.

When the above material was prepared for publication the author learned that the thermal transport in quantum wires was considered recently in Ref. 7. Our results coincide with the ones of the cited paper in the places where two investigations overlap (pre-LL constriction).

The author wishes to thank V. Kravtsov, R. Shekhter and Yu Lu for fruitful discussions. This work was partly supported by the Royal Swedish Academy of Science (KVA) and the Natural Science Research Council (NFR). The hospitality of the Abdus Salam International Center for Theoretical Physics is gratefully acknowledged.

*E-mail: krive@ilt.kharkov.ua

[1] C. L. Kane and M. P. A. Fisher Phys. Rev. Lett. **76**, 3192 (1996).
[2] C. L. Kane and M. P. A. Fisher, Phys. Rev. Lett. **68**, 1220 (1992); Phys. Rev. B **46**, 15233 (1992).
[3] D. L. Maslov and M. Stone, Phys. Rev. B **52**, R5539 (1995); V. V. Ponomarenko, Phys. Rev. B **52**, R8666 (1995); I. Sahfi, and H. J. Schulz, Phys. Rev. B **52**, R170040 (1995).

[4] U. Sivan and Y. Imry, Phys. Rev. B **33**, 551 (1986).
[5] Y. V. Nazarov, A. A. Odintsov, and D. V. Averin, Europhys. Lett. **37**, 213 (1997).
[6] A. Furusaki and N. Nagaosa, Phys. Rev. B **54**, R5239 (1996).
[7] R. Fazio, F. W. J. Hekking, and D. E. Khmelnitskii, ''*Anomalous Thermal Transport in Quantum Wires*'' (unpublished).

This article was published in English in the original Russian journal.